

**COMPUTATIONAL MULTIPHASE FLUID DYNAMICS ANALYSES AND
SYSTEMS-LEVEL MODEL DEVELOPMENT FOR A REACTOR CORE
ISOLATION COOLING SYSTEM TERRY TURBINE**

A Dissertation

by

BRADLEY AARON BEENY

Submitted to the Office of Graduate and Professional Studies of
Texas A&M University
in partial fulfillment of the requirements for the degree of

DOCTOR OF PHILOSOPHY

Chair of Committee,	Karen Vierow Kirkland
Committee Members,	Yassin Hassan
	Pavel Tsvetkov
	Gerald Morrison
Head of Department,	Yassin Hassan

August 2017

Major Subject: Nuclear Engineering

Copyright 2017 Bradley Aaron Beeny

ABSTRACT

The Reactor Core Isolation Cooling (RCIC) system found in certain boiling water reactor (BWR) power plants is intended to provide make-up coolant to the reactor pressure vessel (RPV) when it is isolated from the power-producing steam turbine and condenser. Since the Fukushima-Daiichi nuclear power plant accident in March of 2011, the RCIC system has drawn special attention from members of the nuclear industry and government regulators for its apparent role in removing residual decay heat at units 2 and 3 for far longer – 70 and 20 hours, respectively - than the 4 to 8 hours typically credited. The RCIC system in units 2 and 3 mitigated severe accident progression under circumstances well outside its own design basis, delaying core damage for a time. These observations suggest the RCIC system is perhaps a more robust and capable safeguard against core damage than previously thought, especially in the context of beyond-design-basis accidents like short-term or long-term station blackout events. As such, the RCIC system merits further study in pursuit of an increased level of understanding. If better analytical methods are developed and applied, the findings may lead to revised severe accident management strategies and more resilient nuclear power plants in the United States and abroad. The goals of this dissertation are essentially to develop, implement, apply, and validate sufficiently detailed mathematical models of the RCIC system that it may be better understood. This analysis occurs at two disparate levels of physical detail: the computational multiphase fluid dynamics (CMFD) level and the systems level.

For CMFD level analyses, a quasi-two-fluid dispersed phase flow model was developed for implementation into STAR-CCM+. Results were validated to the extent possible via experimental benchmarks. Data useful for systems level modeling purposes was obtained from CMFD, including several factors for MELCOR turbine velocity stage and pressure stage modeling. For systems level analyses, RCIC system Terry turbine mathematical models (for the pressure and velocity stages) were developed for implementation into MELCOR as was a new centrifugal pump model (homologous pump model). New systems-level model capabilities were demonstrated with example problems. Some important observations were made regarding RCIC system performance under off-normal conditions, namely that: 1) the RCIC turbine could be capable of operating with a wide-open governor valve without reaching its mechanical over-speed set-point, and 2) the RCIC system could be capable of self-regulating under two-phase flow conditions resulting from a cyclic pattern of reactor pressure vessel re-fill and over-fill. The new MELCOR models developed herein will certainly enable users to investigate RCIC system thermal-hydraulic response in greater detail and with higher fidelity.

DEDICATION

For my mother, Brenda, and for my grandmothers, Charline and Joyce. Their unconditional love and support was, is, and remains invaluable to me.

ACKNOWLEDGEMENTS

I most sincerely appreciate and acknowledge my long-time advisor and dissertation committee chair, Dr. Karen Vierow Kirkland, for her consistently positive influence on my academic career throughout my time at Texas A&M. Much of my present and future success I owe directly to her sound guidance and encouragement.

I would also like to thank my department committee members: Dr. Yassin Hassan and Dr. Pavel Tsvetkov. Both have made meaningful contributions to my personal and professional development through their teaching and advising. Thanks also to my external committee member, Dr. Gerald Morrison, for his input and assistance with completion of this dissertation.

Thanks to Matthew Solom and Nicholas Luthman for their complementary, cooperative research efforts on the experimental side of the Nuclear Heat Transfer Systems Laboratories at Texas A&M. It has been a pleasure to collaborate with such capable and insightful engineers.

A large part of this research would have been impossible without the assistance and counsel of my co-workers in the reactor modeling and analysis division at Sandia National Laboratories. My current manager, Randall Gauntt, first took me on as an undergraduate intern and has graciously allowed me a great deal of flexibility in my dual role as a PhD candidate and as one of his graduate interns. Special thanks to Larry Humphries, lead MELCOR developer at Sandia National Labs and my original staff mentor, for his patience, guidance, and confidence in me as a new code developer. Thanks

also to Kyle Ross for his co-investigation and collaboration on the research reported in this dissertation. Thanks to Douglas Osborn for his grand facilitation of numerous research efforts and for his valuable technical insights. Thanks to Jeff Cardoni and Chisom Wilson for giving me a great start on my computational fluid dynamics analyses. Thanks to John Reynolds for all his assistance over the years with computer and software issues. Finally, thanks to Matthew Denman, Jesse Phillips, Donald Kalinich, David Louie, Chun Fu, Andrew Clark, Zachary Jankovsky, and all my other friends and colleagues at Sandia Labs for making it a great place to work.

CONTRIBUTORS AND FUNDING SOURCES

Contributors

This work was supervised by a dissertation committee consisting of Professor Vierow Kirkland (advisor and committee chair), Professors Hassan and Tsvetkov of the Department of Nuclear Engineering, and Professor Morrison of the Department of Mechanical Engineering.

The data used in section 7 was obtained by Nick Luthman under the advisement of Dr. Vierow Kirkland. Some of the basic geometry used for purposes of computational fluid dynamics analyses was furnished by Kyle Ross, Jeff Cardoni, and Chisolm Wilson of Sandia National Laboratories. Some of the basic concepts behind the systems-level models presented in section 6 were first posited by Kyle Ross of Sandia National Laboratories in a Department of Energy report on related research.

Other work pursuant to dissertation objectives was completed independently.

Funding Sources

This work was made possible in part by the United States Department of Energy, Nuclear Energy University Programs, under Award Number DE-NE0008312. Its contents are solely the responsibility of the author and do not necessarily represent the official views of the United States Department of Energy.

Graduate study was supported in part by a graduate assistant research position from Texas A&M University, Department of Nuclear Engineering, and by a fellowship grant from the Texas A&M Energy Institute.

NOMENCLATURE

Acronyms

AC	Alternating Current
BWR	Boiling Water Reactor
CAD	Computer Aided Drafting
CD	Converging-Diverging
CF	Control Function
CFD	Computational Fluid Dynamics
CVH	Control Volume Hydrodynamics
CV	Control Volume
CMFD	Computational Multiphase Fluid Dynamics
COR	Core
CST	Condensate Storage Tank
DC	Direct Current
DCH	Decay Heat Package
DOE	Department of Energy
EXEC	Executive
FL	Flow Path
HS	Heat Structure
IAPWS	International Association for the Properties of Water and Steam
IF97	Industrial Formulation 1997
LTSBO	Long Term Station Black Out

MP	Material Properties
NCG	Noncondensable Gas
NEUP	Nuclear Energy University Programs
NHTS	Nuclear Heat Transfer Systems
NPSH	Net Positive Suction Head
NRC	Nuclear Regulatory Commission
NSS	Nuclear Steam Supply
PWR	Pressurized Water Reactor
RCIC	Reactor Core Isolation Cooling
RPV	Reactor Pressure Vessel
SAMG	Severe Accident Management Guideline
SIMPLE	Semi Implicit Method for Pressure Linked Equations
SNL	Sandia National Laboratories
SRV	Safety Relief Valve
STSBO	Short Term Station Black Out
TAMU	Texas A&M University
TDAFW	Turbine Driven Auxiliary Feed Water
TF	Tabular Function

TABLE OF CONTENTS

	Page
ABSTRACT	ii
DEDICATION	iv
ACKNOWLEDGMENTS.....	v
CONTRIBUTORS AND FUNDING SOURCES.....	vii
NOMENCLATURE.....	viii
TABLE OF CONTENTS	x
LIST OF FIGURES.....	xv
LIST OF TABLES	xix
1 INTRODUCTION.....	1
1.1 Dissertation Objectives	2
1.2 Significance of Work	3
1.3 Technical Approach	4
1.4 Dissertation Overview.....	5
2 REACTOR CORE ISOLATION COOLING SYSTEM OVERVIEW	8
2.1 Background Information: Fukushima-Daiichi Accident.....	8
2.2 RCIC System Description	10
2.3 RCIC Turbo-Pump Assembly and the Terry Turbine.....	14
2.3.1 RCIC Pump	20
2.3.2 RCIC Terry Turbine, Pressure Stage.....	21
2.3.3 RCIC Terry Turbine, Velocity Stage	23
2.3.4 RCIC Terry Turbine Auxiliaries	24
2.4 RCIC Operational Considerations.....	25
2.4.1 Normal Operation.....	25
2.4.2 RCIC System Isolation and Trips.....	26
2.4.3 Off-Normal Operation.....	28
3 COMPUTATIONAL FLUID DYNAMICS CODE OVERVIEW	31
3.1 STAR-CCM+ Introduction	31
3.2 Code Mechanics	32
3.3 General Workflow.....	36

3.4	Selected Code Features and Concepts.....	37
3.4.1	Surface Preparation and Meshing.....	38
3.4.2	Coupled Flow and Coupled Energy Models and Solvers.....	41
3.4.3	Passive Scalar Model and Solver	43
3.4.4	User-defined Equation of State Model.....	43
3.4.5	User-defined Sources via Field Function Utility.....	44
3.4.6	Mixing Planes and Moving Reference Frames	44
3.4.7	Derived Parts and Mesh Refinement via Volumetric Controls.....	47
4	SYSTEMS-LEVEL CODE OVERVIEW (MELCOR)	49
4.1	MELCOR Introduction	49
4.2	Code Mechanics	49
4.3	Modeling Concepts	54
4.3.1	Control Volumes	54
4.3.2	Flow Paths	55
4.3.2.1	Flow Paths and Steam Nozzle Expansion.....	56
4.3.2.2	Flow Paths and the Homologous Pump Formulation	57
4.4	Proposed Enhancements for RCIC System Modeling	58
5	STAR-CCM+ MODEL DEVELOPMENT AND IMPLEMENTATION	59
5.1	Physics of Condensing Steam Flow	59
5.1.1	Homogeneous Nucleation	60
5.1.2	Drop-wise Condensation	72
5.2	Dispersed-Phase Size Distribution Modeling	76
5.2.1	Polydisperse Droplet Size Distribution by Moment Method	76
5.2.2	Size Distribution Moments as Passive Scalars.....	82
5.3	Compressible Flow and Steam Nozzles.....	83
5.3.1	Generic Converging-Diverging Nozzle Flow	83
5.3.2	Condensing Steam Nozzle Flow	87
5.3.3	Miscellaneous Considerations.....	91
5.4	Equation-of-State for Super-Saturated Steam.....	93
5.4.1	IAPWS-IF97 Background.....	93
5.4.2	IAPWS-IF97 Data Table Extraction	95
5.5	Turbulence.....	99
5.5.1	Two-Equation k- ϵ Turbulence Modeling Concepts	100
5.5.2	Turbulent, Compressible, Condensing Steam Flow	103
5.6	Full Pseudo Two-Fluid Formulation for Condensing Steam Flow	106
5.6.1	Coupled Flow Model.....	106
5.6.2	Realizable k- ϵ Two-Layer All- y^+	110
5.7	Ideal Gas Formulation.....	117
6	SYSTEMS-LEVEL MODEL DEVELOPMENT AND IMPLEMENTATION....	118

6.1	Homologous Pump Model	118
6.1.1	Conventional Homologous Pump Representation	119
6.1.2	Polar Homologous Pump Representation.....	123
6.1.3	Universal Pump Correlation Alternative	126
6.1.4	Head and Hydraulic Torque	132
6.1.5	Miscellaneous Pump Model Features.....	133
6.1.5.1	Pump Friction Torque	133
6.1.5.2	Pump Moment of Inertia	134
6.1.5.3	Pump Controls: Speed, Motor Torque, Trips.....	134
6.1.5.4	Pump Energy Dissipation and Efficiency	137
6.1.6	Semi-Implicitness and Integration with MELCOR Solution Scheme.....	139
6.1.6.1	MELCOR Phasic Velocity Equation	139
6.1.6.2	Expansion of ΔP_j	141
6.1.6.3	Modified Velocity Equation	143
6.1.6.4	Derivative Computation, $(dH/dQ)^{n-1}$	144
6.2	Terry Turbine Velocity Stage Model	145
6.3	Terry Turbine Pressure Stage Model	151
6.3.1	Ideal Gas Isentropic Flow.....	155
6.3.2	Ideal Gas Rayleigh Flow	157
6.3.3	Nucleation-Growth Integrals.....	159
6.3.4	Normal Shocks and Aerodynamic Back Pressure Effects.....	163
6.3.5	Saturation Line Equation.....	165
6.3.6	Steam Nozzle Expansion Model	166
6.3.6.1	First Step	166
6.3.6.2	Second Step.....	167
6.3.6.3	Third Step.....	167
6.3.6.4	Fourth Step.....	170
6.3.6.5	Fifth Step.....	172
6.3.6.6	Sixth Step.....	172
6.4	Terry Turbine Shaft Model	174
6.5	MELCOR Implementation and Aspects of Solution Methodology	175
6.5.1	Velocity Stage Model	175
6.5.2	Pressure Stage Model	177
6.5.3	Turboshaft Model	178
6.6	CFD-informed Systems Level Model Parameters	178
6.6.1	Velocity Stage Model Parameters	179
6.6.2	Pressure Stage Model Parameters	180
7	RESULTS AND DISCUSSION	181
7.1	STAR-CCM+ Results	181
7.1.1	Gyarmathy Steam Nozzle Experimental Benchmark.....	181
7.1.1.1	Problem Description and Set-up	181
7.1.1.2	Results.....	184

7.1.1.3	Discussion	196
7.1.2	Nuclear Heat Transfer Systems Labs Experimental Benchmark	197
7.1.2.1	Problem Description and Set-Up	197
7.1.2.2	Results	201
7.1.2.3	Discussion	202
7.1.3	Data to Inform Systems-Level Models	204
7.1.3.1	Problem Description and Set-Up	204
7.1.3.2	Bucket Loss Coefficient	205
7.1.3.3	Bucket Exit Angle	209
7.1.3.4	Reversing Chamber Loss Coefficient	213
7.1.3.5	Reversing Chamber Leakage Coefficient	217
7.1.3.6	Carry-Over Fraction	221
7.1.3.7	Terry Turbine Steam Nozzle Expansion Rate	224
7.1.3.8	Discussion	227
7.2	MELCOR Results	228
7.2.1	Demonstration Problems for New Models	228
7.2.1.1	Homologous Pump Model Demonstration	228
7.2.1.2	Terry Turbine Pressure Stage Demonstration and Benchmark	234
7.2.2	Pseudo-Fukushima Test Variant Descriptions	235
7.2.2.1	General Description and Set-Up	235
7.2.2.2	Revised Nodalization with CF Turbine Model	239
7.2.2.3	Modifications to Accommodate New Models	241
7.2.3	Pseudo-Fukushima Results	244
7.2.3.1	Original Version with Revisions	245
7.2.3.2	New Models, Isentropic Steam Expansion	255
7.2.3.3	New Models, Non-Equilibrium Steam Expansion	260
7.2.3.4	New Models, Long-Term Transient	264
7.2.3.5	Discussion	275
8	CONCLUSIONS AND RECOMMENDATIONS	277
	REFERENCES	280
	APPENDIX A: HOMOLOGOUS PUMP MODEL CURVES AND DATA	287
	APPENDIX B: TERRY TURBINE VELOCITY STAGE MODEL DERIVATIONS	314
	APPENDIX C: TERRY TURBINE PRESSURE STAGE MODEL DERIVATIONS	320
	APPENDIX D: MELCOR USER INPUT FOR NEW MODELS	335
	APPENDIX E: 3D NOZZLE SIMULATION DETAILS AND RESULTS	360
	APPENDIX F: MODIFIED HEM FOR DISPERSED TWO-PHASE FLOW	369

APPENDIX G: INL VIRTUAL NOZZLE JET EXPANSION MODEL	371
APPENDIX H: PLOTTING AND CONTROL FUNCTIONS.....	372

LIST OF FIGURES

FIGURE	Page
2.1 BWR4 MKI RCIC system configuration	12
2.2 BWR 5/6 RCIC system configuration	13
2.3 Terry turbine drawing, casing lifted to show rotor	16
2.4 A typical Terry turbine helical steam flow path	18
2.5 Casing cut-away view of a nozzle, its reversing chambers, and the rotor.....	19
2.6 Terry turbine coupled to a centrifugal pump	20
2.7 Terry turbine nozzle geometry and dimensions (inches).....	21
2.8 Pressure stage geometry used for CFD analyses	22
2.9 Terry turbine velocity stage geometry	24
3.1 Geometry part tessellation (top) and surface triangulation (bottom).....	40
3.2 Mixing plane illustration (shown in purple)	45
3.3 Mixing plane, periodic interfaces, and moving reference frames	46
4.1 MELCOR execution flow diagram.....	50
5.1 Condensation, evaporation, and net growth	67
5.2 Converging-Diverging nozzle flow at various back pressures	86
5.3 Qualitative h-s diagram for condensing steam flow in a nozzle.....	88
5.4 Qualitative pressure plot for condensing steam flow	88
5.5 Qualitative illustration of wetness and pressure along a steam nozzle.....	89
5.6 IAPWS-IF97 regions, dependent/independent variables.....	93
6.1 Semiscale single-phase head curve.....	122
6.2 Polar homologous single-phase head curve, Semiscale	126
6.3 Universal correlation head function, each curve an x on $[0, \pi/2]$	128

6.4	Universal correlation torque function, each curve an x value on $[0, \pi/2]$	129
6.5	Control volume for angular momentum equation	147
6.6	Qualitative h-s diagram, pressure/wetness plots for expansion.....	154
7.1	Gyarmathy experimental nozzle 4B geometry	182
7.2	Pressure [Pa] distribution along nozzle wall	186
7.3	Pressure [Pa] profile in nozzle.....	187
7.4	Super-saturation [-] ratio in nozzle	188
7.5	Mach number [-] in nozzle	189
7.6	Velocity [m/s] vectors in nozzle	190
7.7	Nucleation rate [drop/m ³ /s] in nozzle	191
7.8	Condensation rate [m/s] in nozzle	192
7.9	Droplet two-zero (average) diameter [m] in nozzle	193
7.10	Droplet number density [drop/m ³] in nozzle	194
7.11	Droplet mass fraction [kg _l /kg _g] in nozzle	195
7.12	Full three-dimensional Terry turbine wedge	198
7.13	Terry turbine wedge, rotor and reversing chamber	199
7.14	Cut-away view demonstrating mixing plane configuration.....	200
7.15	Mixing planes used to compute rotor bucket loss coefficients.....	206
7.16	Bucket loss coefficient as a function of rotational speed	207
7.17	Example planes for bucket exit angle computations	210
7.18	Bucket exit angle as a function of rotational speed	211
7.19	Constrained planes to compute reversing chamber loss coefficients	214
7.20	Reversing chamber loss coefficient as a function of rotational speed.....	215
7.21	Reversing chamber crescent hole constrained planes.....	218

7.22	Reversing chamber leakage coefficient as a function of rotor speed	219
7.23	Carry-over fraction as a function of rotor speed.....	222
7.24	Three-dimensional Terry turbine nozzle geometry, inner side.....	224
7.25	Three-dimensional Terry turbine nozzle geometry, outer side.....	225
7.26	Predicted nucleation rate [drop/m ³ /s] for 3D Terry turbine nozzle	226
7.27	Homologous pump model demonstration problem, pump-driven flow	229
7.28	Loop flow problem, pump impeller speed.....	231
7.29	Loop flow problem, pump head.....	232
7.30	Loop flow problem, water velocity at pump discharge	233
7.31	Pseudo-Fukushima RCIC system model diagram	237
7.32	RPV pressure [Mpa]	246
7.33	RPV liquid level [m].....	247
7.34	Steam nozzle steam flow rates [kg/s]	248
7.35	Steam nozzle water flow rates [kg/s].....	249
7.36	Steam nozzle phasic velocities [m/s].....	250
7.37	Pump/Shaft/Rotor rotational speed [rpm].....	251
7.38	Pump head [Pa].....	252
7.39	Pump Flow [m ³ /s].....	253
7.40	Turbine torque from CF-model [N*m].....	254
7.41	Pump/Shaft/Rotor speed [rpm]	255
7.42	Pump Head [Pa].....	256
7.43	Pump Flow [m ³ /s].....	257
7.44	Turbine torque [N*m] from new compound velocity-stage model	258
7.45	Steam line relief valve open fraction	259

7.46	Pump/Shaft/Rotor speed [rpm]	260
7.47	Pump Head [Pa]	261
7.48	Pump Flow [m ³ /s]	262
7.49	Turbine torque [N*m]	263
7.50	RPV pressure [MPa]	265
7.51	RPV liquid level [m]	266
7.52	Steam nozzle phasic velocities [m/s]	267
7.53	Pump/Shaft/Rotor speed [rpm]	268
7.54	Pump Head [Pa]	269
7.55	Pump Flow [m ³ /s]	270
7.56	Total turbine torque (both phases) [N*m]	271
7.57	Turbine torque due to steam flow [N*m]	272
7.58	Turbine torque due to water flow [N*m]	273
7.59	RCIC pump suction water temperature [K]	275

LIST OF TABLES

TABLE		Page
2.1	RCIC-related event timeline, Fukushima-2	8
6.1	Possible pump operating modes	121
6.2	Octant arrangement under the polar homologous representation	124
6.3	Polynomial fit data for curves in Figure 6.3	130
6.4	Polynomial fit data for curves in Figure 6.4	131
7.1	Gyarmathy Nozzle 4B geometry data (constant width 20 mm)	183
7.2	Gyarmathy experimental benchmark, nozzle 4B, run 19A	185
7.3	NHTS experimental benchmark conditions.....	201
7.4	NHTS experimental torque/power comparison and simulation results	202
7.5	Simulation Matrix Stagnation Inlet Boundary Conditions	205
7.6	Bucket loss coefficient data	208
7.7	Bucket exit angle data.....	212
7.8	Reversing chamber loss coefficient data	216
7.9	Reversing chamber leakage coefficient data	220
7.10	Carry-over fraction data.....	223
7.11	GS-1 Terry turbine expansion rate computational details	226
7.12	Code-to-code benchmark results, analytical Wilson point	234
7.13	Key values for original pseudo-Fukushima RCIC system input deck.....	238
7.14	Homologous pump inputs for pseudo-Fukushima run	240
7.15	Block-CVH input for Terry turbine rotor object	242

1 INTRODUCTION

The Reactor Core Isolation Cooling (RCIC) system found in certain boiling water reactor (BWR) power plants consists of safety-related equipment intended to provide make-up coolant to the reactor pressure vessel (RPV) when isolated from the power-producing steam turbine and condenser. The RCIC system is alternating current (AC) independent and can deliver coolant from either the condensate storage tank (CST) or the suppression pool (called the “torus” in a MK-I containment) via a steam-driven Terry turbine coupled on a common shaft to a centrifugal, multistage pump.

Since the accident at the Fukushima-Daiichi nuclear power plant in March of 2011, the RCIC system has drawn special attention from industry and regulators for its apparent role in removing residual decay heat at units 2 and 3 for far longer – 70 and 20 hours, respectively - than the 4 to 8 hours typically credited. The RCIC system in units 2 and 3 mitigated severe accident progression under circumstances well outside its own design basis, delaying core damage for a time. These observations suggest the RCIC system is a more robust and capable safeguard against core damage than previously thought, especially in the context of beyond-design-basis accidents like short-term station blackout (STSBO) events or long-term station blackout (LTSBO) events.

As such, the RCIC system merits further study in pursuit of an increased level of understanding. If better analytical methods are developed and applied to the RCIC system, the findings may lead to revised severe accident management strategies and more resilient nuclear power plants in the United States and abroad. This is, in part, the impetus for a co-investigative effort of the Texas A&M (TAMU) Nuclear Heat Transfer Systems (NHTS)

laboratory and Sandia National Laboratories (SNL) under the auspices of the Department of Energy (DOE) Nuclear Energy University Programs (NEUP).

The RCIC system can be logically divided into two halves for purposes of analysis on either the CMFD level or the systems level: the steam (Terry) turbine side and the centrifugal pump side. Systems-level thermal hydraulics and accident codes, e.g. RELAP5-3D and (due in large part to code development efforts of the author) MELCOR, currently have methods for modeling centrifugal pumps. They typically require a full complement of pump performance data but can model most aspects of centrifugal pump behavior with fair fidelity. However, there are special modeling challenges for the Terry turbine that systems codes cannot accommodate without special provision. Even if a user could, in theory, create their own Terry turbine equation (e.g. through MELCOR control function utility) for use in a calculation, there are reasons beyond mere convenience as to why a built-in code model would be preferable.

1.1 Dissertation Objectives

The aims of this dissertation are:

- To develop appropriately detailed CMFD physics models for the RCIC turbine
- To implement CMFD physics models on a RCIC Terry turbine geometry
- To validate CMFD physics models – to the extent possible – against experiments from literature and/or the NHTS Laboratory at TAMU
- To develop and implement RCIC systems-level models informed by CMFD
- To apply/validate the RCIC systems-level models to the extent possible

- To draw useful conclusions about RCIC system operation from a pseudo-Fukushima MELCOR model targeted at off-normal operating conditions

1.2 Significance of Work

Higher-fidelity RCIC physics models would advance the state of the art of nuclear power plant safety analysis (for conditions up to and beyond design basis) by improving the predictive capability of present analytical tools. If more detailed analyses are possible, the true capabilities of RCIC systems could be better understood in general and the curious behavior of RCIC systems during the Fukushima event could be better understood in particular. The CMFD development activity performed in this dissertation demonstrates the implementation and application of a method for modeling condensing steam flow with a commercial CFD code. Furthermore, some CFD results can be used in the context of higher-level systems models to capture physical effects otherwise lost to mathematical simplification. The systems code development activity performed in this dissertation will help with stand-alone RCIC system analysis but will also integrate new models into the existing MELCOR framework so that they are immediately available for purposes of predictive accident analysis (design basis or beyond).

Furthermore, systems level codes are often used in the process of small-scale or full-scale experimental facility design. For example, estimates for piping and equipment sizing often follow from some sort of calculation or simulation. A higher-quality simulation typically leads to better estimates overall and can guide facility designers in their decision-making. There is currently a great deal of interest on the part of industry

and regulators to plan and perform smaller-scale and full-scale RCIC system experiments, hence another reason why better RCIC system models would be useful [1].

Note also that the benefits of this research extend to pressurized water reactor (PWR) systems analysis because turbine-driven auxiliary feed water (TDAFW) systems use turbo-pumps consisting of a Terry turbine coupled to a centrifugal pump.

1.3 Technical Approach

To achieve aforementioned dissertation goals, a systems-level code and a computational fluid dynamics (CFD) code capable of multiphase modeling were selected. Because of previous experience, prior and concurrent research activity, familiarity, availability, and popularity, MELCOR was chosen as the systems-level (and severe accident) code for the present study. In all likelihood, any RCIC system model developed for MELCOR could be adapted to other thermal-hydraulics codes (e.g. RELAP5-3D). Because of availability, capability, portability, and convenience, STAR-CCM+ was chosen as the CFD/CMFD code for the present study. Most commercial CFD codes are similar in terms of user-defined function versatility and pre-packaged multiphase physics models, so development with STAR-CCM+ is likely reproducible in other CFD codes (e.g. ANSYS-FLUENT).

Prior to model development in MELCOR and STAR-CCM+, the pertinent physics of the RCIC Terry turbine were studied in an extensive literature survey. The physics of interest are typical of steam nozzles, turbines, and separators, i.e. compressible, turbulent two-phase condensing steam/droplet flow with non-equilibrium thermodynamics and homogeneous nucleation. Theoretical expositions of and CMFD formulations for

condensing steam flow were sought in literature and indeed proved helpful in the process of developing Terry turbine physics models. Experiments from the literature offered valuable insight into physical phenomena and provided some excellent benchmark data. Previous and concurrent RCIC system research by SNL helped with:

1. Understanding needs and knowledge gaps of system-level RCIC models,
2. Understanding RCIC geometry and normal/off-normal operation modes
3. Simplifying analyses by supplying computer-aided drafting (CAD) files, and
4. Developing RCIC models compatible with current MELCOR models

This dissertation largely pertains to development, implementation, application, and validation of CMFD and systems-level RCIC turbine models. A quasi-two-fluid dispersed phase flow model was developed and implemented in STAR-CCM+ to capture in sufficient detail the important aspects of normal-mode Terry turbine operation. The physics model was tested and, to an extent, validated with a simple steam nozzle geometry corresponding to a subset of experiments documented in the literature. In parallel, a three-dimensional CAD representation of a RCIC Terry turbine was imported into STAR-CCM+, conditioned for meshing, and surface/volume meshed in such a way as to be compatible with the quasi-two-fluid model. A systems-level physics model - informed by CMFD results - was developed and implemented in MELCOR. A so-called pseudo-Fukushima RCIC system MELCOR input deck was updated to leverage new capabilities.

1.4 Dissertation Overview

Appropriately in-depth overviews of the RCIC system, STAR-CCM+, and MELCOR are given in dissertation sections 2, 3, and 4, respectively. Section 2 includes

background information on the Fukushima accident, a detailed description of the RCIC system (BWR MK-I containment), an overview of the turbo-pump assembly, and a discussion of some RCIC operational characteristics. Section 3 includes an introduction to STAR-CCM+ and sufficiently descriptive summaries of its code mechanics, its solution workflow, and selected code features/concepts of importance to Terry turbine modeling. Section 4 includes an introduction to MELCOR and sufficiently descriptive summaries of its code mechanics, its modeling concepts, and proposed enhancements for purposes of RCIC system modeling.

Sections 5 and 6 detail CFD and systems level model development and implementation. Section 5 outlines, point-by-point, the important phenomenological aspects of condensing steam flow and simultaneously presents equations, formulations, closures, etc. that are useful for CMFD analyses. Section 5 concludes by presenting the full physics formulations for all computations performed pursuant to dissertation objectives. Section 6 outlines formulations for RCIC system turbo-pump analysis beginning with a recap of the existing homologous pump model (with special attention to how it must be modified) and continuing on to cover both Terry turbine stages (pressure and velocity) and the turbo-pump shaft. Then, a discussion of behind-the-scenes implementation in MELCOR is included. This exposition covers solution methodology and any tie-ins to MELCOR phasic velocity and phasic energy equations. Section 6 concludes by drawing attention to the interplay between proposed RCIC systems level models and more detailed CFD computations.

Section 7 presents and discusses results obtained from implementation of models described in sections 5 and 6. The section is divided so that STAR-CCM+ results are presented separately from MELCOR results. The STAR-CCM+ section includes results from certain experimental benchmarks so as to at least partially validate the physics and geometry used for the RCIC Terry turbine. The STAR-CCM+ section also includes data intended for use at the systems level so as to encapsulate certain phenomena beyond the scope of a systems level analysis. The MELCOR section includes results from simple demonstration problems that exercise new physics models as well as results from a pseudo-Fukushima benchmark problem (modified to use the new models). Section 8 draws meaningful conclusions and makes recommendations for additional experiments, benchmarks, and development projects.

2 REACTOR CORE ISOLATION COOLING SYSTEM OVERVIEW

2.1 Background Information: Fukushima-Daiichi Accident

At present – more than 5 years after the fact – several exhaustive studies of the Fukushima-Daiichi accident have been conducted based on available evidence. The reader is referred to any of these (e.g. [2]) for a more complete description. However, it is instructive to review a short timeline of RCIC-related events for unit 2 so as to underscore the point that the RCIC system far exceeded its credited operation time. Table 2.1 - adapted from [3] – summarizes Fukushima-Daiichi unit 2 RCIC-related events.

Table 2.1 RCIC-related event timeline, Fukushima-2

Time Since Earthquake	RCIC-Related Events
0	Earthquake causes loss of off-site power Fission chain reaction terminated, diesel generators start RPV isolated, RCIC starts on low water level
1 min	RCIC automatically shuts down (high level)
11 min	Operators restart RCIC on low water level
47 min	First of seven tsunamis arrives at plant
48 min	RCIC automatically shuts down (high level) Operators restart RCIC
55 min	Start of loss of AC/DC due to flooding
later, same day	Failed attempt to verify RCIC operation Faint metallic sounds heard in RCIC room
11 hr, 14 min	Attempt to verify RCIC operation Discharge pressure high, conclude RCIC is operational
14 hr, 12 min	RCIC pump suction switchover to torus
26 hr, 42 min	RCIC continues injecting
70.5 hr	Operators conclude RCIC failure, restart unsuccessful Water level at ~ 95" above TAF Core degradation commences within hours
9 days	Offsite power restored at unit 2

In the postulated Fukushima-Daiichi unit 2 accident sequence – classified as a LTSBO – the operators, after manually restarting once, were able to get the RCIC system on-line and injecting into the RPV just before AC and DC power delivery was degraded by tsunamis and flooding. The RCIC system ran for the next three days, delaying core degradation all the while. This is significant because, as discussed in subsequent sections, loss of DC power is typically assumed to lead abruptly and inexorably to RCIC system failure. Due to extensive on-site infrastructure damage, off-site power could not be restored until nine days later and core damage was not averted. RCIC system failure - perhaps due to suppression pool saturation – ultimately occurred under unit 2 LTSBO conditions. Nevertheless, the RCIC system operated without DC power under extreme conditions beyond its design envelope for far longer than severe accident management guidelines (SAMGs) typically assume.

The Fukushima-Daiichi unit 2 event sequence (and additionally the unit 3 event sequence as outlined in [3]) is evidence that the RCIC system is perhaps more robust than conventionally assumed. The evidence would suggest that the RCIC system is capable of self-regulating independent of its DC-powered control system and governor (both of which are discussed in subsequent sections). With confirmation from computational models and/or experiments, substantial revisions to SAMGs for certain BWRs (with respect to the RCIC system) and PWRs (with respect to the TDAFW system) may be in order. Such procedural changes could lead to an increased level of plant resilience under accident conditions at minimal cost to existing nuclear installations.

2.2 RCIC System Description

For certain BWR designs such as the BWR3/4 MK-I shown in Figure 2.1 or the BWR 5/6 shown in Figure 2.2, one provision for residual heat removal and/or vessel coolant inventory make-up is the RCIC system. It is functionally classified as a “safety related system” and is regarded for regulatory purposes as an Engineered Safety Feature (ESF) system [4]. It is designed to intervene when:

- The RPV is isolated from the turbine/condenser (the typical heat sink), or
- Off-site (AC) power is lost and other systems are unavailable, or
- Feed-water stops, pressure prohibits shutdown cooling system intervention

The RCIC system is sized to compensate for a high rate of vessel coolant boil-off assuming steam venting through safety relief valves to the suppression pool. It is designed to maintain RPV water inventory 15 minutes after reactor shutdown and valves are in a stand-by lineup such that the system initiates upon a complete loss of AC power [4]. The system will automatically start and stop (via its control system when power is available) at certain low and high RPV water level set-points. The exact RCIC capacity varies with power level of a given BWR, but 400-800 gal/min of coolant delivery is typical. The RCIC system can operate across almost the entire range of possible system pressures from normal operating pressure (or 1135 psig) down to about 150 psig [4]. The RCIC system is entirely independent of off-site AC power and needs no service air or cooling water.

As seen in Figure 2.1, the RCIC system turbo-pump assembly consists of a Terry turbine coupled to a centrifugal pump via a common shaft. There are several lines of piping to and from the turbine and pump in addition to shutoff valves, a trip-and-throttle valve,

and control valves (all of which are AC independent). Support systems (e.g. lube oil cooling), instrumentation, and control systems are also present. The Terry turbine steam supply line splits off a main steam line (MSL) upstream of the inboard isolation valve. Steam admitted to the turbine through its governor valve delivers an impulse to the turbine rotor which exerts a shaft torque to spin the pump impeller. Expanded steam and water exhausts to the suppression pool through a dedicated line from a casing port. Note there are alternate discharge lines for testing purposes, non-condensable gas venting, and RCIC pump minimum flow protection. The RCIC pump is initially aligned to take suction from the CST. It delivers coolant (from either the CST or the wet-well) to a feed-water injection line and thereby to the RPV. The Terry turbine usually has both a mechanical over-speed trip and an electro-hydraulic control system with a governor to regulate steam flow. Note the governor may be manually operated (independent of the DC-powered flow controller). Note Figure 2.2 shows a similar RCIC system for BWR systems with MK III containment.

RCIC system failure can result from:

- Some DC power supply issue causing the governor valve to fully open and leading abruptly to a turbine trip on over-speed
- High suppression pool temperature so that insufficient pump net positive suction head (NPSH) exists (unlikely if AC power allows suppression pool cooling by other systems)
- High containment pressure (and thus high turbine back-pressure)

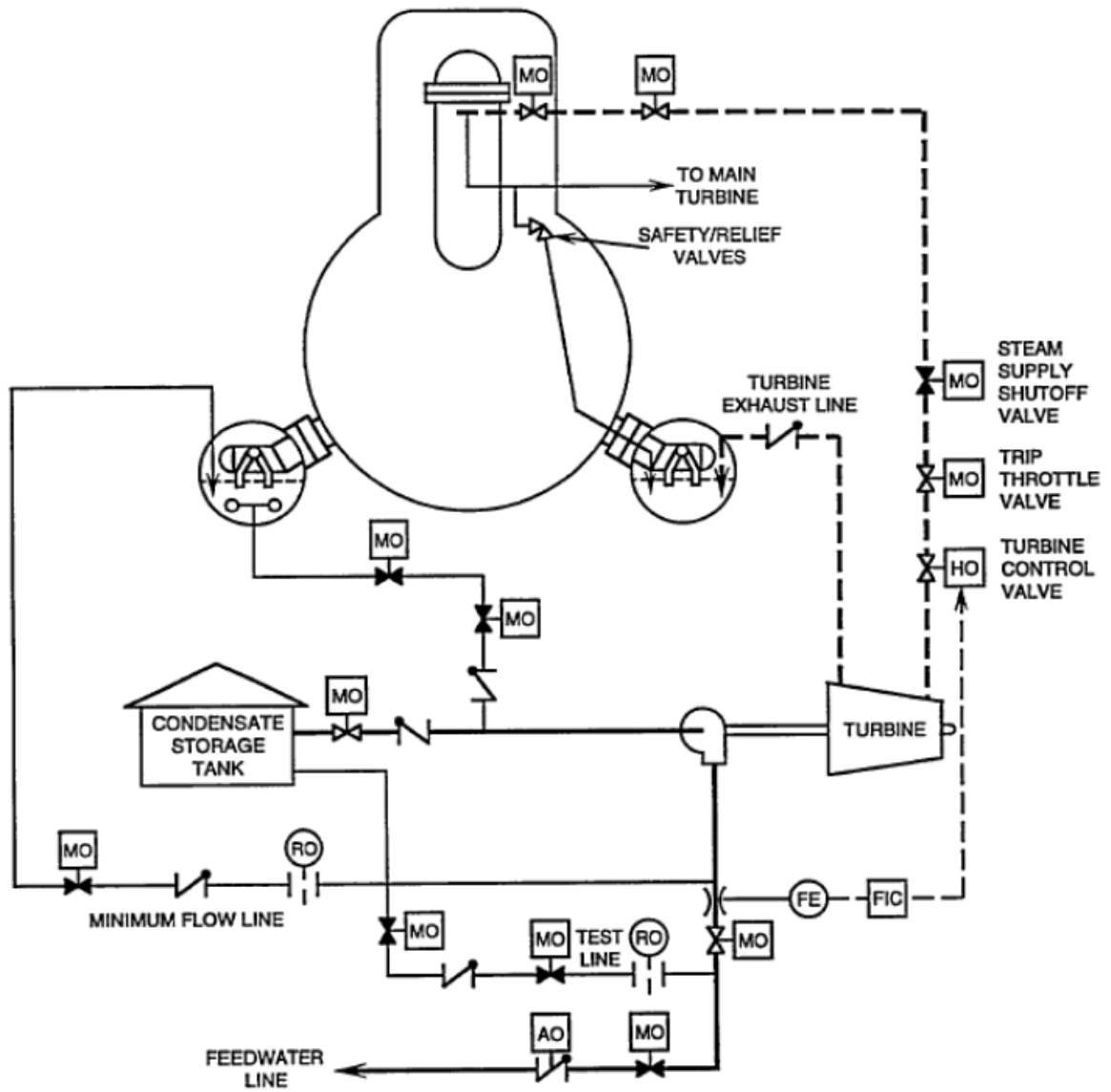


Figure 2.1 BWR4 MKI RCIC system configuration [5]

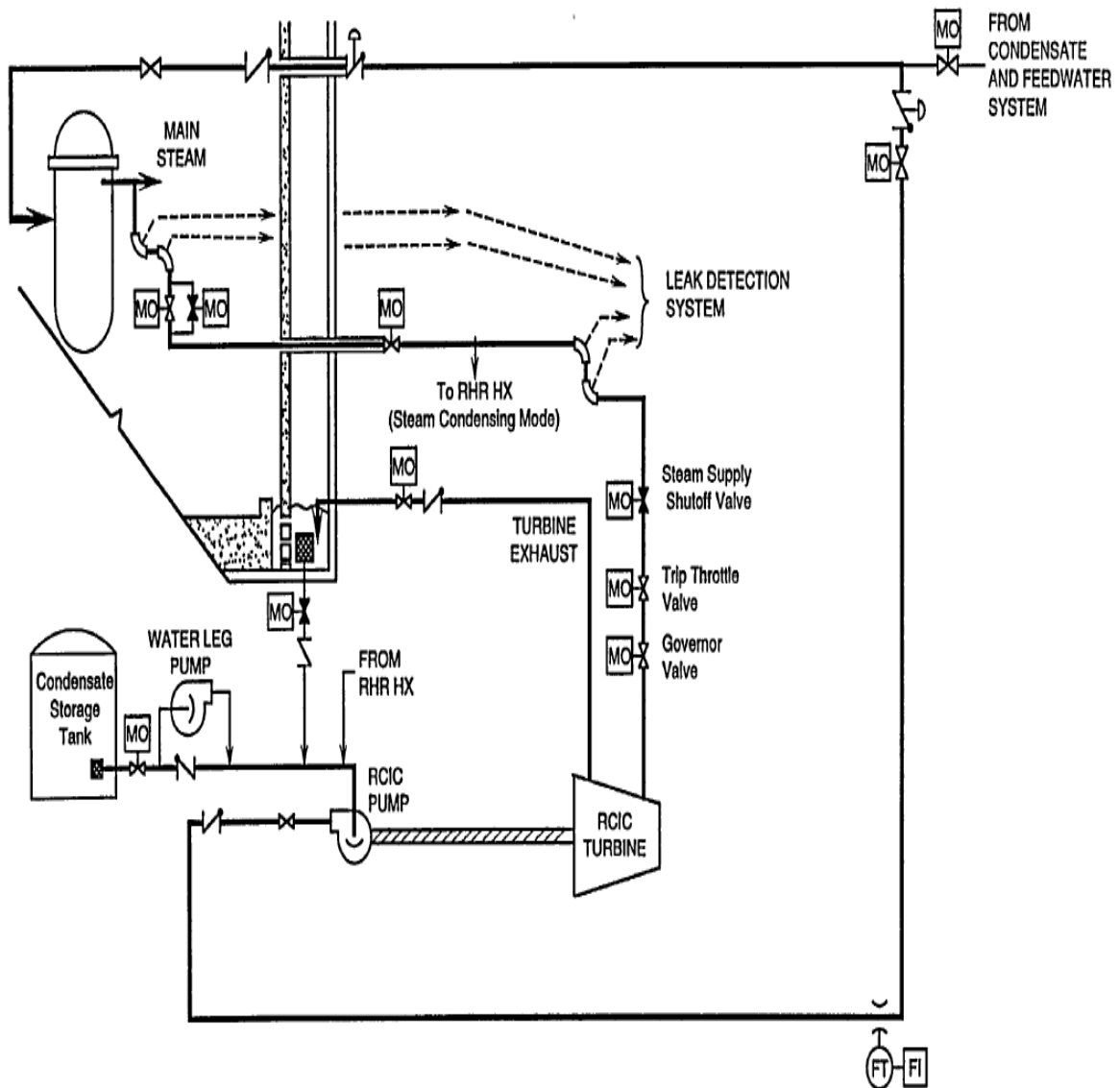


Figure 2.2 BWR 5/6 RCIC system configuration [5]

With respect to RCIC system operational failure, the usual assumption is that – in the absence of AC power – operation ceases in the 4 to 12 hours required for on-site DC power to deplete. The failure mode in this case is a loss of governor control leading directly to an over-speed trip, perhaps after turbine ingestion of water due to pressure vessel over-fill and subsequent steam line flooding. This assumption discounts any and all ability of the

Terry turbine to self-regulate (to maintain vessel inventory and pump NPSH requirements) without DC governor valve control.

A quick run-down of important valve components marked in Figure 2.1 and/or Figure 2.2 is instructive. Note all major RCIC system valves respond to initiation, isolation, or trip signals. The following descriptions are short summaries of content in [4]:

- Steam Supply Isolation Valves (unlabeled in Figure 2.1 and Figure 2.2)
 - Inboard (AC) and outboard (DC), both motor-operated
 - Designed to admit MSL flow to the RCIC steam line
- Steam Supply Shutoff Valve
 - DC, motor-operated, closed when RCIC system in stand-by lineup
 - Designed to open/close on low/high RPV water level signals
- Turbine Trip-and-Throttle Valve
 - Motor-operated, open when RCIC system in stand-by lineup
 - Upstream of governor, trip turbine if signaled or throttle steam flow
- Turbine Governor (Control) Valve
 - Electro-hydraulic, opened by spring force, closed by oil pressure
 - Controls turbine speed via oil pressure (RCIC flow control circuit)

2.3 RCIC Turbo-Pump Assembly and the Terry Turbine

The steam-driven turbine that powers the RCIC system centrifugal pump is based on the early 20th century design of Edward Terry and the Terry Steam Turbine Company. Patents filed as early as 1903 detail a turbine that bears a strong resemblance to not only the GS-1 and GS-2 model turbines in BWR RCIC systems, but also to other smaller

models (e.g. the Z-1) that find application in other industries. Terry turbines of all sizes could be classified as Pelton impulse type with multiple velocity stages [6]. Impulse-type turbines rely on:

- Conversion of steam enthalpy to kinetic energy via expansion in nozzles (expansion occurs in the so-called pressure stage of the turbine)
- Subsequent delivery of an impulse (force) to a turbine blade or bucket from high-velocity steam (occurs in the so-called velocity stage of the turbine)

The Terry turbine certainly conforms to this two-fold description. The single pressure stage consists of a series of converging/diverging nozzles that are circumferentially situated around the rotor. The nozzles are either all around the rotor or only around one half, depending on the specific Terry turbine model. Each nozzle receives steam that is first admitted through the up-stream turbine governor valve. Any given parcel of steam crosses a nozzle and expands only once, hence the single pressure stage. Note that an in-depth discussion of steam expansion and nozzle physics is deferred to a later section. Every nozzle discharges straight into one of the u-shaped buckets milled into the face of the solid rotor wheel.

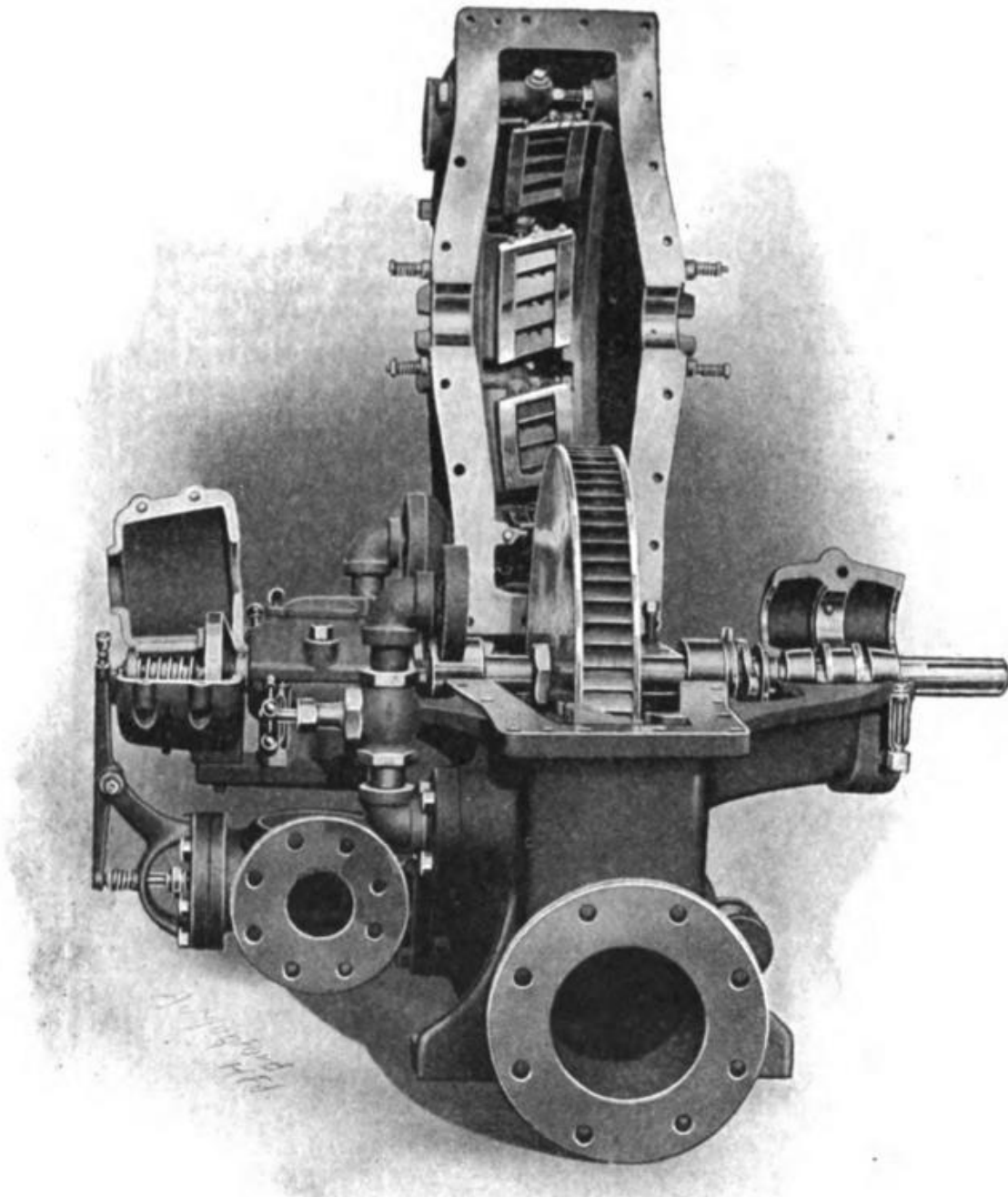


Figure 2.3 Terry turbine drawing, casing lifted to show rotor [7]

Details of the rotor including the buckets are visible in Figure 2.3. Steam enters buckets and reverses direction (turning through 180°) before exiting at the opposite end.

Paired with each nozzle is a series of reversing chambers (typically four per nozzle) affixed to the inside of the casing (visible in Figure 2.3). Reversing chambers constitute the velocity stages of the turbine because they return some portion of the steam flow to the rotor for secondary, tertiary, and quaternary impulse delivery. Each reversing chamber has a semi-circular or crescent-shaped hole in its top lateral surface that permits some expanded steam to vent. Otherwise the flow passages would need to be progressively wider to accommodate the increased steam volume [7].

The typical steam flow path is shown in Figure 2.4. Note the nozzle plenum, the nozzle, and the rotor are shown with reversing chambers omitted. Note also the helical shape of the flow path which indicates the slightly slanted orientation of the reversing chambers with respect to the rotor buckets. Figure 2.5 cuts away the casing wall to show the nozzle, rotor, and four reversing chambers in their actual arrangement. In Figure 2.3, the large flanged pipe at the bottom of the turbine is the steam outlet. Steam exits from the casing here after it vents from a reversing chamber or traverses all four velocity stages. Steam travels through a turbine exhaust line to the suppression pool below the water level, thereby condensing the steam unless the pool is at or near saturation. The exhaust line is protected by vacuum breakers and a high turbine back-pressure trip capability.

Turbines of this type are inefficient but robust since wet steam and even liquid slugs can pass through the turbine with little risk to the structural integrity of turbine internals. Blade pitting and erosion is not a concern with the Terry turbine because steam or water passes through nozzles and impinges on buckets rather than blades. Performance

typically degrades (less shaft torque to drive the pump) with excessive wetness, but the system can often ride out transient conditions and return to normal thereafter.

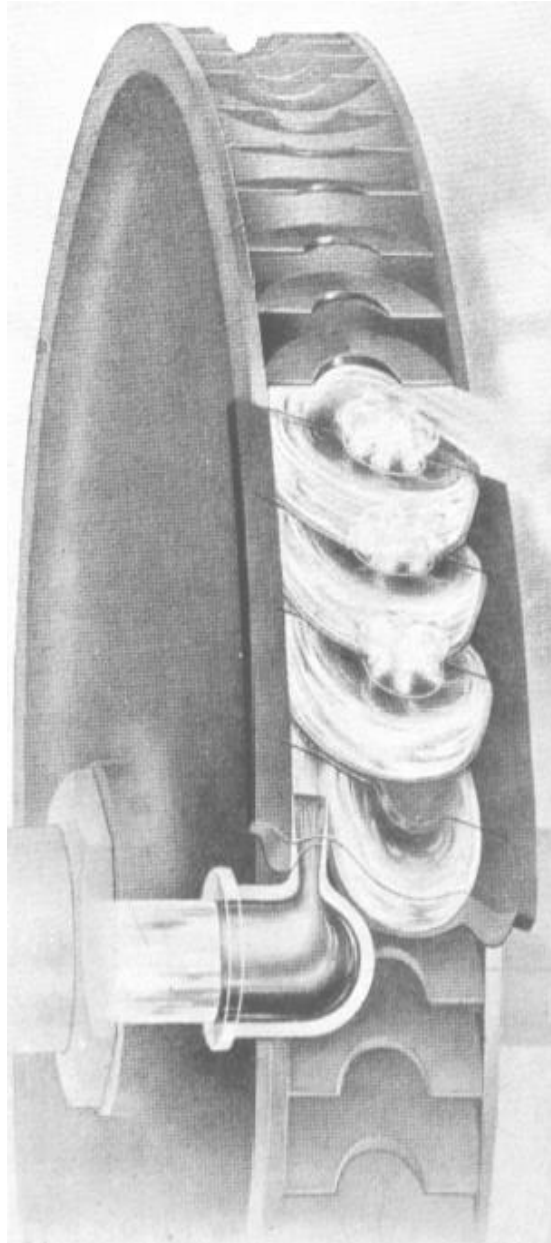


Figure 2.4 A typical Terry turbine helical steam flow path [8]

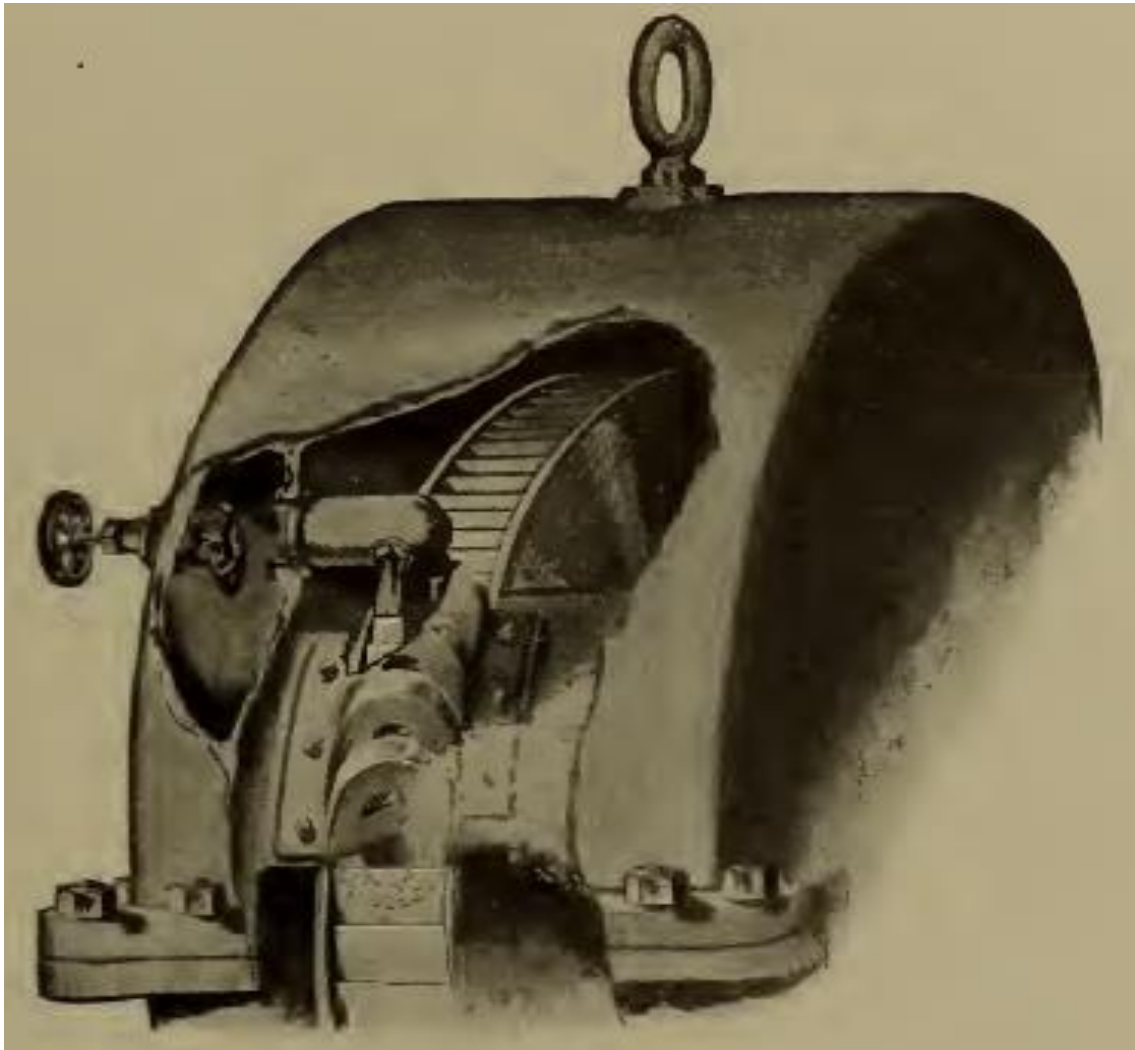


Figure 2.5 Casing cut-away view of a nozzle, its reversing chambers, and the rotor [7]

To illustrate the turbo-pump concept, Figure 2.6 shows a Terry turbine (on the right) coupled to a centrifugal pump (on the left) via a torque shaft (spanning the space between). The RCIC system employs a similar turbo-pump concept to deliver make-up feed water to the RPV.

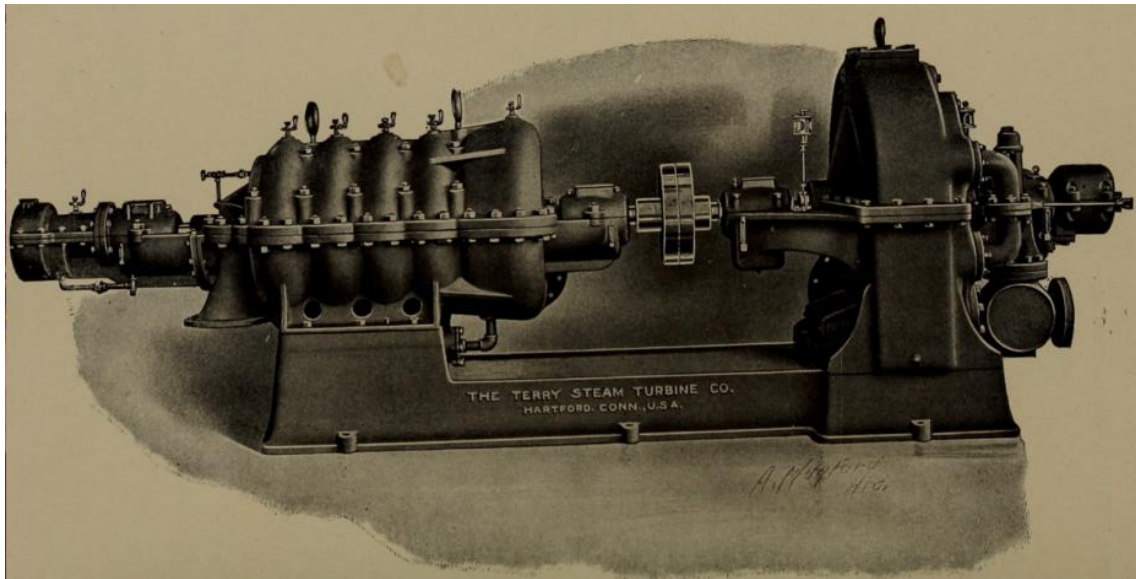


Figure 2.6 Terry turbine coupled to a centrifugal pump [7]

2.3.1 RCIC Pump

As previously mentioned, the turbine-driven RCIC pump draws water from either the CST or the suppression pool. The CST suction line is physically lower in elevation relative to other system suction lines also found within the CST [4]. Switch-over (CST to suppression pool) will occur upon indication of a low water level in the CST. The pump itself is horizontally-mounted, multi-stage, and centrifugal. The majority of water drawn in at suction is sent to the RPV, but a small fraction is conveyed to Terry turbine auxiliaries [4]. To help preserve RCIC pump NPSH, the physical elevation of the pump is lower than any possible suction elevation [4]. Note from Figure 2.1 that there are two motor-operated valves on the pump discharge line. Two flow paths (one for turbine auxiliaries and one for minimum flow) tap off upstream of the first discharge valve and another test line taps off just downstream of the first discharge valve [4].

2.3.2 RCIC Terry Turbine, Pressure Stage

The Terry turbine pressure stage is that part of the turbomachine within which a significant reduction in steam pressure occurs by virtue of rapid expansion in a converging-diverging nozzle. Typically, steam is superheated or high-quality saturated (if not totally dry) at the nozzle inlet after passing through the turbine governor. In accordance with the operating principles of an impulse-type turbine, a conversion of enthalpy to kinetic energy accompanies the steam expansion across the nozzle. This process allows for high-velocity steam to exit the nozzle. There are typically several nozzles in a Terry turbine, but these do not constitute multiple pressure stages because any given parcel of steam admitted through the governor valve expands only once in only one of the nozzles.

With respect to nozzle shape and geometry, dimensional estimates can be made from available sources including actual measurements of representative Terry turbine steam nozzles. Figure 2.7 depicts nozzle cross-sectional shape and dimensional estimates.

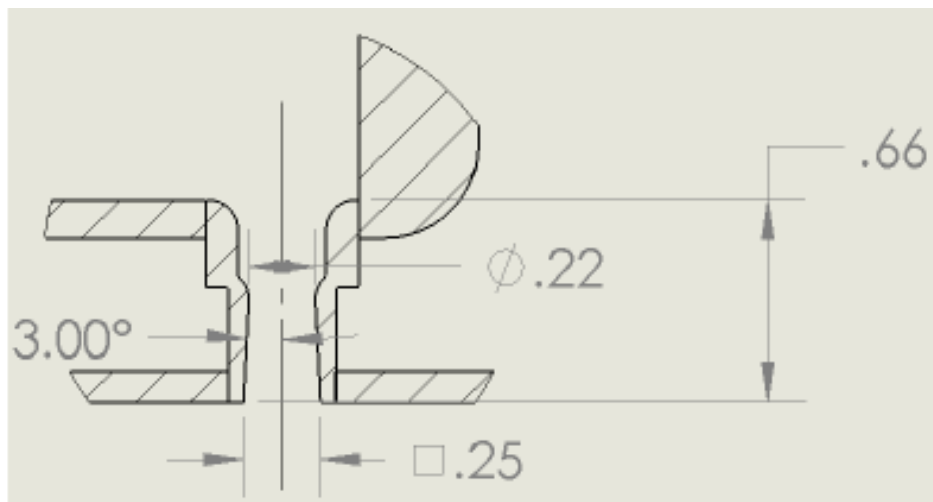


Figure 2.7 Terry turbine nozzle geometry and dimensions (inches) [1]

The nozzle cross-sectional shape and area both evolve along the direction of flow. In the converging section, the cross-section is circular and decreasing in area. At the throat (diameter of 0.22 in), the cross-section is still circular but begins transitioning to a square shape thereafter along the gradually diverging (3° angle) section. At the nozzle outlet, the cross-sectional shape is square with length and width of 0.25 in. The entire length of the nozzle is approximately 0.669 in (1.7 cm) so that the transition from circular to square cross-section occurs over a short length. Preceding dimensional estimates correspond to a typical BWR RCIC Terry turbine (GS-1 or GS-2). CAD renderings in Figure 2.8 show the geometry used for CFD analyses.

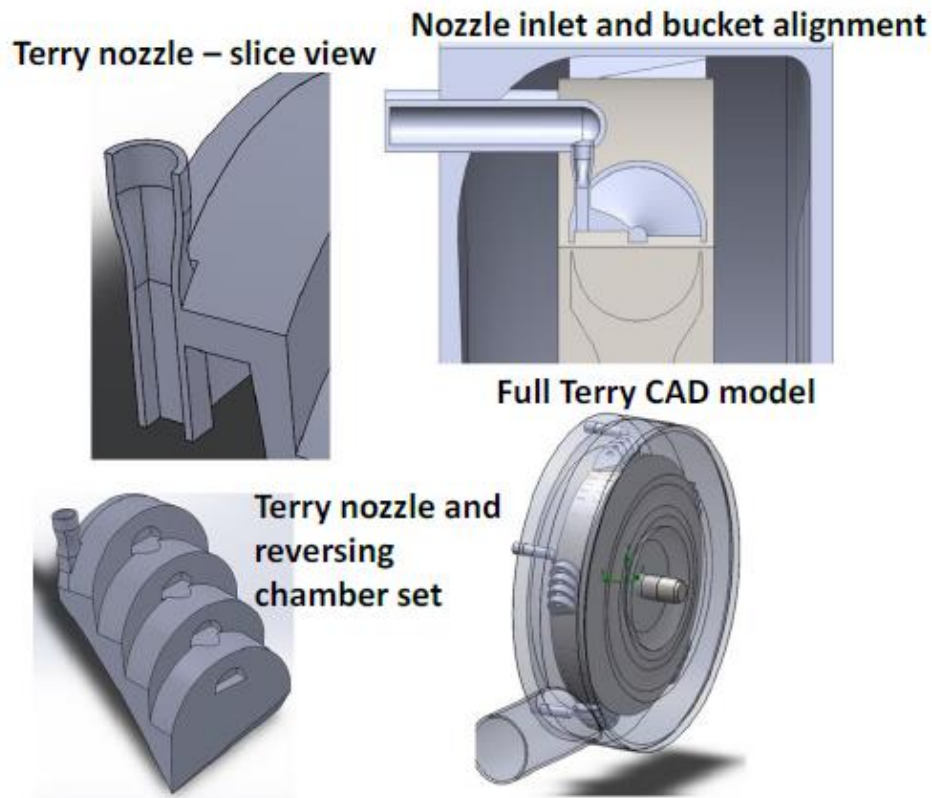


Figure 2.8 Pressure stage geometry used for CFD analyses [1]

2.3.3 RCIC Terry Turbine, Velocity Stage

The Terry turbine velocity stage consists of rotor buckets and reversing chambers and is characterized by a momentum exchange between impinging steam and the rotor. Because reversing chambers can return steam to the rotor after the first (or previous) impingement, the Terry turbine is technically a compound velocity stage machine. The first velocity stage involves a nozzle and the rotor whereas subsequent velocity stages involve reversing chambers and the rotor. In accordance with the operating principles of an impulse-type turbine, steam enters the rotor and delivers an impulse as it turns through a bucket. A force is generated in the local direction of bucket motion, acting with the leverage of a moment arm roughly equal in length to the turbine wheel radius. This creates a twisting moment, or torque, on the turbine shaft.

All Terry turbines found in domestic BWR RCIC systems have a wheel diameter of 24 in [1]. Anywhere between five and ten nozzles are situated circumferentially about the Terry turbine rotor. The turbine wheel/bucket width is estimated at 2.756 in (7 cm) and four reversing chambers per nozzle are assumed. About eighty-four buckets would fit around the perimeter of the rotor and there is a distance of about 0.59 in (1.5 cm) between the steam nozzle outlet and the rotor. Figure 2.9 shows oblique and side views of the full Terry turbine geometry.

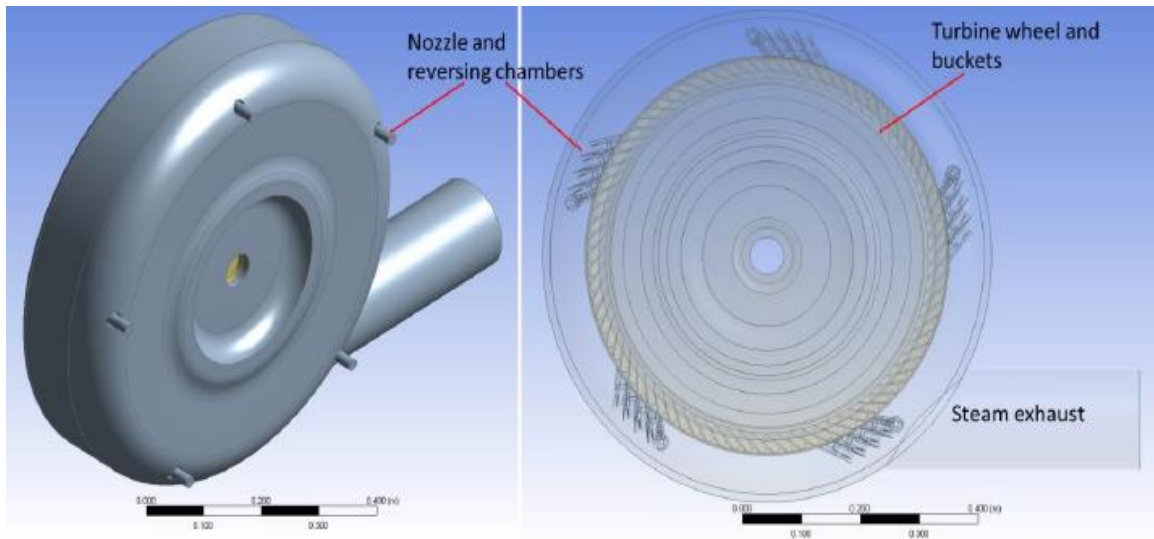


Figure 2.9 Terry turbine velocity stage geometry [1]

2.3.4 RCIC Terry Turbine Auxiliaries

A brief summary of a few important auxiliary systems (adapted from [4]) completes the physical description of the Terry turbine. These auxiliaries include an oil system, a barometric condenser system, and a line fill system.

The oil system supplies lubricating oil to turbine and pump bearings as well as control oil to the governor valve. A small pump is attached to the turbine rotor for purposes of distributing oil. Thus, oil pressure is a function of turbine speed and there are provisions for pressure regulation (preservation of a minimum oil pressure, handling of excess oil).

The barometric condenser system consists of a barometric condenser, a vacuum pump, and a condensate pump. It prevents steam leakage from the turbine shaft seals (gland seals, trip-and-throttle valve and governor valve stems) and the exhaust casing

drain. Steam collected by the system is condensed and the condensate is sent back to the RCIC pump. There are also provisions for handling noncondensable gases.

The line fill system draws water inventory from the CST and fills the RCIC pump discharge line so as to both minimize injection time and to prevent potentially destructive water hammer phenomena.

2.4 RCIC Operational Considerations

2.4.1 Normal Operation

In the context of normal, expected operations, the RCIC system behaves as [4]:

- An initiation signal is sent either automatically (sufficiently low RPV water level) or manually (pushbutton activation in control room)
- Several valves and some turbine auxiliaries actuate:
 - Outboard steam isolation valve opens
 - Steam supply shutoff valve opens
 - Minimum flow valve (pump discharge line) opens, closes if flow increases
 - Inboard pump discharge valve (leading to RPV) opens
 - Test line valve closes if it was open
 - Outboard pump discharge valve receives a signal to open
 - CST suction valve (usually open) receives a signal to open
 - Barometric condenser auxiliary system starts
- Turbine speeds up, bringing turbine oil system pressure up

- RCIC flow controller modulates the governor valve position using a comparison of measured flow with desired flow
- Pump flow and discharge pressure hold once target is reached
- RCIC system operates until an isolation signal, trip signal, high RPV level signal, or manual shutdown signal is sent

Normal and expected RCIC system operations include situations wherein [2]:

- The RPV is isolated and in a hot standby condition
- The fission chain reaction is terminated but primary pressure is too high for shutdown cooling system intervention
- The plant experiences a complete loss of AC power

Note that in each of these scenarios, RCIC system capacity is more than enough to compensate for inventory losses due to boil-off from decay heat generation. Note also that the RCIC system does not regulate primary system pressure. Thus, any steam boiled off in the RPV by residual heat vents to the suppression pool via safety relief valves (SRVs). Therefore, the suppression pool ultimately receives decay heat and would heat up (approach saturation) if not for the AC-powered Residual Heat Removal (RHR) system.

2.4.2 RCIC System Isolation and Trips

The RCIC system flow loop is outside of primary containment (Figure 2.1 and Figure 2.2) and the RCIC steam supply line is the sole connection to the radioactive Nuclear Steam Supply (NSS) system. As such, provisions for RCIC isolation must exist in order to minimize the potential for containment bypass and radioactive release. In particular, leak detection (explicitly marked in Figure 2.2) is an imperative. Several

indicators possibly indicate a RCIC steam supply line leak and can trigger RCIC system isolation [4]:

- Low RCIC steam supply line pressure
- High RCIC steam supply line differential pressure
- High RCIC steam line space temperature

Additionally, a high pressure between turbine exhaust rupture diaphragms can trigger isolation as could a manually-transmitted signal [4]. Once an isolation signal is received, the inboard and outboard steam supply isolation valves (and their corresponding warm-up valves) are closed off. Because steam supply is cut off, the turbine trips coincident with isolation.

RCIC turbine trips follow isolation signals but can also occur independent of them as there are other scenarios wherein a running RCIC system must be shut down. In some instances, the system is brought off-line with the steam supply valve - not the trip-and-throttle valve - such that system reactivation can occur automatically without a trip reset.

For example, a high RPV water level signal would close the turbine steam supply valve but not the trip-and-throttle valve such that the RCIC system may be automatically restarted upon receipt of a low RPV water level signal. The trip-and-throttle valve does not close and there is no need to reset it.

In other instances, shut down occurs via the trip-and-throttle valve such that a trip reset is required before RCIC system reactivation. Such shutdowns occur by trip because there is often a need to protect the integrity of the RCIC system. Scenarios include [4]:

- Turbine over-speed, trip-and-throttle valve closure, either electrical (with AC/DC) at 110% max speed or mechanical (No DC) at 125% max speed
- Low pump suction pressure
- High turbine exhaust pressure (back pressure)
- Receipt of any RCIC system isolation signal
- Receipt of any manual trip signal

Note that in the above scenarios, some sort of extra action is required to bring the RCIC system back on-line. If an electrical trip-and-throttle valve closure occurs (electrical over-speed trip, low pump suction pressure, high turbine exhaust pressure), operators have to re-latch the trip by closing and re-opening the motor that operates the trip-and-throttle valve [4]. If a mechanical over-speed trip occurs, a manual reset from the RCIC room is required [4]. If any isolation signal trips the turbine, isolation logic (i.e. the capability to again send an isolation signal if necessary) must be manually reset [4].

2.4.3 Off-Normal Operation

With particular attention to LTSBO conditions, some aspects of RCIC system operation merit further discussion. In the absence of off-site or on-site AC power and upon depletion of on-site DC power and assuming no steam supply line valves close, the turbine governor valve fully opens (loss of electro-hydraulic speed regulation) and the turbine runs in an uncontrolled manner. There can be no RCIC system isolation or stoppage signals received (e.g. for high RPV water level) and there can be no electronic turbine trips (e.g. on 110% over-speed).

The mechanical turbine trip (125% over-speed) is presumably still in play as it requires no AC or DC power. Without the capability to close the steam supply line valve on high RPV water level and assuming no manual modulation of the trip-and-throttle valve from the RCIC room, the turbine will continue to run the pump as it draws inventory from the CST (at first) or the suppression pool (if switch-over was successful). The turbine speed is governed chiefly by incoming flow conditions (temperature, void fraction) of both the turbine and the pump. Two-phase flow into the turbine (due to water carry-over into the steam lines) could degrade turbine performance (speed) which would in turn degrade pump capacity and could decrease the RPV water inventory as decay heat boil-off catches up with RCIC system delivery. Two-phase flow or even a nearly-saturated water flow into the pump (due to long-term suppression pool heat-up) could degrade pump performance (inadequate NPSH) and lube oil cooling. Pump cavitation could also lead to a turbine over-speed if less hydraulic resistance from the pump impeller factors into the coupling shaft torque balance. Investigators [9] have posited a self-regulating mode of RCIC turbo-pump operation in the absence of AC and DC power and with a fully open governor valve:

- RCIC overfills RPV, causing two-phase flow ingestion and water carry-over into the steam supply line, turbine “rides out” conditions and continues running
- RCIC turbine performance degrades accordingly, allowing RPV level to deplete and for single-phase steam to enter the supply line
- Cyclic operation as above

If the RCIC system operates in this cyclic, self-regulating mode, residual heat is ultimately still conveyed to the suppression pool as the turbine exhaust line and SRVs

(assuming no malfunction) continue to dump steam into the wetwell. In the long term, the suppression pool may approach saturation conditions (without RHR operation) and the RCIC pump could suffer from inadequate NPSH and cavitation. The RCIC turbine – without AC and DC power – could only be shut down by mechanical trip on over-speed or perhaps by operator intervention from the RCIC room (e.g. trip-and-throttle valve closure).

Gauntt [9] and Mizokami [10] postulate the aforementioned scenario as a possible explanation for RCIC system operation without AC/DC power for nearly 70 hr in Fukushima unit 2. RCIC system stoppage – according to this hypothesis – occurred by turbine mechanical over-speed trip coincident with inadequate NPSH on the pump side due to a nearly-saturated suppression pool. Experiments and computational models – for purposes of experimental design and predictive computations – could confirm or refute this hypothesis.

3 COMPUTATIONAL FLUID DYNAMICS CODE OVERVIEW

3.1 STAR-CCM+ Introduction

STAR-CCM+ is a computer code managed, maintained, and developed by CD-ADAPCO. It is capable of a wide variety of engineering physics simulations, but is used only as a CFD tool for purposes of this dissertation. The code employs an object-oriented architecture that readily lends itself to parallelization across multiple computing resources without extra effort from the user. The code itself is essentially a suite of integrated components, including [11]:

- A 3D CAD modeler with CAD imbedding
- Surface preparation tools
- Automated meshing technology
- Physics modeling (including turbulence)
- Post-processing tools and CAE integration

The 3D CAD modeler was not used extensively for the present work since the complicated geometry was imported from pre-existing Solidworks models [1]. Once the geometry was imported, surface preparation tools were used to condition for meshing. Several off-the-shelf physics models were applied as-is or were customized with user-defined functions and external tables. Physics models applied to the RCIC turbine include:

- Coupled flow and coupled energy model/solver with user-defined source terms and user-defined passive scalars
- Steady state time model/solver
- Turbulence model/solver

- User-defined equation of state model (ideal gas too)
- Mixing planes and a moving reference frame where applicable

A student license issued exclusively for research purposes was used for analyses in this dissertation. The configuration is convenient because any computer with STAR-CCM+ installed can launch one or more simulations via the CD-ADAPCO portable on-demand remote licensing server. The only requirement is an internet connection to communicate with the license server (to periodically verify connectivity). Computational speed is in no way dependent on internet connection quality.

3.2 Code Mechanics

Some general concepts in STAR-CCM+ including simulations, parts, continua, models, regions, boundaries, interfaces, solvers, and reports, monitors, plots, and scenes are described in turn below.

A simulation holds the solution state and data for some given STAR-CCM+ analysis. The simulation is accessed and manipulated via the graphic user interface after a client has connected to a server. The simulation is fully described by an object tree through which the user may manipulate the simulation (e.g. define physics models, set boundary conditions, etc.).

Parts are components of a simulation that define its attributes. There are several subsets including geometry parts, model parts, and derived parts. Geometry parts represent the geometry of the simulation and have their own branch on the object tree. 3D CAD bodies must be converted into geometry parts before those parts can be used in a

simulation. Geometry parts can be manipulated by operations (splitting, combining, etc.) that work on surfaces, curves, and contacts comprising the geometry part. Model parts are related to geometry parts and include regions, boundaries, and interfaces. Model parts represent portions of the geometry being analyzed and physics models are applied directly to model parts. Derived parts are typically used in the creation of analysis reports or flow visualization scenes (e.g. a plane derived part applied to a vector scene to show the solution velocity field on that plane). Derived parts are often inputs to other objects. A subsequent section discusses salient details of types of derived parts used in this study.

Continua are themselves STAR-CCM+ objects but are applied to one or more region objects. Continua have no associated geometry but instead consist of physics and/or meshing model objects that define a simulation as described below. A mesh continuum holds mesh model objects (e.g. surface mesher, volume meshers) that get applied to a region (which has geometry parts assigned to it, see description of regions below). A physics continuum holds physics model objects (solvers, time and motion models, etc.) that get applied to a region.

There are generally two types of models: mesh models (surface mesher, polyhedral mesher, prism layer mesher, etc.) and physics models (flow, time, motion). Mesh models control the creation of a computational domain (or rather the faces, cells, and vertices that comprise a computational domain) within a given region. Mesh models are not associated directly with any geometry parts but instead are indirectly linked with geometry parts through common affiliation with a region. Physics models characterize the problem that will ultimately be solved on a given computational domain. Physics models are also

indirectly associated with geometry through a region. The mesh and physics models applied to a given region are not always independent of one another, e.g. certain kinds of turbulence physics models may require a sufficiently well-resolved near-wall mesh generated with the prism layer mesh model. Also, the geometry part assigned to a region might dictate certain features of the mesh model applied to that region, e.g. a finer volume mesh might be desired near certain geometric features (a sharp corner or the throat of a converging flow channel).

Regions are volume domains (for 3D simulations) or area domains (for 2D simulations) in space that are entirely enclosed by boundaries. Regions are discretized according to their assigned mesh models. Regions also have geometry parts assigned to them and thus they link the mesh models with problem geometry (the notion of boundaries also come from geometry part definition). Separate regions (with different mesh and physics models in general) can be joined with interfaces so that solution information may pass from region to region.

Boundaries are surfaces (for 3D simulations) or lines (for 2D simulations) that – alone or in combination with other boundaries - entirely surround a region. Regions do not share boundaries and so a given boundary belongs to only one region. Boundaries can come from the surfaces defined in a geometry part upon assignment of that part to a region. Boundaries can also come from interfaces created between geometry parts or from other manipulations like splitting. Boundaries have associated properties that determine behavior (e.g. wall, stagnation inlet, pressure outlet, etc.)

Interfaces serve as connections between boundaries during the meshing and solution processes. Recall that each region has its own unique boundaries but that regions must be allowed to communicate. An interface facilitates that communication via its definition between two boundaries of two regions. When meshing, interfaces are necessary to generate a conformal mesh where two regions meet. When performing a solution on a volume mesh (computational domain), interfaces permit the flow of information (i.e. flow of mass, energy, other continuum properties) between regions. Interfaces have associated types that determine what is done with/to the information moving across it.

Solvers are activated once per solution iteration and control the progress of a solution. They are related to but distinct from physics models. Physics models often dictate the type of solver employed for a given simulation (e.g. the coupled flow model invokes the coupled solver) and some physics models have their own dedicated solvers. Solvers manage the algebraic multigrid procedure and control everything associated with the process of obtaining a converged solution.

Reports, monitors, plots, and scenes are all methods of conveying the progress and results of a simulation. Reports are often used to convey certain metrics from the solution data, e.g. a volume-averaged pressure or an area-averaged mass flow rate. Monitors are used to sample certain quantities (and perhaps plot them) as the solution progresses. Physical quantities (e.g. pressure) can be monitored but the most common use of monitors involves solver residuals. Reports can be used to create monitors. Plots show line graphs of solution data and monitors can be used to create plots. Scenes are used to visualize

simulation properties like geometry, the mesh, or solution data. There are a few types of scenes including geometry, mesh, scalar, and vector. Geometry scenes are used to show geometry parts while mesh scenes will show surface or volume meshes from mesh models associated with regions. Scalar and vector scenes are used to display scalar or vector solution data. A pressure distribution might be shown in a solution scene, while a velocity field might be shown in a vector scene.

3.3 General Workflow

A comprehensive though simplified STAR-CCM+ simulation work-flow is [11]:

1. Plan the regions layout
2. Prepare geometry (working with geometry-level objects)
3. Construct the regions layout (working with region-level objects)
4. Generate mesh after defining mesh continua (working with mesh objects)
5. Define physics, configure physics continua
6. Prepare for analysis (define boundary conditions)
7. Run the simulation(s) (tweak solver settings, boundary conditions as needed)
8. Analyze results

In step 1, the number of regions and their connectivity is determined. Several different factors may influence modeling decisions at this point including the physics of the problem, the number of materials, the type of boundary conditions on the problem, and any special region-wise interfacial requirements (mixing planes, etc.)

In step 2, 3D CAD is drawn up and translated into geometry parts. Alternatively, files from external CAD programs (e.g. Solidworks) can be read in as geometry parts. Then, surface repairs and part transformations/augmentations may be made as necessary. Generally the modeler should configure geometry parts and underlying surfaces in such a way that boundary condition assignment is straightforward upon assigning parts to regions. Also, part contacts can be either automatically or manually defined.

In step 3, a “map” between the geometrical definition of a problem and the computational or physical definition of the problem is created [11]. Region interfaces may be manufactured out of part contacts (which were defined in step 2) and region boundary conditions may be defined using part surfaces (likewise defined in step 2). Mesh models can run (step 4) only after valid regions with boundaries/interfaces are present, but physics models can be assigned to regions separate and apart from mesh models at this point.

Steps 4 through 8 above are often iterative in nature and one rarely proceeds directly from 4 to 8. In fact, each step could be an iterative process unto itself within the outer iterative loop over steps 4 to 8. For example, a solution might be poorly converged on a certain mesh, necessitating a return to 4 from 8. In the process of discovering that the solution needs a better mesh, step 7 might be performed over and over with different solver settings to assist the solution procedure on its way.

3.4 Selected Code Features and Concepts

A brief discussion of certain code features and concepts is useful at this point given their significance to the present analyses. These include the surface preparation tool, the

surface mesher, the polyhedral mesher, the prism layer mesher, the coupled flow/energy model and solver, the passive scalar model and solver, the user-defined equation-of-state model, the user-defined scalar/vector field function utility, mixing planes, and moving reference frames. Any mathematical details or in-depth technical discussions of phenomenological models are deferred to later sections.

3.4.1 Surface Preparation and Meshing

The surface preparation tool works on tessellated geometry parts to prepare their surfaces for meshing upon assignment to a region. Note that a tessellated surface is a surface discretized by small triangles so as to capture all features of its geometry. If imported, tessellated surfaces may have defects like improperly intersecting (i.e. pierced) faces, free edges, or non-manifold edges. These must be repaired before attempting to mesh the surface so as to avoid mesh generation errors. Launching the surface repair tool brings up a repair scene (for visualization) and a graphic user interface from which certain actions can be taken to remedy any defects. The surface repair tool is also useful for other applications like imprinting parts, performing Boolean operations on parts, and redefining surfaces/curves. A general surface repair workflow is as follows [11]:

1. Launch the repair tool with one or more input surfaces
2. Perform repairs, run leak detection, or do merging, imprinting, and any surface Boolean operations
3. Run diagnostics, highlight problem areas, and graphically display them
4. Repair any remaining surface/feature errors

Surface preparation and repair was required for the present analyses. After importing three-dimensional RCIC turbine geometry into STAR-CCM+, several surfaces comprising different turbine parts were split out from the single initial surface. A few mating surfaces had pierced face errors and/or free-edge errors that required repair. Interfaces were needed between certain surface pairs to ensure a conformal volume mesh, a conformal periodic boundary condition, and mixing planes. With the surface preparation tool, part contacts for said interfaces were defined manually.

The surface mesher is a surface mesh model used to generate high-quality triangulated surfaces from either a geometry parts tessellation or the surface wrapper. A valid surface mesh is a prerequisite for volume meshing. The surface mesher is usually applied to a closed (i.e. water-tight) geometry and as such is usually executed only after:

- The surface wrapper is used to close all holes in the geometry, or
- The surface preparation tool has been used to zip edges, fill holes, etc.

The user has control over target size for triangles created by the surface mesher, and the target value can apply globally or locally according to a volumetric control. Figure 3.1 below illustrates the difference between a geometry tessellation (e.g. for an imported part) and a triangulation from the surface mesher. A part of the RCIC turbine is shown, including a steam nozzle assembly, a set of reversing chambers, and a section of the rotor and its buckets. The triangles are much coarser in the geometry tessellation, but note all details of the geometry (curves, corners, etc.) are well resolved. The surface mesher triangulation shows darker clusters of triangles in places, a result of applying volumetric

controls. The surface mesher triangulation gives a high-quality surface representation from which the volume mesh models may manufacture a fluid domain mesh.

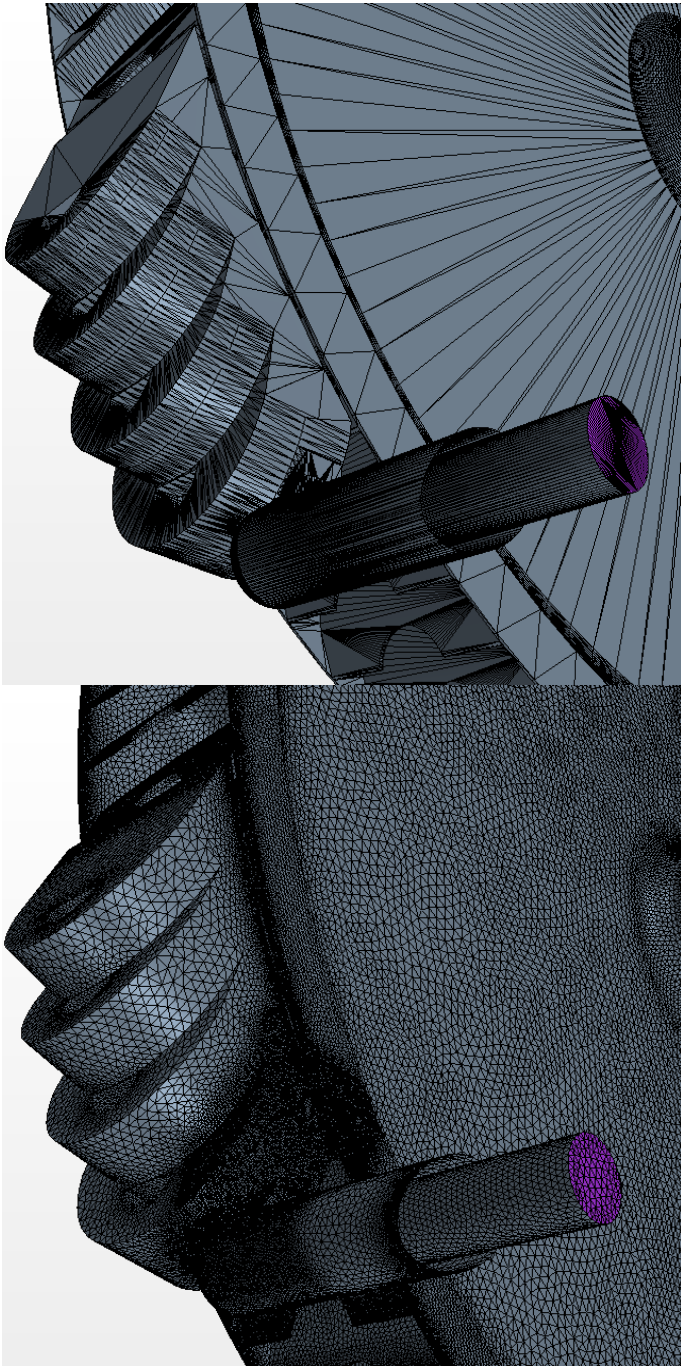


Figure 3.1 Geometry part tessellation (top) and surface triangulation (bottom)

The polyhedral mesher and the prism layer mesher are both volume mesh models typically applied to fluid domains. The polyhedral mesher forms a core mesh comprised of arbitrary polyhedral cells. The prism layer mesher works in tandem with a core mesher (e.g. tetrahedral or polyhedral) to form near-wall parallel layers of rectangular-shaped cells. The user has control over polyhedral mesh cell density (global parameters or local refinement by volumetric control) and may specify several parameters for the prism layer including total layer thickness, the number of constituent cells across the total layer, and the cell size distribution. The polyhedral mesher is a good choice for most meshing problems. The prism layer mesher has more specific applications, namely the resolution of near-wall (i.e. boundary layer) flows for purposes of turbulence modeling, conjugate heat transfer modeling, and reduction of numerical diffusion (increased accuracy) near the wall [11]. For analyses in this dissertation, the prism layer mesher is used for turbulence modeling and for more accurate computation of fluid/surface interactions.

3.4.2 Coupled Flow and Coupled Energy Models and Solvers

The coupled flow model is the best option available in STAR-CCM+ for compressible, trans/super-sonic flows in which aerodynamic shocks are expected [11]. The coupled flow and energy approach is appropriate for the RCIC turbine because both aerodynamic and condensation shocks in compressible steam are possible. The shock-capturing capability of the coupled method - owing to its density-based solution approach - is beneficial for present analyses of compressible flow. Also, one aspect of the pseudo two-fluid model (described more fully in a later section) is the incorporation of algebraically large mass, momentum, and energy sources. According to [11], the coupled

flow model is preferable to the segregated flow model when large energy sources are present in the simulation. The segregated flow model will not be described any further.

The coupled flow and coupled energy models collectively solve mass, momentum, and energy equations simultaneously rather than sequentially as might occur in a Semi-Implicit Method for Pressure-Linked Equations (SIMPLE) solution approach. Pseudo-time-marching is used for transient problems in tandem with either the explicit or implicit time model. For steady-state analyses, the unsteady forms of conservation equations are “driven” towards steadiness with the same pseudo-time marching scheme. The coupled flow model is compatible with several methods for finite volume face convective and diffusive flux computation, e.g. the second-order upwind method. Coupled flow also makes use of pre-conditioning for efficient solution of both compressible and incompressible flows at all speeds [12]. Additionally, inviscid flux discretization by Roe’s scheme or Liou’s AUSM+ scheme is employed.

The coupled solver manages the solution procedure for the coupled flow/energy models. The solver uses implicit spatial integration (or, alternatively, an explicit Runge-Kutta option) and algebraic multi-grid (AMG) methods to numerically solve discretized, finite-volume equations. There are several miscellaneous options available in the solver that may or may not be appropriate for a given application. Certain options pertain to solution initialization, e.g. expert initialization for grid sequencing. Other options are designed to assist the solution while running, e.g. convergence accelerators, and the expert solution driver.

3.4.3 Passive Scalar Model and Solver

The passive scalar model allows the user to simulate the convective/diffusive transport of some arbitrarily-valued scalar variable. With careful definition of source terms, passive scalars can be manipulated to model several phenomena. For the pseudo two-fluid condensing steam flow model of these analyses, passive scalars are used for a dispersed water droplet phase that evolves from and interacts with single-phase steam. Passive scalar transport generally consists of convection and diffusion (molecular and turbulent). The user can disable one or the other as appropriate.

3.4.4 User-defined Equation of State Model

The user-defined equation of state model allows the user to specify how the working fluid density depends on temperature and pressure. It also determines how other quantities are evaluated such as density derivatives, enthalpy, speed of sound (for compressible fluids), and certain transport properties like thermal conductivity, dynamic viscosity, and specific heat. While there are several built-in options available in STAR-CCM+, for certain fluids or certain states of a fluid (e.g. super-saturated state of steam), no data is available in the STAR-CCM+ database. In such situations, the user has the latitude to define (usually by tabular input) all equation of state data. For RCIC turbine modeling, steam is expected to exist in super-heated, saturated, and super-saturated states at various points in the simulation. Since STAR-CCM+ built-in steam/water data does not cover all the aforementioned thermodynamic states, user-defined data from International Association for the Properties of Water and Steam (IAPWS) Industrial Formulation-1997 (IF97) was used [13].

3.4.5 User-defined Sources via Field Function Utility

The user-defined scalar/vector field function utility is a means by which conservation equation source terms can be specified. A litany of field function arguments from the simulation are available for use. Field functions are updated on-the-fly as the solution progresses. Once defined a scalar/vector field function can be plotted, visualized in a scene, or used in the simulation directly (e.g. through source term definition).

3.4.6 Mixing Planes and Moving Reference Frames

Mixing plane interfaces and moving reference frames play an important role in RCIC system turbine simulations of this dissertation. Both are used together in order to get time-averaged, steady-state solutions for turbo-machinery flows involving rigid-body rotational/translational motion which are inherently unsteady.

Mixing planes are implemented as interfaces across which circumferentially-averaged flow field data is transferred in a conservative manner between two rotationally periodic regions that share the same axis [11]. The averaging of quantities (mass, momentum, energy, etc.) across a mixing plane occurs according to “bins” or uniformly-thick patches of area spanning the entire length and breadth of the boundary associated with the mixing plane interface. The transfer of information is such that identical, average quantities are used for each and every cell within a given bin. There are explicit and implicit options, the difference being the update strategy for circumferential averages. The user has limited control over mixing plane bin characteristics. At the geometry parts level, surface contacts can be designed so as to tailor a mixing plane interface to a limited area. Also, the so-called “bin coarsening factor” grants some control over the circumferential

bin thickness. Figure 3.2 shows a mixing plane with two circumferential bins between two regions (a stator at left, a rotor at right). As the right-most region rotates or is subjected to a moving reference frame, the upstream flow quantities from the stator region are “mixed out” or averaged across mixing plane bins so that a time-averaged flow across the mixing plane is used.

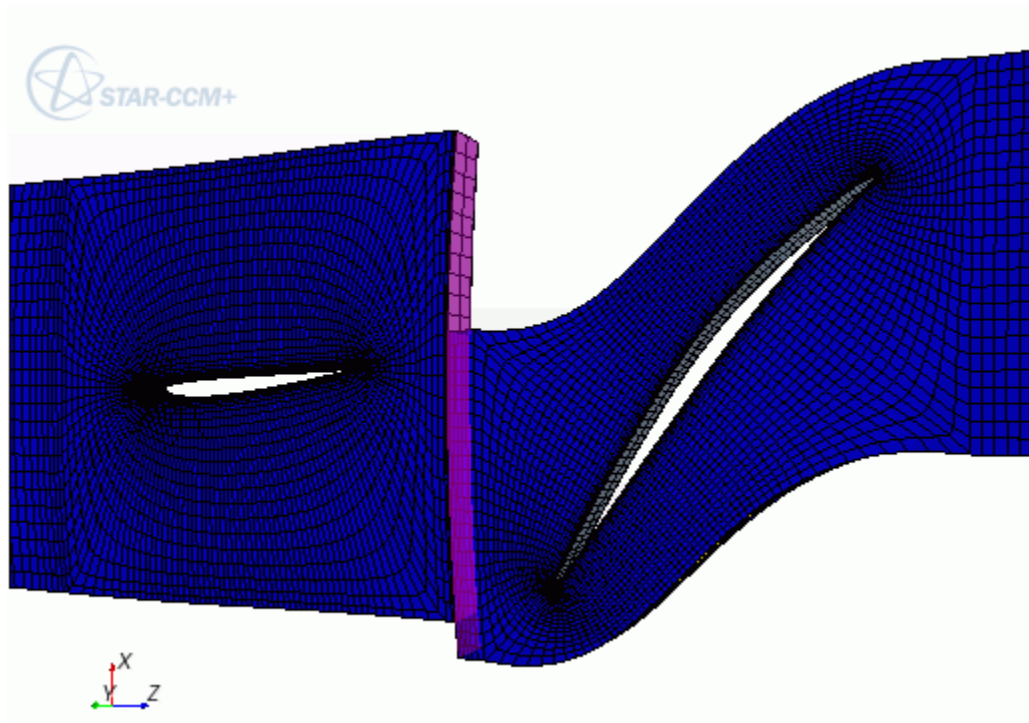


Figure 3.2 Mixing plane illustration (shown in purple) [11]

With a moving reference frame, some effects of rotational and/or translational motion on a flow field can be captured without the heavy computational burden of a moving mesh. Similar to the mixing plane interface formulation, moving reference frames are appropriate in the context of steady-state analyses and can help provide a time-averaged depiction of turbo-machinery flows that are inherently unsteady. Applying a

moving reference frame to a region, e.g. the right-most region of Figure 3.2, generates grid fluxes (new terms) in the conservation equations that approximate the effects that would be seen with true grid vertex motion [11]. Figure 3.3 illustrates (in a two-dimensional view) the use of a mixing plane, periodic interfaces, and a moving reference frame in the context of a turbo-machine which has a stator region (at left) and a rotor region (at right) containing the imposed moving reference frame.

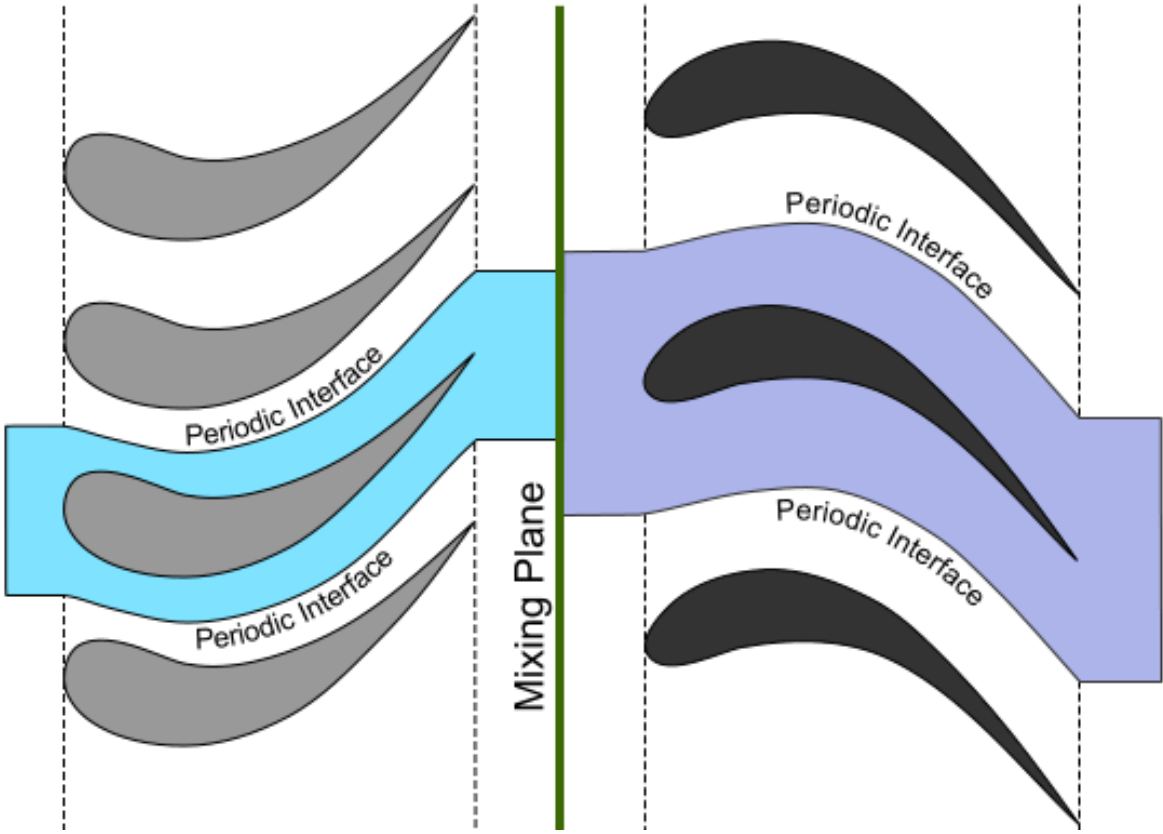


Figure 3.3 Mixing plane, periodic interfaces, and moving reference frames [11]

3.4.7 Derived Parts and Mesh Refinement via Volumetric Controls

Derived parts are one mechanism by which solution data may be accessed and/or manipulated (through certain operations like surface or volume averaging) in a STAR-CCM+ simulation. Essentially, the user has the capability to extract data for any part of the solution space without limit to defined regions, boundaries, cells, etc. [11]. Derived parts can generally be described as user-defined parts based on other so-called “parent” parts (usually these are geometry parts). There are several types, but extensive use is made here of “implicit section” derived parts and, more specifically, planes and constrained planes. Implicit section parts are functions of coordinates and are useful for generating reports that tally solution quantities (e.g. mass flow rates and velocities) across certain user-defined surfaces of interest. For example, a user could insert a plane that spans the height and depth of a steam nozzle or that covers the exit area of a rotor bucket.

When properly coupled with a report, such use of derived parts can yield surface (plane) averaged solution quantities. For example, when a surface-average report is created using a plane derived part and the mass flow rate scalar field function, one can ascertain an average mass flow rate corresponding to the derived part. As explained in the results section, just such a calculation is done at the CFD level to ascertain factors entering into the systems-level Terry turbine velocity stage model.

Mesh refinement is sometimes necessary to better resolve the physics of certain regions of interest in a simulation. Two examples most important to this study are near-wall regions (where prism layers are constructed for turbulence modeling) and the nucleation/condensation zone of a steam nozzle. Volumetric controls apply to the mesh models utilized in a given simulation. With respect to this study, the polyhedral and prism layer mesh models are in play.

For the polyhedral mesh model, a control on target cell size can be set for a geometry part (a user-defined cylinder, sphere, box, cone, etc.) overlaid onto the problem geometry. Within the geometry part, the mesh is altered according to control target cell size. In areas where sharp gradients in solution quantities are expected, the mesh may be refined for better resolution and presumably higher fidelity. An example that applies to steam nozzle analyses would be the diverging section downstream of the throat where nucleation and condensation is expected to occur over a short distance. Nucleation rate can change by an order of 10^{20} or more, so a large number of small cells in the vicinity of the nucleation front would help with resolution.

For the prism layer mesh model, controls are available for the number of layers, their spacing, and their overall thickness. Across a steam nozzle along the direction of main flow, velocities can change by two or three orders of magnitude such that the nearest-wall prism layer thickness must decrease in order to keep y^+ within range for whatever turbulence model is in use. This requirement could be met by increasing the number of prism layers along the nozzle flow direction or possibly by altering size distribution and/or total thickness.

4 SYSTEMS-LEVEL CODE OVERVIEW (MELCOR)

4.1 MELCOR Introduction

Created by SNL for the Nuclear Regulatory Commission (NRC), MELCOR was originally conceived as a flexible, fast-running probabilistic risk assessment tool that has since evolved in to a best-estimate, systems-level severe accident analysis code primarily for light water reactors. MELCOR development began in 1982 - a few years after the events at TMI unit 2 - and has continued to the present day. MELCOR is capable of tracking severe accident progression up to source term generation. It can be employed in alternate capacities to study various thermal hydraulic, heat transfer, and aerosol transport phenomena. This is due in large part to the lumped parameter control volume/flow path modeling approach that is quite general and adaptable. MELCOR is under active development and maintenance by the reactor modeling and analysis division at SNL.

4.2 Code Mechanics

MELCOR is comprised of a suite of packages that each fit in to one of three categories: basic physical phenomena, reactor-specific phenomena, or support functions [14]. Program execution involves two steps, MELGEN and MELCOR, as shown in Figure 4.1. All code packages used for a given problem communicate with one another as directed by an overseeing executive package. User input is processed by MELGEN, checked against code requirements, initialized, and used to write a restart file before running MELCOR. Calculation advancement through a specified problem time is performed by MELCOR. Text output and plot data are written to certain output files with a user-

prescribed frequency. Certain code packages important to systems-level BWR and RCIC system modeling are described below.

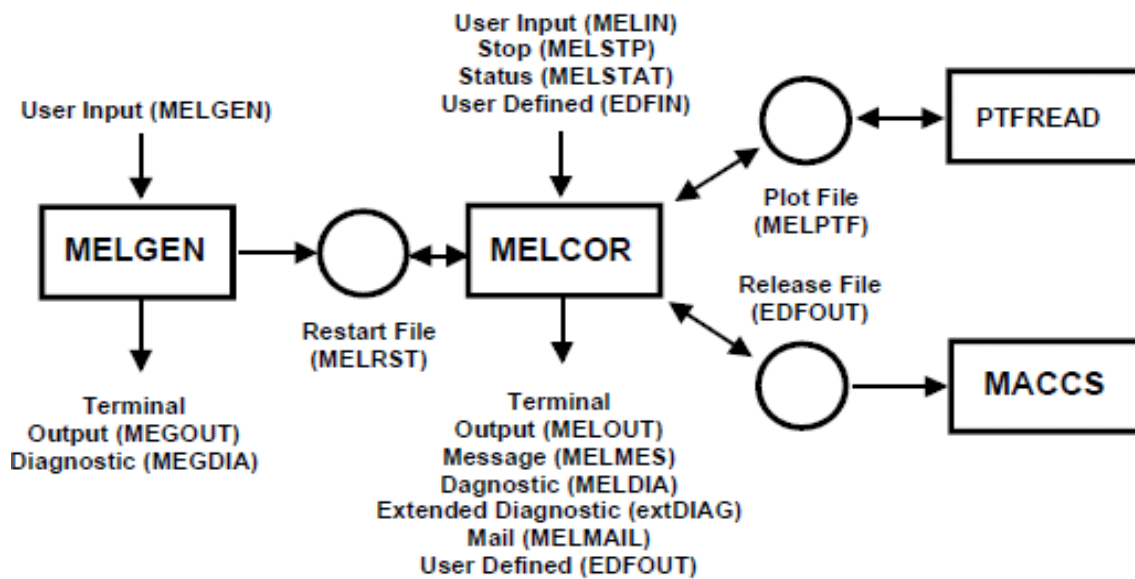


Figure 4.1 MELCOR execution flow diagram [15]

The executive (EXEC) package is a support functions module responsible for overall execution control when running MELGEN or MELCOR. It essentially coordinates processing tasks for all other packages. It performs file handling functions, input and output processing, sensitivity coefficient modifications, time-step selection, problem time advancement, and calculation termination [15].

The Control Volume Hydrodynamics (CVH) package is a basic physical phenomena module. It models, in part, the thermal-hydraulic behavior of all hydrodynamic materials that are assigned to control volumes in a calculation. Control volume altitudes (relative to some chosen reference) as well as material volumes are

specified by CVH input. The initial thermodynamic states of all control volumes are defined by CVH input as are any energy or material sources/sinks. As part of this dissertation, the CVH package was modified to include a Terry turbine velocity stage model that is capable of interfacing with a Terry turbine pressure stage model (via the new “steam nozzle” type flow path). This development with the CVH package directly benefits current and future RCIC system (or TDAFW system) modeling. Much more technical detail on this new development is included in a subsequent section.

The Flow Path (FL) package is a basic physical phenomena module that works in tandem with the CVH package to predict thermal-hydraulic response. The FL input defines all characteristics of the control volume connections through which hydrodynamic material can relocate. However, no material can physically reside within a flow path in any given time-step. Instead, the FL package is concerned with momentum and heat transport of single or two phase material as it moves from one control volume to another. Friction losses (e.g. to pipe walls), form losses, flow blockages, valves, and momentum sources (e.g. pumps) are defined through the FL package. As part of this dissertation, the FL package was modified (new user input and new physics models in MELCOR source code) to include a homologous pump model so that a more mechanistic treatment of centrifugal pumps is available. Also, the FL package was modified to include a Terry turbine pressure stage (steam nozzle expansion) model that co-opts some features of the “time-independent” flow path. A turbo-shaft model capable of interfacing with homologous pumps and the new Terry turbine models was also integrated into the FL

package as part of this dissertation. Obviously, these developments benefit RCIC system modeling directly, and further technical details are included in subsequent sections.

The Heat Structure (HS) package is another basic physical phenomena module that calculates one-dimensional heat conduction within any so-called heat structures. The structures are intact, solid, and comprised of some material with some definite geometry. The HS package also models energy transfer at a heat structure surface. This might include convection heat transfer to hydrodynamic material of an adjacent control volume or radiation heat transfer to separate heat structures.

The core (COR) package is a reactor-specific phenomena module because the physics models employed generally depend on reactor type. It predicts the thermal response of the core and lower plenum. It frequently communicates with CVH, FL, and HS packages as fission power ultimately goes to hydrodynamic material or heat structures.

The Material Properties (MP) package is a support functions module that acts as a repository for material properties data. Apart from the NCG package that treats noncondensable gases, the MP package is the sole reference for all thermo-physical data of materials. There are built-in properties for certain materials (most of which are common to LWR's), but the user may optionally overwrite those defaults or create new materials entirely. Density, thermal conductivity, specific heat capacity, and enthalpy/melt point can be defined as functions of material temperature.

The Noncondensable Gases (NCG) package is a basic physical phenomena module in that it predicts noncondensable gas properties via the ideal gas law. Similar to the MP package, it acts in a support functions capacity because it passes requisite materials data

to other physics packages for use. In the NCG package, a gas is characterized by its molecular weight, energy of formation, and specific heat capacity at constant volume which is assumed to be an analytic function of the gas temperature [15]. There are over a dozen built-in noncondensable gases. As with the MP package, the user may overwrite any default properties or create entirely new materials.

The Decay Heat (DCH) package is a basic physical phenomena module. It can be deployed in “whole-core” mode so that the power at all times subsequent to reactor scram is computed using a version of the ANS standard decay curve.

The Control Function (CF) package is a support functions module. It can be leveraged to create real or logical functions for use by the physics packages. Real-valued control functions return a real value (i.e. floating point value), while logical control functions return one of two integer values that are interpreted as either “true” or “false”. Most mathematical and logical functions available in FORTRAN are available for use in the CF package. A real-valued control function might be used to compute the density of some user-defined material via a user-defined function of material temperature. A logical-valued control function might be used to signal the start of a reactor scram or to close a user-defined valve in some flow path. Physics packages often reference control functions for required information. Control functions can also be helpful when a user is interested in calculating or plotting some variable that MELCOR does not compute by default.

The Tabular Function (TF) package is a support functions module. Tabular functions are utilized when definition of some dependent variable (e.g. decay heat) is required as a tabular function of some independent variable (usually time or temperature).

As an example, the MP package often references tabular functions to retrieve material property values as a function of temperature. The user retains the option to define many input variables as either tabular or control functions. There are situations wherein a tabular function is more appropriate (e.g. material property data is known only at certain values of temperature), and there are cases in which a control function is more useful (e.g. material property data is approximated by an analytic function of temperature).

4.3 Modeling Concepts

Since the MELCOR development efforts undertaken for this work deal primarily with the CVH package and the FL package - and because the new RCIC system physics models must fit within pre-existing MELCOR paradigms - a more detailed overview of control volumes and flow paths is in order. The intent is to support subsequent mathematical descriptions of the new RCIC system models.

4.3.1 Control Volumes

The MELCOR CVH/FL approach to model building is abstract and flexible relative to methods of other thermal-hydraulics codes. There are no pre-defined reactor components or structures. The user has the latitude to create pipes, vessels, ducts, core coolant channels, etc. using control volumes, flow paths, and heat structures in whatever manner deemed appropriate. Control volumes contain hydrodynamic material mass and associated energy consisting of internal energy and flow work (or just enthalpy, by definition). These materials can be liquids, vapors, and noncondensable gases so that in general all control volumes contain a “pool” of liquid and an “atmosphere” of vapor or

gas. Control volume geometry specification is required, as the user must give an altitude and describe, indirectly, a control volume shape by specifying the available hydrodynamic volume between control volume elevations. Thermodynamic conditions of the pool and atmosphere are initially set by the user and may evolve with time (subject to solution of the governing equations) or not. Thermodynamic states of active control volumes are advanced by solving linearized-implicit finite difference equations for mass, momentum, and energy [15]. These equations are not reproduced here (see [16]), but note that the control volume mass and energy equations contain source terms that could be leveraged by new RCIC system models to account for the evolution of a dispersed droplet (or fog) field upon condensation or the effects of a turbine as it extracts work from a control volume atmosphere.

4.3.2 *Flow Paths*

Flow paths are code constructs that model the flow and momentum transport of hydrodynamic material between control volumes. As mentioned before, hydrodynamic material has no residence time in a flow path across any time-step. The tacit assumption is that any amount of hydrodynamic material that would occupy the physical volume of the flow path connection is negligibly small compared to hydrodynamic volume of the connected control volumes [15]. The flow path package does account for friction losses, form losses, and inter-phase momentum/heat transport that would be associated with actual flow between connected volumes. Any single flow path connects only two control volumes, but there are no restrictions on the number of flow paths attached to any given

control volume. Flow paths may be vertical or horizontal with several versions of each (e.g. atmosphere-first, pool-first, etc.)

The user must designate a “from”, or “donor”, control volume and a “to”, or “acceptor”, control volume, as well as several geometric parameters like from/to elevations, junction opening heights, flow path area, flow path length, and open fraction. Junction heights and from/to elevations have implications for any gravitational head terms appearing in the flow equations. The flow path length is related to the distance over which inter-phase momentum transport occurs. The importance is diminished in cases of single phase flow, and normally this length is assumed to be the center-to-center distance between connected control volumes. Flow paths may be fully open, partially open, or completely closed.

Regarding momentum transport, all dissipative pressure drops related to wall friction and form losses are accounted for in FL package input. The user must specify any and all form loss coefficients directly, as there are no predictive models for these values. Conversely, wall friction is handled by treating the flow path as one or more segments (in series along the flow direction), calculating an appropriate mixture Reynolds number based on a segment velocity, and deriving a Fanning friction factor that is used to compute a pressure drop in each segment [15]. All that is needed from the user are segment geometric parameters such as area, length, and hydraulic diameter.

4.3.2.1 Flow Paths and Steam Nozzle Expansion

Much like control volumes, flow paths can be “active” or “time-independent” with the distinction being that phasic velocity equations are solved to predict evolution of flow

conditions in the former. For the latter, user input instead dictates phasic velocities. For purposes of RCIC system turbine pressure stage modeling, this “time independent” flow path functionality can be co-opted to implement a new steam nozzle expansion model. Essentially, the usual phasic velocity equations can be bypassed (in source code) for specially-flagged steam nozzle flow paths. These special flow paths would be treated as time-independent up until the point where look-ups for user-specified velocities would normally be performed. At that point, new steam nozzle physics subroutines could be called to compute, among other things, the phasic velocities (for atmosphere and/or fog). The results from these phasic velocity calculations could be used in a CVH package Terry turbine velocity stage model. Details of the new turbine pressure stage (steam nozzle physics) models are deferred to a subsequent section.

4.3.2.2 Flow Paths and the Homologous Pump Formulation

The phasic velocity equations used to “solve” flow paths contain an explicit pressure head term reserved for momentum sources from influences external to the flow, e.g. a pump impeller. There are also semi-implicit terms in the phasic velocity equations that accounting for various other physics but not for pump head. Before homologous pump model development, CF-specified pumps were allowed in MELCOR but only a numerically explicit treatment of their effects was possible. As will be demonstrated in a subsequent section, the pre-existing explicit pump head term and the in-place semi-implicit terms of the general phasic velocity equation can be manipulated to create a numerically semi-implicit pump head term treatment. The homologous pump performance model can be coded in MELCOR source and interfaced to both sides (implicit and explicit)

of the phasic velocity equation pressure head term. Details of this new homologous pump model are deferred to a subsequent section.

4.4 Proposed Enhancements for RCIC System Modeling

As a quick recapitulation of the proposed enhancements to MELCOR source code for purposes of RCIC system modeling:

- Build a new centrifugal pump performance model (homologous pump model) and integrate it into the current CVH/FL solution framework with “semi-implicitness”
- Conceptualize a Terry turbine pressure stage (steam nozzle expansion) model and integrate it into the current CVH/FL framework using a strategy similar to that of “time-independent” flow paths
- Conceptualize a Terry turbine velocity stage model and integrate it into the current CVH/FL framework
- Conceptualize a turbo-shaft model capable of interfacing with the homologous pump model and the Terry turbine velocity stage model, integrate it into the current CVH/FL framework

A great deal of extra coding comes along with these models, namely the provisions for user input processing and text/plot output.

5 STAR-CCM+ MODEL DEVELOPMENT AND IMPLEMENTATION

This section focuses largely on the physical and mathematical details of the pressure stage model developed for CMFD analyses of the RCIC turbine. The full formulations used for both pressure and velocity stage analyses of the turbomachine (with steam and air) are covered in this section. In the sequence of sub-sections below, a topic will be theoretically expounded and then described in sufficient (often simplified) physical and mathematical detail for CMFD analyses.

5.1 Physics of Condensing Steam Flow

The RCIC turbine pressure stage constitutes a complex thermodynamic system featuring non-equilibrium dispersed steam/water flow. Heat and mass transfer processes take place under super-saturated and saturated conditions and in continuum and free molecular regimes. In this section, the thermodynamics of phase change (droplet formation) in a mostly pure, homogeneous medium (steam) will be reviewed as will the process of drop-wise steam condensation. Both bear relevance to the problem at hand because the CMFD model incorporates conservation equation source terms to account for them. Compressible flow, turbulence in dispersed two-phase flow, and equation-of-state treatments for steam/water thermodynamic systems will be discussed also.

Thermodynamic aspects of steam-to-water phase change are covered in some detail here because a basic comprehension promotes understanding of the CMFD model and the fluid dynamics of a real-world RCIC turbine pressure stage. Across a steam nozzle in the RCIC turbine, incoming steam (dry superheated or high-quality saturated) is expanded such that enthalpy is converted into kinetic energy that may then be imparted to

rotor buckets and converted into a torque on the pump shaft. The expansion occurs first in the converging section of the nozzle (while the flow is sub-sonic) and continues in the diverging section of the nozzle (while the flow is super-sonic). The steam pressure declines rapidly, and saturation conditions are reached somewhere at or slightly beyond the nozzle throat. From there, the assumption of thermodynamic equilibrium throughout the remainder of expansion has been shown [17] to yield under-predictions in steam mass flow at the nozzle discharge. More specifically, if non-equilibrium effects due to supersaturation are neglected, there is typically a 2-4% under-estimation in the steam mass inventory at nozzle discharge. The discrepancy is due to non-equilibrium effects, namely steam super-saturation and an attending delay in the onset of phase change (droplet formation and subsequent drop-wise condensation). The RCIC turbine relies primarily upon an impulse from impinging steam to turn the rotor, so an accurate prediction of steam discharge from the nozzles is crucial for accurate modeling. Thus, the CMFD model must account for non-equilibrium effects to some extent.

5.1.1 Homogeneous Nucleation

To understand the nature of the problem at hand, one must first distinguish between two mechanisms of water droplet formation from steam: homogeneous nucleation and heterogeneous nucleation. The term “nucleation” refers to the first formation of thermodynamically stable droplet embryos in the midst of saturated or super-saturated vapor. Nucleation occurs in a condensing vapor as a result of the tendency to minimize free energy in a thermodynamic system. Heterogeneous nucleation is of secondary importance here but refers to a situation in which some “nucleation site” in or adjacent to

the condensing vapor – e.g. impurities, ions, or a rough wettable surface – aids the process of phase change. Nucleation sites effectively lower the Gibbs free energy barrier to nucleation (an explanation of which is given in the context of homogeneous nucleation below). Homogeneous nucleation is of primary interest here and refers to a situation in which a pure condensing vapor manufactures its own embryonic droplets without any assistance from nucleation sites in overcoming the Gibbs free energy barrier to nucleation. The following paragraphs include a detailed description of homogeneous nucleation as a thermodynamic, kinetic, and inherently probabilistic phenomenon. The excellent exposition put forth by McDonald ([18], [19]) serves well as a guide for discussion.

Considering pure, condensing steam (water vapor at the saturation pressure for its current temperature) and accepting without further evidence that the steam is inclined to minimize its free energy, the only way this minimization occurs is by phase change, i.e. the formation of small, embryonic droplets of water and subsequent growth by drop-wise condensation. When this happens, the bulk free energy of the steam decreases in an amount proportional to the mass (or volume) of the droplet formed. Therefore, the bulk free energy of the vapor decreases by an amount proportional to the cube of the drop embryo radius. The process actually unfolds in three parts:

1. isothermal decrease of vapor pressure to the saturation pressure,
2. conversion of vapor at saturation to liquid at saturation, and
3. isothermal increase of pressure to higher internal pressure of curved droplet

The first step is the most energetically consequential and the other two may be ignored for present purposes. Condensation would seem to move the system to a lower

level of free energy except that along with droplet formation comes an increase in droplet surface area and an attending increase in system free energy. Thus, the system free energy increases as the square of the radius of the droplet formed. An equation for the change in free energy ΔF accompanying drop formation then looks like:

$$(5.1) \quad \Delta F = 4\pi r^2 \sigma - \left(\frac{4}{3}\right) \pi r^3 \rho_{liq}(T_{stm}) R T_{stm} \ln(S)$$

Where:

r = radius of just-formed droplet [m] ; T_{stm} = steam temperature [K]

R = gas constant of steam [J/mol/K] ; $\rho_{liq}(T_{stm})$ = liquid density at T_{stm} [kg/m³]

$S = P/P_{sat}$ = super-saturation ratio ; σ = Surface tension [N/cm]

There are dueling terms in the free energy equation. For small but positive r , the first term will mathematically dominate the second and keep the net free energy change of vapor condensation above zero, rendering the process of drop-wise condensation thermodynamically unfavorable. Condensation cannot move the system to a stable state of lower free energy and drop-wise condensation is no longer a spontaneous process. Phase change is delayed and the steam stays dry in a metastable state called “super-saturated” or “super-cooled”. The term “super-saturated” indicates a vapor pressure greater than the saturation pressure for the current vapor temperature, i.e. the super-saturation ratio exceeds unity. The term “super-cooled” indicates a vapor temperature lower than the saturation temperature for the current vapor pressure. Note from equation

(5.1 that the bulk free energy term – which becomes larger in magnitude with increasing super-saturation ratio – ensures that $\Delta F(r)$ has a maximum, i.e. an activation energy barrier, at some critical drop radius. Also, note that this critical drop radius decreases as super-saturation increases (since, approximately, the droplet forms isobarically and isothermally). The free energy barrier must be surmounted somehow for vapor condensation to become a spontaneous process and for the system to move towards thermodynamic equilibrium. Until the barrier is overcome, the steam stays in the metastable super-saturated state. Very small liquid embryos can still evolve from steam, but they cannot grow to critical size by steam condensation.

By differentiating equation (5.1 with respect to r (holding other variables constant) and setting the result equal to zero, the critical droplet radius r^* may be found as:

$$(5.2) \quad r^* = 2\sigma(T_{stm}) / \rho_{liq}(T_{stm})RT_{stm} \ln(S)$$

The maximum height of the energy barrier, ΔF^* , corresponding to the critical droplet radius:

$$(5.3) \quad \Delta F^* = 16\pi\sigma(T_{stm})^3 / 3(\rho_{liq}(T_{stm})RT_{stm} \ln(S))^2$$

Note that equation (5.3 is simply Kelvin's equation describing the change in vapor pressure due to a curved liquid/vapor interface. The curvature of a critical embryo is such

that it would raise the vapor pressure to the super-saturated pressure P from the saturation pressure P_{sat} . Equivalently, a droplet must reach the critical size in order to exist in metastable equilibrium with its super-saturated condensing vapor (which is itself a metastable state). A broad definition of metastability is given by Guggenheim [18] as:

“Any state which is stable with respect to all states differing only infinitesimally from the given state, but unstable with respect to some other state differing finitely from the given state”

The super-saturated condensing vapor satisfies Guggenheim’s definition as does the critical droplet. If conditions change by some finite amount in either case, the super-saturated vapor can undergo reversion to thermodynamic equilibrium and the critically-sized droplet could either evaporate (if radius falls just below critical) or spontaneously grow (if radius climbs just above critical).

The question remains: how can critical droplets form and grow if embryonic droplet growth is disallowed by system thermodynamics? Since a droplet is merely a collection of water molecules, the question becomes: are there avenues other than condensation growth whereby water molecules may aggregate to possibly form a critical droplet? One may also ask if the free energy barrier could be lowered such that a critical droplet requires a smaller collection of water molecules. As already explained, the thermodynamic barrier ΔF^* and the required critical radius r^* tend to decrease as steam super-saturation ratio S increases. So the longer the steam expands in a metastable state,

the larger S grows and the smaller r^* becomes. Regardless of the manufacturing mechanism, critical droplets are more probably formed at higher steam super-saturation.

To identify the alternate means of critical droplet formation, McDonald [18] points out that super-heated (sub-saturated) or saturated steam (with $S < 1$) is not entirely free of liquid phase embryos. Rather, embryos exist in a statistically-steady Boltzmann-like size distribution according to change in free energy for a given embryo size (size directly correlates to number of constituent water molecules). This distribution is supported by so-called “fluctuation phenomena” or random interactions of water molecules in vapor. As super-saturation increases, there is a general increase in embryo population across every point in the size distribution. Sufficient super-saturation ought to simultaneously lower the required r^* and increase the population of larger-sized embryos, thus making it more probable that collisions between larger embryos (fluctuation phenomena) could assemble a critical or supercritical embryo. Supercritical embryos have surmounted the free energy barrier such that their growth by vapor condensation is a thermodynamically-favorable, spontaneous process. Going back to equation (5.1, this means that the decrease in bulk free energy associated with droplet growth outmatches the increase in surface free energy accompanying that growth. Hence free energy is minimized by drop-wise condensation on supercritical embryos. Reversion to equilibrium from metastability coincides with spontaneous condensation growth of sufficiently many supercritical embryos.

Nucleation in the specific context of steam nozzle flow is discussed later, but it is important to note that phase change delay by steam super-saturation amounts to mere fractions of a millisecond assuming a super-heated or dry saturated nozzle inlet condition.

Strictly speaking, the evolution of critical droplets is a kinetic process that unfolds over that small but finite period of time. However, as will be shown subsequently, critical droplet formation can be modeled as instantaneous with a steady-state critical droplet nucleation rate that depends on steam supersaturation and other parameters. The reader is referred to McDonald's overview of nucleation kinetics [19] for a complete discussion, but a few highlights of that discourse are included here.

Liquid droplet embryos evolved from steam are born sub-critical and at once are exposed to an environment in which, on average, evaporation (loss of water molecules) from the embryo exceeds condensation (gain of water molecules) on the embryo. Conversely, super-critical embryos have an excess of growth by condensation over decay by evaporation. A critically-sized embryo sees a balance in growth and decay of constituent water molecules. Dynamics of molecular exchange are illustrated by Figure 5.1 which shows evaporation, condensation, and net appearance rates as a function of embryo size (g being the number of water molecules). The condensation rate increases monotonically as embryo surface area increases with increasing g . The evaporation rate will eventually increase under action of increasing surface area but initially decreases due to a rapid rise in net work of escape (for an evaporating molecule) as the number of nearest-neighbors increases (g increases). This latter effect is considerable at first but becomes less consequential as g increases. The net loss rate curve shows a sub-critical region, a critical point, and a super-critical region. To develop a useful mathematical description of nucleation, the chaotic, statistical molecular interactions encapsulated by

Figure 5.1 may be described by differential equations under simplifying assumptions.

McDonald [19] gives valuable insight into embryo population dynamics.

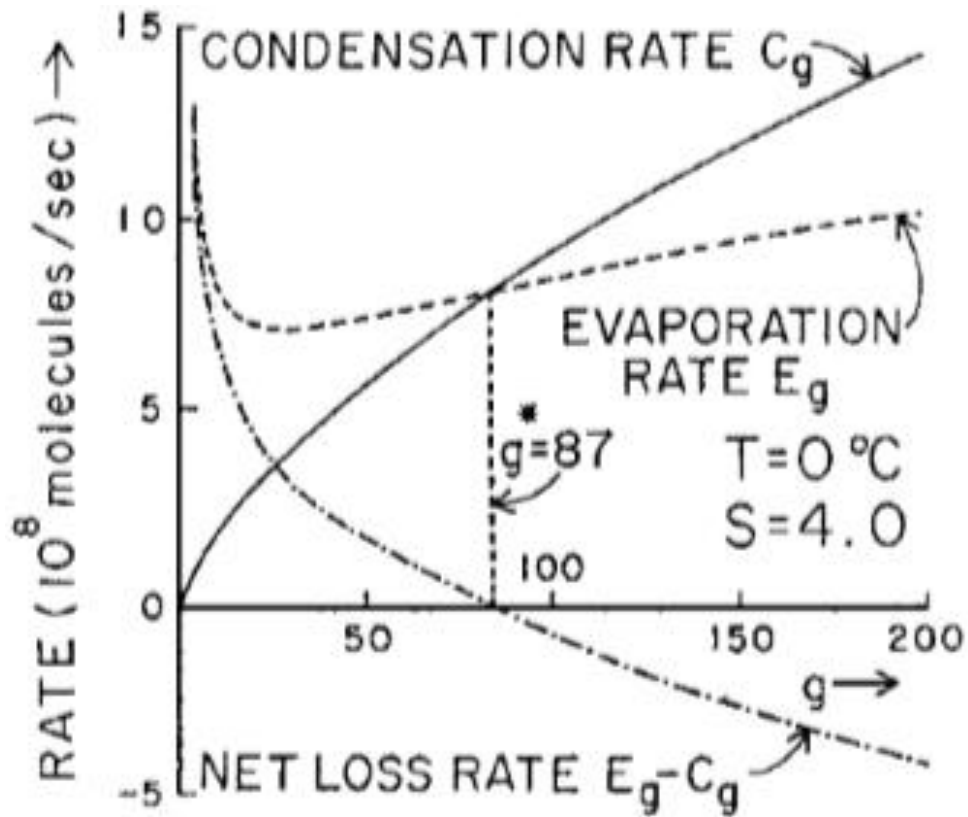


Figure 5.1 Condensation, evaporation, and net growth [19]

The stage of unbalanced, nonsteady-state embryo growth refers to a transient condition just after vapor has entered a super-saturated state (via isothermal compression or adiabatic expansion). The liquid embryo population (recall from above that a distribution exists before super-saturation) is at this point building up due to collisional processes. Condensation occurs when molecules collide with and stick to the embryo, and

evaporation occurs when molecules escape. This stage can be described with a differential balance equation for concentration N_g of embryos containing g water molecules (g -mers):

$$(5.4) \quad \frac{\partial N_g}{\partial t} = I_{g-1} - I_g$$

Where:

$$I_g = C_g N_g - E_{g+1} N_{g+1} = \text{Current flowing between } (g-1)\text{-mers and } g\text{-mers}$$

$$C_g = \text{Condensation rate for a } g\text{-mer} \quad ; \quad E_g = \text{Evaporation rate for a } g\text{-mer}$$

When the current (I_g) equals zero for all g -mers and when the current equals some non-zero value for all g -mers, there exists a balanced and an unbalanced steady-state, respectively. In particular, the unbalanced steady-state case serves as the basis for a mathematically convenient and physically realistic predictor of the steady-state droplet embryo population. One simplifying assumption which is credible in light of the physical timescales involved is that the nucleation process may be divided into two distinct parts:

- 1) Short (tens of μs) transient build-up of an embryo population containing moderately large g -mers, and
- 2) Longer (tens to hundreds of ms) period of sustained supercritical embryo generation throughout the vapor

The latter period concludes when reversion to equilibrium commences. For a steam nozzle, this reversion is due to latent heat effects that relieve super-saturation.

Moving forward with this slightly simplified view of the nucleation process, the first and briefest period can be assumed instantaneous while the second and longest period can be approximated by the unbalanced steady-state idealization. For the unbalanced steady-state, the concentration of g -mer embryos, for all g in the embryo size distribution, does not evolve with time because the same nonzero current (for all g -mers) flows through the entire embryo chain. This is equivalent to saying that the same balance between condensation and evaporation is preserved between every $(g-1)$ -mer and g -mer for all g in the embryo size distribution. A non-zero, positive current (where condensation dominates evaporation) between every neighboring g in the embryo size distribution is preserved by a statistical excess of condensational gain over evaporative loss. Note that this is true even when $g < g^*$ where the loss rate of g -mers by evaporation outpaces the appearance rate of g -mers by condensation. Even though the loss rate exceeds the gain rate, total condensation can dominate total evaporation if the concentration of $(g-1)$ -mers (any of which may grow to g -mers by condensation) sufficiently exceeds the concentration of g -mers (which may decay to smaller size by evaporation).

Another artifice is introduced along with the unbalanced steady-state approximation: at some size $G \gg g^*$, let all molecules comprising G be reintroduced as monomers (single water molecules) at the “bottom” of the embryo chain. This is the so-called Szilard artifice [19] and its purpose is to maintain the steady state with a finite number of water molecules in the system. It also imposes a boundary condition on the nucleation problem, thus helping with the mathematical description of nucleation. Predictions from the eventual nucleation model are insensitive to the exact choice of G .

Another boundary condition on the nucleation problem is needed. It is gotten from an observation of the balanced steady-state case: the concentration of g -mers for the unbalanced steady-state case and the balanced steady-state case are very nearly equal in the limit as g approaches unity [19].

An expression for the constant current may be derived by putting these pieces together and manipulating the mathematical description of the current. The result is that the current may be written in terms of known quantities (condensation rates, g -mer concentrations, the Szilard boundary condition, and the asymptotic boundary condition from the previous paragraph). The reader is referred to McDonald [19] for further mathematical details, but the end result is an expression for the generation rate of super-critical embryos. This expression has an exponential factor encapsulating the effects of super-saturation that tends to dominate the kinetics of the nucleation process.

The review given by McDonald ([18], [19]) comprises much of the so-called classical nucleation theory. Revisions outlined by Bakhtar and Young [20] have been made to classical theory. The nucleation model employed in the CMFD studies here assumes classical nucleation theory and uses corrections posited by Courtney [21] and Kantrowitz [22] pertaining, respectively, to partial pressure of molecular clusters and the non-isothermal nature of nucleation. Courtney's correction amounts to a reduction in the nucleation rate by a factor equal to the super-saturation ratio, while Kantrowitz's correction amounts to a multiplicative factor on the classical nucleation rate. Finally, an expression for the nucleation rate (appearance of critically-sized embryos) is:

$$(5.5) \quad J = \left(\frac{1}{1+\nu} \right) \left(\frac{2\sigma(T_{stm})}{\pi m^3} \right)^{1/2} \left(\frac{\rho_{stm}^2}{\rho_{liq}(T_{stm})} \right) e^{\left(\frac{-4\pi r^*{}^2 \sigma(T_{stm})}{3KT_{stm}} \right)}$$

Where:

J = Nucleation rate of droplets at r^* [drops/m³/s] ; m = Mass of water molecule [kg]

ρ_{stm} = Steam density [kg/m³] ; K = Boltzmann constant = 1.380648*10⁻²³ [J/K]

$\nu = 2 \left(\frac{\gamma-1}{\gamma+1} \right) \left(\frac{h_{fg}(P)}{RT_{stm}} \right) \left(\frac{h_{fg}(P)}{RT_{stm}} - 0.5 \right)$ = Kantrowitz isothermal correction factor

γ = Specific heat ratio ; h_{fg} = Latent heat of vaporization [J/kg]

For modeling purposes, this nucleation rate is instantaneously evolved according to local conditions. Gyarmathy [23] outlines a brief derivation of the nucleation time delay corresponding to typical steam nozzle conditions. By this estimate, the delay is approximately a nanosecond which is clearly negligible even with respect to the microsecond scale. This is some justification of the aforementioned assumption that steady-state nucleation is instantaneous.

One noteworthy source of uncertainty in classical and modified-classical nucleation theory regards the use of the bulk surface tension of a plane liquid interface despite the highly-curved surfaces of freshly-nucleated embryos. At present, no conclusions can be drawn as to the truly correct value for surface tension, but note that the choice of values may drastically influence nucleation theory predictions.

5.1.2 *Drop-wise Condensation*

Once the steam super-saturation lowers the thermodynamic barrier to condensation, critical droplets appear at a high volumetric rate throughout the vapor. Drop-wise vapor condensation on critical embryos is a spontaneous process that quickly relieves super-saturation by the phenomenon of condensation shock. The underlying heat and mass exchanges, which strongly depend on droplet size, must be mathematically modeled because they contribute to inter-phase terms in the CMFD formulation.

Drop-wise condensation heat/mass transfer cannot be considered a continuum phenomenon for all embryo sizes, particularly sizes on the order of r^* . Rather, heat/mass transfer must initially be considered from a free-molecular perspective and, as an embryo grows by condensation through a broad transition regime, the continuum approximation becomes valid [23]. The pertinent measure for size regime is the Knudsen number:

$$(5.6) \quad Kn = \frac{\ell}{2r}$$

Where:

ℓ = Mean free path of steam molecule [m]

The mean free path can be computed from one of several prescriptions using, for example, steam properties at saturation conditions. It represents the average distance of free travel by steam molecules before collision or interaction. A large Knudsen number implies the steam mean free path exceeds the droplet size, so the droplet “sees” individual molecules

streaming around the vapor space. A small Knudsen number implies the droplet is much larger than the steam mean free path, so the droplet “sees” a continuous medium instead. Typically, Knudsen number less than or equal to 0.01 indicates continuum flow whereas Knudsen number greater than or equal to 4.5 indicates free-molecular flow [23].

Regardless of Knudsen number, the process of condensation is governed by latent heat removal from droplet to vapor via conduction heat transfer. Upon condensation, mass moves from vapor to droplet with an attending latent heat release to the droplet (as condensation is an exothermal process). In actuality some small fraction of latent heat is stored in the droplet while the remainder transfers back to vapor. To good approximation however, the entirety of the latent heat transfers back to vapor. This is the energy balance maintained throughout the process of drop-wise condensation, with the final result being sensible heat transfer through a finite temperature difference from droplet to vapor. Size regime is important when choosing a conduction heat transfer coefficient to characterize drop/vapor heat transfer so that:

$$(5.7) \quad h_{fg}(P) \frac{dm}{dt} = h_{fg}(P) 4\pi r^2 \rho_{liq}(T_{stm}) \frac{dr}{dt} = 4\pi r^2 \alpha_r (T_r - T_{stm}) \\ = 4\pi r^2 \alpha_r (T_{sat|P} - T_{stm}) \left(1 - \frac{r^*}{r}\right)$$

Where:

α_r = Droplet/vapor heat transfer coefficient [W/m²/K] ; T_r = Droplet temperature [K]

$T_{sat|P}$ = Saturation temperature at system pressure [K]

The drop-to-vapor heat transfer constitutes an increase in steam entropy and raises steam pressure rapidly, giving rise to the condensation shock phenomenon that corrects the system to equilibrium. Note the temperature change that characterizes the heat transfer is the difference between the droplet and the vapor, but a capillarity relation [23] may be used to eliminate droplet temperature as an unknown. The capillarity relationship says that the steam sub-cooling multiplied by a geometric factor approximates the difference between droplet temperature and steam temperature.

In the free molecular regime, kinetic theory is often employed to predict heat and mass transfer to droplets, e.g. by taking the difference between condensation and evaporation rates [24]. Under the assumptions of negligible droplet slip velocity, uniform steam temperature, and negligible temperature variations within the small droplets, Hill [24], Young [25], and Zori and Kelecyc [26] suggest a free-molecular condensation rate:

$$(5.8) \quad \frac{dr}{dt} = \left(\frac{\gamma+1}{2\gamma}\right) C_{p,stm} (T_{sat|P} - T_{stm}) \left(\frac{P}{\rho_{liq}(T_{stm}) h_{fg}(P)} (2\pi RT_{stm})^{-1/2} \right)$$

Where:

$C_{p,stm}$ = Specific heat capacity at constant pressure of steam [J/kg/K]

In the continuum regime, the typical approach is to employ a theoretically-developed and empirically-tuned heat transfer coefficient. Gyarmathy [23] proposes a heat transfer coefficient of the form:

$$(5.9) \quad \alpha_r = \begin{cases} \frac{k_{stm}}{r} \left(1 + \left(\frac{2\sqrt{8\pi}}{1.5*Pr_{stm}} \right) \left(\frac{\gamma}{\gamma+1} \right) \left(\frac{Kn}{a_{th}} \right) \right)^{-1} & , \text{ free molecular} \\ 0.357 \left(\frac{k_{stm}}{r} \right) \sqrt{Re_r Pr_{stm} + 7.96} & , \text{ continuum} \end{cases}$$

Where:

k_{stm} = Thermal conductivity of steam [W/m/K] ; Pr_{stm} = Steam Prandtl Number

a_{th} = Thermal accommodation coefficient ; Re_r = Droplet Reynolds Number

With a droplet growth law given by:

$$(5.10) \quad \frac{dr}{dt} = \left(\frac{k_{stm}}{\rho_{liq}(T_{stm})h_{fg}(P)} \right) \left(\frac{1 - \frac{r^*}{r}}{1 + \left(\frac{2\sqrt{8\pi}}{1.5*Pr_{stm}} \right) \left(\frac{\gamma}{\gamma+1} \right) \left(\frac{Kn}{a_{th}} \right)} \right) \left(\frac{(T_{sat|P} - T_{stm})}{r} \right)$$

Or, more approximately:

$$(5.11) \quad \frac{dr}{dt} = \left(\frac{k_{stm}}{\rho_{liq}(T_{stm})h_{fg}(P)} \right) \left(\frac{1 - \frac{r^*}{r}}{r + 1.59\ell} \right) ((T_{sat|P} - T_{stm}))$$

Where the following values are assumed: $Pr_{stm} = 1.3$, $\gamma = 1.2$, $a_{th} = 1$

Note the thermal accommodation coefficient [24] essentially quantifies the amount of energy carried away by molecules that, upon colliding with a droplet surface, reflect from it rather than condense (and stick) to it. The very concept of a thermal accommodation coefficient assumes a condensation coefficient less than unity. Hill [24] describes the

condensation coefficient as the fraction of collided molecules that condense rather than reflect from a droplet surface. Both the thermal accommodation coefficient and the condensation coefficient factor into growth law formulations.

5.2 Dispersed-Phase Size Distribution Modeling

5.2.1 *Polydisperse Droplet Size Distribution by Moment Method*

Consider some general droplet population evolved from super-saturated steam. The phenomena of nucleation and condensation both drastically alter the size distribution of that population. Nucleation rapidly generates new droplets at the critical size while condensation quickly grows existing droplets to larger sizes. Since heat and mass transfer between vapor and droplets depends on droplet number density, size, and surface area, it is important to model the dispersed-phase size distribution in fair fidelity. The assumption of mono-dispersity at a suitably averaged droplet size has been used in the literature with some success. However, a more appealing alternative is put forth by Giordano [27]. Polydispersity is captured by solving scalar transport equations for the first few statistical moments of a size distribution. A brief synopsis follows.

Assume a continuous droplet size distribution in radius r with number density function f such that the product $f * dr$ is the number of drops per unit mass of steam falling within the size range $(r, r + dr)$. Also assume a four-dimensional phase space consisting of three spatial dimensions x, y, z and a droplet size (radius) dimension r . In a volume V' of this phase space, there is a total droplet population N_V :

$$(5.12) \quad N_V = \int_{V'} \rho_{stm} f dV'$$

The trajectories of droplets in the four-dimensional phase space are described by the usual components of velocity plus a droplet growth rate which could be interpreted as a droplet growth velocity:

$$(5.13) \quad \vec{u}' = \left[\frac{dx}{dt}, \frac{dy}{dt}, \frac{dz}{dt}, \frac{dr}{dt} \right] = [\mathbf{u}_x, \mathbf{u}_y, \mathbf{u}_z, \mathbf{G}]$$

Note that if zero phase slip is assumed (appropriate for sufficiently small droplets) the velocity components in the vector \vec{u}' are those of steam. A conservation equation may be written for droplet number in an elemental volume of the phase space under the assumption that only nucleation and condensation affect the population (to the exclusion of coagulation/coalescence and break-up, which is a good approximation). Droplets appear in the phase space volume by nucleation (rate J) and stream through the phase space volume control surface S' under the influence of the velocity vector \vec{u}' . Note that by the definition of the phase space and of \vec{u}' , the “control surface” must also consist of boundaries on droplet size. So droplets enter/exit the phase space volume by streaming across x , y , or z boundaries but also by condensation growth across r boundaries with “velocity” G . The droplet conservation equation is:

$$(5.14) \quad \frac{\partial}{\partial t} \int_{V'} \rho_{stm} f dV' + \int_{S'} \rho_{stm} f (\vec{u}' \cdot d\vec{S}') = \int_{V'} \rho_{stm} J dV'$$

Applying Gauss' divergence theorem to the last term on the left-hand side, one obtains a differential balance equation for the droplet population in an Eulerian frame of reference that includes a transient term, two flux terms, and a volumetric source term:

$$(5.15) \quad \frac{\partial}{\partial t} (\rho_{stm} f) + \vec{\nabla} * (\rho_{stm} f \vec{u}) + \frac{\partial}{\partial r} (\rho_{stm} f G) = \rho_{stm} J$$

Note that the one flux term resulting from application of the divergence theorem is split into two: one for the usual convective flux involving flow velocity $\vec{u} = [u_x, u_y, u_z]$ and one for the convective flux involving drop growth velocity G .

Now, consider the definition of the j^{th} moment of size distribution f :

$$(5.16) \quad \mu_j = \int_0^{\infty} r^j f dr$$

Here, the statistically-distributed radius r is raised to the j^{th} power and multiplied into the distribution function. The result is then integrated over all possible r . Given that r has units of length and the distribution function has units of inverse length times inverse mass, one could discern from dimensional considerations that the 0th moment is related to droplet number [$drop/kg$], the 1st moment is related to droplet size [$m * drop/kg$], the 2nd moment is related to droplet surface area [$m^2 * drop/kg$], and the 3rd moment is related to droplet volume [$m^3 * drop/kg$]. These first four moments may be used in conservation equation inter-phase heat/mass transfer source terms so as to capture the poly-disperse

nature of the droplet population. Such an approach is more detailed than the mono-disperse treatment and simpler to implement than a discretized size binning approach. Each of the moments is a passive scalar quantity transported by the flow field. A general transport equation for the moments is still required.

Taking the product of r^j with the differential droplet balance equation, moving r^j across differential operators where possible, and integrating over all radii:

$$(5.17) \int_0^\infty \left[\frac{\partial}{\partial t} (\rho_{stm} r^j f) + \bar{\mathbf{v}} * (\rho_{stm} r^j f \bar{\mathbf{u}}) + r^j \frac{\partial}{\partial r} (\rho_{stm} f G) = \rho_{stm} J r^j \right] dr$$

The first and second terms are straightforward. The term on the right-hand side is evaluated by allowing the nucleation rate to be represented as a step function since the source term produces droplets of one radius only (the critical radius). The third term on the left-hand side requires integration by parts:

$$(5.18) \int_0^\infty \left[r^j \frac{\partial}{\partial r} (\rho_{stm} f G) \right] dr = (r^j \rho_{stm} f G)_0^\infty - \int_0^\infty j r^{j-1} \rho_{stm} f G dr =$$

$$-j \rho_{stm} \int_0^\infty r^{j-1} f G dr$$

Where:

$$(r^j \rho_{stm} f G)_0^\infty = 0$$

$\int_0^\infty r^{j-1} f G dr$, requires knowledge about $G(r)$ before it can be evaluated

Finally, the general moment transport equation is:

$$(5.19) \quad \frac{\partial}{\partial t} (\rho_{stm} \mu_j) + \bar{\mathbf{V}} * (\rho_{stm} \mu_j \bar{\mathbf{u}}) = j \rho_{stm} \int_0^{\infty} r^{j-1} f G dr + \rho_{stm} J_* r^{*j}$$

Where:

$$J_* = \text{Nucleation rate} \left[\frac{drop}{kg*s} \right] \text{ of droplets, size } r^*, \text{ from integration of } J_* \delta(r - r^*)$$

A further closure describing the condensation growth ($G = dr/dt$) dependence on r is required to evaluate the integral in the moment transport equation. Considering the possible definitions of droplet growth laws from above, $G(r)$ could be a constant. Even if G depends on r somehow, the dependence might be approximated as a constant by using a certain definition of r , e.g. the “two-zero” diameter as proposed by Giordano [27]. Other measurements of significance could also be used, e.g. the “three-two” diameter also known as the Sauter mean diameter. In any case, the droplet growth rate G comes outside the integral on r and the definition of the size distribution moment is applied, i.e:

$$(5.20) \quad \int_0^{\infty} r^{j-1} f dr = \mu_{j-1}$$

In writing out the four moment equations, it is readily apparent that they are coupled through the condensation growth term:

$$(5.21) \quad \frac{\partial}{\partial t} (\rho_{stm} \mu_0) + \bar{\nabla} * (\rho_{stm} \mu_0 \bar{\mathbf{u}}) = \rho_{stm} J_*$$

$$(5.22) \quad \frac{\partial}{\partial t} (\rho_{stm} \mu_1) + \bar{\nabla} * (\rho_{stm} \mu_1 \bar{\mathbf{u}}) = \rho_{stm} (G \mu_0 + J_* r^*)$$

$$(5.23) \quad \frac{\partial}{\partial t} (\rho_{stm} \mu_2) + \bar{\nabla} * (\rho_{stm} \mu_2 \bar{\mathbf{u}}) = \rho_{stm} (2G \mu_1 + J_* r^{*2})$$

$$(5.24) \quad \frac{\partial}{\partial t} (\rho_{stm} \mu_3) + \bar{\nabla} * (\rho_{stm} \mu_3 \bar{\mathbf{u}}) = \rho_{stm} (3G \mu_2 + J_* r^{*3})$$

Notice that the 0th moment (proportional to total droplet number) has no condensation source term, only a nucleation source term. So the 0th moment equation accounts for the effects of nucleation on total droplet number. The 2nd moment equation accounts for the effects of both condensation and nucleation on droplet surface area distribution. The 3rd moment equation accounts for the effects of both condensation and nucleation on droplet volume and/or wetness fraction. Some useful droplet population measures are related to size distribution moments:

$$(5.25) \quad n \left[\frac{drop}{m_{stm}^3} \right] = \rho_{stm} \mu_0, \text{ Droplet number density}$$

$$(5.26) \quad d_{32} [m] = \frac{\mu_3}{\mu_2} = \text{Sauter mean diameter}$$

$$(5.27) \quad \bar{r} [m] = \frac{d_{32}}{2} = \text{Droplet average radius}$$

$$(5.28) \quad \beta \left[\frac{kg_l}{kg_{stm}} \right] = \rho_{liq}(T_{stm}) \mu_0 \frac{4}{3} \pi \left(\frac{\mu_3}{2\mu_2} \right)^3 = \text{Droplet mass (wetness) fraction}$$

$$(5.29) \quad \alpha \left[\frac{m_l^3}{m_{stm}^3} \right] = \beta \left(\frac{\rho_{stm}}{\rho_{liq}(T_{stm})} \right) = \text{Droplet volume fraction}$$

$$(5.30) \quad \bar{m} \left[\frac{kg_l}{drop} \right] = \frac{\beta}{\mu_0} = \text{Mass of average}$$

$$(5.31) \quad \rho_{stm}^l \left[\frac{kg_l}{m_{stm}^3} \right] = \beta \rho_{stm} = \text{Droplet density in vapor}$$

$$(5.32) \quad \bar{A} \left[\frac{m_l^2}{drop} \right] = 4\pi \bar{r}^2 = \text{Surface area of average droplet}$$

$$(5.33) \quad a \left[\frac{m_l^2}{m_{stm}^3} \right] = \bar{A} n = \text{Droplet areal density}$$

Note from the formulae above that mass, length, area, and volume units sometimes have subscripts indicating a phase (l for liquid, stm for vapor/steam). This is helpful in clarifying the physical meaning of certain droplet parameters.

5.2.2 *Size Distribution Moments as Passive Scalars*

As an interesting side note, the formulation above bears some resemblance to the S- γ model for dispersed-phase size distribution modeling in STAR-CCM+ [11]. Since the S- γ model is compatible only with certain two-phase flow formulations (e.g. multiphase segregated Eulerian/Eulerian) that are not being exercised in CMFD analyses here, the S-

γ model cannot be used directly. Instead, the four size distribution transport equations can be cast as passive scalar transport equations which assume the form [11]:

$$(5.34) \quad \frac{\partial}{\partial t} \int_V (\rho \phi_j) dV + \oint_A (\rho \phi_j \vec{u}) \cdot d\vec{A} = \oint_A J_j \cdot d\vec{A} + \int_V S_{\phi_j} dV$$

Where:

ϕ_j is a passive scalar component

J_j a diffusion flux ; S_{ϕ_j} is a source term for the passive scalar component

Comparing equation (5.34) to equations (5.21) through (5.24), it is readily apparent that the moments of the droplet size distribution are passive scalars that experience convective transport only (zeroed diffusion flux) and that have source terms equal to the right hand sides of equations (5.21) through (5.24).

5.3 Compressible Flow and Steam Nozzles

Nucleation and drop-wise condensation have already been discussed as stand-alone phenomena. It is useful to now consider them in the context of compressible, condensing steam flow in a converging-diverging nozzle as may be found in the pressure stage of the RCIC turbine.

5.3.1 Generic Converging-Diverging Nozzle Flow

A quick overview of compressible converging-diverging (CD) nozzle flow is in order. The discussion provided by Cengel and Boles [28] is an excellent review of some

basic concepts of compressible flow in nozzles. It is devoid of any two-phase non-equilibrium flow considerations, but the same concepts of choking and aerodynamic shock are important in condensing steam nozzle flow. Figure 5.2 shows the various possibilities for nozzle flow with stagnation inlet pressure P_0 , back pressure P_b , and exit plane pressure P_e . There are several cases of back pressure (A through G) shown graphically in terms of pressure and Mach number. They run the gamut from no flow to choked flow with/without aerodynamic shocks inside/outside the nozzle.

For flow to occur at all, the back pressure must be less than the inlet pressure (case A shows no flow, no pressure drop). As the back pressure is reduced below the inlet pressure but held above $P_c = P^*$, flow along the nozzle commences and there is a pressure drop until the throat is reached (maximum velocity, mass flow rate, and Mach number). Since P_b is above critical pressure of the working fluid (the lowest pressure attainable at the throat regardless of back pressure), the Mach number at the throat is less than one and flow never reaches sonic speed. As such, the diverging section of the nozzle behaves like a diffuser and increases fluid pressure at the expense of decreasing velocity. Flow is sub-sonic throughout the nozzle and no aerodynamic shocks occur.

When the back pressure is lowered to just equal the critical pressure, flow goes sonic at the throat ($Ma=1$) but slows to sub-sonic in the diverging section of the nozzle. The maximum mass flow rate through the nozzle is just established at the throat where sonic flow prevails. Because of the choked condition at the nozzle throat, further drop in back pressure will not influence flow in the converging section. Therefore the throat

velocity and mass flow rate will not increase beyond their values for back pressure P_b equal to critical pressure P^* .

As back pressure is lowered below critical, flow at the throat remains choked but flow in the diverging section accelerates to super-sonic velocity since the diverging cross-section now behaves like a nozzle. A standing, compressive, normal shock occurs inside the diverging section of the nozzle while $P_b > P_E$. Since in this illustration P_E is the back pressure at which flow is approximately isentropic across the nozzle, if back pressure is higher an introduction of entropy is required. The shock is highly irreversible (non-isentropic) and suddenly decelerates the flow to sub-sonic while raising pressure. The rest of the diverging section acts as a diffuser, decelerating the flow and raising the pressure.

Reducing the back pressure towards P_E will effectively lengthen the region of super-sonic flow in the diverging section and push the location of the normal shock down the nozzle. Ultimately the normal shock is pushed to the nozzle exit plane when $P_b = P_E$. Flow across the nozzle is approximately isentropic and super-sonic conditions prevail beyond the throat until the shock at/near the exit plane. The shock leads to an emanating jet that is sub-sonic.

Decreasing the back pressure still further below P_E leads to expansion to pressure P_F (approximately isentropic) at the exit plane regardless of the value of P_b . The relative values of back pressure and P_F determine what happens just beyond the exit plane. If $P_b > P_F$, the flow is over-expanded because back pressure exceeds the exit plane pressure. This causes the standing shock at the exit plane to bow outward and leads to a mixed sub/super-sonic jet emanating from the nozzle. The shock is still compressive and there is also some

degree of jet contraction because the shock is not perpendicular to the nozzle wall. If $P_b = P_F$, there will be no shocks inside or beyond the nozzle. If $P_b < P_F$, the flow is under-expanded because exit plane pressure exceeds back pressure. This causes a complex pattern of oblique, expansive shocks (tending to lower pressure) to appear outside the nozzle, leading to a slightly expanded jet. These considerations underscore the need for a strong shock-capturing CMFD solution.

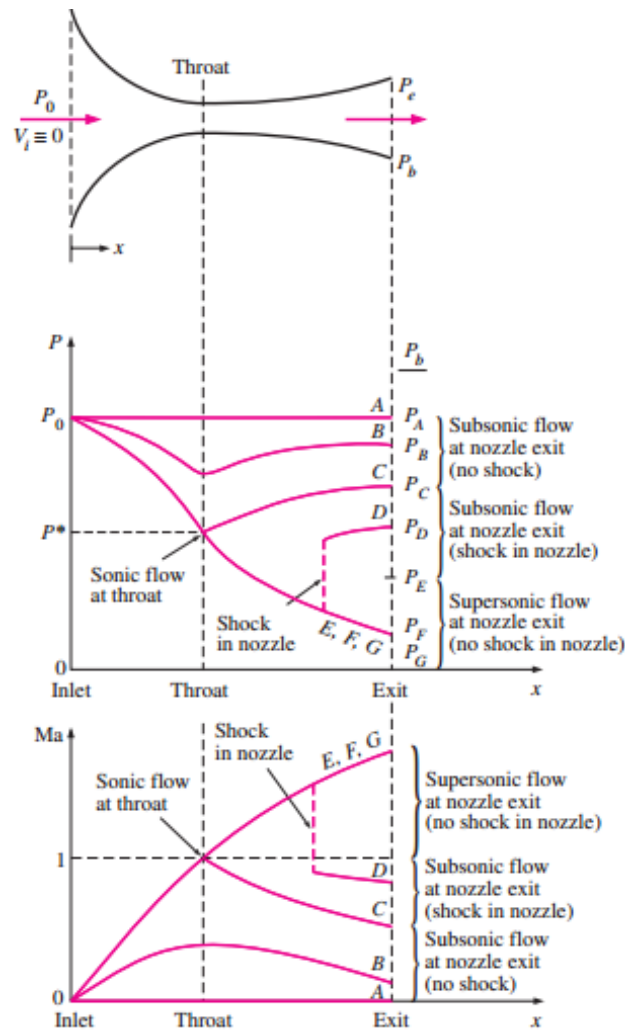


Figure 5.2 Converging-Diverging nozzle flow at various back pressures [28]

5.3.2 *Condensing Steam Nozzle Flow*

When super-heated or saturated steam expands in a converging-diverging nozzle, the steam pressure and temperature both decrease, eventually crossing into the saturation region. At this point, the steam temperature equals the saturation temperature for the steam pressure and one might expect phase change to commence. As discussed previously however, homogeneous condensation is often the only route for phase change and some short but finite amount of time is required to surmount the Gibbs free energy barrier. In the interim, steam exists in the usual saturation region but remains dry in a sub-cooled or, equivalently, a super-saturated state of thermodynamic non-equilibrium. Condensation becomes a thermodynamically-favorable (spontaneous) process when some sufficient degree of sub-cooling or super-saturation is established. The point at which this happens (inside the saturation dome) is called the Wilson point and, for different nozzle inlet conditions, the locus of Wilson points forms the Wilson line. Typically, the Wilson line falls around the 4-5 % wetness curve in the saturation region and is often approximated as the 4% moisture line [28]. Thus, super-saturated steam will not begin condensing until its saturation conditions would dictate roughly a 96% quality.

The thermodynamics of steam nozzle flow are illustrated in an h-s diagram in Figure 5.3 [29]. The numbers on the diagram correspond to the pressure plot along the steam nozzle as shown in Figure 5.4. Super-heated inlet conditions are assumed at (1), and expansion to saturation at (3) and then to the Wilson line at (4) is shown.

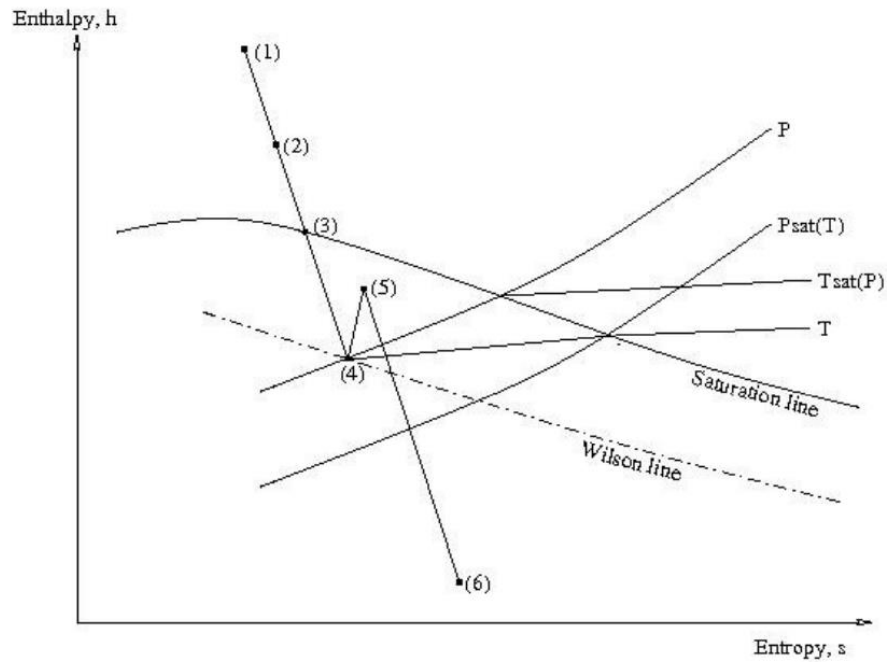


Figure 5.3 Qualitative h-s diagram for condensing steam flow in a nozzle [29]

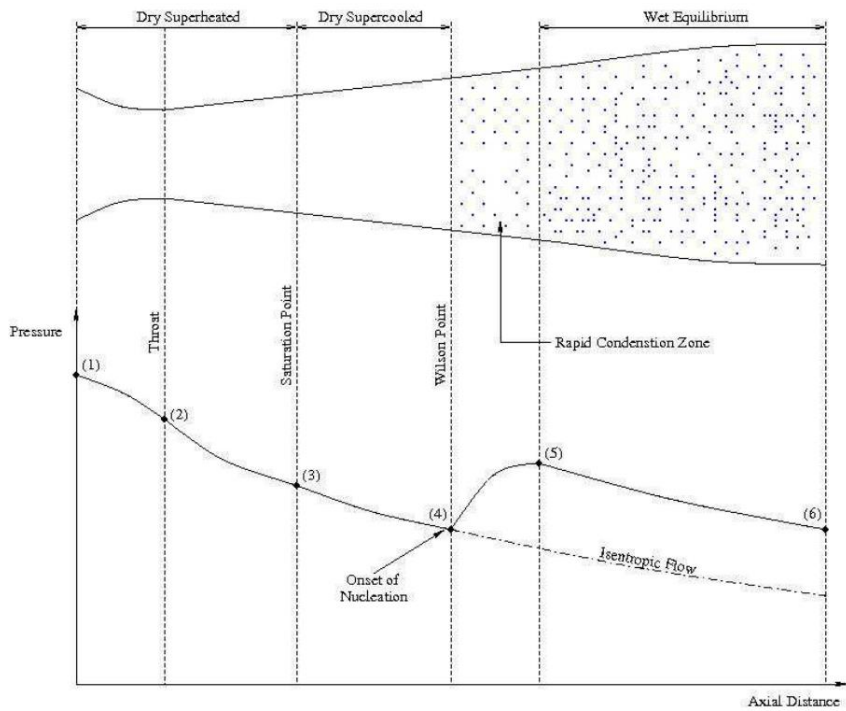


Figure 5.4 Qualitative pressure plot for condensing steam flow [29]

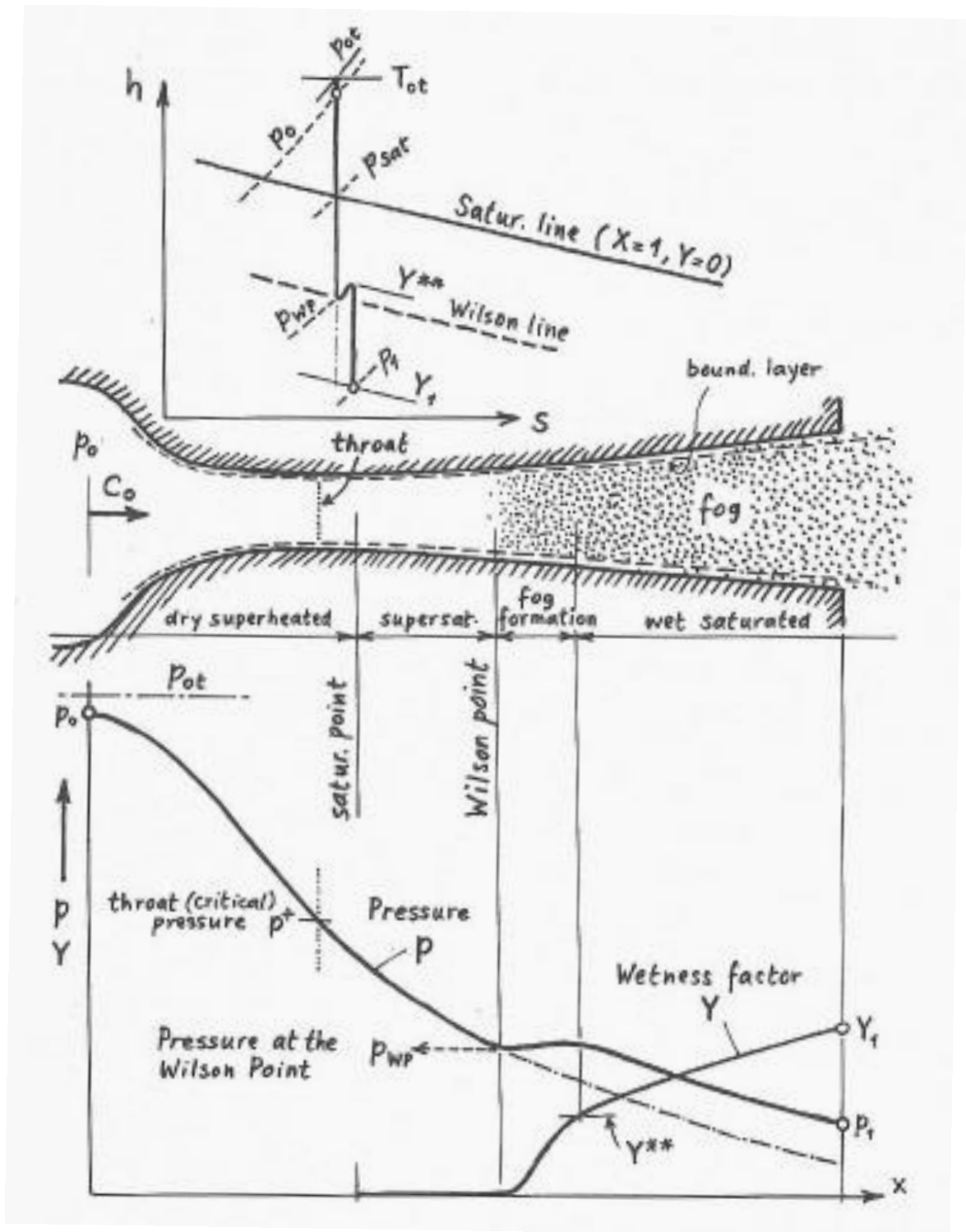


Figure 5.5 Qualitative illustration of wetness and pressure along a steam nozzle [23]

The region between (3) and (4) is the “nucleation zone” where dry sub-cooled (super-saturated) steam exists. The nucleation zone eventually terminates at the Wilson point (point of maximum sub-cooling and super-saturation) as nucleation furnishes a large number density of critically-sized droplets on which steam may condense unhindered by a thermodynamic barrier. The “condensation zone” begins at the Wilson point and terminates when condensation shock (pressure bump between (4) and (5)) has corrected the two-phase system back to thermodynamic equilibrium. The point of equilibrium at (5) is somewhere between the Wilson line and the top of the saturation dome. As seen from the wetness curve in Figure 5.5, the condensation delay (zero wetness after saturation point until Wilson point) and shock (rapid condensation) leads to different nozzle outlet conditions (pressure, wetness) relative to an approximately isentropic expansion predicted by steam tables or a Mollier diagram. A few special considerations for steam nozzle flow:

- Two-dimensional effects cause asymmetric or v-shaped condensation fronts
- Latent heat release during condensation lowers Mach number so that a super-sonic flow can be made super-sonic (lower Ma) or sub-sonic with transient, pulsating patterns possible
- Pre-existing wetness or foreign nuclei (impurities in steam) could lead to some amount of condensation soon after saturation conditions are reached
- Droplet flashing (cavitation boiling and subsequent fragmentation due to a sudden expansion pressure drop) within or just outside the nozzle is something is unlikely for sufficiently small droplets
- Flashing of larger liquid parcels in the nozzle or jet is more probable.

5.3.3 *Miscellaneous Considerations*

With respect to latent heat release and its effects on super-sonic nozzle flow, an interesting transient phenomenon can potentially occur if latent heat release (condensation shock) is sufficient to decelerate the flow to sonic velocity. This could occur if condensation takes place close enough to the throat where the Mach number is only slightly larger than unity. When condensation shock does not cause reversion to sonic flow, condensation is referred to as sub-critical and there is no “thermal choking”. In this case, a steady-state flow can be established. When condensation shock is sufficiently strong to cause reversion to sonic flow, condensation is referred to as super-critical and there is thermal choking. An adiabatic shock sets up inside the diverging section of the nozzle. The shock moves upstream towards the nozzle throat if it cannot establish a position downstream at which flow remains super-sonic upon crossing it [30]. If the shock moves far enough upstream, it will inhibit nucleation by virtue of the attending steam temperature increase across the shock. This disrupts the very phenomenon that leads to condensation and, in turn, the shock disappears. Nucleation within super-sonic flow is re-established downstream of the throat, condensation begins again, and the strong condensation shock re-appears. This oscillatory pattern repeats itself with some frequency due to the self-sustaining nature of the phenomenon [30]. Should this occur in the pressure stage of a RCIC turbine, it could lead to more thermodynamic losses, and an altered droplet size distribution (fewer droplets that are larger in size).

With respect to modeling heterogeneous nucleation sites, the same drop-wise condensation source terms can be applied and a special set of size distribution equations

could be utilized. The effect of any nucleation sites or inlet wetness is to decrease the steam super-saturation that would otherwise occur because steam can readily condense out on heterogeneous sites without appreciable hindrance from a thermodynamic barrier. If inlet moisture is excessive or if impurities exist in large concentrations, condensation shock might not occur in the nozzle or might be much less pronounced.

With respect to modeling droplet flashing/cavitation, Gyarmathy [23] briefly describes the physics. Droplet flashing (by cavitation) can only proceed if a rapid pressure decrease (expansion) occurs in ambient steam and internal droplet temperature cannot quickly adjust (cool by heat transfer) to the new pressure environment. In this scenario, the whole droplet “feels” the lower pressure instantly and thus the liquid droplet has new saturation conditions immediately. However, the internal droplet temperature can only decrease by heat transfer with the drop surface and the surrounding steam. If internal droplet temperature cannot decrease quickly enough, cavitation boiling (flashing) could occur. This would cause the droplet to fragment as some liquid vaporizes. Gyarmathy [23] proposes an equation for the maximum droplet size that escapes flashing as a function of the pressure drop and the time interval of expansion. Most droplets evolved from condensing steam flow are likely small enough to avoid flashing under normal conditions.

5.4 Equation-of-State for Super-Saturated Steam

5.4.1 IAPWS-IF97 Background

STAR-CCM+ has certain built-in data for water as a working fluid, be it in the liquid or vapor state. It even incorporates a few of the five IAPWS-IF97 regions as show in Figure 5.6 below [13].

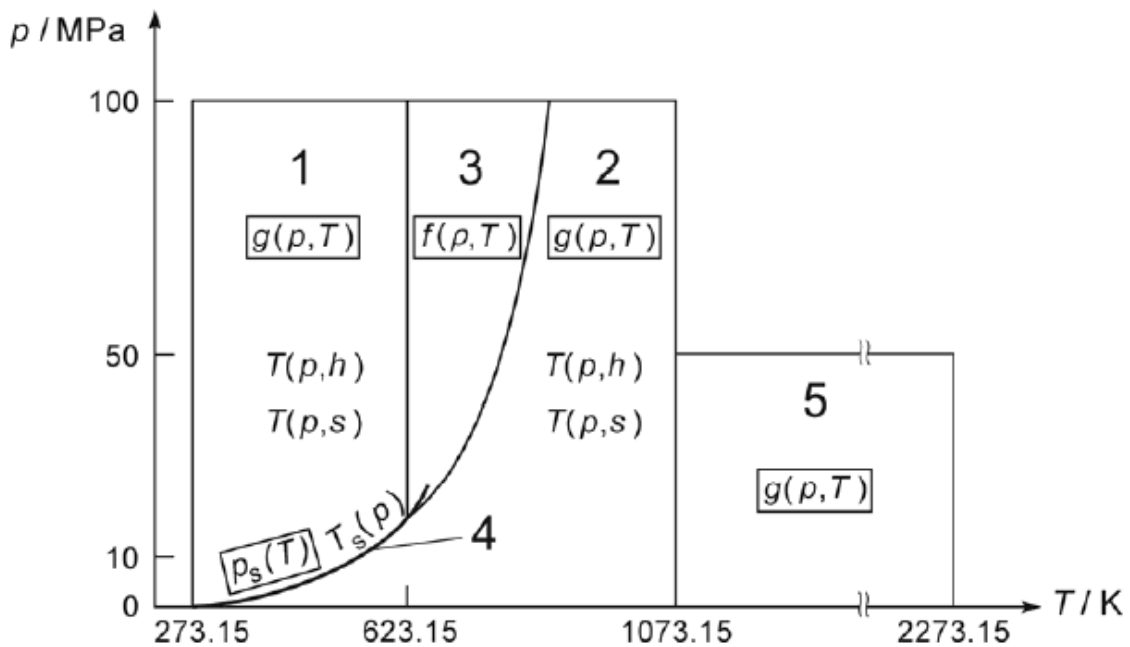


Figure 5.6 IAPWS-IF97 regions, dependent/independent variables [13]

The STAR-CCM+ material database does not contain equation-of-state data for saturated and super-saturated steam, two states of water that must be modeled in a CMFD calculation of condensing steam flow in particular and steam turbines in general. The code does, however, allow a user to totally define equation-of-state closures for compressible

fluids via external data tables. IAPWS-IF97 provides the requisite data (by furnishing the necessary equations, constants, exponents, etc.) for saturated, super-saturated, and super-heated steam as well as saturated and sub-cooled water. Regions 2 and 2m from Figure 5.6 (2m not explicitly marked in the diagram) represent super-heated and super-saturated steam, respectively. Region 4 (actually just a curve) represents saturated steam/water. Region 1 represents sub-cooled (or compressed) water.

IAPWS-IF97 provides region-wise equations and tables of fitting exponents and constants which are derived empirically or – in the case of metastable super-saturated steam – from special extrapolations of experimental data. Using, for example, a suitably-written MATLAB script or EXCEL spreadsheet, one can borrow from IAPWS-IF97 as needed and compile whatever water data tables are required for a given application. In this case, tables of data are needed for thermodynamic and transport properties of steam in the super-heated, saturated, and super-saturated states as well as for water in the saturated and sub-cooled states. The following properties as functions of both temperature and pressure (excluding saturation where temperature and pressure are dependent) were required:

- Density
- Specific enthalpy
- Dynamic (absolute) viscosity
- Thermal conductivity
- Speed of sound

Certain other properties like isobaric and isochoric specific heat and certain required property derivatives are obtained from numerical differentiation or integration in STAR-

CCM+. With data tables input, all requisite equation-of-state closures for compressible steam and incompressible water are known. Furthermore, interpolating field functions can be written to retrieve steam and water properties for use in other instances like conservation equation source terms.

5.4.2 IAPWS-IF97 Data Table Extraction

The IAPWS-IF97 methodology for predicting steam and meta-stable steam properties is described subsequently. Then, an outline is given for a short MATLAB script that produces data tables for import into STAR-CCM+. Though IAPWS-IF97 was employed for the present condensing steam CMFD analyses, note that other alternatives are viable and have been used in the literature. One popular method employs the Vukalovich virial equation of state [31] which is expected to give reasonable results when extrapolated into the super-saturated region.

For regions 2 and 2m of Figure 5.6, IAPWS-IF97 proposes a fundamental equation for specific Gibbs free energy as a function of pressure and temperature - $g(P, T)$ - consisting of a sum of two parts: 1) an “ideal gas” part γ^0 , and 2) a “residual” part γ^r :

$$(5.35) \quad \frac{g(P, T)}{RT} = \gamma \left(\pi = \frac{P}{P^*}, \tau = \frac{T^*}{T} \right) = \gamma^0(\pi, \tau) + \gamma^r(\pi, \tau)$$

Where:

P = Steam pressure ; T = Steam temperature ; P^* = Reducing pressure = 1 MPa

T^* = Reducing temperature = 540 K ; π = Dimensionless pressure

τ = Dimensionless temperature

The ideal-gas and residual terms consist of equations in dimensionless pressure and temperature including a litany of empirical coefficients and exponents. For super-heated and super-saturated steam, the ideal-gas part is identical in form, uses slightly different empirical coefficients n^0 , and uses identical empirical exponents J^0 :

$$(5.36) \quad \gamma^0(\pi, \tau) = \ln(\pi) + \sum_{i=1}^9 n_i^0 \tau^{J_i^0}$$

The residual part differs in form for super-heated and super-saturated steam. For super-heated steam, the expression for the residual part is:

$$(5.37) \quad \gamma^r(\pi, \tau) = \sum_{i=1}^{43} n_i \pi^{I_i} (\tau - 0.5)^{J_i}$$

For super-saturated steam, the expression for the residual part is:

$$(5.38) \quad \gamma^r(\pi, \tau) = \sum_{i=1}^{13} n_i \pi^{I_i} (\tau - 0.5)^{J_i}$$

Thermodynamic properties – specific volume (density), specific internal energy, specific entropy, specific enthalpy, specific heat capacity (isobaric), specific heat capacity (isochoric), and speed of sound – are all expressed as functions of specific Gibbs free energy and derivatives thereof. These can be found in [13] along with all empirical coefficients and exponents. Since Gibbs free energy is written as a sum of two terms, all thermodynamic properties may be written as functions of the ideal-gas term (and derivatives thereof) and the residual term (and derivatives thereof).

To compute desired steam properties one must select a temperature and pressure (or rather a matrix of those independent variables) inside the range of validity for a region in question, compute all the ideal-gas and residual terms (including the various derivatives), and then compute thermodynamic variables of interest. This is the rather simple approach followed for equilibrium states of steam and water, i.e. super-heated steam, saturated steam/water, and sub-cooled water. For metastable super-saturated steam, the floor on the range of validity is the 5% equilibrium moisture line (95% quality) [13]. To compile super-saturated steam property tables – where independent variables are temperature and pressure - the minimum valid steam sub-cooled temperature for a given pressure was recovered from a Newton’s method solution (for temperature T) of:

$$(5.39) \quad h = g(P, T) - T \left(\frac{\partial g}{\partial T} \right)_P = RT\tau(\gamma_t^0 + \gamma_t^r)$$

Where:

$$h = h_{95} = h_{f,sat} + 0.95 * (h_{g,sat} - h_{f,sat})$$

For each pressure the range of validity on super-saturated steam temperature is

$(T_{stm_{h_{95}}}, T_{sat})$ with $T_{stm_{h_{95}}}$ coming from the Newton’s method solution.

Thermodynamic properties of super-saturated steam follow from IAPWS-IF97 prescriptions. There are special IAPWS-IF97 documents for thermal conductivity [32], viscosity [33], and surface tension [34].

A MATLAB function file IAPWS_IF97.m [35] was called from a specially-developed script to compute steam and water properties. The super-saturated region 2m computations and the Newton's method solution for steam sub-cooling were coded around IAPWS_IF97 function calls as necessary. Generally, the script proceeds as:

- Define pressure P array (logarithmically spaced between 0.01 – 100 MPa)
- Get a saturation temperature T_{sat} array, a value for each member of the P array
- Define a T_{stm} matrix, 500 points for each P between $T_{sat}(P)$ to 1073.0 K
- Get $h_{f,sat}$, $h_{g,sat}$, and h_{95} for each member of the P array
- Initialize/zero arrays for h_{stm} , ρ_{stm} , C_{stm} , μ_{stm} , k_{stm}
- Specify arrays of IAPWS-IF97 data (coefficients, exponents)
- Newton's method for array of $T_{stm,min}$, the maximum sub-cooling for each P
- Use region 2m formulae for h_{stm} , ρ_{stm} , C_{stm} , μ_{stm} , k_{stm}
- Use region 2 formulae for h_{stm} , ρ_{stm} , C_{stm} , μ_{stm} , k_{stm} of super-heated steam
- Compute saturated steam/liquid properties
- Print all data to text files in tabular format, condition for STAR-CCM+ import

5.5 Turbulence

In trans-sonic condensing steam flow, turbulence could conceivably impact the process of spontaneous condensation and affect both inter-phase mass/momentum/energy transfer and condensation shock formation. There are two general mechanisms by which turbulence could impact the condensation process [36], though one is negligible with respect to the other:

- The impact of turbulent transfers on the hydrodynamic pattern of flow
- The impact of statistical, turbulent fluctuations on nucleation and condensation

The former is thought more consequential than the latter [36], thus much of the research in this area has focused on how turbulence affects a condensing steam flow field rather than how statistical fluctuations of, say, steam pressure and temperature might secondarily impact nucleation and condensation. Turbulence modeling for condensing steam flow is usually limited to a two-equation approach, typically a modified k - ϵ formulation which retains special source/sink terms for dispersed phase effects. A third equation for dispersed phase turbulence kinetic energy is sometimes added [37] if inter-phase slip (dispersed phase velocity) is not neglected. Some basic concepts of two-equation turbulence modeling are reviewed below as are the special modifications necessary for application to compressible condensing steam flow. The realizable k - ϵ two-layer all y^+ model as it applies in STAR-CCM+ will be presented in a subsequent section.

5.5.1 Two-Equation k - ϵ Turbulence Modeling Concepts

A detailed discussion of fundamental turbulence concepts is omitted here, but the reader is referred to textbooks such as [38], [39], and [40] for proper introductions to turbulence theory. Every type of k - ϵ formulation seeks to address the closure problem of turbulence introduced upon Reynolds averaging of the non-linear Navier-Stokes equations. To solve for the mean turbulent flow, one requires a set of closures for Reynolds stresses that arise because of turbulent velocity fluctuations. These closures should describe how Reynolds stresses relate to mean flow strain (mean flow velocity gradients or the mean flow strain rate tensor). The k - ϵ formulations use the Boussinesq eddy viscosity approximation to correlate Reynolds stresses and mean flow velocity gradients. Thus, the turbulent stresses assume the mathematical form of a molecular stress.

An expression is required for the turbulent viscosity which is the constant of proportionality between the Reynolds stress tensor and the strain rate tensor (consisting of mean flow velocity gradients). The k - ϵ approach follows Prandtl's proposal of connecting the turbulent viscosity to a characteristic velocity scale of turbulence via the specific turbulence kinetic energy. This obviates the need for a mixing length approximation but assumes some method to compute turbulence kinetic energy is available. The trace of the Reynolds stress tensor is proportional to specific turbulence kinetic energy [39]. A transport equation for the Reynolds stress can be obtained – see [39] for a walk-through – by averaging the moment equation formed upon multiplying the Navier-Stokes equation component-wise by turbulent velocity fluctuations. Taking the trace of the Reynolds stress transport equation leads to a scalar equation for turbulence kinetic energy.

A by-product of that operation is a turbulence kinetic energy sink (loss) term that is known as the turbulence energy dissipation. It measures the loss of turbulence kinetic energy (its dissipation into thermal energy) by action of viscosity. It too requires a closure of some kind. Certain so-called one-equation models make assumptions that follow purely from dimensional arguments, algebraically correlating the dissipation to turbulence kinetic energy, length scales, and fluid properties. The k - ϵ model instead proposes a scalar transport equation for the turbulence dissipation which follows from averaging of a certain moment of the Navier-Stokes equation [39].

The two scalar transport equations for turbulence kinetic energy and turbulence energy dissipation require further closures before they can be solved. The gradient transport hypothesis provides one closure and posits that turbulent Reynolds stress is proportional to mean flow velocity gradients. Another gradient transport closure is enforced on the so-called turbulent transport and pressure diffusion terms, thus defining:

- a triple correlation among fluctuating velocity components, and
- a correlation between fluctuating pressure and fluctuating velocity

Further closures involve approximations to certain terms in the kinetic energy and dissipation equations that include tuning constants. Thus, the model must be calibrated via experiments or with some other strategy.

There are actually eight different types of k - ϵ model available in STAR-CCM+ including a few varieties of the so-called standard k - ϵ formulation. It is left to the user to decide which form is most appropriate for a given application, but there are general guidelines [11] that aid the user in weighing the various trade-offs. One particularly

attractive alternative is the so-called “realizable, two-layer $k-\varepsilon$ ” model which can be combined with an all- y^+ wall treatment. Subsequent paragraphs expound on the three aspects of this particular turbulence model: realizable, two-layer, and all- y^+ . These explanations are drawn from the STAR-CCM+ users’ guide [11] which has references to original papers.

The term “realizable” indicates certain augmentations to the standard model that make the mathematics more consistent with empirically-observed physics of turbulence. Specifically, a different turbulence energy dissipation equation is employed. Also, one particular model coefficient assumed constant in the standard model is instead made a function of mean flow and turbulence properties.

The term “two-layer” refers to a scheme that makes the $k-\varepsilon$ model applicable in the viscous sub-layer of a turbulent boundary layer (near a wall). A wall function approach to near-wall modeling is rendered unnecessary because, in the computational cell nearest the wall, both the dissipation and turbulent viscosity assume a functional dependence on wall distance while the normal transport equation for turbulence kinetic energy is solved. In computational cells farther from the wall, the full complement of $k-\varepsilon$ transport equations is solved. There is then a blending between the near-wall layer and the outer layers. There are different prescriptions for near-wall dissipation and turbulent viscosity as well as for the blending method. With respect to two-layer models, STAR-CCM+ has two slightly different shear-driven flow formulations and one buoyancy-driven flow formulation.

The term “all- y^+ ” refers to a hybrid treatment that compromises between low- y^+ (the mesh is fine enough to resolve the near-wall viscous sublayer) and high- y^+ (the mesh

is coarse and wall laws are used to represent near-wall regions). All y^+ treatment attempts to duplicate low- y^+ results when the mesh is fine and high- y^+ results when the mesh is coarse. It also gives reasonable results when the mesh is somewhere between low and high y^+ . The all- y^+ model provides an expression for u^* (friction velocity) near the wall and also affects the turbulence kinetic energy production term in the near-wall layer. Furthermore, when combined with the two-layer scheme a special algebraic prescription for near-wall dissipation is used.

5.5.2 Turbulent, Compressible, Condensing Steam Flow

Modifications have been proposed to a certain term in the turbulence kinetic energy transport equation that increases its predictive accuracy for compressible flows. Wilcox notes [39], for example, that the stand-alone k - ϵ model without compressibility modifications cannot predict the experimentally-observed decrease in spreading rate for a compressible mixing layer. The turbulence kinetic energy sink (dissipation) term proposed by Sarkar is targeted at correcting just this defect. While it is demonstrably imperfect in some respects [39], the Sarkar compressibility modification is adopted in STAR-CCM+ for purposes of computing the so-called dilation dissipation term in the turbulence kinetic energy equation. This term comes from an expansion of the turbulence kinetic energy dissipation term into two parts: solenoidal dissipation related to fluctuating vorticity and dilation dissipation related to divergence of fluctuating vorticity. The dilation part, nonzero only for compressible flows, is taken as proportional to the turbulent Mach number and the solenoidal dissipation. The equality is substituted into the turbulence

kinetic energy equation, completing the compressibility treatment in either the standard or the realizable k - ϵ model.

The dispersed droplet phase present in condensing steam flow will influence continuous phase turbulence kinetic energy and dissipation. In the literature (e.g. [36], [37]) the influence of droplets and nucleation is treated via source terms. The turbulence kinetic energy source/sink term accounts for:

- Turbulence modulation due to the presence of droplets, and
- Loss of steam phase turbulence kinetic energy due to nucleation.

The turbulence energy dissipation source/sink term is typically assumed proportional to the kinetic energy source/sink term according to time scaling arguments [41]. Turbulence modulation refers to any effect a dispersed particle/droplet phase has on the turbulence of its carrier phase. Several categories of such effects have been observed empirically [41]:

- Surface effects
- Loading effects (dispersed phase concentration including fluid displacement)
- Inertial effects (related to the relative Reynolds number of drops/particles)
- Response effects (droplet response/relaxation time, Stokes number, etc.)
- Interaction effects (particle-particle and/or particle-wall effects)
- Enhanced turbulence dissipation due to drop/particle presence
- Extra turbulence kinetic energy transfer due to drop/particle presence
- Effects due to wakes of moving drops/particles

Experimentally, such effects manifest themselves in the turbulence statistics of the continuous phase, as they are altered relative to the case of single-phase flow. For the dilute, dispersed two-phase condensing steam flow, some of the effects listed above are in play. Namely, the steam turbulence kinetic energy is modulated by additional dissipation due to droplet presence. Also, nucleation and condensation (essentially a mass transfer from steam phase to droplet phase) will cost the steam turbulence some of its specific kinetic energy and some of its dissipation.

Turbulence modulation due to droplet presence is not modeled in these studies, though they possibly could be following the example in [36]. Here, the authors appeal to a Lagrangian stochastic model of turbulent dispersion to characterize a coefficient of droplet response to turbulent steam velocity fluctuations. Sawford's Lagrangian stochastic model [42] considers Lagrangian position, velocity, and acceleration to be collectively Markovian. More specifically, memory effects are neglected at the 0th order but encapsulated by two time-scales at the 1st and 2nd order. The 1st order time scale characterizes the energy-containing scales and the 2nd order time scale is the familiar Kolmogorov time scale which characterizes the dissipative scales. To fully understand the methods [42], a working knowledge of turbulence statistics, e.g. as presented in [38] is required. Results from [42] are borrowed [36] to formulate a steam turbulence kinetic energy dissipation term (appearing in the turbulence kinetic energy equation as a source term) which describes a modulation effect – more specifically a response effect – of the condensed droplets. The dispersed droplets impact steam turbulence kinetic energy dissipation but are themselves impacted by steam turbulent dispersion. Such effects are

accounted for by this method, and it would be particularly attractive for RCIC turbine CMFD modeling because it does not require computation of phase slip as other methods do, e.g. the k - ϵ - k_p model from [37]. Instead, the only turbulence kinetic energy and turbulence dissipation source terms in this study are those corresponding to phase change.

5.6 Full Pseudo Two-Fluid Formulation for Condensing Steam Flow

5.6.1 Coupled Flow Model

Conservation equations for the steam phase are solved via the coupled flow model in STAR-CCM+. These equations in their general integro-differential form are first presented. Then, the particular equations for the condensing steam flow problem at hand are reviewed. Add-ons to the coupled flow model such as the passive scalar model and user-defined sources were discussed in section 3.

The general coupled flow conservation equations for an infinitesimal control volume dV with differential surface area dA in integro-differential operator form are:

$$(5.40) \quad \frac{\partial}{\partial t} \int_V \vec{W} dV + \oint_A (\vec{F} - \vec{G}) * (d\vec{A}) = \int_V \vec{H} dV$$

Where:

$$\vec{W} = \begin{cases} \rho \\ \rho \vec{u} \\ \rho E \end{cases} \text{ a vector of dependent variables (density and flux variables)}$$

$$\vec{F} = \begin{cases} \rho(\vec{u} - \vec{u}_{grid}) \\ (\rho(\vec{u} - \vec{u}_{grid}) X \vec{u}) + P\vec{I} \\ (\rho(\vec{u} - \vec{u}_{grid})H) + P\vec{u} \end{cases} \text{ a vector of convective fluxes and pressure terms}$$

$$\vec{G} = \begin{cases} 0 \\ \vec{T} \\ \vec{T} * \vec{u} + \vec{q}'' \end{cases} \text{ a vector of molecular fluxes}$$

$$\vec{H} = \begin{cases} S_m \\ \vec{f}_r + \vec{f}_g + \vec{f}_p + \vec{f}_u + \vec{f}_\omega + \vec{f}_L \\ S_e \end{cases} \text{ a vector of various source terms}$$

E = total specific energy [J/kg] ; P = pressure [Pa] ; \vec{I} = Identity tensor

$$H = E + \frac{P}{\rho_{stm}} = h + \frac{|\vec{u}|^2}{2} = C_p T + \frac{|\vec{u}|^2}{2} = \text{Total specific enthalpy [J/kg]}$$

\vec{T} = viscous stress tensor [Pa] ; $\vec{q}'' = -k\nabla T$ = Heat flux vector [W/m²]

S_m = Mass source term ; S_e = Energy source term

\vec{f}_x , $x = r, g, p, u, w, L$ are various momentum source terms

The major assumptions of the physics model presented here are:

- Droplet phase is represented by passive scalar transport equations
- The droplet volume fraction is negligibly small
- Mechanical equilibrium (no slip) between the steam and any droplets evolved
- Droplet temperature follows from capillarity considerations (Gyarmathy [23])
- Classical nucleation theory (with corrections) applies

- Process of steam/droplet heat and mass exchange is simplified, e.g. no droplet energy storage or internal heat transfer
- Two-layer, all y+, realizable k-epsilon turbulence model

The specialized continuity, momentum, and energy equations in integro-differential form for the continuous steam phase in the RCIC turbine CMFD model are:

$$(5.41) \quad \frac{\partial}{\partial t} \int_V \rho_{stm} dV + \oint_A \rho_{stm} (\bar{\mathbf{u}} * d\bar{\mathbf{A}}) = \int_V S_m dV$$

$$(5.42) \quad \frac{\partial}{\partial t} \int_V \rho_{stm} \bar{\mathbf{u}} dV + \oint_A [\rho_g (\bar{\mathbf{u}} \times \bar{\mathbf{u}}) + P\bar{\mathbf{I}} - \bar{\mathbf{T}}] * d\bar{\mathbf{A}} = \int_V \bar{\mathbf{S}}_u dV$$

$$(5.43) \quad \frac{\partial}{\partial t} \int_V \rho_{stm} \left(h_{stm} + \frac{|\bar{\mathbf{u}}|^2}{2} - \frac{P}{\rho_{stm}} \right) dV +$$

$$\oint_A \left[\rho_{stm} \bar{\mathbf{u}} \left(h_{stm} + \frac{|\bar{\mathbf{u}}|^2}{2} \right) - (\bar{\mathbf{T}} * \bar{\mathbf{u}}) + \bar{\mathbf{q}}'' \right] * d\bar{\mathbf{A}}$$

$$= \int_V S_e dV$$

The droplet phase equations (reproduced below) are:

$$(5.44) \quad \frac{\partial}{\partial t} (\rho_{stm} \mu_0) + \bar{\mathbf{V}} * (\rho_{stm} \mu_0 \bar{\mathbf{u}}) = \rho_{stm} J_*$$

$$(5.45) \quad \frac{\partial}{\partial t} (\rho_{stm} \mu_1) + \bar{\mathbf{V}} * (\rho_{stm} \mu_1 \bar{\mathbf{u}}) = \rho_{stm} (G \mu_0 + J_* r^*)$$

$$(5.46) \quad \frac{\partial}{\partial t} (\rho_{stm} \mu_2) + \vec{\nabla} * (\rho_{stm} \mu_2 \vec{u}) = \rho_{stm} (2G \mu_1 + J_* r^{*2})$$

$$(5.47) \quad \frac{\partial}{\partial t} (\rho_{stm} \mu_3) + \vec{\nabla} * (\rho_{stm} \mu_3 \vec{u}) = \rho_{stm} (3G \mu_2 + J_* r^{*3})$$

Interphase transfer terms G , S_m , \vec{S}_u , S_e remain to be specified. Note also that $\rho_{stm} J_*$ equals J . One possible expression for a constant condensation growth rate was already presented and is reproduced here:

$$(5.48) \quad \frac{dr}{dt} = G = \left(\frac{k_{stm}}{\rho_{liq}(T_{stm})h_{fg}(P)} \right) \left(\frac{1 - \frac{r^*}{r}}{r + 1.59\ell} \right) ((T_{sat}|_P - T_{stm}))$$

The mass, momentum, and energy source terms will contain nucleation and condensation parts in general. The steam mass source term is negative when nucleation and condensation occur and can be written as:

$$(5.49) \quad S_m = -\frac{4}{3}\pi r^{*3} \rho_{liq}|_{T_{stm}} J - 4\pi \left(\frac{D_{32}}{2} \right)^2 \rho_{liq}|_{T_{stm}} N G$$

The steam momentum source is negative when nucleation and condensation occur and can be written as:

$$(5.50) \quad \vec{S}_u = (\vec{u}S_m) + (\vec{v}S_m) + (\vec{k}S_m)$$

Where:

$\vec{u}, \vec{v}, \vec{k}$ are Cartesian components of the steam velocity vector

The steam energy source is negative when nucleation and condensation occur:

$$(5.51) \quad S_e = -S_m h_{fg}(P)$$

Where:

$h_{fg}(P)$ is latent heat of vaporization at steam pressure P

Combining equations (5.41 through (5.51 with the turbulence model presented in the next section completes the coupled flow, pseudo two-fluid formulation.

5.6.2 Realizable k - ϵ Two-Layer All- y^+

The full set of realizable k - ϵ two-layer all- y^+ equations with terms for compressibility effects and dispersed-phase effects is presented below in integro-differential form. The transport equations are taken directly from [11] and the turbulence modulation source terms are taken from [36] and [37]. Note the transport equations are for turbulence kinetic energy and dissipation in the steam phase exclusively. There is no modeling of dispersed phase turbulence parameters.

The steam turbulence kinetic energy transport equation is:

$$(5.52) \quad \frac{\partial}{\partial t} \int_V \rho_{stm} k dV + \oint_A \rho_{stm} k \left((\vec{u} - \vec{u}_{grid}) * d\vec{A} \right) =$$

$$\oint_A \left(\mu_{stm} + \frac{\mu_t}{\sigma_k} \right) (\vec{\nabla} k * d\vec{A}) +$$

$$\int_V (f_c G_k + G_b - \rho_{stm} ((\epsilon - \epsilon_0) + Y_M) + S_k) dV$$

Where:

k = Turbulent kinetic energy [J/kg] ; \vec{u}_{grid} = Grid velocity [m/s]

μ_t = Turbulent viscosity [Pa*s] ; σ_k = Turbulent Prantl number

f_c = Curvature factor ; G_k = Production source term for k

G_b = Buoyancy production source term for k

ϵ = Turbulence dissipation rate [J/kg/s] ; ϵ_0 = Ambient turbulence value

Y_M = Dilation dissipation ; S_k = Miscellaneous source term for k

The steam turbulence dissipation rate transport equation is:

$$(5.53) \quad \frac{\partial}{\partial t} \int_V \rho_{stm} \epsilon dV + \oint_A \rho_{stm} \epsilon \left((\bar{\mathbf{u}} - \bar{\mathbf{u}}_{grid}) * d\bar{\mathbf{A}} \right) =$$

$$\oint_A \left(\mu_{stm} + \frac{\mu_t}{\sigma_\epsilon} \right) (\nabla \epsilon * d\bar{\mathbf{A}}) +$$

$$\int_V \left(f_c C_{\epsilon 1} S_\epsilon + \frac{\epsilon}{k} (C_{\epsilon 1} C_{\epsilon 3} G_b) - \left(\frac{\epsilon}{k + \sqrt{\nu_{stm} \epsilon}} \right) (C_{\epsilon 2} \rho_{stm} (\epsilon - \epsilon_0) + S_\epsilon) \right) dV$$

Where:

$$S_\epsilon = \text{Miscellaneous source term for } \epsilon \quad ; \quad \nu_{stm} = \frac{\mu_{stm}}{\rho_{stm}}$$

$\sigma_\epsilon, C_{\epsilon 1}, C_{\epsilon 3}, C_{\epsilon 2}$ are model coefficients

The various closures needed for the two transport equations include the turbulence production term, the buoyancy production term, the dilation dissipation (compressibility modification) term, and the turbulent viscosity expression. The model closure coefficients must also be specified. All closures are discussed in turn. The turbulence production term representing the rate at which kinetic energy is transferred to the turbulence from mean flow (an interaction between mean flow strain rate and turbulent stresses) is:

$$(5.54) \quad G_k = \mu_t S^2 - \frac{2}{3} \rho_{stm} k (\nabla * \bar{\mathbf{u}}) - \frac{2}{3} \mu_t (\nabla * \bar{\mathbf{u}})^2$$

Where:

$$S = |\bar{S}| = \sqrt{2\bar{S}:\bar{S}}; \bar{S} = \frac{1}{2}(\nabla\vec{u} + \nabla\vec{u}^T), \text{ for } S \text{ the strain rate tensor}$$

The buoyancy production term is:

$$(5.55) \quad G_b = \beta \frac{\mu_t}{\sigma_t} (\nabla T * \vec{g})$$

Where:

β = thermal expansion coefficient

The dilation dissipation term proposed by Sarkar [39] is:

$$(5.56) \quad Y_M = \frac{2k\epsilon}{c^2}$$

Where:

c is the speed of sound in steam (from equation-of-state prescription)

The turbulent viscosity assumes the form of:

$$(5.57) \quad \mu_t = \rho_{stm} C_\mu \frac{k^2}{\epsilon}$$

Where:

$$C_\mu = 1/A_0 + A_s U^{(*)} \frac{k}{\epsilon} ; U^{(*)} = \sqrt{\bar{S}:\bar{S} + \bar{W}:\bar{W}} ; \bar{W} = \frac{1}{2}(\nabla\bar{u} - \nabla\bar{u}^T)$$

$$\bar{W} \text{ is the rotation rate tensor ; } A_0 = 4.0 ; A_s = \sqrt{6}\cos(\phi)$$

$$\phi = \frac{1}{3} \arccos(\sqrt{6}W) ; W = \frac{S_{ij}S_{jk}S_{ki}}{(\sqrt{S_{ij}S_{ij}})^3} \text{ and } S = |\bar{S}|$$

$$C_{\epsilon 1} = \max\left(0.43, \frac{\eta}{5+\eta}\right) ; \eta = \frac{Sk}{\epsilon} ; C_{\epsilon 2} = 1.9 ; \sigma_k = 1.0 ; \sigma_\epsilon = 1.2$$

The turbulence kinetic energy equation is solved everywhere in the two-layer approach. However, the near-wall layer has special prescriptions for turbulent viscosity, dissipation, and turbulence kinetic energy production. The two-layer approach coupled with an all- y^+ wall treatment aims to blend the one-equation near-wall layer treatment with the normal two-equation treatment elsewhere. Blending is done for the dissipation and turbulence kinetic energy production. The turbulent viscosity depends on a length scale function and a wall proximity indicator. Also, the near-wall layer dissipation depends on the length scale function.

The length scale function and turbulent viscosity ratio in general look like:

$$(5.58) \quad l_\epsilon = f(y, Re_y)$$

$$(5.59) \quad \frac{\mu_t}{\mu_{stm}} = f(Re_y)$$

There are different prescriptions for the length scale function and the turbulent viscosity ratio, but all correlations are written in terms of a wall-distance (y) Reynolds number:

$$(5.60) \quad Re_y = \frac{\sqrt{k}y}{\nu_{stm}}$$

Additionally, all correlations have the same algebraic dissipation equation:

$$(5.61) \quad \epsilon = \frac{k^{3/2}}{l_\epsilon}$$

For all correlations of length scale function and turbulent viscosity ratio, the layer blending depends on a wall proximity indicator:

$$(5.62) \quad \lambda = \frac{1}{2} \left[1 + \tanh \left(\frac{Re_y - Re_y^*}{A} \right) \right]$$

Where:

$$Re_y^* = 60 \quad ; \quad A = |\Delta Re_y| / \operatorname{atanh}(0.98) \quad ; \quad \Delta Re_y = 10$$

Such that the blended turbulent viscosity is expressed as:

$$(5.63) \quad \mu_t = \lambda \mu_{t_{k-\epsilon}} + (1 - \lambda) \mu \left(\frac{\mu_t}{\mu} \right)_{2-layer}$$

Where:

$$\mu_{t_{k-\epsilon}} = \text{Realizable } k-\epsilon \text{ turbulent viscosity}$$

The remainder of the two-layer model formulation depends on the choice of either the Norris-Reynolds or the Wolfstein models. Neither is clearly preferable over the other [11]. Norris-Reynolds length scale function and turbulent viscosity is:

$$(5.64) \quad l_{\epsilon}(Re_y, y) = \frac{C_l Re_y y}{Re_y + C_{\epsilon}}$$

Where:

$$C_{\epsilon} = 5.3 \quad ; \quad C_l = k C_{\mu}^{-3/4} \quad ; \quad k = 0.42$$

$$(5.65) \quad \frac{\mu_t}{\mu}(Re_y) = Re_y k C_{\mu}^{1/4} \left[1 - \exp\left(\frac{-Re_y}{A_{\mu}}\right) \right]$$

Where:

$$A_{\mu} = 50.5$$

As for the kinetic energy production blending and the dissipation blending, it is accomplished via a blending function:

$$(5.66) \quad g = \exp\left(\frac{-Re_y}{11}\right)$$

Then, the friction velocity (u^*), near-wall cell turbulence energy production (G_k), and near-wall cell dissipation (ϵ), can be expressed in terms of the blending function:

$$(5.67) \quad u^* = \sqrt{\frac{g\nu_{stm}u}{y} + (1-g)C_\mu^{1/2}k}$$

$$(5.68) \quad G_k = g\mu_t S^2 + (1-g)\frac{1}{\mu_{stm}}\left(\rho u^* \frac{u}{u^*}\right)^2 \frac{\partial u^+}{\partial y^+}$$

$$(5.69) \quad \epsilon = g\frac{2\nu_{stm}k}{y^2} + \frac{k^{3/2}}{l_\epsilon}$$

Where:

u^+ is wall-parallel velocity, non-dimensionalized with u^*

y^+ is non-dimensional wall distance (from near-wall cell centroid)

5.7 Ideal Gas Formulation

For certain simulations, air is used as a working fluid. The ideal gas approximation applies as the equation of state describing density, temperature, and pressure:

$$(5.70) \quad \rho = P_{abs}/RT$$

Where:

P_{abs} = Absolute pressure [Pa] ; T = Absolute temperature [K] ; $R = R_u/M$

$R_u = 8.3144621$ [J/mol/K] ; M = Molecular weight [g/mol]

6 SYSTEMS-LEVEL MODEL DEVELOPMENT AND IMPLEMENTATION

6.1 Homologous Pump Model

A homologous pump model was integrated into the MELCOR flow path (FL) package to predict the attending fluid momentum source (pressure head) of a centrifugal pump as a function of the pump impeller speed and the pump capacity (volumetric flow). This addition to MELCOR increases light water reactor modeling capability in general and RCIC system modeling in specific as a more mechanistic model of pump performance is available. The model also computes hydraulic torque (indicative of the brake power), pump friction torque, pump inertia, and pump energy dissipation (and thus efficiency). The homologous pump performance model therefore predicts the “brake power” (proportional to hydraulic torque) and the “hydraulic power” (proportional to the product of head and flow), with the difference between the two being the pump dissipation energy. Pump inefficiencies are “baked-in” to the pump performance model, but user input of rated conditions can account for extra inefficiencies if necessary.

The new MELCOR homologous pump model is similar to that of RELAP [43] but with some distinguishing features including a polar homologous pump curve representation and a “universal correlation” as discussed in a later section. Several new MELGEN input records have been added that, in general, allow the user to fully specify:

1. Rated pump conditions,
2. Single/two-phase pump performance via homologous curve input,
3. Pump friction torque as a polynomial in pump speed ω , or rather the non-dimensional ratio $|\omega/\omega_R|$ with ω_R the rated pump speed,

4. Pump inertia as a polynomial in the quantity $|\omega/\omega_R|$,
5. Pump speed and motor torque controls,
6. Pump trips,
7. Pump numerical treatment options

Additionally, pump data from both the Semiscale [44] and Loft [45] experiments are available as “built-in” performance modeling options. A “universal correlation” [46] is included. These features are described below.

6.1.1 Conventional Homologous Pump Representation

The essential goal of the homologous pump model is to characterize centrifugal pump performance by predicting the pressure head (ΔP) and the hydraulic torque (τ_H) given inputs of impeller speed (i.e. pump speed) ω and pump capacity (volumetric flow rate) Q . Empirical homologous curves are one way of compactly summarizing pump performance in response to given conditions ω, Q . In this representation, non-dimensional ratios α and ν are formed as:

$$(6.1) \quad \alpha = \frac{\omega}{\omega_R}$$

$$(6.2) \quad \nu = \frac{Q}{Q_R}$$

Where:

ω_R, Q_R are rated pump impeller speed and rated pump capacity (volumetric flow)

Homologous ratios α/ν and ν/α are formed from the non-dimensional ratios. The entire domain of pump operation (4 modes) is covered by an independent variable space:

- $\left| \frac{\nu}{\alpha} \right| \leq 1$, then in the “ α range” of the independent variable space
- $\left| \frac{\alpha}{\nu} \right| < 1$, then in the “ ν range” of the independent variable space

These homologous ratios become the independent variables for the homologous curve dependent variables which include single-phase pump head, single-phase hydraulic torque, fully-degraded pump head, and fully-degraded hydraulic torque. For each dependent variable, a plot can be created that traces out 4 possible operating mode curves, each with 2 pieces (called octants): the α range piece and the ν range piece. Thus, a homologous curve for a given dependent variable consists of 8 octants each representing different combinations of pump speed (≥ 0 or < 0) and capacity (≥ 0 or < 0). When ω and Q are such that $|\nu/\alpha|$ is less than or equal to 1, this indicates pump operation in the ν range of the current mode, and as soon as ν grows large enough that $|\nu/\alpha|$ would exceed 1, the independent variable is changed to $|\alpha/\nu|$ such that pump operation enters the α range of the current mode. Therefore, the magnitude of the independent variable is never greater than 1 and is bounded by $[-1, 1]$. Note that α and ν ranges deal exclusively with non-dimensional pump speed/capacity magnitudes and their ratios. The pump modes account for the 4 possible combinations of negative/positive speed and negative/positive capacity. The modes are summarized in Table 6.1 below.

Table 6.1 Possible pump operating modes

Plot Quadrant	Non-dimensional Speed/Capacity	Mode Identifier
1 st (upper right)	$\alpha \geq 0$ and $v \geq 0$	Normal (N)
2 nd (Upper Left)	$\alpha > 0$ and $v < 0$	Dissipation (D)
3 rd (Lower Left)	$\alpha \leq 0$ and $v \leq 0$	Turbine (T)
4 th (Lower Right)	$\alpha < 0$ and $v > 0$	Reversal (R)

Note that the possibility of negative speed and negative capacity requires the independent variable to cross the zero value. The dependent variable also changes depending on the range (α or v) in question. In the homologous formulation, non-dimensional values for pump head and hydraulic torque are:

$$(6.3) \quad h = \frac{H}{H_R}$$

$$(6.4) \quad t = \frac{\tau_H}{\tau_{H,R}}$$

Where:

$H_R, \tau_{H,R}$ are rated head and rated hydraulic torque

Furthermore, these quantities are divided by either α^2 or v^2 depending upon the range (α or v). An example of the final form for a homologous curve is shown in Figure 6.1. Note that Appendix A contains all Semiscale [44] and Loft [45] homologous pump curves.

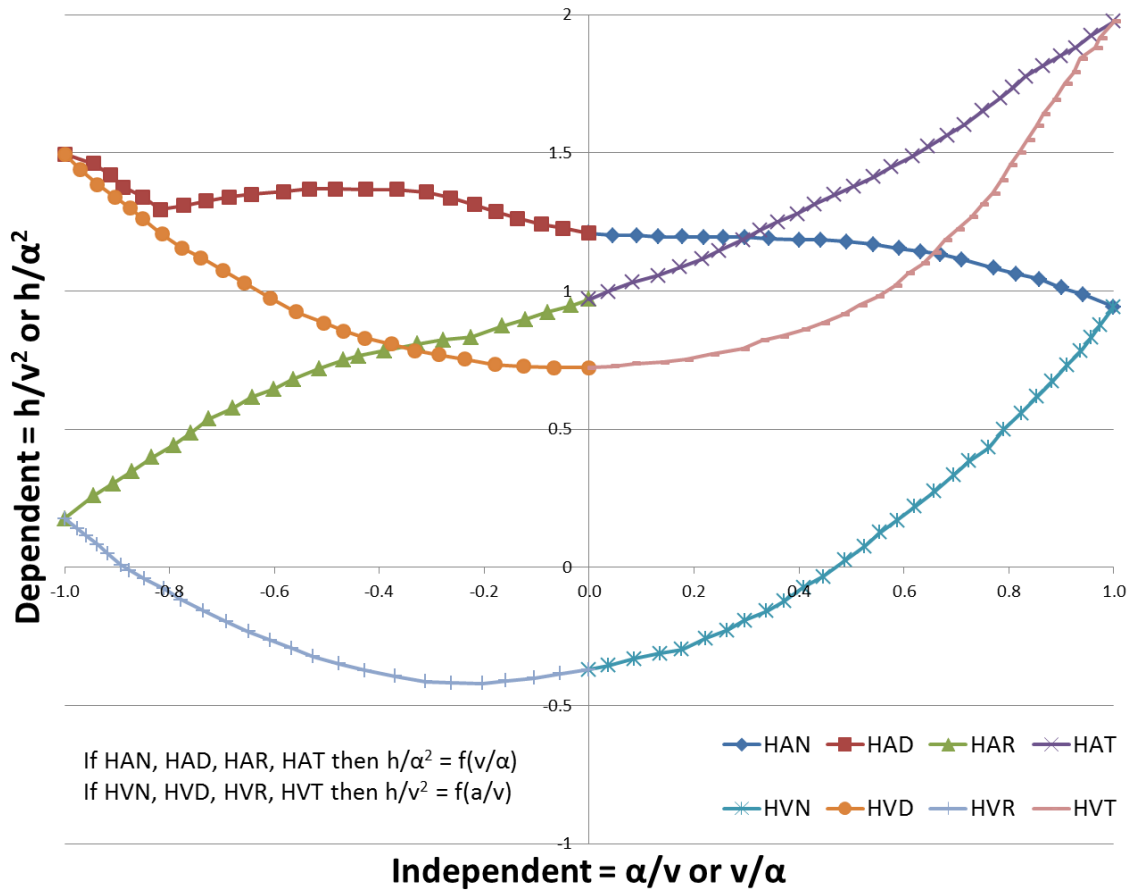


Figure 6.1 Semiscale single-phase head curve [44]

Note that a system of three-letter octant identifiers is used. Each octant identifier indicates at once the dependent variable, the independent variable, and the pump mode. The general identifier is $[H/B][A/V][N/D/T/R]$, where the first $[]$ denotes head (H)/torque (B), the

second [] denotes α range (A) or v range (V), and the third [] denotes normal (N)/dissipation (D)/turbine (T)/reversal (R).

6.1.2 Polar Homologous Pump Representation

For several reasons related to programming convenience, MELCOR internally employs the so-called polar homologous representation ([47], [48]) of pump performance. It bears some resemblance to the conventional homologous method, but uses different variable definitions such that the independent variable is always positive and bounded on $[0, 2\pi]$. The variable transformation allows all octants to be ordered in monotonically-increasing fashion with respect to a single independent variable. This obviously simplifies data interpolation logic, since with the homologous data representation a total of 8 separate data tables (one per octant) are used. Essentially, the polar homologous variable transformation results in one independent variable and one dependent variable.

The polar homologous representation is identical to the homologous representation until the point where independent and dependent variables are chosen. The new independent variable is:

$$(6.5) \quad x = C + \tan^{-1} \left(\frac{\alpha}{v} \right)$$

Where:

α, v are defined as before for the conventional homologous pump representation

The constant C assumes different values depending upon the mode of pump operation. Regardless of the negative/positive sign of speed or capacity, the argument of the inverse tangent function does not change. Some useful properties of the inverse tangent function:

- Defined for an argument equal to zero
- Bounded ($\pm \pi/2$) as its argument goes to infinity on either side of zero

One could foresee a problem if capacity and hence v equals zero, but in fact the division by zero can simply be treated as a case of the argument α/v approaching $\pm \infty$. The homologous octants, under this definition of x , are arranged in a predictable way on $[0, 2\pi]$ as summarized in Table 6.2.

Table 6.2 Octant arrangement under the polar homologous representation

Octant Identifier (C Value)	Portion of Domain on $[0, 2\pi]$
[H/B]VN (0)	$[0, \pi/4]$
[H/B]AN (0)	$[\pi/4, \pi/2]$
[H/B]AD (π)	$[\pi/2, 3\pi/4]$
[H/B]VD (π)	$[3\pi/4, \pi]$
[H/B]VT (π)	$[\pi, 5\pi/4]$
[H/B]AT (π)	$[5\pi/4, 3\pi/2]$
[H/B]AR (2π)	$[3\pi/2, 7\pi/4]$
[H/B]VR (2π)	$[7\pi/4, 2\pi]$

The dependent variables (head and torque functions, WH and WT) are:

$$(6.6) \quad WH = \left(\frac{h}{\alpha^2} \mid \frac{h}{v^2} \right) / \left(\mathbf{1} + \left(\left(\frac{v}{\alpha} \right)^2 \mid \left(\frac{\alpha}{v} \right)^2 \right) \right)$$

$$(6.7) \quad WT = \left(\frac{t}{\alpha^2} \mid \frac{t}{v^2} \right) / \left(\mathbf{1} + \left(\left(\frac{v}{\alpha} \right)^2 \mid \left(\frac{\alpha}{v} \right)^2 \right) \right)$$

Where:

h, t, α, v are defined as before under

(|) a decision where left and right correspond to α range and v range, respectively

One observes that WH, for example, is readily obtained from data pairs corresponding to any given octant, e.g. HAN where the homologous data pairs are ($v/\alpha, h/\alpha^2$). Thus, there is no need for extra programming logic as the data pairs of each octant can be substituted into the WH and WT equations directly. After converting independent and dependent variables into polar homologous form, new plots (encapsulating the very same information) can be created. An example is shown in Figure 6.2 and may be compared to Figure 6.1. Clearly Figure 6.2 is more convenient for lookups and interpolation. Appendix A contains all polar homologous plots for Semiscale and Loft data.

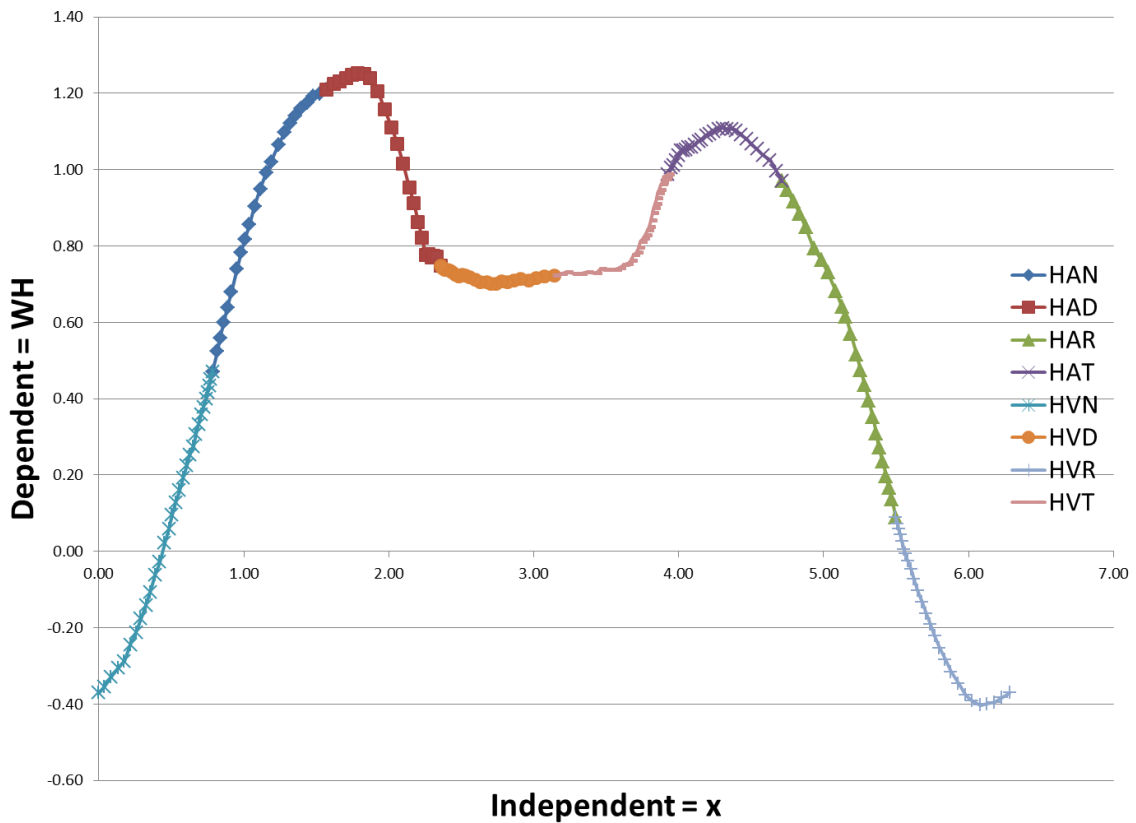


Figure 6.2 Polar homologous single-phase head curve, Semiscale

6.1.3 Universal Pump Correlation Alternative

If not enough information is known about a given centrifugal pump to furnish a full set of performance data for the homologous pump model, an alternative “universal correlation” is available that requires only the specific pump speed as an input. Based upon several data sets, head and hydraulic torque functions were derived as a function of pump specific speed for a given set of pump conditions $x(\omega, Q)$ [46]. These functions are only valid in the normal pump operating mode (x on $[0, \pi/2]$). Pump specific speed is defined, in this context, as a dimensional quantity:

$$(6.8) \quad N_s = \frac{\omega_R \sqrt{Q_R}}{H_R^{3/4}}$$

Where:

ω_R, Q_R, H_R are rated pump impeller speed, rated capacity, and rated head

Given specific speed and given pump conditions ω and Q , a double interpolation may be performed on independent variable x and dependent variable WH (WT) to recover an estimate of WH (WT) from which a dimensional head (hydraulic torque) can be recovered. Outside the normal mode and/or for two-phase considerations, the universal correlation cannot apply. The actual MELCOR implementation follows the method in [46] so that each curve of Figure 6.3 and Figure 6.4 is fitted with a 3rd order polynomial $f(N_s)$. Interpolation is done with fits rather than with raw tabular pump data. Arrays of curve fit data are included in Table 2.1 and Table 6.4. The constants A through D represent polynomial coefficients:

$$(6.9) \quad (WH|WT) = A + BN_s + CN_s^2 + DN_s^3$$

A user with knowledge only of rated conditions for a given pump may predict its performance for the normal operating mode. Semiscale and LOFT data are included in the universal correlation data set.

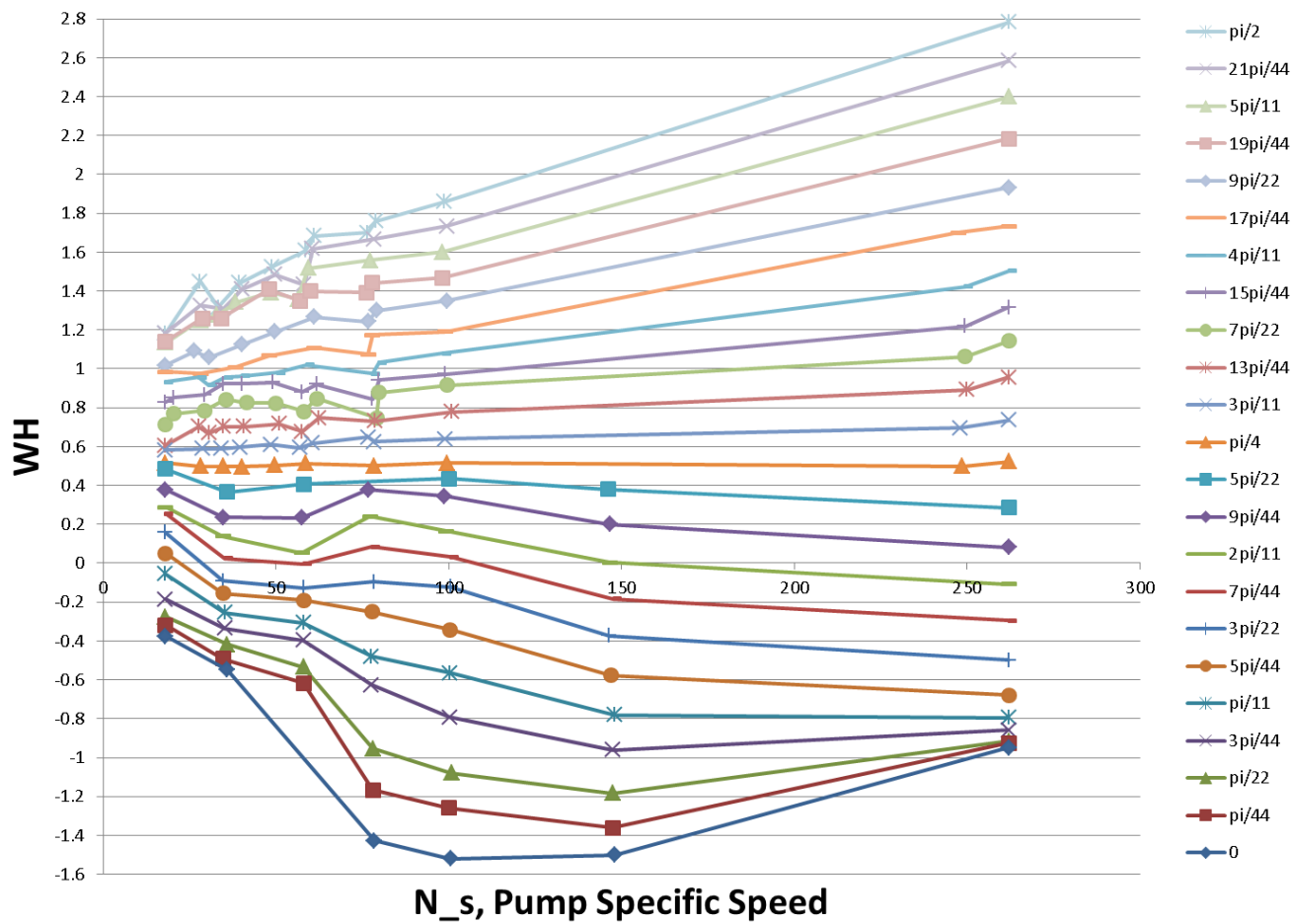


Figure 6.3 Universal correlation head function, each curve an x on $[0, \pi/2]$ [46]

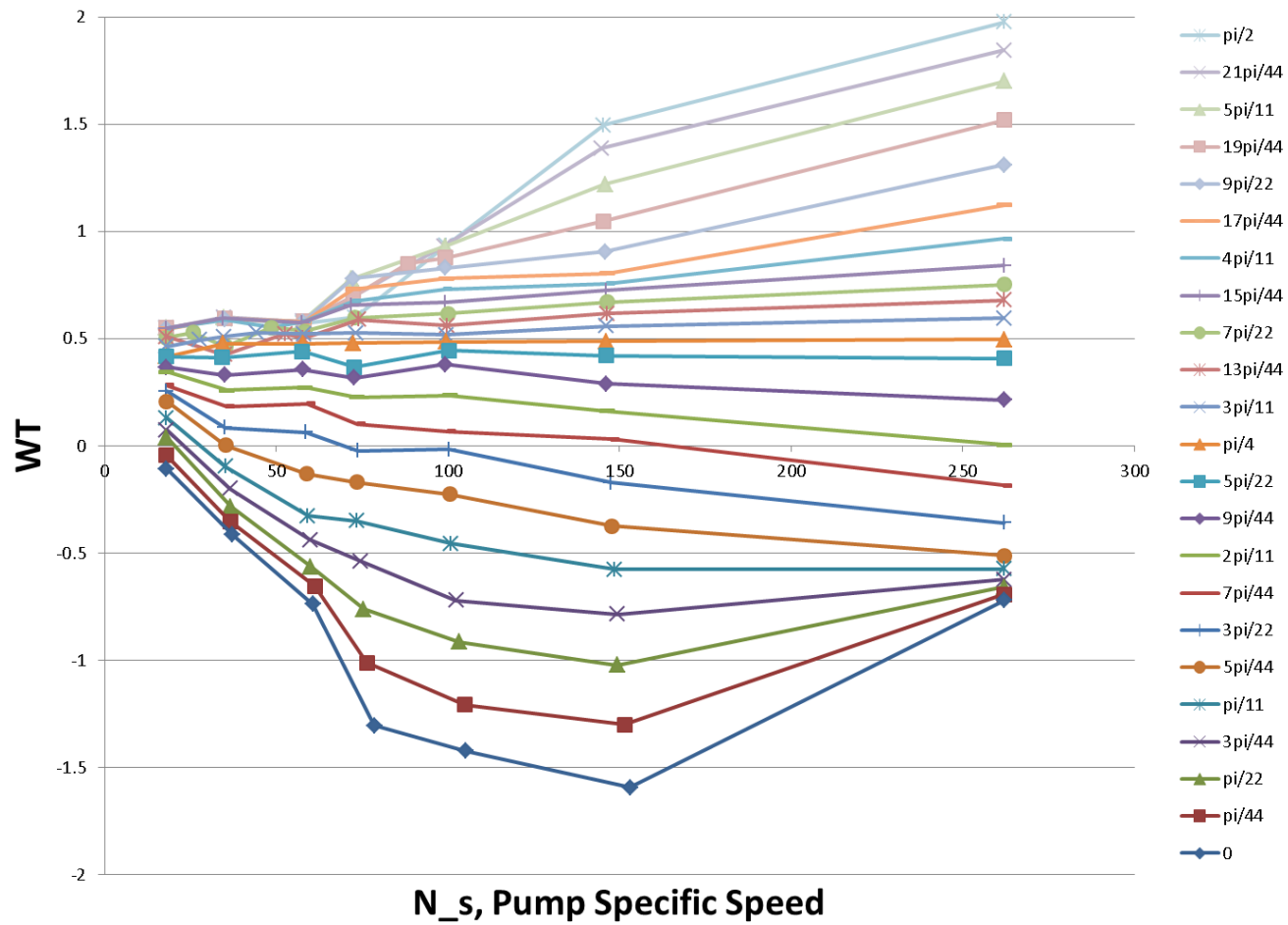


Figure 6.4 Universal correlation torque function, each curve an x value on $[0, \pi/2]$ [46]

Table 6.3 Polynomial fit data for curves in Figure 6.3

x	A	B	C	D	x	A	B	C	D
$\pi/2$	1.0946	0.0088	-9.5600E-06	0.00	$5\pi/22$	0.4515	-0.0062	0.0000E+00	0.0000E+00
$21\pi/44$	1.0855	0.0077	-8.2443E-06	0.00	$9\pi/44$	0.3630	-0.0010	0.0000E+00	0.0000E+00
$5\pi/11$	1.0813	0.0063	-5.3857E-06	0.00	$2\pi/11$	0.2595	-0.0021	7.1163E-06	-1.7401E-08
$19\pi/44$	1.0486	0.0049	-2.6536E-06	0.00	$7\pi/44$	0.2138	-0.0025	-5.8728E-07	1.0494E-08
$9\pi/22$	0.9948	0.0038	-1.0063E-06	0.00	$3\pi/22$	0.1375	-0.0038	2.6036E-06	9.2164E-09
$17\pi/44$	0.9508	0.0021	2.7905E-06	0.00	$5\pi/44$	0.1218	-0.0063	1.2390E-05	0.0000E+00
$4\pi/11$	0.9048	0.0011	4.1812E-06	0.00	$\pi/11$	0.0200	-0.0065	-2.8421E-07	4.9910E-08
$15\pi/44$	0.8508	0.0007	3.4325E-06	0.00	$3\pi/44$	-0.1975	0.0022	-1.7558E-04	1.1621E-06
$7\pi/22$	0.7454	0.0012	7.6247E-07	0.00	$\pi/22$	0.0130	-0.0143	3.8180E-05	1.0995E-08
$13\pi/44$	0.6240	0.0017	-2.1960E-06	0.00	$\pi/44$	0.0541	-0.0184	5.7827E-05	-8.7150E-09
$3\pi/11$	0.5494	0.0012	-1.9922E-06	0.00	0	0.2704	-0.0346	2.0041E-04	-3.2951E-07
$\pi/4$	0.5000	0.0000	0.0000E+00	0.00					

Table 6.4 Polynomial fit data for curves in Figure 6.4

x	A	B	C	D	x	A	B	C	D
$\pi/2$	0.3014	0.0068	-1.00E-06	0.00E+00	$5\pi/22$	0.4089	0.0002	-6.00E-07	0.00E+00
$21\pi/44$	0.3385	0.0065	-3.00E-06	0.00E+00	$9\pi/44$	0.3540	0.0000	-2.00E-06	0.00E+00
$5\pi/11$	0.3909	0.0056	-2.00E-06	0.00E+00	$2\pi/11$	0.3371	-0.0012	-3.00E-07	0.00E+00
$19\pi/44$	0.4370	0.0041	2.00E-07	0.00E+00	$7\pi/44$	0.3522	-0.0048	3.00E-05	-6.00E-08
$9\pi/22$	0.4532	0.0044	-1.00E-05	3.00E-08	$3\pi/22$	0.2704	-0.0039	6.00E-06	0.00E+00
$17\pi/44$	0.4577	0.0044	-2.00E-05	5.00E-08	$5\pi/44$	0.3547	-0.0108	6.00E-05	-1.00E-07
$4\pi/11$	0.4992	0.0021	-1.00E-06	0.00E+00	$\pi/11$	0.3614	-0.0153	8.00E-05	-1.00E-07
$15\pi/44$	0.5235	0.0016	-1.00E-06	0.00E+00	$3\pi/44$	0.3814	-0.0190	1.00E-04	-1.00E-07
$7\pi/22$	0.4573	0.0018	-3.00E-06	0.00E+00	$\pi/22$	0.4123	-0.0227	1.00E-04	-1.00E-07
$13\pi/44$	0.4382	0.0016	-3.00E-06	0.00E+00	$\pi/44$	0.3134	-0.0210	7.00E-05	0.00E+00
$3\pi/11$	0.4750	0.0007	-1.00E-06	0.00E+00	0	0.3756	-0.0257	8.00E-05	0.00E+00
$\pi/4$	0.4294	0.0008	-2.00E-06	0.00E+00					

6.1.4 Head and Hydraulic Torque

Speed and flow are used to deduce a value of the polar homologous independent variable x which can then be used to interpolate the polar homologous functions WH and WT . In general, two-phase effects must also be accounted for and x may be used to interpolate WH_2 and WT_2 . Note WH_2 and WT_2 are the two-phase (fully-degraded) head and torque functions obtained from empirical data. The void fraction (or in the case of a MELCOR flow path, the atmosphere area fraction) can be used to interpolate the so-called head and torque degradation multipliers MH and MT . These functions of void fraction are included in Appendix A. Note that the LOFT report [45] provides degradation multipliers as well. This information is used to compute overall head and torque functions:

$$(6.10) \quad \mathbf{WH}_{overall} = \mathbf{WH} - \mathbf{MH} * (\mathbf{WH} - \mathbf{WH}_2)$$

$$(6.11) \quad \mathbf{WT}_{overall} = \mathbf{WT} - \mathbf{MT} * (\mathbf{WT} - \mathbf{WT}_2)$$

Using definitions already presented, the non-dimensional head and hydraulic torque are obtained from these overall functions. The dimensional head and hydraulic torque is then:

$$(6.12) \quad \mathbf{H} = \mathbf{hH}_R$$

$$(6.13) \quad \mathbf{\tau}_H = \mathbf{t\tau}_{H,R}$$

If the user chooses an explicit numerical formulation, the pump pressure head is included as a momentum source term in the flow path phasic velocity equations (like FANA and QUICK-CF pump types in the MELCOR FL package [16]). The user may also request a semi-implicit numerical formulation for which pump head is expanded into implicit and explicit terms such that new-time phasic velocities do depend on new-time pump head terms. The details of this implementation are included in a subsequent section.

6.1.5 *Miscellaneous Pump Model Features*

6.1.5.1 *Pump Friction Torque*

The frictional torque associated with a pump is modeled as in RELAP [43] with a polynomial in the quantity $|\omega/\omega_R|$, according to:

$$(6.14) \quad \tau_{fr} = \begin{cases} \tau_{frn}, & \left| \frac{\omega}{\omega_R} \right| < S_{PF} \\ \tau_{fr0} + \tau_{fr1} \left| \frac{\omega}{\omega_R} \right|^{x1} + \tau_{fr2} \left| \frac{\omega}{\omega_R} \right|^{x2} + \tau_{fr3} \left| \frac{\omega}{\omega_R} \right|^{x3}, & \left| \frac{\omega}{\omega_R} \right| \geq S_{PF} \end{cases}$$

The user specifies each of the constants and exponents in the above equations as well as the critical speed ratio S_{PF} below which the frictional torque is constant. The sign convention is that frictional torque is negative for a positive pump speed but positive for a negative pump speed. The exponents $x1$, $x2$, and $x3$ cannot equal 0 but there are no restrictions on the torque coefficients.

6.1.5.2 Pump Moment of Inertia

The pump inertia may be variable in certain situations, so a model similar to that of frictional torque is applied. A 3rd order polynomial is written as:

$$(6.15) \quad I_p = \begin{cases} I_{pn}, & \text{for } \left| \frac{\omega}{\omega_R} \right| < S_{PI} \\ I_{P0} + I_{P1} \left| \frac{\omega}{\omega_R} \right| + I_{P2} \left| \frac{\omega}{\omega_R} \right|^2 + I_{P3} \left| \frac{\omega}{\omega_R} \right|^3, & \text{for } \left| \frac{\omega}{\omega_R} \right| \geq S_{PI} \end{cases}$$

The user may specify each polynomial coefficient but not the exponents. The pump inertia is a positive nonzero quantity and, as with friction torque, may be held constant for pump speed below a threshold.

6.1.5.3 Pump Controls: Speed, Motor Torque, Trips

Pump speed is controlled either by the user via CF or TF or by the code via solution of a torque-inertia equation. The user has three options for speed control:

1. Always specified by CF/TF,
2. Always obtained by torque-inertia equation solution, or
3. CF/TF specified until a trip indicates switchover to torque-inertia equation

Option 1 would be appropriate if, for example, some externally-imposed CF model was dictating pump speed. Option 3 would be appropriate for modeling a pump coast-down during off-normal operating conditions after some time of normal pump operation. Option 2 allows the net torque (motor torque less the sum of hydraulic and friction torque)

to determine whether pump speed increases (net positive torque), decreases (net negative torque), or stays constant (net zero torque, motor balances friction and hydraulic torques).

To model a scenario in which the pump speed can ramp up and coast down repeatedly, option 2 would allow for finer control over motor torque and hence net torque so as to drive pump speed in the desired direction. The convention for a pump motor under MELCOR TRIP CF (see [15] for a description) control is: if the TRIP CF is ON-FORWARD, motor torque is zero and if TRIP CF is ON-REVERSE motor torque is given by CF/TF. Given the motor torque/trip convention, virtually any pump shut off and restart sequence can be modeled. The torque-inertia equation is:

$$(6.16) \quad I_p \frac{d\omega}{dt} = \tau_{net} = \tau_{motor} - (\tau_H + \tau_{fr})$$

In general, the net torque has three components shown above (motor, hydraulic, friction), but the motor torque is only nonzero if:

- the pump trip has not occurred or
- a pump trip CF is in an ON-REVERSE state

The assumptions are that an ON-FORWARD trip CF state signifies a pump disconnection from its driving motor while an ON-REVERSE trip CF state allows pump connection to its driving motor. Equation (6.16) above is treated either:

- explicitly in time via a forward Euler technique with all terms being functions of old-time pump speed, or

- implicitly in time via a backward Euler technique and fixed-point iteration such that all terms depend on new-time pump speed

For the forward Euler method, the difference equation for pump speed update is:

$$(6.17) \quad \omega^n = \omega^{n-1} + \frac{\tau_{net}(\omega^{n-1})}{I_p(\omega^{n-1})} \Delta t$$

Where:

n = current time level ; $n - 1$ = old time level ; Δt = time-step

For the backward Euler method, the fixed-point iteration scheme is:

$$(6.18) \quad \begin{cases} \omega^n_{[0]} = \omega^{n-1} \\ \omega^n_{[i+1]} = \omega^{n-1} + \frac{\tau_{net}(\omega^n_{[i]})}{I_p(\omega^n_{[i]})} \Delta t, \text{ for } i = 1 \dots i_{lim} \end{cases}$$

The fixed-point iteration scheme starts with the guess that pump speed at time level n is that of time level $n-1$. Then, an iterative solution proceeds wherein the net torque and pump inertia are evaluated at the latest-iterate pump speed to approximate the next-iterate value. Eventually, the next-iterate pump speed matches the last-iterate pump speed within some convergence tolerance. This solution method incorporates n -level information into the solution of the n -level pump speed and ought to improve code performance when the torque-inertia equation is being solved.

6.1.5.4 Pump Energy Dissipation and Efficiency

The total power imparted to a pumped fluid by an impeller rotating at a given speed is equal to the product of that speed and the delivered hydraulic torque. This quantity is also known as “brake power” or “brake horsepower”. In reality, not all the power delivered to the fluid is manifest as a pressure (head) increase (and therefore as “hydraulic power”) because some fraction is lost to dissipation, appearing as thermal energy added to the fluid. If the brake power is known and the hydraulic power can be calculated, the energy dissipation DISS is:

$$(6.19) \text{ DISS} = (\text{brake power}) - (\text{hydraulic power}) =$$

$$\tau_H \omega \frac{2\pi}{60} - gH \left((1 - \alpha_g) \rho_f V_f + \alpha_g \rho_g V_g \right) Af$$

This suggests one measure of pump efficiency EFF:

$$(6.20) \text{ EFF} = \frac{gH \left((1 - \alpha_g) \rho_f V_f + \alpha_g \rho_g V_g \right) Af}{\tau_H \omega \frac{2\pi}{60}}$$

By this definition, efficiency is the quotient of hydraulic power (i.e. used for pumping) and brake power (the sum of useful and lost power).

The dissipated energy heats up the pumped fluid and cannot, in general, be neglected. A simple way to account for dissipation energy addition is to assume that both the pool and the atmosphere (if both are present) receive amounts of thermal energy that would lead to identical increases in their respective phasic temperatures [43]. Therefore, if the pool and atmosphere were in thermal equilibrium before the dissipation energy addition, they remain so afterwards. Accordingly, a phasic split fraction is computed as:

$$(6.21) \quad f_{P,DISS} = \frac{((1-\alpha_g)\rho_f C_{p,f})}{((1-\alpha_g)\rho_f C_{p,f} + \alpha_g \rho_g C_{p,g})}$$

Then, the rate of dissipation energy addition to the pool is:

$$(6.22) \quad DISS_P = DISS * f_{P,DISS} =$$

$$\left(\tau_H \omega \frac{2\pi}{60} - gH \left((1 - \alpha_g) \rho_f V_f + \alpha_g \rho_g V_g \right) Af \right) \left(\frac{((1-\alpha_g)\rho_f C_{p,f})}{((1-\alpha_g)\rho_f C_{p,f} + \alpha_g \rho_g C_{p,g})} \right)$$

While the rate of dissipation energy addition to the atmosphere is:

$$(6.23) \quad DISS_A = DISS * (1 - f_{P,DISS}) =$$

$$\left(\tau_H \omega \frac{2\pi}{60} - gH \left((1 - \alpha_g) \rho_f V_f + \alpha_g \rho_g V_g \right) Af \right) \left(\frac{(\alpha_g \rho_g C_{p,g})}{((1 - \alpha_g) \rho_f C_{p,f} + \alpha_g \rho_g C_{p,g})} \right)$$

Note that the dissipation energy source is essentially equivalent, in MELCOR terms, to two external sources (one AE-type and one PE-type, see [15]) with a RATE interpretation. The dissipation energy is effectively treated as such when the user chooses to model dissipation energy addition.

6.1.6 Semi-Implicitness and Integration with MELCOR Solution Scheme

6.1.6.1 MELCOR Phasic Velocity Equation

The general set of linearized phasic velocity equations MELCOR solves [16] is included below as equation (6.24). The left-hand side includes new-time phase ϕ velocities for the j^{th} flow path ($V_{j,\phi}^n$ and $V_{j,-\phi}^n$) as well as terms for other flow paths interfaced to the same from/to CVs with which flow path j communicates. The right-hand side includes old-time information, i.e. velocity equation terms that are treated explicitly. Currently, the term ΔP_j appears on the right-hand side of the j^{th} flow path velocity equation and is treated as an explicit source term.

$$\begin{aligned}
(6.24) \quad & \left(1 + \frac{K_{j,\varphi}^* \Delta t}{2L_j} |v_{j,\varphi}^{n-} + v'_{j,\varphi}| + \frac{\alpha_{j,-\varphi} f_{2,j} L_{2,j} \Delta t}{\rho_{j,\varphi} L_j} \right) v_{j,\varphi}^n - \frac{\alpha_{j,-\varphi} f_{2,j} L_{2,j} \Delta t}{\rho_{j,\varphi} L_j} v_{j,-\varphi}^n \\
& + \sum_{s,\psi} C(j,\varphi : s,\psi) v_{s,\psi}^n \\
& = v_{j,\varphi}^{o+} + \frac{K_{j,\varphi}^* \Delta t}{2L_j} |v'_{j,\varphi}| v_{j,\varphi}^{n-} + \frac{\Delta t}{\rho_{j,\varphi} L_j} (\hat{P}_i + \Delta P_j - \hat{P}_k) \\
& + (\rho g \Delta z)_{j,\varphi}^o + \frac{\partial(\rho g \Delta z)_{j,\varphi}}{\partial M_{i,P}} (\hat{M}_{i,P}^o - M_{i,P}^{o+}) \\
& + \frac{\partial(\rho g \Delta z)_{j,\varphi}}{\partial M_{k,P}} (\hat{M}_{k,P}^o - M_{k,P}^{o+}) \Big]
\end{aligned}$$

It is through ΔP_j that any type of pump must deliver a pressure head (momentum source) to its assigned flow path. For the newly-implemented homologous pump model to be semi-implicit such that phasic velocity calculations do not totally treat pump head as an “old-time” quantity, then:

- ΔP_j must be expanded into implicit and explicit terms, and
- Equation (6.24) above must be rearranged such that:
 - Terms multiplying $V_{j,\varphi}^n$ and $V_{j,-\varphi}^n$ on the left account for the implicit part of ΔP_j
 - The explicit part of ΔP_j is retained on the right-hand side

6.1.6.2 Expansion of ΔP_j

The new pump model predicts, among other things, the pump performance in terms of delivered pressure head H as a result of pumping the fluid. The pressure head is computed as a function of pump speed, ω , and pump capacity (volumetric flow rate), Q . The pump capacity is a function of phasic velocities and is computed, for flow path j , as:

$$(6.25) \quad Q_j = Af(V_{j,P} + V_{j,A})$$

Where:

Q_j = Volumetric flow rate, flow path j [m^3/s] ; A = Flow path j area [m^2]

f = Flow path j open fraction ; $V_{j,X}$ = Velocity, $X=P$ (pool), $X=A$ (atmosphere)

Note Af is the product of flow path area and flow path open fraction. Thus Q_j depends on phasic velocities so that pump head can be expressed as a function of phasic velocities. Neglecting the dependence of head on pump speed (i.e. assuming pump speed is constant) and expanding via a two-term Taylor series about Q_j^{n-} for n - the latest-iterate value (computed with n - velocities during the inner velocity iteration) one recovers:

$$(6.26) \quad H_j^n = H_j^{n-1} + \left(\frac{dH}{dQ}\right)^{n-1} (Q_j^n - Q_j^{n-})$$

Alternatively, expanding ΔP_j with respect to Q :

$$(6.27) \Delta P_j = \Delta P_j^{n-1} + \left(\frac{d\Delta P}{dQ}\right)^{n-1} (Q_j^n - Q_j^{n-})$$

Where:

$$\Delta P_j^{n-1} = \rho_m g H_j^{n-1}, \text{ relating pressure [Pa] to head [m]}$$

$$\left(\frac{d\Delta P}{dQ}\right)^{n-1} = \rho_m g \left(\frac{dH}{dQ}\right)^{n-1}, \text{ relating derivatives}$$

Substituting from equation (6.25) :

$$(6.28) \Delta P_j = \rho_m g H_j^{n-1} + \rho_m g A f \left(\frac{dH}{dQ}\right)^{n-1} (V_{j,P}^n + V_{j,A}^n) - \rho_m g A f \left(\frac{dH}{dQ}\right)^{n-1} (V_{j,P}^{n-} + V_{j,A}^{n-})$$

Separating out the terms further:

$$(6.29) \Delta P_j = \rho_m g H_j^{n-1} - \rho_m g A f \left(\frac{dH}{dQ}\right)^{n-1} (V_{j,P}^{n-}) - \rho_m g A f \left(\frac{dH}{dQ}\right)^{n-1} (V_{j,A}^{n-}) + \rho_m g A f \left(\frac{dH}{dQ}\right)^{n-1} (V_{j,P}^n) + \rho_m g A f \left(\frac{dH}{dQ}\right)^{n-1} (V_{j,A}^n)$$

6.1.6.3 Modified Velocity Equation

This expression for ΔP_j can be substituted back into equation (6.24). Also, the new-time information can be moved to the left side while the old-time information can be kept on the right side. This results in:

$$\begin{aligned}
 (6.30) \quad & V_{j,\varphi}^n \left(1 + \left(\frac{K_{j,\varphi}^* \Delta t}{2L_j} \right) |V_{j,\varphi}^{n-} + V'_{j,\varphi}| + \left(\frac{\alpha_{j,-\varphi} f_{2,j} L_{2,j} \Delta t}{\rho_{j,\varphi} L_j} \right) - \right. \\
 & \left. \zeta \left(\frac{\Delta t}{\rho_{j,\varphi} L_j} \right) \rho_m g A f \left(\frac{dH}{dQ} \right)^{n-1} \right) - \\
 & V_{j,-\varphi}^n \left(\frac{\alpha_{j,-\varphi} f_{2,j} L_{2,j} \Delta t}{\rho_{j,\varphi} L_j} + \zeta \left(\frac{\Delta t}{\rho_{j,\varphi} L_j} \right) \rho_m g A f \left(\frac{dH}{dQ} \right)^{n-1} \right) + \\
 & \sum_{s,\psi} [C(j, \varphi: s, \Psi) V_{s,\psi}^n] = \\
 & V_{j,\varphi}^{o+} + \left(\frac{K_{j,\varphi}^* \Delta t}{2L_j} \right) (|V'_{j,\varphi}| V_{j,\varphi}^{n-}) + \\
 & \left(\frac{\Delta t}{\rho_{j,\varphi} L_j} \right) \left(\hat{P}_i + \left(\rho_m g H_j^{n-} - \zeta \rho_m g A f \left(\frac{dH}{dQ} \right)^{n-1} (V_{j,\varphi}^{n-} + V_{j,-\varphi}^{n-}) \right) - \hat{P}_k \right) \\
 & + (\rho g \Delta z)_{j,\varphi}^o + \frac{\partial(\rho g \Delta z)_{j,\varphi}}{\partial M_{i,P}} (\hat{M}_{i,P}^o - M_{i,P}^{o+}) + \frac{\partial(\rho g \Delta z)_{j,\varphi}}{\partial M_{k,P}} (\hat{M}_{k,P}^o - M_{k,P}^{o+})
 \end{aligned}$$

Thus linearizing ΔP_j leads to:

- New terms in coefficient multipliers of $V_{j,\varphi}^n$ and $V_{j,-\varphi}^n$ for implicit part of ΔP_j
- a modified explicit term for ΔP_j

The new terms are written in bold, red text in equation (6.30). Note the factor ζ is positioned so that if set to 1 the semi-implicit formulation can be used while if set to 0, the solution reverts to a fully explicit treatment for ΔP_j ($\Delta P_j = \rho_m g H_j^{n-}$). Note the “old-time” information is denoted (n-1) while the “latest-iterate” information is denoted n-, the distinction being that n-1 quantities are set before the level n velocity iteration loop is entered while n- quantities change with each level n velocity iteration.

Within the doubly-iterative MELCOR solution (an outer pressure iteration, an inner velocity iteration), the evaluation of pump semi-implicit terms happens within the innermost phasic velocity solution. Changes in provisional flow path phasic velocities impact flow path volumetric flow rates and thus new $\frac{dH}{dQ}$ values and new explicit and semi-implicit terms are evaluated with each velocity iteration.

6.1.6.4 Derivative Computation, $(dH/dQ)^{n-1}$

The change in pump head with respect to flow (at constant speed) must be evaluated at level n-1 conditions (speed and flow). This derivative describes how the pump head (generally a function of single and two-phase pump performance) varies with capacity in the neighborhood of Q_j^{n-1} . A cubic spline interpolation method is used to evaluate the derivative. An outline of the method is as follows:

- Use cubic spline fit formula to approximate user-specified single-phase head $H_{1\phi}$ data and two-phase head $H_{2\phi}$ data as a function of the polar homologous independent variable $x = C + atan\left(\frac{\omega Q_R}{\omega_R Q}\right)$

- Compute $\frac{dH_{1\phi}}{dx}$ and $\frac{dH_{2\phi}}{dx}$ from cubic spline prescriptions for the first derivative of a spline-fitted function (involves function values and 2nd derivatives)

An approach outlined in [49] was followed to obtain cubic spline fits of the functions $H_{1\phi}$ and $H_{2\phi}$ in addition to their respective derivatives $\frac{dH_{1\phi}}{dx}$ and $\frac{dH_{2\phi}}{dx}$. A “natural cubic spline” was assumed, i.e. the 2nd derivatives at both boundaries of the function were set to zero. The procedure amounts to solving a tridiagonal system of equations for second derivatives of the function in question and then substituting those values into formulae for interpolated values of the function and its first derivative. The total head derivative is:

$$(6.31) \quad \frac{dH}{dQ} = \frac{dH_{1\phi}}{dQ_{x(Q)}} + \frac{dH_{2\phi}}{dQ_{x(Q)}} = \frac{dx}{dQ_Q} \left(\frac{dH_{1\phi}}{dx_{x(Q)}} + \frac{dH_{2\phi}}{dx_{x(Q)}} \right)$$

Where:

$$\frac{dx}{dQ_Q} = -\omega Q_R \omega_R / (\omega_R^2 Q^2 + \omega^2 Q_R^2) \text{ since } x = C + a \tan\left(\frac{\omega Q_R}{\omega_R Q}\right)$$

6.2 Terry Turbine Velocity Stage Model

The Terry turbine compound velocity stage model is a somewhat more generalized version of a single control-volume angular momentum balance approach originally proposed for Pelton turbine analysis [50]. It is the method proposed for a CF model in a pre-existing RCIC system MELCOR deck [1], but with explicit accounting for:

- Several separate nozzles and their jets of steam/water

- Each bucket/reversing chamber pair (i.e. each velocity stage)
- A general number ‘n’ of reversing chambers allotted per steam nozzle, with the proposed capability to model any user-requested number of steam nozzles that may be circumferentially-situated about the rotor wheel

For a given Terry turbine wheel with x steam nozzles around its perimeter and with y reversing chambers per nozzle, this model could be applied in all x instances with different steam nozzle jet effluents for every instance. The steam jets would be predicted by separate applications of a Terry turbine pressure stage model as described in a subsequent section.

The mathematical model of the velocity stage of a Terry turbine is based on a control volume (CV) formulation for conservation of angular momentum [1]. A simpler form of the model presented in this section has already been applied in MELCOR via user-defined control functions with some success.

The quantity of interest in a velocity stage model of an impulse-type turbine is the momentum flux delivered to the rotor because the attending force ultimately turns the rotor and exerts a “positive” torque on a coupled shaft. For a compounded velocity stage, the total momentum flux and/or force integrated over all velocity stages is of interest. The velocity stage model developed hereafter predicts a turbine torque that is intended to factor into a shaft torque/inertia (angular speed) equation which dictates pump impeller speed and hence turbo-pump performance.

Conceptually, the CV used for analysis resembles the sketch in Figure 6.5. Note the CV is drawn around a Terry turbine rotor in such a way that the turbo-pump shaft is

cut by the control surface. Rotor buckets reside within the cylindrical CV while steam nozzles and any reversing chambers in the turbine casing interior are outside the CV.

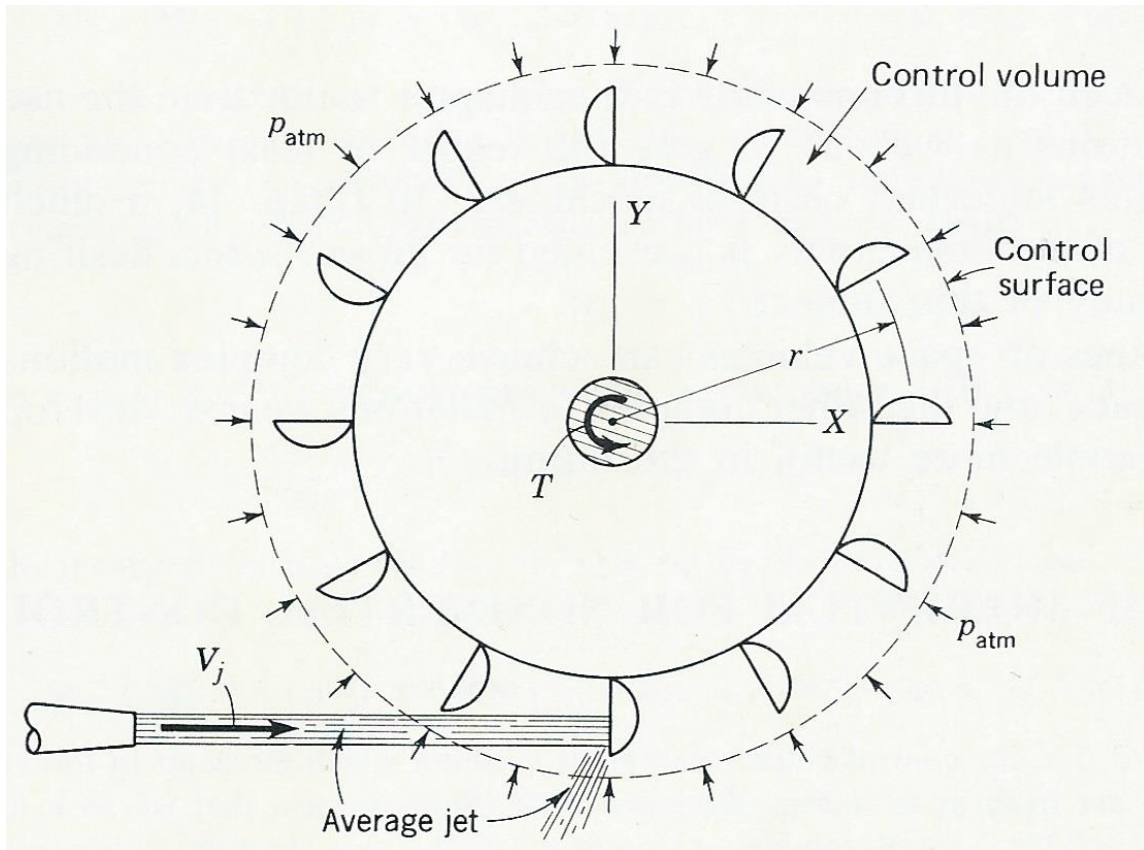


Figure 6.5 Control volume for angular momentum equation [1]

Figure 6.5 shows how the steam jet emanating from a nozzle crosses the CV boundaries. Presumably, the fluid jet would cross the control surface several more times (steam enters, exits the CV while passing through rotor bucket and reversing chambers) in a compound velocity stage though this is not explicitly shown. Working in cylindrical coordinates, the θ component of angular momentum has a scalar equation written as:

$$(6.32) \oint r T_{\theta} dA + \iiint r B_{\theta} dV = \oint r u_{\theta} (\rho \bar{u} * d\bar{A}) + \frac{\partial}{\partial t} \iiint \rho r u_{\theta} dV$$

Where:

\bar{u} is the fluid velocity vector incoming to a rotor bucket

u_{θ} is the tangential component of the fluid velocity vector exiting a rotor bucket

r is the turbine rotor radius

The first term in equation (6.32) accounts for any torques crossing the control surface. In this case, only the shaft crosses the boundary. The second term accounts for body forces and may be neglected. The third term accounts for net moment of momentum flux delivered by any fluid flow crossing the control surface. This term may be expanded so that compound velocity stages (multiple entries/exits of a fluid stream across the control surface) may be taken into account. The fourth term is a transient term that is shown in Appendix B to contain the moment of inertia and time derivative of rotor angular speed.

The net moment of momentum flux term may be written for the CV as:

$$(6.33) \oint r u_{\theta} (\rho \bar{u} * d\bar{A}) = \sum_{OUT} [|\bar{R} \times \bar{u}|_{out} \dot{m}_{out}] - \sum_{IN} [|\bar{R} \times \bar{u}|_{in} \dot{m}_{in}]$$

Details behind the evaluation of this term for a compound velocity stage turbine are included in Appendix B which resembles the derivations in [1]. The OUT sum consists of n+1 distinct fluid streams exiting n+1 distinct rotor buckets, where n is the number of reversing chambers per steam nozzle. The IN sum consists of one fluid stream emanating

from a nozzle and n distinct fluid streams entering n distinct buckets after exiting from one of n reversing chambers. Velocity triangles (a typical analysis tool for Pelton-type turbines) can be leveraged to describe the IN summation in terms of bucket loss coefficients and angles between the bucket velocity vector and fluid inlet/outlet velocity vectors (details in Appendix B). The OUT summation can be written in terms of the tangential component of fluid velocity exiting the bucket. Thus:

$$(6.34) \quad \sum_{OUT} \left[\left| \vec{R} \times \vec{u} \right|_{out} \dot{m}_{out} \right] = \sum_{i=1}^{n+1} \left[r u_{\theta,i} \dot{m}_{out,i} \right]$$

$$(6.35) \quad \sum_{IN} \left[\left| \vec{R} \times \vec{u} \right|_{in} \dot{m}_{in} \right] = \sum_{i=1}^{n+1} \left[r V_{j,i} \cos(\beta_i) \dot{m}_{in,i} \right]$$

Employing relationships from velocity triangles (Appendix B), the moment of momentum flux term looks like:

$$(6.36) \quad \oint r u_{\theta} (\rho \vec{u} * d\vec{A}) =$$

$$\sum_{i=1}^{n+1} \left[r^2 \omega \dot{m}_{in,i} \left(1 + C_{B,i}(\cos(\beta_i)) \right) - r V_{j,i}(\cos(\beta_i)) (C_{B,i} + 1) \dot{m}_{in,i} \right]$$

Furthermore, there are relationships between terms in the above equation (Appendix B):

$$(6.37) \quad \dot{m}_{in,i} = \gamma_{RC,i-1} \xi_{i-1} \dot{m}_{in,i-1}$$

$$(6.38) \quad V_{j,i} = u_{\theta,i-1} C_{RC,n} = \\ C_{RC,i-1} \left(r\omega - C_{B,i-1} (V_{j,i-1} - r\omega) (\cos(\beta_{i-1})) \right)$$

These essentially capture the effects of reversing chambers. Reversing chamber crescent holes can vent some steam mass to the casing, hence the factor γ_{RC} . Also, they can cause some decrease in steam velocity, hence the factor C_{RC} analogous to C_B for a rotor bucket.

Turning now to the transient term, it can be shown (Appendix B) through use of velocity triangle relationships and with some mathematical manipulations that:

$$(6.39) \quad \frac{\partial}{\partial t} \iiint \rho r u_{\theta} dV = \sum_{i=1}^{n+1} \left[\frac{\partial}{\partial t} \iiint \rho r u_{\theta,i} dV \right] = \\ I_T \frac{\partial \omega}{\partial t} \left(\mathbf{1} + C_{B,i} (\cos(\beta_i)) \right)$$

Assembling all pieces and accounting for multiple nozzles, the torque-inertia equation is:

$$(6.40) \quad -\tau_{shaft} = -\tau_{pump} = I_T \frac{\partial \omega}{\partial t} \sum_{k=1}^m \left[\sum_{i=1}^{n+1} \left[\mathbf{1} + C_{B,i} (\cos(\beta_i)) \right] \right] + \\ \sum_{k=1}^m \left[\sum_{i=1}^{n+1} \left[\left[r^2 \omega \dot{m}_{in,i} \left(\mathbf{1} + C_{B,i} (\cos(\beta_i)) \right) \right] \right. \right. \\ \left. \left. - \left[r V_{j,i} (\cos(\beta_i)) (C_{B,i} + \mathbf{1}) \dot{m}_{in,i} \right] \right] \right]$$

$$(6.41) \quad \dot{m}_{in,i} = \begin{cases} \dot{m}_{jet} & i = 1 \\ \gamma_{RC,i-1} \xi_{i-1} \dot{m}_{in,i-1} & i > 1 \end{cases}$$

$$(6.42) \quad V_{j,i} = \begin{cases} V_{jet} & i = 1 \\ C_{RC,i-1} \left(r\omega - C_{B,i-1} (V_{j,i-1} - r\omega) (\cos(\beta_{i-1})) \right) & i > 1 \end{cases}$$

Where:

$\dot{m}_{in,i} = \dot{m}_{out,i}$, for $i > 1$, mass into bucket equals mass out of bucket

n = number of reversing chambers in k^{th} nozzle ; m = number of nozzles in turbine

Therefore, the turbine torque can be calculated in terms of the nozzle jet conditions and a set of bucket loss coefficients $C_{B,i}$, steam exit angles β_i , steam carry-over fractions ξ_{i-1} , reversing chamber loss coefficients $C_{RC,i}$, and reversing chamber leakage coefficients $\gamma_{RC,i}$. These various coefficients will be left for the user to specify or, as described in a subsequent section, CMFD results could furnish a “built in” data set. Note also that in Equation (6.40), the pump moment of inertia and any friction torques can be added in to round out the full torque-inertia equation for the entire RCIC turbo-pump.

6.3 Terry Turbine Pressure Stage Model

The pressure stage model treats the flow of steam (dry saturated or superheated) through a converging/diverging nozzle as a sequence of expansion processes:

- An isentropic expansion from the nozzle inlet through the throat and to a point where condensation heat release begins to introduce entropy

- A Rayleigh flow process between the end of the last isentropic expansion and the Wilson point (point of maximum nucleation, maximum steam super-saturation)
- A Rayleigh flow process between the Wilson point and the point of full reversion from thermodynamic non-equilibrium (re-establishment of saturation)
- An isentropic expansion between the end of the last Rayleigh flow process and the nozzle outlet with provision for standing normal shocks
- A standing normal shock (over-expanded flow with respect to back-pressure) or a jet expansion (if under-expanded flow with respect to back-pressure)

Implementation in MELCOR follows the example of a time-independent, user-specified flow path (see [15], [16]) except an expansion model is applied for phasic velocities in a steam nozzle.

The expansion process without any consideration of aerodynamic shocks is shown in Figure 6.6 below. The states included on the h-s diagram are:

- **01**, representing inlet stagnation conditions
- **2**, representing the point where expanding steam crosses the saturation line
- **m**, representing the point where condensation starts to release latent heat to the steam such that significant entropy is introduced
- **n**, representing the Wilson point (point of maximum nucleation and maximum super-saturation), reached at a time t_n after point 2 is reached

- **a**, representing the state that expanding steam would have reached if it expanded on an isentropic line for a time t_n after point 2 is reached
- **3**, representing the point where thermodynamic phase equilibrium is re-established
- **4**, representing the nozzle exit state (on an isentropic line with state 3, no shocks)

The only distinguishing feature from conventional isentropic compressible flow theory is the latent heat release between states m and 3. This process can be modeled by a Rayleigh flow process which assumes:

- One dimensional flow through a constant cross-sectional area duct
- Steady flow
- Frictionless flow
- Heat addition (non-adiabatic flow)

In the present case, thermal energy is added to flowing steam as a consequence of latent heat release. Heat addition in this case equals the product of latent heat and wetness fraction. Thus, the heat addition is proportional to evolved wetness which can be obtained by evaluation of the so-called nucleation-growth integrals [51] as will be discussed below. The Rayleigh flow relationships ([28], [51], [52]) are such that a downstream state (e.g. state 'n') can be determined from an upstream state (idealized state 'a' in this case) and a known heat addition between the two states.

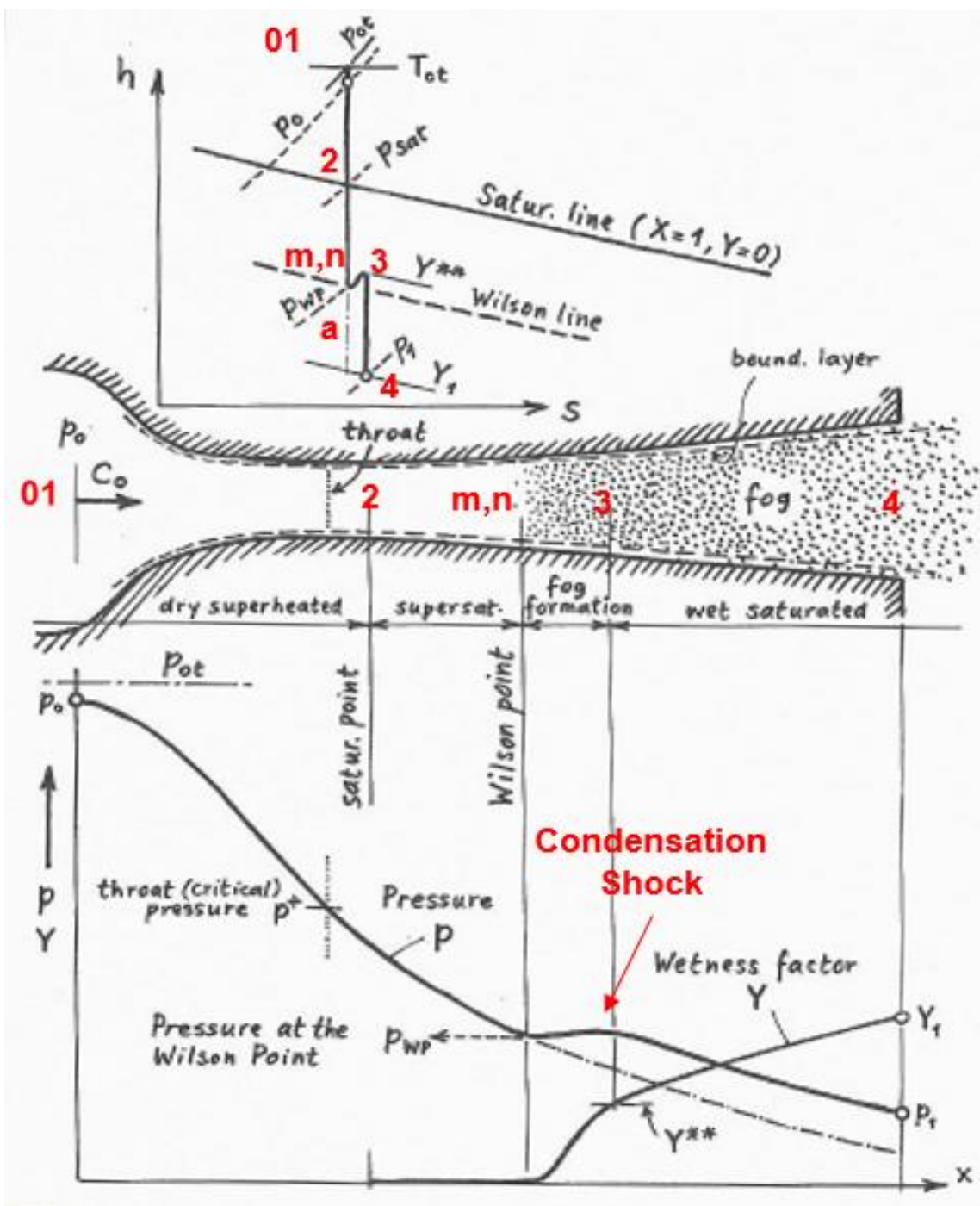


Figure 6.6 Qualitative h-s diagram, pressure/wetness plots for expansion

An ideal gas equation-of-state relationship is typically chosen for analytical Wilson point solutions, and this assumption has been shown to compare well with more rigorous computations and experiments. The error is certainly low enough to justify the assumption in light of the considerable complexity in implementing more complicated equations of state.

Note that a user input option for purely isentropic steam expansion (to the neglect of any and all steam phase metastability) is included. This particular formulation is discussed in turn below.

6.3.1 *Ideal Gas Isentropic Flow*

Isentropic flow in this case implies one-dimensional, steady, frictionless, adiabatic flow such that stagnation enthalpy and entropy both remain constant during the expansion process. Isentropic flow property relations that connect any downstream location 2 to the inlet stagnation state 01 are [28]:

$$(6.43) \quad \frac{T_2}{T_{01}} = \left(1 + \left(\frac{\gamma-1}{2}\right) M_2^2\right)^{-1} \quad \text{Temperature Ratio}$$

$$(6.44) \quad \frac{P_2}{P_{01}} = \left(1 + \left(\frac{\gamma-1}{2}\right) M_2^2\right)^{-\gamma/\gamma-1} \quad \text{Pressure Ratio}$$

$$(6.45) \quad \frac{\rho_2}{\rho_{01}} = \left(1 + \left(\frac{\gamma-1}{2}\right) M_2^2\right)^{-1/\gamma-1} \quad \text{Density Ratio}$$

Relating entropy and enthalpy:

$$(6.46) \quad T * ds = du + P * dv = dh - v * dP$$

Using specific heat definitions (isochoric and isobaric):

$$(6.47) \quad c_v = \frac{\partial u}{\partial T_v} ; c_p = \frac{\partial h}{\partial T_p}$$

Thus, for an isentropic process and using static temperatures and pressures:

$$(6.48) \quad R * \ln \left(\frac{P_2}{P_1} \right) = \int_{T_1}^{T_2} c_p(T) * \left(\frac{dT}{T} \right)$$

Rearranging leads to a pressure ratio equation:

$$(6.49) \quad \frac{P_2}{P_1} = \exp \left[-\frac{1}{R} * \int_{T_2}^{T_1} c_p(T) * \left(\frac{dT}{T} \right) \right]$$

Additionally, a Mach number relationship can be derived from the fact that stagnation enthalpy remains constant across the expansion (pressure and kinetic energy trade-off):

$$(6.50) \quad M_2^2 = \frac{2}{kRT_2} \int_{T_2}^{T_1} c_p(T) * dT$$

Note that with the above isentropic flow relations, the state 2 pressure and Mach number may be evaluated from known state 2 temperature (or from a guessed value in an iterative procedure). In a computational procedure, constant specific heats may be assumed if appropriate or a Gaussian quadrature approach could be applied (see Appendix C).

6.3.2 *Ideal Gas Rayleigh Flow*

Rayleigh flow implies one-dimensional, steady, compressible, frictionless flow through a constant-area duct. It is an idealized representation of steam nozzle flow locally at/around the Wilson point and rapid condensation zone. Conservation equations between two states 1 and 2 are [28]:

$$(6.51) \quad \rho_1 v_1 = \rho_2 v_2 \quad \text{Continuity}$$

$$(6.52) \quad P_1 + \rho_1 v_1^2 = P_2 + \rho_2 v_2^2 \quad \text{Momentum}$$

$$(6.53) \quad q + h_1 + \frac{v_1^2}{2} = h_2 + \frac{v_2^2}{2} \quad \text{Energy}$$

Thus:

$$(6.54) \quad q = c_p(T_2 - T_1) + \frac{v_1^2 - v_2^2}{2} = h_{02} - h_{01} = c_p(T_{02} - T_{01})$$

Giving rise to property relations in terms of Mach number Ma for a Rayleigh process [28]:

$$(6.55) \frac{p_2}{p_1} = \frac{(1 + \gamma M_1^2)}{(1 + \gamma M_2^2)} \quad \text{Pressure Ratio}$$

$$(6.56) \frac{T_2}{T_1} = \frac{(M_2^2(1 + \gamma M_1^2)^2)}{(M_1^2(1 + \gamma M_2^2)^2)} \quad \text{Temperature Ratio}$$

$$(6.57) \frac{\rho_2}{\rho_1} = \frac{v_1}{v_2} = \frac{(M_1^2(1 + \gamma M_2^2))}{(M_2^2(1 + \gamma M_1^2))} \quad \text{Density Ratio}$$

Additionally, there are stagnation property relations not reproduced here. It should be mentioned however that during a Rayleigh flow process with heat addition, the stagnation enthalpy (and hence the stagnation temperature) changes as a result of heat addition [28]:

$$(6.58) \frac{h_{02} - h_{01}}{c_p} = (T_{02} - T_{01}) = \frac{q}{c_p} = \frac{h_{fg} Y_2}{c_p}$$

Where:

Y = Wetness fraction

The dimensionless entropy change can be written as [28]:

$$(6.59) \frac{s_2 - s_1}{c_p} = \ln \left[\left(\frac{M_2^2}{M_1^2} \right) \left(\frac{1 + \gamma M_1^2}{1 + \gamma M_2^2} \right)^{\gamma+1/\gamma} \right]$$

The wetness fraction Y must come from nucleation-growth integral evaluation across the Rayleigh process (discussed subsequently), and it will be shown how these relationships can be employed in an iterative solution process to deduce Wilson point conditions and to predict flow properties at the point of reversion from non-equilibrium.

6.3.3 *Nucleation-Growth Integrals*

The nucleation-growth integral assists with determining wetness evolved from super-saturated steam. The wetness fraction (mass of liquid water per unit mass of steam) is predicted at a downstream state 2 from an upstream state 1 by integrating the effects of nucleation and condensation growth between states. Gyarmathy [23] and Dobbins [51] present two slightly different takes on the nucleation-growth integral. Both will be presented here because both help to solidify the concept.

Gyarmathy's discussion [23] of the nucleation growth integral begins with the definition of a spatial variable x and a spatial variable of integration ξ defined between x_s (the spatial location of state 2 where saturation line is first crossed by expanding steam) and x . Then, the wetness fraction is:

$$(6.60) \quad Y(x) = \frac{4\pi}{3} \rho_l \int_{x_s}^x r(x, \xi)^3 v(\xi) d\xi$$

Where:

$r(x, \xi)$ = Radius of droplet at x assuming droplet born at upstream location ξ

$v(\xi)d\xi$ = Drop number per mass of steam, born between $x = \xi$ and $x = \xi + d\xi$

This wetness fraction expression can be differentiated to yield:

$$(6.61) \quad Y'(x) = \frac{4\pi}{3} \rho_l \left[\frac{d}{dx} \left(\int_{x_s}^x r(x, \xi)^3 v(\xi) d\xi \right) + \int_{x_s}^x \frac{d}{dx} (r(x, \xi)^3 v(\xi) d\xi) \right]$$

$$= \frac{4\pi}{3} \rho_l \left[\frac{d}{dx} \left(\int_{x_s}^x r(x, \xi)^3 v(\xi) d\xi \right) + \int_{x_s}^x 3 \left(r(x, \xi)^2 \frac{\partial r(x, \xi)}{\partial x} v(\xi) d\xi \right) \right]$$

Furthermore:

$$(6.62) \quad r(x, \xi) = r^*(\xi) + \int_{\xi}^x \frac{\partial r(x', \xi)}{\partial x'} dx', \text{ for } x' \text{ between } \xi \text{ and } x$$

$$(6.63) \quad \dot{r} = \frac{\partial r(x, \xi)}{\partial t}, \text{ expressing condensation growth rate of droplet radius}$$

$$(6.64) \quad v(x) = \frac{I(x)}{v(x)} = \frac{\text{Nucleation rate} \left[\frac{\text{drop}}{\text{kg/s}} \right]}{\text{velocity} \left[\frac{\text{m}}{\text{s}} \right]}$$

$$(6.65) \quad Y'(x) = \frac{4\pi}{3} \rho_l r^*(x) \frac{I(x)}{v(x)} + \frac{4\pi \rho_l}{v(x)} \int_{x_s}^x \left[r^*(\xi) + \int_{\xi}^x \frac{\dot{r}}{v(x)} dx' \right]^2 \dot{r} \frac{I(\xi)}{v(\xi)} d\xi$$

Dobbins [51] proposes a slightly different formulation in which spatial variables are converted into time variables. Beginning with a similar definition of wetness fraction:

$$(6.66) \quad Y(x) \dot{m} = \int_{-\infty}^x m(x_1, x) J(x_1) A_c(x_1) dx_1$$

Where:

$m(x_1, x)$ = Mass of a droplet at x , born at location x_1

$A_c(x_1)dx_1$ = Local volume element

$J(x_1)$ = Embryo formation rate per unit volume per time

Dividing through by $\dot{m} = \rho_g vA$ leads to a conversion from space to time coordinates:

$$(6.67) \quad Y = \int_0^t \frac{4\pi}{3} \rho_l r(t_1, t)^3 \left(\frac{J(x_1)}{\rho_g} \right) \left(\frac{dx_1}{v} \right) = \int_0^t \frac{4\pi}{3} \rho_l r(t_1, t)^3 I(t_1) dt_1$$

Differentiating with respect to time:

$$(6.68) \quad Y' = 4\pi\rho_l \int_0^t r(t_1, t)^2 I(t_1) \frac{\partial r(t_1, t)}{\partial t_1} dt_1 + \frac{4\pi\rho_l}{3} I(t) r^{*3}$$

The nucleation-growth integrals for wetness fraction and its time derivative are now defined with respect to time, and certain other assumptions can be used to evaluate the integrals between two states, i.e. between two times.

Firstly, elements of classical nucleation theory may be assumed so that the following relationships hold for nucleation rate and condensation growth rate:

$$(6.69) \quad I = A e^{-B\eta} \quad \text{Nucleation Rate}$$

Where:

$$\eta = \frac{1}{T^3 (\ln(S))^2}$$

$$A = \frac{\rho_g}{\rho_l} \left(\frac{2\sigma}{\pi m_v^3} \right)^{1/2}$$

$$B = \frac{16\pi\sigma^3}{K(\rho_l R)^2}$$

$$(6.70) \quad \frac{\partial r}{\partial t} = \dot{r} = \left(\frac{\lambda_g \Delta T}{\rho_l h_{fg}} \right) \frac{1 - r^*/r}{1 + 1.59\lambda/r} \quad \text{Condensation Rate}$$

The critical radius (size of freshly-nucleated drops) comes from a thermodynamic relation:

$$(6.71) \quad r^* = \frac{2\sigma}{\rho_l R T \ln(S)}$$

Assuming an approximately constant condensation growth rate and assuming a definition of vapor molecule mean free path leads to a simplified droplet growth rate equation:

$$(6.72) \quad \frac{\partial r}{\partial t} = \dot{r} = c_g = \frac{\rho_g c_p \Delta T}{2.4 \rho_l h_{fg} P r_g} \sqrt{RT}$$

Both integrals (for Y and Y' as in Equations (6.67 and (6.68 or Equations (6.60 and (6.61) can be evaluated (Laplace method, see Appendix C) to ascertain wetness at the Wilson point. Note the integration is from time zero at state '2' to time t_n at Wilson point.

However, the problem is not quite so straightforward, and several auxiliary relationships are derived based on a mixture of assumptions and physical observations about the Wilson point (Appendix C). The entire set of nucleation/growth closures can be used along with Rayleigh flow property relationships (and isentropic flow relationships for upstream states) in an iterative approach to resolve a self-consistent set of Wilson point conditions.

6.3.4 Normal Shocks and Aerodynamic Back Pressure Effects

Converging-diverging nozzle flow of an ideal gas is largely governed by back pressure. Choked flow at the throat will only occur if the ratio of inlet to back pressure reaches a sufficiently low value. When treating steam as an ideal gas, this critical pressure ratio is approximately 0.546 or 0.576 depending upon whether the steam is superheated or saturated, respectively. As the back pressure is lowered and the inlet-to-back pressure ratio falls further below the critical value, certain quantities remain unchanged:

- The throat Mach number reaches a maximum (unity, sonic flow),
- The flow velocity reaches a maximum (speed of sound of the medium),
- The pressure reaches a minimum, and
- The mass flow rate reaches a maximum

However, the decreasing back pressure will affect the flow beyond (downstream of) the throat as discussed previously in section 5.3.1. One outcome of that review was that nozzle back pressure, at certain values, can lead to standing normal shocks within or just outside the diverging section. Across a shock plane, pressure increases and velocity decreases in an approximately step-wise fashion such that the flow becomes subsonic.

To account for aerodynamic effects in a systems-level, control volume oriented solution approach, some simplifications must be made. Most importantly, the physical location of the shock inside the diverging section cannot be resolved. If the known back pressure indicates it, the flow may be assumed to pass through a standing normal shock at the nozzle exit plane. There are conservation equations that must be satisfied upstream (1) and downstream (2) of the shock [28]:

$$(6.73) \quad \rho_1 v_1 A_1 = \rho_2 v_2 A_2 \quad \text{Continuity}$$

$$(6.74) \quad A(P_1 - P_2) = \dot{m}(v_2 - v_1) \quad \text{Momentum}$$

$$(6.75) \quad h_1 + \frac{v_1^2}{2} = h_2 + \frac{v_2^2}{2}, \text{ or } h_{02} = h_{01} \quad \text{Energy}$$

Note there is an attending increase in entropy such that $s_2 > s_1$. Thus, for a one-dimensional ideal gas flow across a normal shock, these property relations hold [28]:

$$(6.76) \quad M_2 = \left[\frac{M_1^2(\gamma-1)+2}{2\gamma M_1^2 - \gamma + 1} \right]^{1/2} \quad \text{Mach Number}$$

$$(6.77) \quad \frac{P_2}{P_1} = \frac{1+\gamma M_1^2}{1+\gamma M_2^2} = \frac{2\gamma M_1^2 - \gamma + 1}{\gamma + 1} \quad \text{Pressure Ratio}$$

$$(6.78) \quad \frac{\rho_2}{\rho_1} = \frac{P_2/P_1}{T_2/T_1} = \frac{(\gamma+1)M_1^2}{2+(\gamma-1)M_1^2} = \frac{V_1}{V_2} \quad \text{Density Ratio}$$

$$(6.79) \quad \frac{T_2}{T_1} = \frac{2+M_1^2(\gamma-1)}{2+M_2^2(\gamma-1)} \quad \text{Temperature Ratio}$$

Stagnation pressure relationships [28]:

$$(6.80) \quad \frac{P_{02}}{P_{01}} = \left(\frac{M_1}{M_2}\right) \left[\frac{1+M_2^2\left(\frac{\gamma-1}{2}\right)}{1+M_1^2\left(\frac{\gamma-1}{2}\right)} \right]^{(\gamma+1)/(2\gamma-2)}$$

$$(6.81) \quad \frac{P_{02}}{P_1} = \frac{(1+\gamma M_1^2)\left(1+M_2^2\left(\frac{\gamma-1}{2}\right)\right)^{\gamma/\gamma-1}}{1+\gamma M_2^2}$$

Normal shock effects can be at least partially captured by application of these shock relations at the nozzle exit plane if back pressure suggests a standing normal shock should exist. Several aspects of shock physics (multi-dimensional effects, impact on condensation, boundary layer separation, etc.) are beyond the scope of a simple systems-level control volume formulation.

6.3.5 Saturation Line Equation

A saturation line equation which expresses the inter-dependence of pressure and temperature for saturated steam is used for purposes of fixing thermodynamic states along the steam expansion. The saturation equation is [51]:

$$(6.82) \quad \ln(P_{sat}) = A_0 - A_1/T_{sat} - A_2/T_{sat}^2$$

Where:

$$A_0 = 23.24348 \quad ; \quad A_1 = 3757.8699 \quad ; \quad A_2 = 229190.7$$

6.3.6 Steam Nozzle Expansion Model

A strategy for “marching” through the one-dimensional, steady, frictionless ideal gas converging-diverging nozzle steam flow is proposed here. Concepts of isentropic flow and Rayleigh flow are applied for different segments of the nozzle. Reference is made to Figure 6.6 as its state points (01, 2, m, n, a, 3, 4) are treated as “expansion waypoints” that guide the expansion model calculation. The process is outlined in subsequent paragraphs for each step to computing steam nozzle expansion.

6.3.6.1 First Step

First, a stagnation state **01** (T_{01} , P_{01}) is fixed from known CV conditions upstream of the nozzle FL and from assumed specific heat ratio $\gamma = 1.3$ or 1.14 for superheated or saturated steam, respectively. The relationships are purely algebraic and need no iteration:

$$(6.83) \quad T_{01} = T_1 + \frac{v_{cv}^2}{2c_p(T_1)}$$

$$(6.84) \quad P_{01} = P_1 \left(\frac{T_{01}}{T_1} \right)^{\gamma/\gamma-1}$$

6.3.6.2 Second Step

Second, the saturated state **2** (T_2, P_2) is fixed using known conditions at **01**, isentropic flow relations, and a saturation line equation. A system of two equations are solved with a Newton iteration scheme as generally outlined in Appendix C:

$$(6.85) \quad R * \ln \left(\frac{P_2}{P_1} \right) = \int_{T_1}^{T_2} c_p(T) * \left(\frac{dT}{T} \right)$$

$$(6.86) \quad \ln(P_2) = A_0 - A_1/T_2 - A_2/T_2^2$$

Note that if no solution is found for a given set of nozzle inlet conditions, an isentropic expansion of steam (superheated throughout expansion) is assumed through the nozzle.

6.3.6.3 Third Step

Third, states **a** and **n** are solved ($T_a, P_a, M_a, T_n, P_n, M_n, Y_n, Y'_n$) with an iterative technique. This “wetness iteration” attempts to arrive at a self-consistent set of conditions for the isentropic reference state **a** and the Wilson point **n** according to a highly non-linear set of equations that encapsulate all applicable isentropic flow, Rayleigh flow, and nucleation/growth relationships. The process is more completely outlined in Appendix C, but some important property relations that must hold are:

$$(6.87) \quad \frac{P_a}{P_{01}} = \exp \left[\left(\frac{-1}{R} \right) \int_{T_a}^{T_{01}} c_p(T) * \left(\frac{dT}{T} \right) \right] \quad (\text{Isentropic flow, 01 to a})$$

$$(6.88) \quad M_a^2 = \frac{2}{\gamma R T_a} \int_{T_a}^{T_{01}} c_p(T) * dT \quad (\text{Isenthalpic (stagnation) flow, 01 to a})$$

$$(6.89) \quad \frac{T_n}{T_a} = 1 + \left(\frac{\gamma M a^2 - 1}{M a^2 - 1} \right) \left(\frac{h_{fg} Y}{T_a c_{p,a}} \right) \quad (\text{Rayleigh flow, a to n, simplified})$$

$$(6.90) \quad \frac{P_n}{P_a} = 1 + \left(\frac{\gamma M a^2}{M a^2 - 1} \right) \left(\frac{h_{fg} Y}{T_a c_{p,a}} \right) \quad (\text{Rayleigh flow, a to n, simplified})$$

Wilson point wetness:

$$(6.91) \quad Y_n = \frac{2\pi}{3} \rho_l I_n \alpha^4 c_{gn}^3 \left(1 + \frac{3\sqrt{\pi}}{2} \left(\frac{r_n^*}{c_{gn}\alpha} \right) + 3 \left(\frac{r_n^*}{c_{gn}\alpha} \right)^2 + \sqrt{\pi} \left(\frac{r_n^*}{c_{gn}\alpha} \right)^3 \right)$$

$$(6.92) \quad Y'_n = \pi^{3/2} \rho_l I_n \alpha^3 c_{gn}^3 \left(1 + \frac{4}{\sqrt{\pi}} \left(\frac{r_n^*}{c_{gn}\alpha} \right) + 2 \left(\frac{r_n^*}{c_{gn}\alpha} \right)^2 + \frac{4}{3\sqrt{\pi}} \left(\frac{r_n^*}{c_{gn}\alpha} \right)^3 \right)$$

The solution procedure involves a Regula-Falsi search for a Wilson point temperature that leads to convergence of nucleation pulse half-width as predicted by two separate prescriptions (outlined in Appendix C). The converged nucleation pulse half-width yields Wilson point wetness directly and thereby all state **a** and **n** properties. At the end of each wetness iteration, the updated state properties at **a** and **n** including wetness are checked with equations (6.87 through (6.92, among others, to judge “convergence”. Iteration-to-iteration changes in quantities are also tracked.

If the searching algorithm and regula-falsi solution method cannot establish a Wilson point temperature leading to sufficiently converged nucleation pulse half-width,

metastability is discounted and an isentropic steam expansion from state **2** to state **4** is assumed. Note this expansion occurs upon user request too. The solution process is:

- Using the assumed critical pressure ratio, get nozzle throat conditions
- Compute the state **4** properties from throat properties and user-input area fraction (nozzle exit to nozzle throat) using an iterative bisection approach with Y_4 the variable and an entropy equation the function
- Compute a normal shock or jet expansion depending on back pressure

Some important aspects of the **2-to-4** isentropic steam expansion:

- The critical pressure ratio is

$$(6.93) \quad P^* / P_{01} = \left(\frac{2}{\gamma+1} \right)^{\gamma/\gamma-1}$$

- Saturation conditions are assumed at the throat and stagnation enthalpy is constant between state **2** and the throat
- The Mach number relation used in the throat-to-**4** bisection scheme:

$$(6.94) \quad M_4 = \frac{A_t}{A_e} \left[\left(\frac{2}{\gamma+1} \right) \left(1 + \left(\frac{\gamma-1}{2} \right) M_4^2 \right) \right]^{\gamma+1/2(\gamma-1)}$$

- The entropy relation used in the bisection scheme is:

$$(6.95) \quad \bar{C}_{p,4} \ln \left(\frac{T^4}{T_t} \right) = R \ln \left(\frac{P^4}{P_t} \right), \bar{C}_{p,4} = \left(\frac{1}{1+Y_4} \right) (C_{pg,t} + Y_4 C_{pl,t})$$

- The calculation of velocity at 4 uses $\bar{C}_{p,4}$

6.3.6.4 Fourth Step

Fourth, a Rayleigh flow process is followed from the Wilson point **n** to the reversion point **3** (solving for P_3 , M_3 , Y_3) which is the point where saturation conditions are re-established. Four equations are involved (recall $M_n = M_a$):

$$(6.96) \quad \frac{P_3}{P_n} = \frac{(1 + \gamma M_n^2)}{(1 + \gamma M_3^2)}$$

$$(6.97) \quad \frac{T_3}{T_n} = \frac{(M_3^2 (1 + \gamma M_n^2)^2)}{(M_n^2 (1 + \gamma M_3^2)^2)}$$

$$(6.98) \quad P_3 = \exp \left(A_0 - \frac{A_1}{T_3} - \frac{A_2}{T_3^2} \right)$$

$$(6.99) \quad \frac{\Delta s_{3n}}{c_p} = \frac{\Delta y_{3n} h_{fg}}{c_p} = \ln \left[\left(\frac{M_3}{M_n} \right)^2 \left(\frac{1 + \gamma M_n^2}{1 + \gamma M_3^2} \right)^{1 + \gamma/\gamma} \right]$$

Also, wetness relates to flow quality as:

$$(6.100) Y_3 = \frac{1-X_3}{X_3}$$

Newton's method is used to solve a two-equation system consisting of equation (6.96 and (6.97 for T_3 and M_3 . Saturation pressure P_3 follows immediately from T_3 according to equation (6.98. Equations (6.99 and (6.100 yield wetness and flow quality. Then, state **3** entropy and enthalpy can be calculated using flow quality and saturated liquid/vapor entropy and enthalpy.

If no solution is found during the Newton's method system solve, an assumption of thermally-choked flow is applied. In this case, the latent heat released during reversion from the Wilson point is sufficient to either:

- Lower the Mach number to unity if M_n was larger than unity, or
- Raise the Mach number to unity if M_n was smaller than unity

This behavior is consistent with the nature of the "Rayleigh line" which the Rayleigh flow process follows from **n** to **3** [28]. The choked Rayleigh flow property relations and an entropy equation similar to (6.99 may be applied in this case where M_3 is unity:

$$(6.101) T_3 = T_n \left(\frac{1+\gamma M_n^2}{M_n(1+\gamma)} \right)^2$$

$$(6.102) P_3 = P_n \left(\frac{1+\gamma M_n^2}{1+\gamma} \right)$$

$$(6.103) \frac{\Delta s_{3n}}{c_p} = \frac{\Delta y_{3n} h_{fg}}{c_p} = \ln \left[\left(\frac{1}{M_n} \right)^2 \left(\frac{1+\gamma M_n^2}{1+\gamma} \right)^{1+\gamma/\gamma} \right]$$

6.3.6.5 Fifth Step

In the fifth step, a specialized homogeneous-equilibrium two-phase flow model is employed to model the expansion of saturated steam between states **3** and **4**. As suggested in [53], a two-phase mixture of an ideal gas and a dilute, dispersed secondary phase may be treated with the conventional HEM plus augmented specific heats depending on the mass fraction of the dispersed phase. Details are expounded in Appendix F. This approach holds under the assumption of thermal equilibrium between the continuous gas phase and dilute liquid phase (as would occur under saturation conditions) Thus, the pseudo-gas is treated as ideal but with modified specific heat and specific heat ratio. To get to state **4**:

- A Newton's method solution to an ideal gas expansion law and the saturation line equation is done to recover P_4 and T_4
- A Newton's method solution to a stagnation pressure relation is used to get M_4
- A Newton's method solution to a stagnation enthalpy relation is used to get Y_4

6.3.6.6 Sixth Step

Sixth, if an oblique shock ought to exist according to turbine back pressure (i.e. if over-expansion occurs such that P_4 is lower than the back pressure), the effects of such a phenomenon are approximated by those of a standing normal shock and are imposed on the nozzle outlet state **4**. In this case, expansion state **4p** is computed with:

$$(6.104) M_{4p} = [(M_4^2(\gamma - 1) + 2)/(2\gamma M_4^2 - \gamma + 1)]^{1/2}$$

$$(6.105) P_{4p}/P_4 = (1 + \gamma M_4^2)/(1 + \gamma M_{4p}^2) = (2\gamma M_4^2 - \gamma + 1)/(\gamma + 1)$$

$$(6.106) T_{4p}/T_4 = (2 + M_4^2(\gamma - 1))/(2 + M_{4p}^2(\gamma - 1))$$

If instead the flow at 4 is under-expanded (i.e. if P_4 is higher than the back pressure), an algebraic formulation proposed by Idaho National Laboratories (INL) [54] is used to predict the jet expansion that occurs between the nozzle outlet plane and the rotor bucket inlet. The model is summarized in Appendix G and is based on the “virtual nozzle” concept. Three sequentially-solved algebraic equations are used to predict:

- Velocity and Mach number at end of virtual nozzle
- Temperature at end of virtual nozzle (pressure is known turbine back pressure)
- Density at end of virtual nozzle

Because the jet expands further beyond the nozzle exit plane, the velocity at the end of the virtual nozzle will be higher and the pressure lower. The equations for 4p in this case are:

$$(6.107) V_{4P} = \frac{P_4 - P_B + \rho_4 V_4^2}{\rho_4 V_4}$$

$$(6.108) T_{4P} = T_4 + \frac{V_4^2 - V_{4P}^2}{2 * C_{p4}}$$

$$6.109 \quad \rho_{4P} = \left(\frac{\rho_4 T_4}{\rho_4} \right) \left(\frac{\rho_{4P}}{T_{4P}} \right)$$

The nozzle outlet conditions feed into the Terry turbine compound velocity stage model so that impulses delivered by steam on the turbine can be calculated. One pressure stage FL (representing one steam nozzle) feeds one “set” of rotor buckets and reversing chambers. Several steam nozzles are typically situated around the rotor circumferentially and there is no need to assume all nozzles have the same flow conditions. However, the capability to model multiple, identical nozzles with a sole flow path is included via a so-called steam nozzle multiplicity factor.

6.4 Terry Turbine Shaft Model

The shaft torque-inertia equation represents the rigid coupling between the driving steam turbine rotor on one end and the following/resisting centrifugal pump impeller on the other. Shaft speed is computed as a function of torques exerted on the shaft by the turbine (typically in a “positive” direction via steam impinging on the rotor buckets) and on the shaft by the pump (typically in a “negative” direction via hydraulic resistance of the pumped fluid against the impeller). The resistance of the pumped fluid is “felt” immediately on the turbine side via the rigid shaft. Additional terms for turbine and pump friction torque ought to be included. Additionally, some extra user-defined torque ought to be allowed. The shaft speed equation can be written as:

$$(6.110) \quad (I_T + I_P) \frac{\partial \omega}{\partial t} = \tau_T - \tau_P - \tau_{fr,T} - \tau_{fr,P} - \tau_{user}$$

Where:

T denotes “turbine” ; P denotes “pump” ; fr denotes “friction”

Note that the moments of inertia and the friction torques are user-defined quantities. The turbine moment of inertia and friction torque are formulated just as they are for the pump model (see sections 6.1.5.1 and 6.1.5.2). The turbine and pump torques come from the new Terry turbine compound velocity stage (and pressure stage) model and the homologous pump model, respectively. Note in the above equation that τ_T must consider all pressure stage nozzles (each associated with a set of reversing chambers) circumferentially-situated about a rotor

The numerical solution method for the shaft speed equation will resemble that of the homologous pump model torque-inertia equation (see section 6.1.5.3). Thus, an explicit (forward Euler) or a fully implicit (backward Euler with fixed-point iteration) numerical solution technique will be employed.

6.5 MELCOR Implementation and Aspects of Solution Methodology

Below, user input provisions are described and some discussion of MELCOR solution strategy is included. Each aspect of the Terry turbine model is taken in turn.

6.5.1 *Velocity Stage Model*

With respect to user input in MELCOR, provisions were added to the CVH block input structure. For any CV, a Terry turbine rotor may be defined by (see Appendix D):

- CV_ROT card for rotor name and number, number of reversing chambers per nozzle for all nozzles in the rotor, and rotor radius
- CV_RIN for turbine moment-of-inertia calculations
- CV_RFR for turbine friction torque calculations
- CV_RBE for bucket steam exit angles, CF or constant, one per each bucket associated with steam nozzles
- CV_RCB for bucket loss coefficients, CF or constant, one per each bucket associated with steam nozzles
- CV_RGR for reversing chamber leakage coefficients, CF or constant, one per each reversing chamber associated with steam nozzles
- CV_RCR for reversing chamber loss coefficients, CF or constant, one per each reversing chamber associated with steam nozzles
- CV_RXZI for steam carry-over fractions, CF or constant, one per each reversing chamber associated with steam nozzles
- CV_NFP to identify all steam nozzle FLs associated with rotor

In terms of actually solving for the Terry turbine velocity stage, the pertinent Terry turbine code is triggered when a homologous pump is being used and when that pump is specified as coupled to a turbine (FL_TSH, see Appendix D). The Terry turbine calculations (moment-of-inertia, friction torque, total turbine torque due to steam impingement on rotor) are called from within the inner velocity iteration that solves for phasic velocities.

Due to observed numerical wiggles in time, a temporal relaxation was added to the homologous pump model when it is used in tandem with the new RCIC turbine-side physics models. The temporal relaxation is applied to the pump flow path volumetric flow rate because this quantity is a function of phasic velocities following from the MELCOR phasic velocity equation system solution. The formulation is:

$$(6.111) \dot{Q}_{relax} = \omega * \dot{Q}_{new-time} + (1 - \omega) * \dot{Q}_{old-time}$$

The factor ω is the temporal relaxation factor, defined with a time-scale T as:

$$(6.112) \omega = MIN(1, \Delta t / T)$$

The temporal relaxation factor is a user input and essentially defines the allowable time-scale on which the pump volumetric flow rate is allowed to change. If the current problem time-step Δt is smaller than the prescribed time-scale, the change in pump volumetric flow is limited via a blending between old and new quantities. This approach helps to eliminate oscillations of model parameters in time that naturally arise due to the application of steady-state models to a transient.

6.5.2 Pressure Stage Model

With respect to user input in MELCOR, new FL tabular input records were added. For any given FL, a steam nozzle may be defined via FL_VTM and a pump object may be associated with a rotor object via FL_TSH. Further details are in Appendix D.

In terms of actually solving for the Terry turbine pressure stage, the pertinent steam nozzle code is triggered when user-specified flow path is found and furthermore when that flow path is both:

- Flagged with a special keyword as a steam nozzle
- Associated with a rotor object in some CV

6.5.3 *Turboshaft Model*

No special user input provisions exist exclusively for the turboshaft. A turboshaft is implied when an association is made between a pump object and a rotor object (FL_TSH, see Appendix D). When this occurs, a torque-inertia equation is solved subject to torques from the turbine and pump. The shaft speed equals the pump impeller speed which in turn equals the turbine rotor speed due to the assumed rigidity of the shaft.

To actually solve for the turbo-shaft speed, a subroutine is called just after all of the following occur:

- A pump associated with a turbine is found
- The turbine torques are resolved and turbine moment-of-inertia is computed
- The pump torques are resolved and pump moment-of-inertia is computed

The calculation itself resembles that of a stand-alone homologous pump with impeller speed coming from a torque-inertia equation solution.

6.6 CFD-informed Systems Level Model Parameters

The systems-level RCIC Terry turbine formulations have parameters that account for effects beyond the scope of systems-level modeling. Generally, these parameters must

be supplied by the MELCOR user but some CFD studies undertaken in this dissertation can furnish a “built-in” data set. The parameters will be discussed briefly in turn below. Appendix D gives an idea as to required user input in MELCOR for these new parameters.

6.6.1 Velocity Stage Model Parameters

Referring back to section 6.2 and equations (6.40 through (6.42, there are several factors in the velocity stage model formulation that require user specification:

- Bucket loss coefficients C_B ,
- Steam exit angles β ,
- Carry-over fractions ξ ,
- Reversing chamber loss coefficients C_{RC} , and
- Reversing chamber leakage coefficients γ_{RC}

Physical insights as to the significance of these terms may be gleaned from Appendix B. To quickly recapitulate:

- Bucket loss coefficients capture the attending decrease in flow velocity when steam traverses a given rotor bucket
- Steam exit angles figure into moment-of-momentum computations and bear significance to the torque exerted by steam on a bucket
- Steam carry-over fractions account for the mismatch in steam flow exiting a given bucket and entering the downstream reversing chamber
- Reversing chamber loss coefficients capture the attending decrease in flow velocity when steam traverses a given reversing chamber

- Reversing chamber leakage coefficients account for loss of steam mass through the crescent hole in a given reversing chamber

These factors are specified by steam nozzle for all steam nozzles in a rotor object. There is some user-defined number of buckets and reversing chambers per steam nozzle and user input for all factors are organized as such.

6.6.2 Pressure Stage Model Parameters

The only pressure stage model parameter required of the user that must be informed by CFD or by experiments is the steam nozzle expansion rate (\dot{P}). This parameter factors into the nucleation/growth closures. The expansion rate is essentially an externally-imposed feature of nozzle geometry with units of inverse time. Mathematically, it is [51]:

$$(6.113) \dot{P} = \frac{1}{P} \frac{dP}{dt} = \frac{1}{P} \left(\mathbf{u} \frac{dP}{dx} \right)$$

7 RESULTS AND DISCUSSION

7.1 STAR-CCM+ Results

The purpose of the STAR-CCM+ calculations was two-fold:

- Validate - to the greatest extent possible - the condensing steam flow physics models so as to judge their appropriateness for the RCIC Terry turbine nozzle
- Gather information useful for systems-level RCIC Terry turbine models

Experiments – one from the literature and one from NHTS tests – were compared to STAR-CCM+ results for validation purposes. A matrix of STAR-CCM+ calculations ranging over the entire spectrum of possible Terry turbine rotor speeds was used to gather data for systems-level models.

7.1.1 Gyarmathy Steam Nozzle Experimental Benchmark

The purpose of Gyarmathy’s Laval nozzle experiments [55] was to study nucleation characteristics in high-pressure saturated/subcooled condensing steam. The experimental test section included a cylindrical steel vessel and several ramp inserts forming different Laval nozzle geometries with disparate expansion rates. An optical measurement technique based on red laser light beam attenuation was used to discern wetness/droplet characteristics. With certain assumptions, measurements were backwards-extrapolated to ascertain Wilson point properties.

7.1.1.1 Problem Description and Set-up

The experimental test section [55] numbered 4B – pictured in Figure 7.1 and described in Table 7.1- was reproduced in two dimensions in STAR-CCM+. Note that the data table gives the height of the “roller coaster” insert above its bottom that forms the

bottom surface of the nozzle channel. A physics model including equations/closures for condensing steam outlined in the previous section was applied to the geometry. Some of these equations are available as options in STAR-CCM+ while others (e.g. the nucleation theory and condensation growth equations) were built with user-defined field functions and applied as source terms. A polygonal, unstructured mesh with near-wall prism layers was applied as a spatial discretization of the geometry. Stagnation inlet and pressure outlet boundary conditions (consistent with known experimental conditions) were used. No-slip, adiabatic conditions were applied at walls.

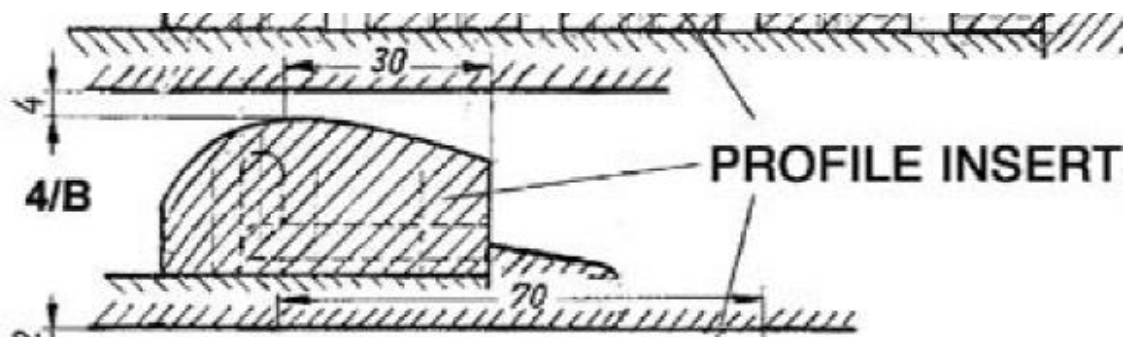


Figure 7.1 Gyarmathy experimental nozzle 4B geometry [53]

Table 7.1 Gyarmathy Nozzle 4B geometry data (constant width 20 mm) [53]

Axial Coord [mm]	Insert Height [mm]	Axial Coord [mm]	Insert Height [mm]
-20	9.59	16	20.26
-18	12.04	18	19.81
-16	14.24	20	19.34
-14	16.17	22	18.83
-12	17.85	24	18.28
-10	19.27	26	17.69
-8	20.44	28	17.07
-6	21.34	30	16.40
-4	21.98		
-2	22.37		
0 (throat)	22.50 (throat)		
2	22.42		
4	22.23		
6	21.99		
8	21.71		
10	21.40		
12	21.05		
14	20.67		

The steam nozzle 4B (run 19A) expansion rate is reported as approximately 50,000 [1/s] and the throat cross-sectional is: 4 mm in height, 20 mm in width, and 0.8 cm² in area [53]. Superheated steam inlet conditions were: stagnation (or total) pressure of 6.147×10^6 [Pa] and stagnation (or total) temperature of 583.55 [K]. A pressure outlet (supersonic) simply extrapolates the boundary values of variables using the neighboring cell values and computed reconstruction gradients. This is consistent with the physics of supersonic flow, as “one-way street” behavior occurs and information does not propagate upstream into the computational domain from the outlet boundary. Initial conditions were linearly-varying estimates of solution variables based on experimental results, isentropic flow hand calculations, or otherwise educated guesses.

7.1.1.2 Results

In Table 7.2, certain derived quantities from the simulation are compared to reported values from [53] which constitute either experimental measurements or extrapolations based on certain assumptions such as isentropic flow. Additionally, profiles of solution quantities are included in several figures. These more detailed descriptions of the flow cannot be directly benchmarked against experimental data because the Gyarmathy experiments yielded point value measurements (from pressure taps, optical scattering, etc.) as opposed to spatial profiles.

Table 7.2 Gyarmathy experimental benchmark, nozzle 4B, run 19A

<u>Parameter</u>	<u>Units</u>	<u>Gyarmathy</u>	<u>CMFD</u>
Wilson Point Pressure	<i>MPa</i>	1.57-1.6	1.03
Critical Drop Size	<i>M</i>	4.314-4.469 *10 ⁻⁸	1.318*10 ⁻⁸
Drop Per Mass	<i>Drop/kg_{steam}</i>	11.99-13.40*10 ¹⁶	5.69*10 ¹⁵
Wilson Point Enthalpy	<i>kJ/kg</i>	2712.72-2716.32	2748.99
Wilson Point Temp	<i>C</i>	177.14-178.92	173.98
Wilson Point Sub-cooling	<i>K</i>	22.46-23.33	17.33

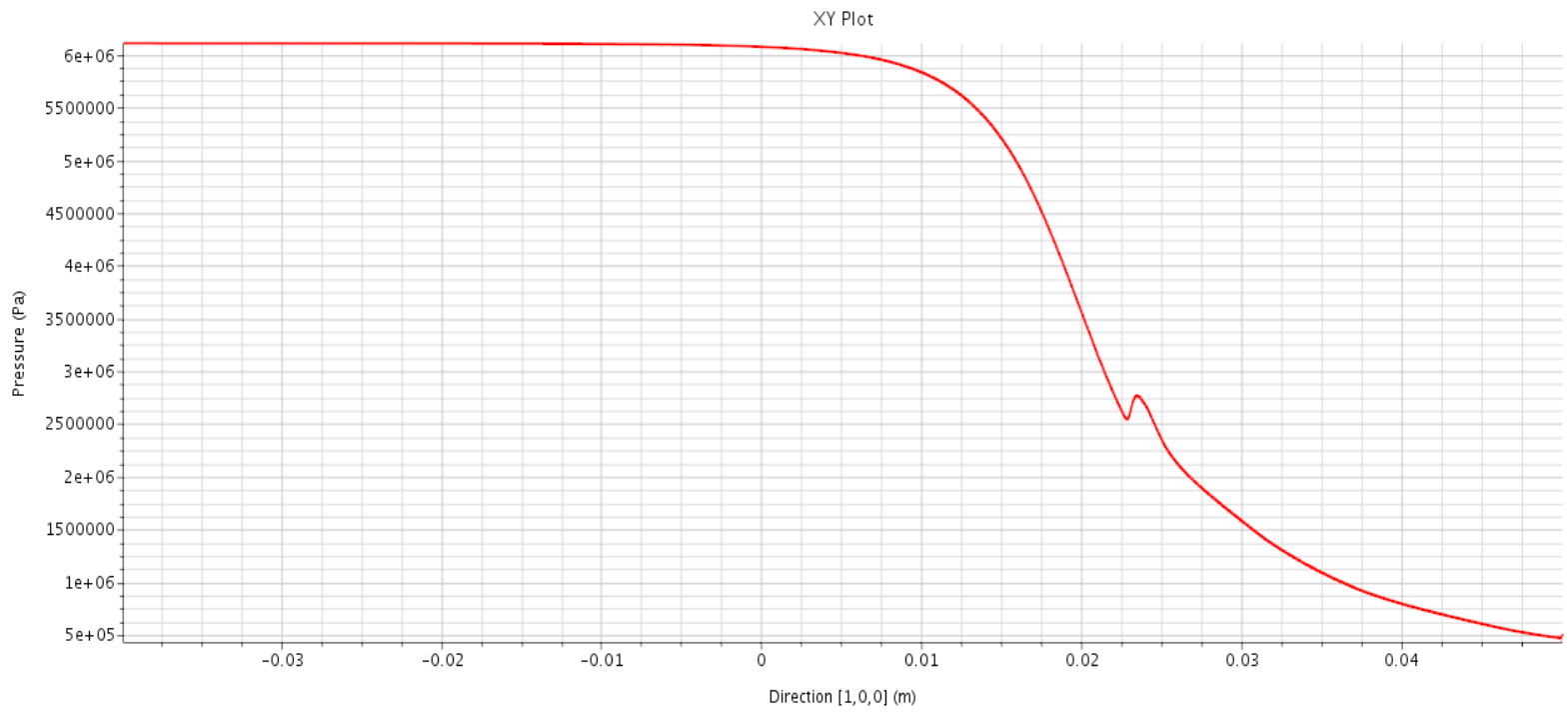


Figure 7.2 Pressure [Pa] distribution along nozzle wall

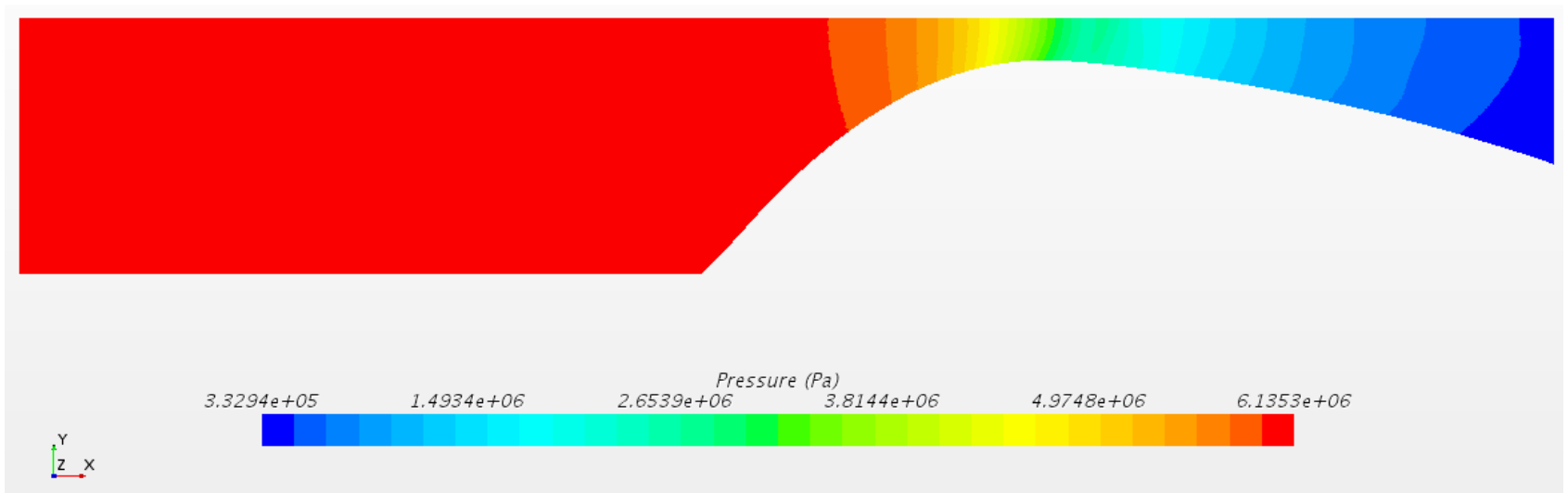


Figure 7.3 Pressure [Pa] profile in nozzle

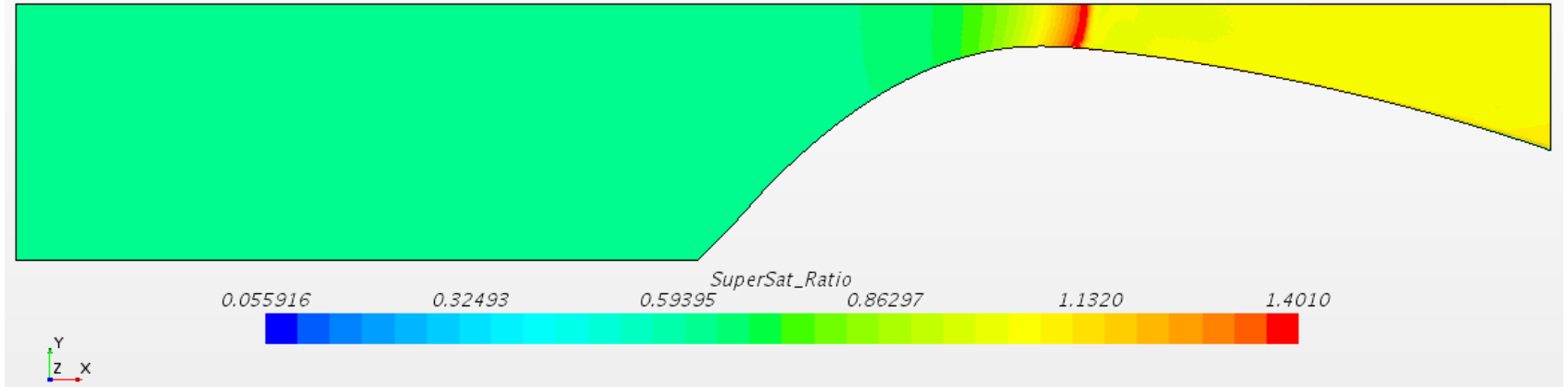


Figure 7.4 Super-saturation [-] ratio in nozzle

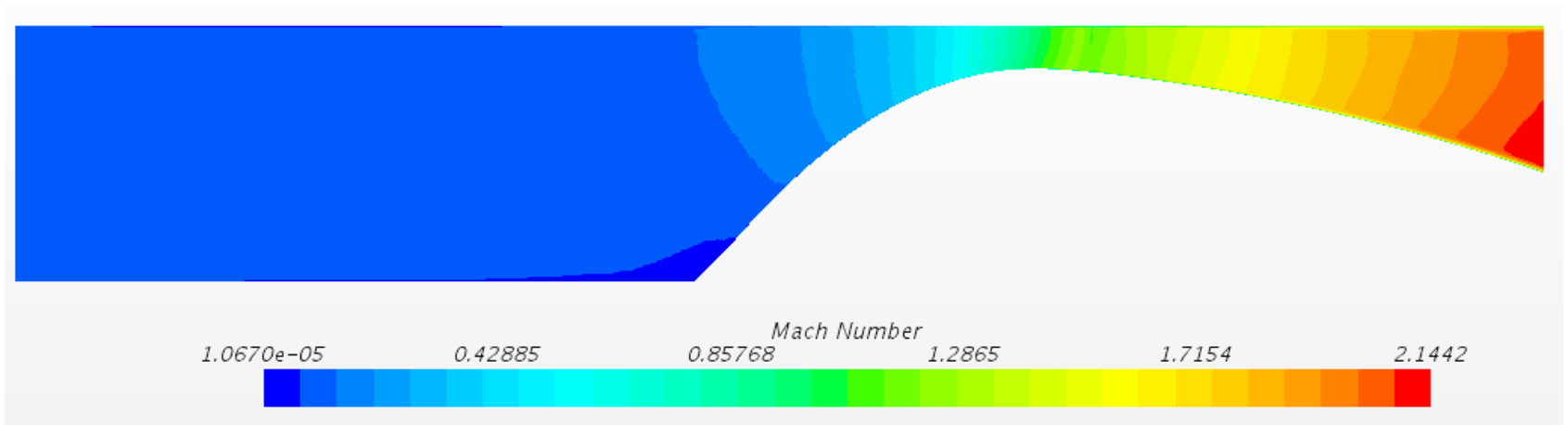


Figure 7.5 Mach number [-] in nozzle

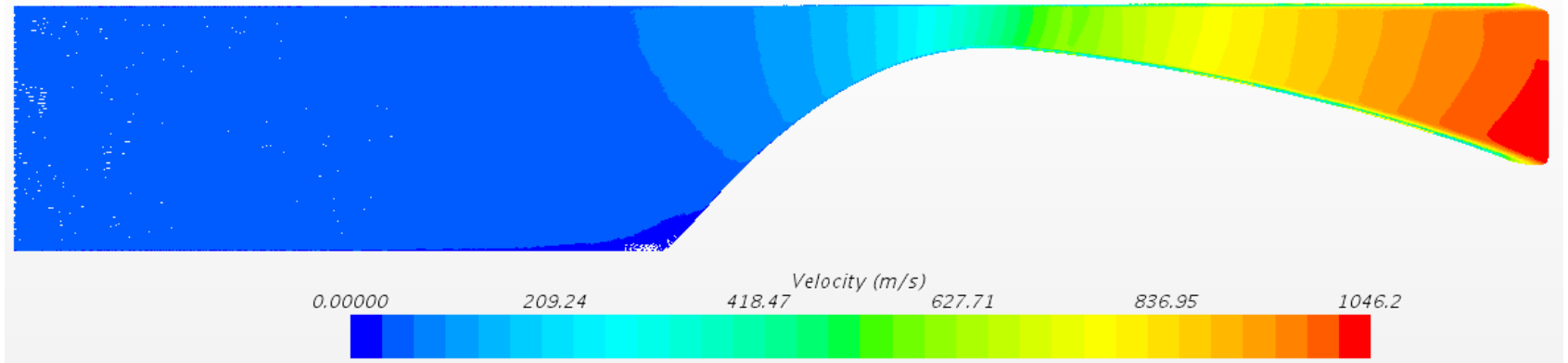


Figure 7.6 Velocity [m/s] vectors in nozzle

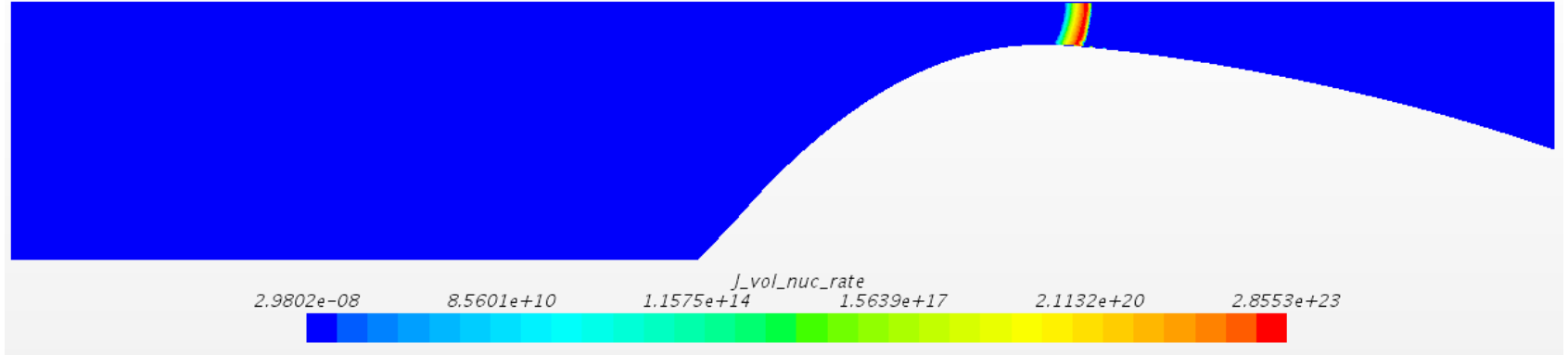


Figure 7.7 Nucleation rate [drop/m³/s] in nozzle

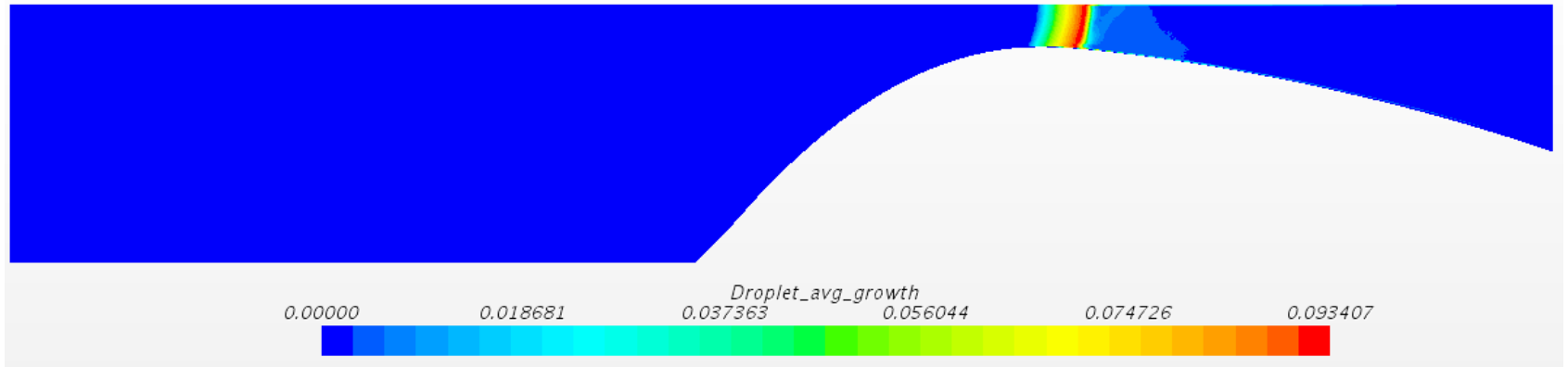


Figure 7.8 Condensation rate [m/s] in nozzle

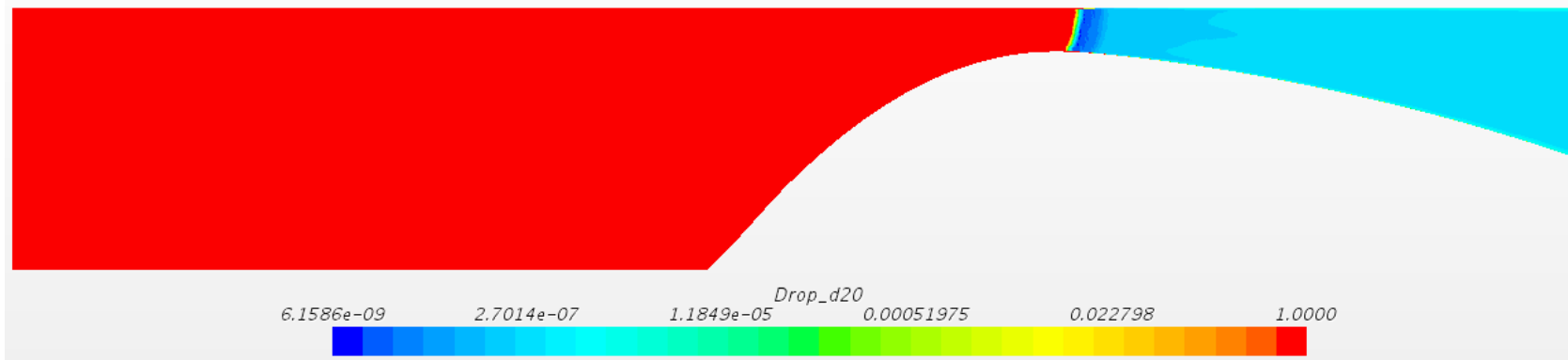


Figure 7.9 Droplet two-zero (average) diameter [m] in nozzle

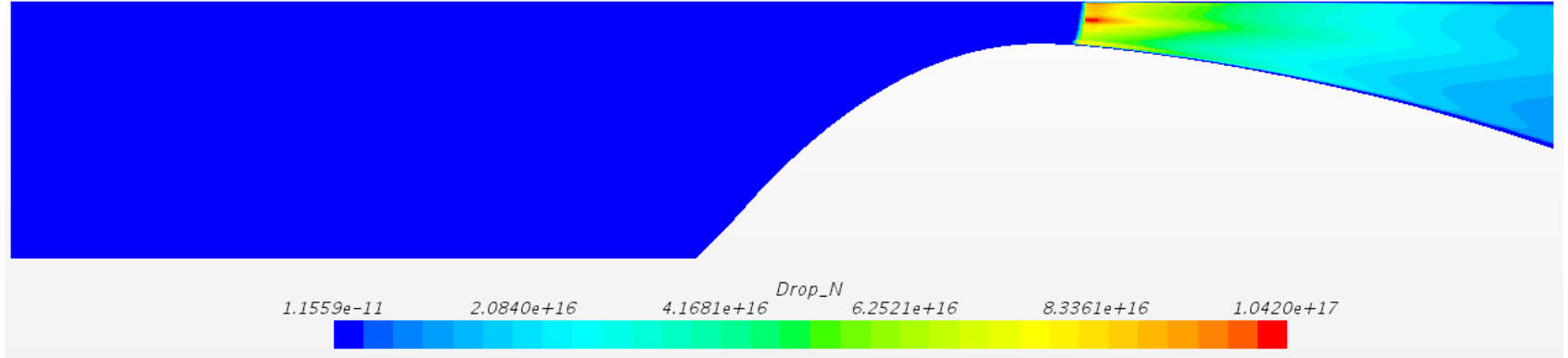


Figure 7.10 Droplet number density [drop/m³] in nozzle

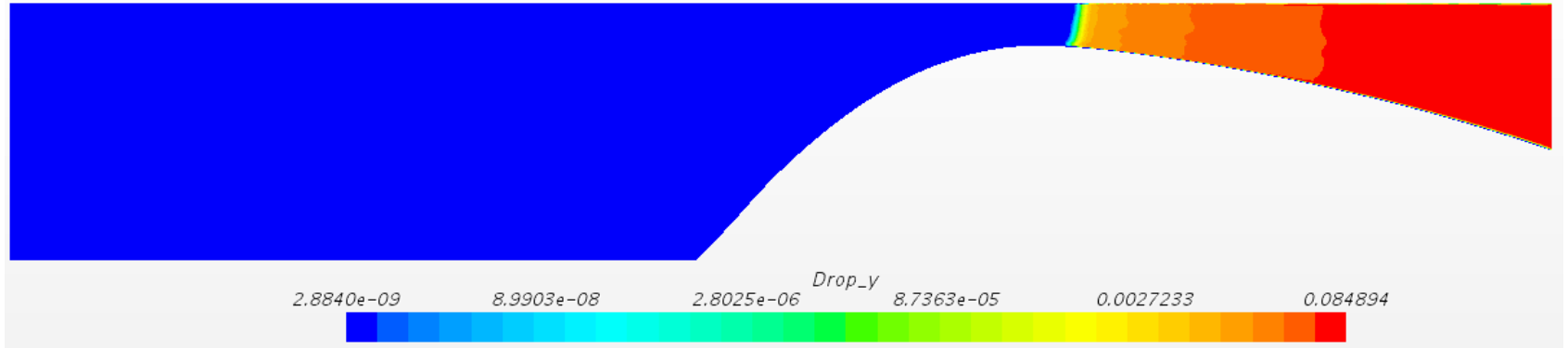


Figure 7.11 Droplet mass fraction [kg_l/kg_g] in nozzle

7.1.1.3 Discussion

The results from Figure 7.2 through Figure 7.11 demonstrate the converged solution obtained with steam physics models in STAR-CCM+. The metastability is evidenced by:

- Figure 7.2 where the pressure effects of condensation shock are visible (i.e. the “pressure bump” in the wall distribution from latent heat release to steam)
- Figure 7.3 where the effects of condensation shock on spatial pressure distribution are visible from the subtle blue-green-blue transition
- Figure 7.4 illustrating super-saturation (implying steam sub-cooling) that invariably leads to formation and growth of droplets
- Figure 7.5 where the steam slow-down due to momentum transfer associated with phase change is visible from the yellow-green-yellow transition
- Figure 7.6 where again the steam slow-down due to phase change is visible (changes of as much as 100 m/s near nucleation/condensation fronts)
- Figure 7.7 where predictions of the nucleation closures are shown
- Figure 7.8 where predictions of the condensation closures are shown, with a condensation front lagging a nucleation front in space (physically reasonable)
- Figure 7.9 where the passive scalar equation solutions are indirectly evidenced by the “two-zero” diameter (from second and zeroth moments)
- Figure 7.10 where the passive scalar equation solutions are indirectly evidenced by the droplet number density formed out of the zeroth size distribution moment

- Figure 7.11 which shows the dispersed mass fraction increasing along the flow direction as droplets grow in size/mass

7.1.2 Nuclear Heat Transfer Systems Labs Experimental Benchmark

The NHTS experimental test section [56] is designed to send wet or dry air through a ZS-1 model Terry turbine (similar to the larger GS-1 and GS-2 models in use at domestic PWR and BWR installations). Certain characteristics of turbine performance are measured such as rotational speed, shaft torque, and shaft power. By selecting an NHTS experimental run, matching boundary conditions in STAR-CCM+ on a three-dimensional Terry turbine geometry, running a simulation, and comparing results to measurements, the validity of certain CMFD modeling constructs can be examined. Primarily in question is the technique of combining a moving reference frame (set at the experimentally-observed rotational speed) with mixing planes to get a time-averaged depiction of turbine flow.

7.1.2.1 Problem Description and Set-Up

A three-dimensional wedge of a full GS-1 Terry turbine geometry was used for purposes of the NHTS benchmark calculation. Snapshots of the Terry turbine wedge geometry are shown in Figure 7.12 and Figure 7.13. The wedge was crafted with the STAR-CCM+ surface repair tool by essentially cutting a symmetric slice out of the full Terry turbine CAD model and creating periodic boundary conditions on the lateral wedge faces. The geometry was also split into inner (left and right) and outer (left and right) regions to facilitate mixing plane definitions. Inner regions (both left and right) were assigned a moving reference frame to simulate rigid body rotation of the turbine rotor.

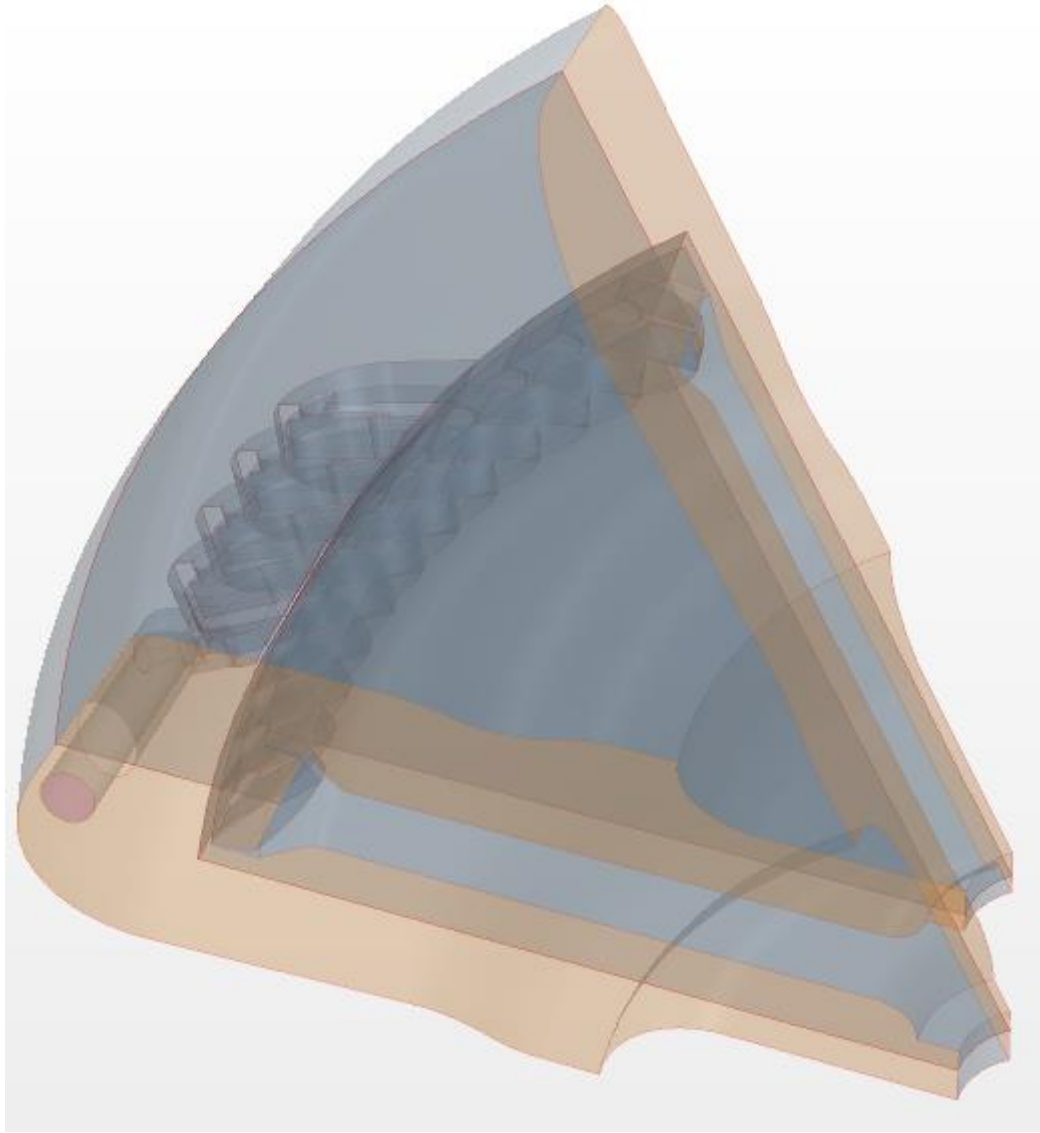


Figure 7.12 Full three-dimensional Terry turbine wedge

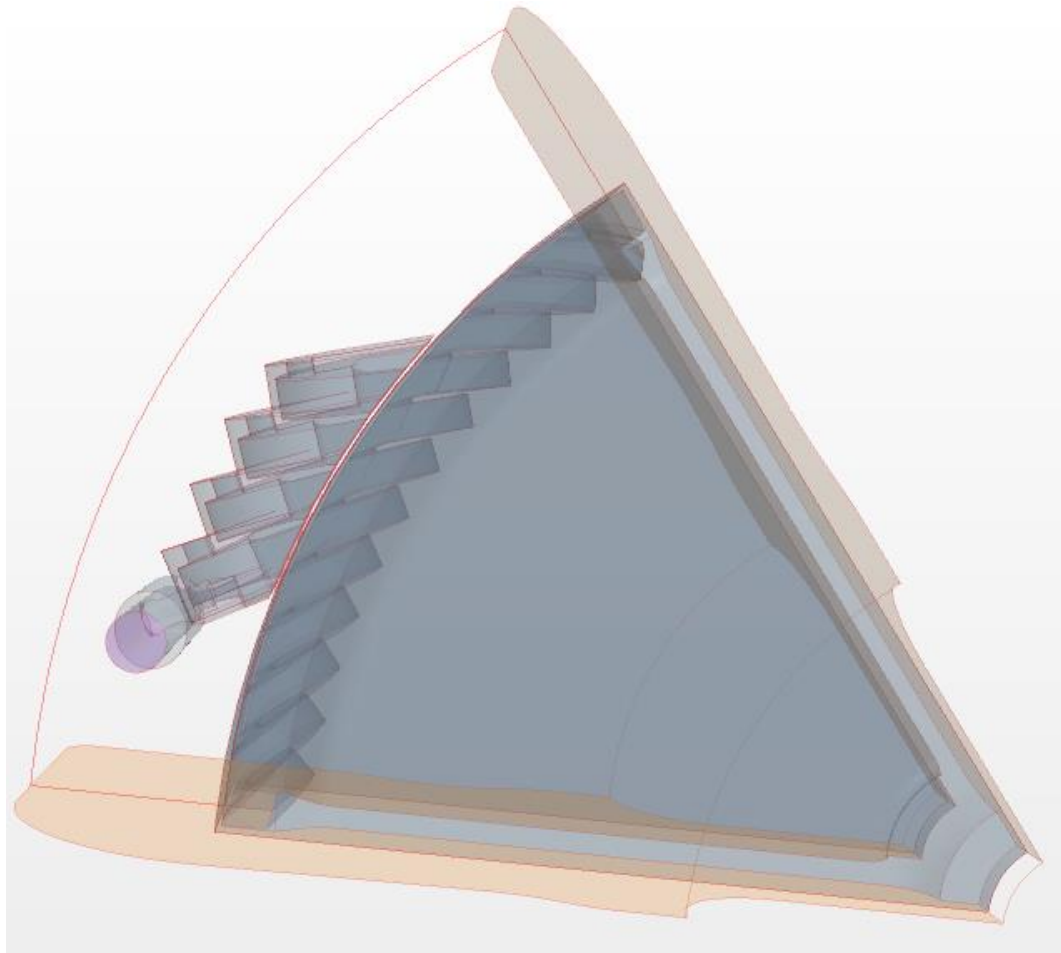


Figure 7.13 Terry turbine wedge, rotor and reversing chamber

Interfaces were set up between regions as necessary. The lateral wedge faces (orange-tinted in Figure 7.13) are periodic interfaces. In-place interfaces were used at all region-wise points of contact. Figure 7.14 demonstrates mixing plane configurations. The interface area between reversing chambers and accompanying rotor buckets was subdivided into three roughly equal patches. Each patch was defined as a mixing plane and arranged such that eighteen circumferential bins spanned the width of the patch.

Averaging occurs over each bin in each patch, and this choice of configuration produces average solution variable profiles across bucket and reversing chamber width.

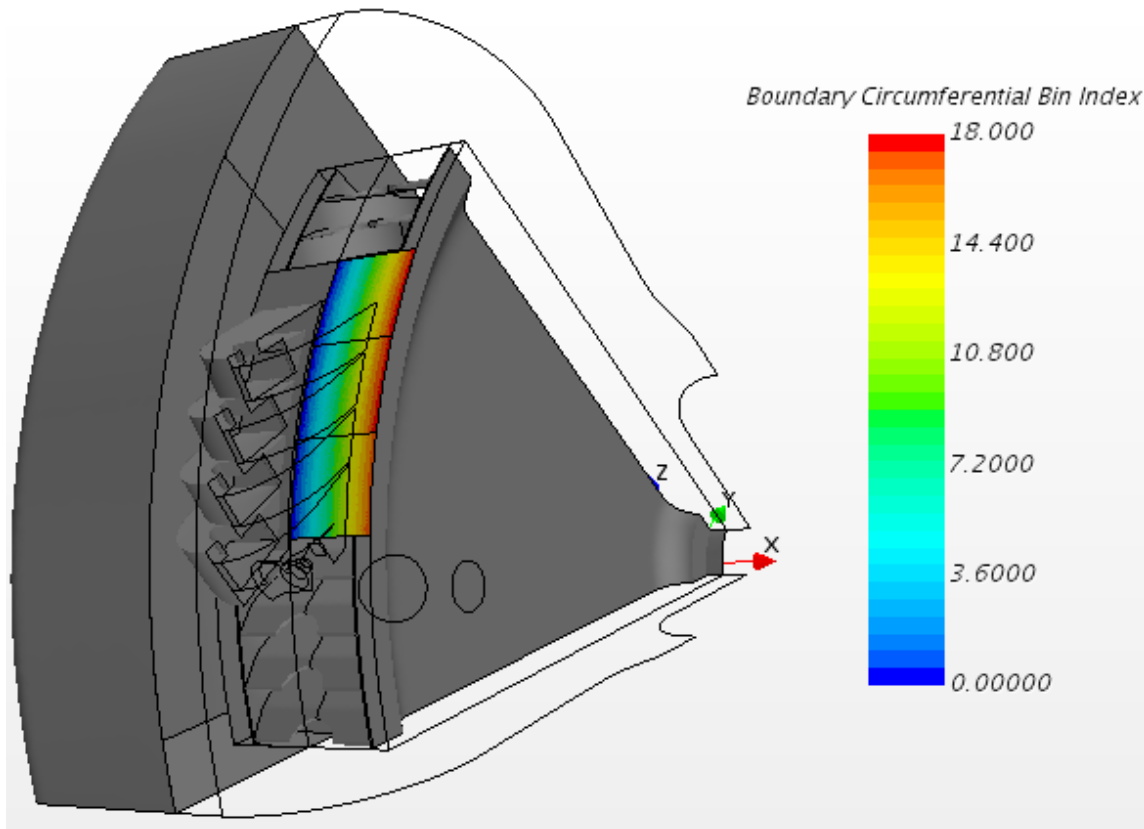


Figure 7.14 Cut-away view demonstrating mixing plane configuration

Boundary conditions are required at all solid surfaces (no slip, adiabatic), at the Terry turbine nozzle plenum inlet (stagnation inlet conditions), and at the periodic lateral wedge surfaces (pressure outlet). Additionally, a rotational speed must be specified for the moving reference frame assigned to the rotor. In this case, conditions were dictated by NHTS experimental conditions as summarized in Table 7.3 below.

Table 7.3 NHTS experimental benchmark conditions [56]

<u>Boundary/Condition</u>	<u>Value</u>	<u>Units</u>
Inlet/Pressure	360395.8	<i>Pa</i>
Inlet/Temperature	296.55	<i>K</i>
Inlet/Turbulence Intensity	0.01	-
Inlet/Turb Viscosity Ratio	10.0	-
Out/Pressure	106179.3	<i>Pa</i>
Out/Temperature	282.83	<i>K</i>
MRF/Rotational Speed	1500	<i>RPM</i>

7.1.2.2 Results

NHTS dynamometer measurements for torque and power were compared against simulation results. The single average torque value was computed in the simulation with the aid of a force report, which tallies the sum of pressure and shear force on a designated surface (or a collection thereof) by Cartesian coordinate. With all three components of force computed for the rotor bucket u-surfaces, a torque computation can be performed assuming a moment arm position vector with magnitude equal to the rotor radius and direction radially outward through the center of the Terry turbine wedge. Note the NHTS test section consisted of a ZS-1 Terry turbine (18” diameter wheel) containing just one steam nozzle. Therefore, the simulated GS-1 Terry turbine (24” diameter wheel) wedge with just one nozzle directly compares to the experiment, though the turbomachine

diameters and bucket sizes do differ. Table 7.4 below summarizes the torque/power comparison. Some details about the torque computation follow.

Table 7.4 NHTS experimental torque/power comparison and simulation results

<u>Metric</u>	<u>Value</u>	<u>Units</u>
NHTS torque/power	7.077 / 1115.56	$N*m / W$
Simulation torque/power	8.125 / 1276.27	$N*m / W$
Simulation F_j	0.405	N
Simulation F_k	61.64	N
Moment arm azimuth angle	0.4538	rad

7.1.2.3 Discussion

As previously mentioned, STAR-CCM+ furnishes the x, y, and z components of force exerted by air on the rotor bucket u-surfaces. The torque measurement of interest is along a direction tangential to the axis of rotor rotation and acting at a perpendicular distance approximately equal to the rotor radius. In a cylindrical coordinate system, the component of torque that turns the rotor is the azimuthal θ component which, according to a change of basis vectors from Cartesian to cylindrical, depends on the j^{th} and k^{th} Cartesian components of force:

$$(7.1) \quad F_{\theta} = F_j \cos(\theta) - F_k \sin(\theta)$$

Once the report furnishes Cartesian force components, the azimuthal component of force is computed assuming a known angle of the moment arm, θ (which lies in the Cartesian XZ plane for purposes of this simulation geometry). Multiplying F_θ by the moment arm radius yields a torque and multiplying torque by a fixed rotational speed (units of rad/s, not RPM) yields a shaft power.

The agreement in terms of experimental ZS-1 and computational GS-1 shaft torque/power lends some measure of confidence to the analytical approach, namely:

- Use of a moving reference frame (to approximate effects of a spinning rotor on local fluid motion)
- Use of mixing planes (to obtain a time-averaged, steady-state depiction of turbomachine response under all nozzle/rotor configurations)

The comparison in Table 7.4 is not perfect and was not expected to demonstrate exact agreement because of inherent differences in the experimental apparatus and the simulation geometry. Nevertheless, an air flow of similar temperature and pressure exerts a comparable torque despite difference in rotor size, velocity stages, etc.

7.1.3 Data to Inform Systems-Level Models

The systems-level Terry turbine models contain certain factors that must be informed by either experiments or CFD computations. They generally characterize some facet of turbomachine operation and are functions of rotor speed (except for the steam nozzle expansion rate). Some factors follow from a simplified velocity triangles analysis of a rotor bucket and/or a reversing chamber whereas other factors are needed to account for effects of multiple velocity stages. All factors discussed below pertain to the systems-level velocity stage model notwithstanding the steam nozzle expansion rate which is a required input to the pressure stage model.

7.1.3.1 Problem Description and Set-Up

The problem set-up is identical to that of the NHTS benchmark calculation in terms of geometry, analysis approach (mixing planes, moving reference frame), and boundary condition type. The simulation matrix is a set of twenty-seven runs with identical stagnation inlet and pressure outlet boundary conditions but with different moving reference frame rotational speed settings. All mixing planes and all derived part planes (used to track mass flow rates, average velocities, etc.) are identical in all simulations. Stagnation inlet conditions are summarized in Table 7.5. The moving reference frame assumes rotational speeds between 0 and 5625 rpm (the typical mechanical over-speed trip setting for Terry turbines).

Table 7.5 Simulation Matrix Stagnation Inlet Boundary Conditions

<u>Property</u>	<u>Value</u>	<u>Units</u>
Supersonic Static Pressure	6.147×10^6	<i>Pa</i>
Total Pressure	6.147×10^6	<i>Pa</i>
Total Temperature	550.0	<i>K</i>
Turbulence Intensity	0.01	-
Turbulent Viscosity Ratio	10.0	-

Upon convergence, a given simulation generates a series of reports, each one representing some physical quantity of significance used to compute one or more factors as described in turn below. The actual derived parts and/or reports used for each metric are explained in the respective sections below, but in general there are mass flow reports and velocity reports operating on one or more planes or curved surfaces strategically positioned throughout the solution domain.

7.1.3.2 Bucket Loss Coefficient

The bucket loss coefficient, denoted C_B in the systems-level velocity stage model, is computed for each bucket (downstream of a reversing chamber in the solution domain) as a ratio of surface-averaged velocity magnitudes. The surfaces in question for this parameter are not derived parts but rather the mixing planes that constitute the interface between the stationary outer regions of the model and the rotating inner regions of the model. Surface-averaged flow velocity magnitudes are calculated (via surface-average type reports) for mixing plane patches and ratios are taken.

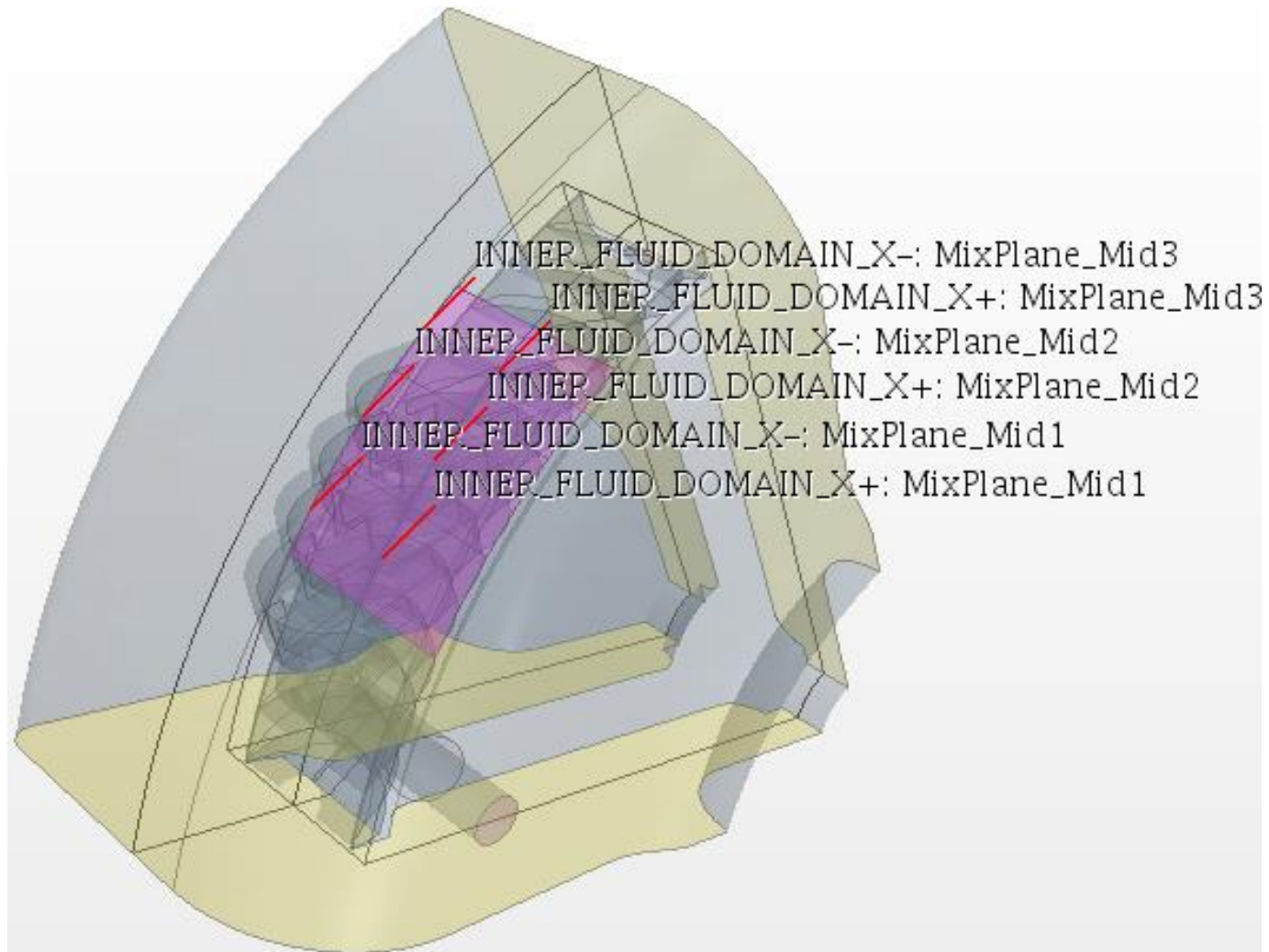


Figure 7.15 Mixing planes used to compute rotor bucket loss coefficients

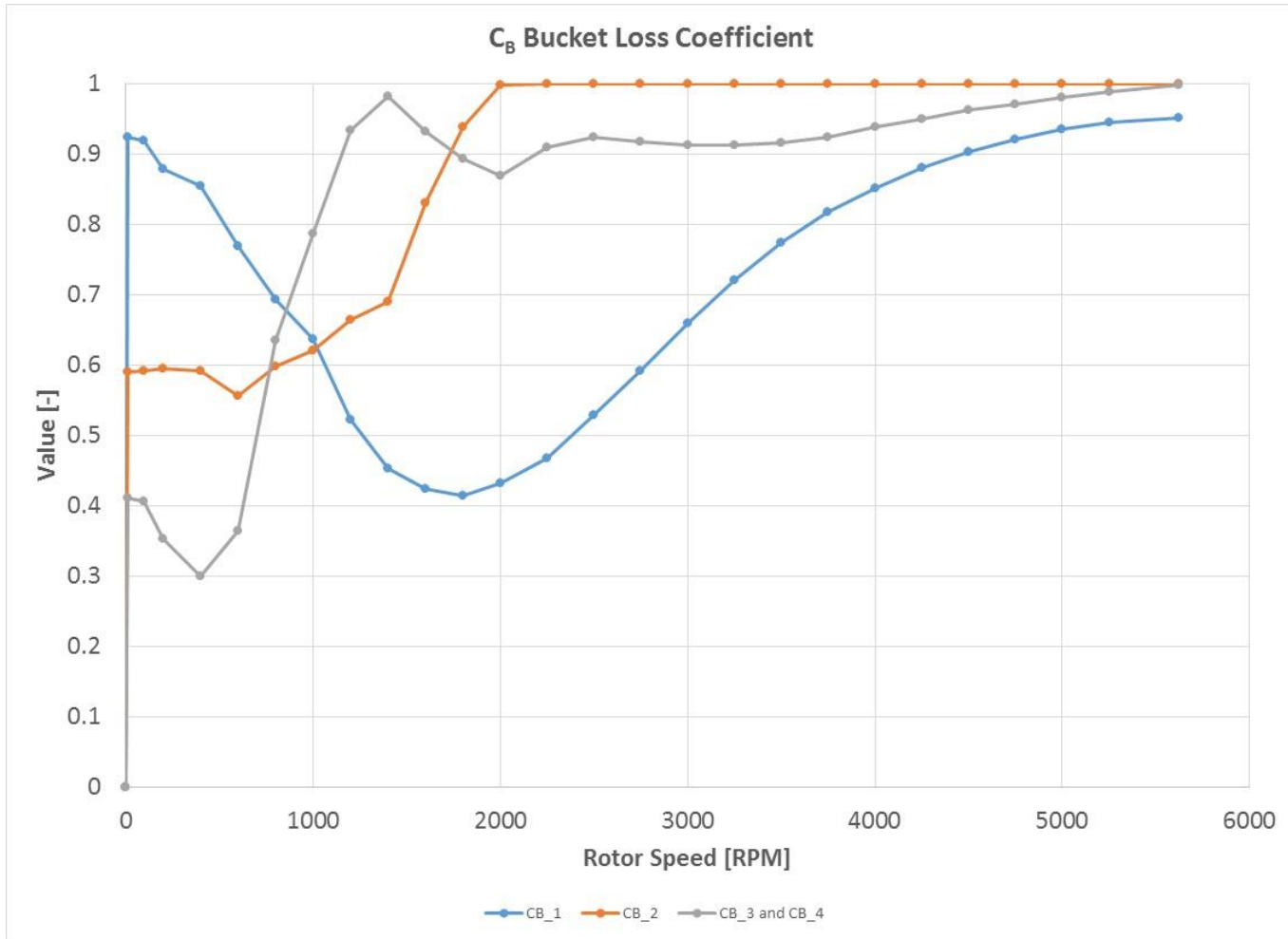


Figure 7.16 Bucket loss coefficient as a function of rotational speed

Table 7.6 Bucket loss coefficient data

RPM	CB1	CB2	CB3 & CB4
0	0.924	0.590	0.410
10	0.919	0.591	0.405
100	0.878	0.594	0.352
200	0.854	0.591	0.300
400	0.768	0.555	0.363
600	0.693	0.597	0.635
800	0.636	0.621	0.787
1000	0.522	0.663	0.934
1200	0.453	0.690	0.981
1400	0.424	0.830	0.932
1600	0.414	0.938	0.893
1800	0.432	0.997	0.868
2000	0.467	1.000	0.909
2250	0.528	1.000	0.923
2500	0.592	1.000	0.916
2750	0.659	1.000	0.912
3000	0.720	1.000	0.912
3250	0.774	1.000	0.916
3500	0.817	1.000	0.924
3750	0.852	1.000	0.938
4000	0.880	1.000	0.950
4250	0.903	1.000	0.962
4500	0.920	1.000	0.971
4750	0.934	1.000	0.980
5000	0.945	1.000	0.989
5250	0.952	1.000	0.998
5625	0.959	1.000	1.000

The expected loss of flow velocity for each bucket as a function of rotor speed is thereby obtained. Figure 7.15 shows the mixing plane surfaces while Figure 7.16 and Table 7.6 summarize the value of this parameter as a function of rotational speed. To get the bucket outlet velocity (magnitude), the inlet velocity magnitude can be multiplied by the factor C_B .

The bucket loss coefficient is defined such that the outlet velocity magnitude for a given bucket is the inlet velocity magnitude of that bucket multiplied by C_B . As the loss coefficient decreases, there is more loss across the bucket in terms of velocity magnitude. The general trend from Figure 7.16 is that all velocity stages (buckets 1 through 4) have greater loss in the buckets at lower rotational speeds.

7.1.3.3 *Bucket Exit Angle*

The bucket exit angle, denoted β in the systems-level velocity stage model, is computed for each bucket (downstream of a reversing chamber in the solution domain) from a dot product of unit vectors directed along:

- the bucket exit plane normal
- the bucket exit plane surface-averaged velocity vector

The bucket exit plane surfaces are derived parts (specifically, constrained planes) with which surface-averaged flow velocity components are calculated (via surface-average type reports). Then, with both unit normal vectors known, the angle between the two is obtained from:

$$(7.2) \quad \cos(\beta) = (\hat{\mathbf{u}} \cdot \hat{\mathbf{n}}) / (|\mathbf{u}| |\mathbf{n}|)$$

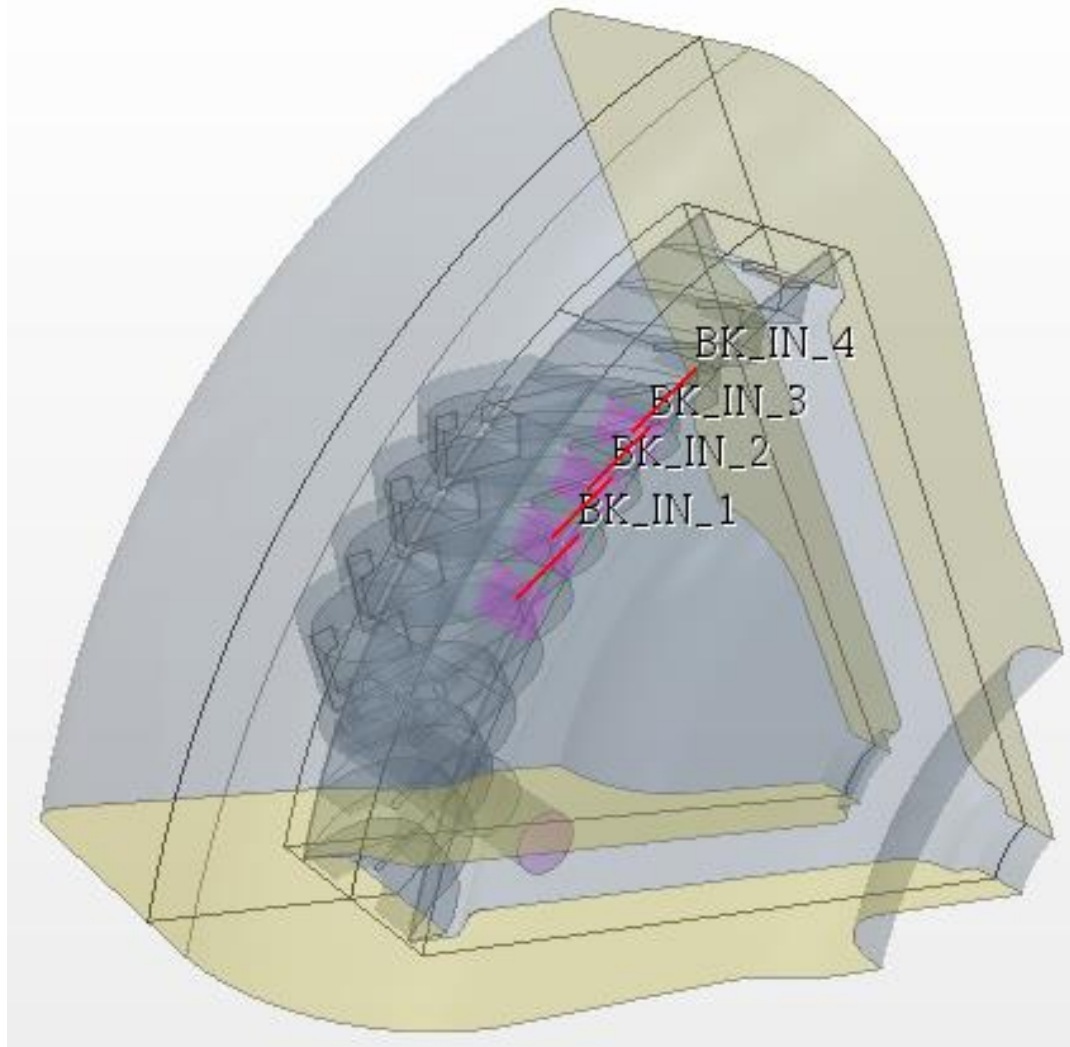


Figure 7.17 Example planes for bucket exit angle computations

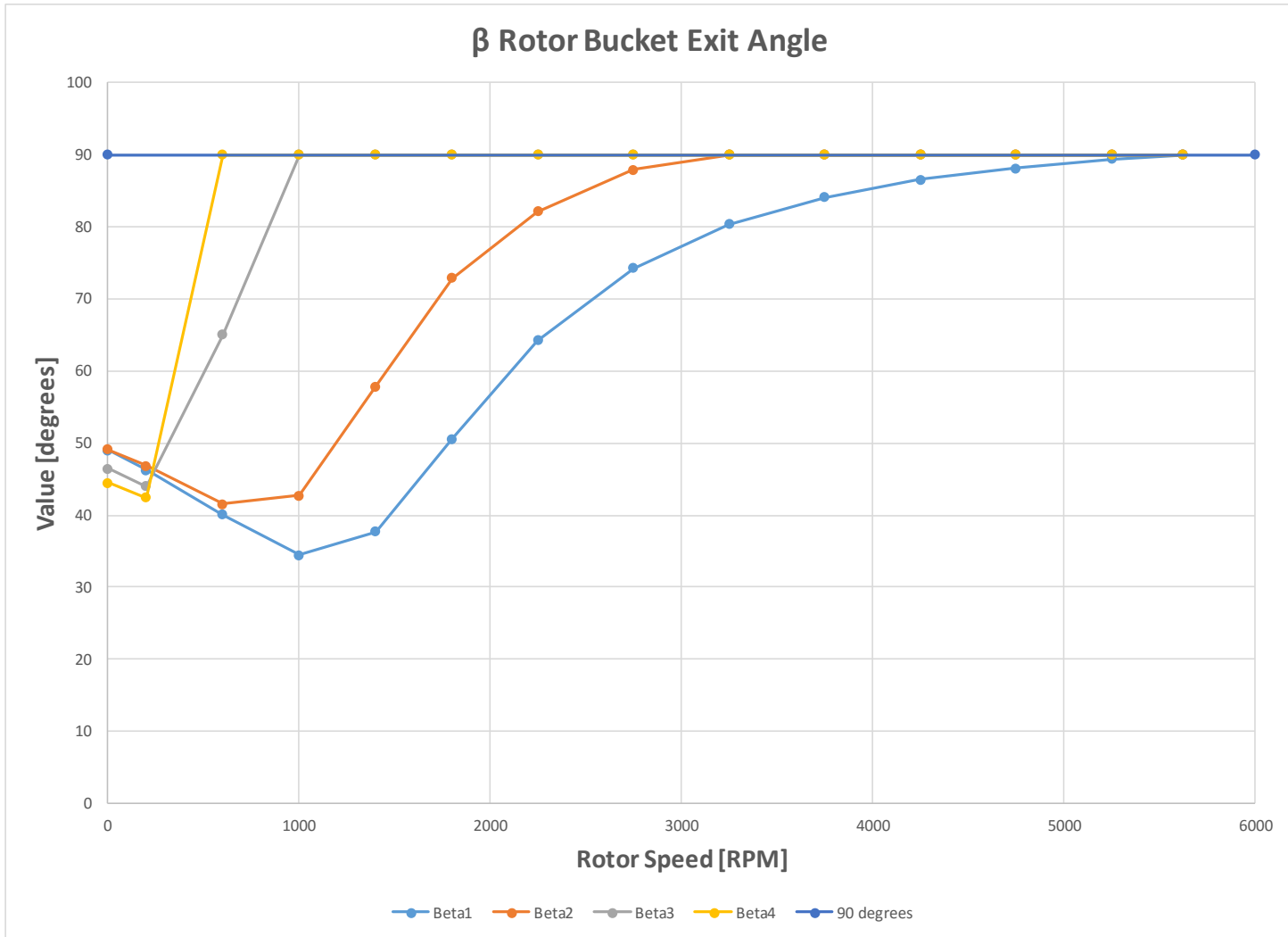


Figure 7.18 Bucket exit angle as a function of rotational speed

Table 7.7 Bucket exit angle data

<u>RPM</u>	<u>Beta1</u>	<u>Beta2</u>	<u>Beta3</u>	<u>Beta4</u>
0	49.046	49.138	46.430	44.452
200	46.251	46.838	44.028	42.416
600	40.035	41.496	65.057	89.976
1000	34.452	42.684	90.000	90.000
1400	37.704	57.904	90.000	90.000
1800	50.557	72.887	90.000	90.000
2250	64.264	82.176	90.000	90.000
2750	74.259	87.910	90.000	90.000
3250	80.390	90.000	90.000	90.000
3750	84.115	90.000	90.000	90.000
4250	86.533	90.000	90.000	90.000
4750	88.189	90.000	90.000	90.000
5250	89.402	90.000	90.000	90.000
5625	90.000	90.000	90.000	90.000

Figure 7.17 shows example planes configured for tracking bucket flow while Figure 7.18 and

Table 7.7 summarize the value of this parameter as a function of rotational speed. An angle of less than 90 degrees signifies a bucket exit plane velocity vector that carries fluid “downstream” to the next velocity stage or to turbine exhaust.

The bucket exit angles monotonically increase as a function of rotor speed for all buckets. The latter stage exit angles reach 90° at lower rotational speed and therefore those buckets contribute to net torque only at lower rotational speeds.

7.1.3.4 Reversing Chamber Loss Coefficient

The reversing chamber loss coefficient, denoted C_{RC} in the systems-level velocity stage model, is computed for each reversing chamber as a ratio of surface-averaged velocity magnitudes. The surfaces in question for this parameter are derived parts (specifically, constrained planes) that constitute reversing chamber inlets and outlets. Surface-averaged flow velocity magnitudes are calculated (via surface-average type reports) and ratios are taken. The expected loss of flow velocity for each reversing chamber as a function of rotor speed is thereby obtained. Figure 7.19 shows the constrained planes while Figure 7.20 and Table 7.8 summarize the value of this parameter as a function of rotational speed. To get the reversing chamber outlet velocity (magnitude), the inlet velocity magnitude can be multiplied by the factor C_{RC} .

The reversing chamber loss coefficient is defined such that the outlet velocity magnitude for a given chamber is the inlet velocity magnitude of that chamber multiplied by C_{RC} . As the loss coefficient decreases, there is more loss across the chamber in terms of velocity magnitude. The first and second reversing chambers (downstream of the first and second buckets) – as seen in Figure 7.20 – decrease in loss coefficient after peaking around 1000 rpm. Therefore, more velocity loss (lower downstream velocity and less net torque contribution from downstream buckets) occurs at higher rotational speeds.

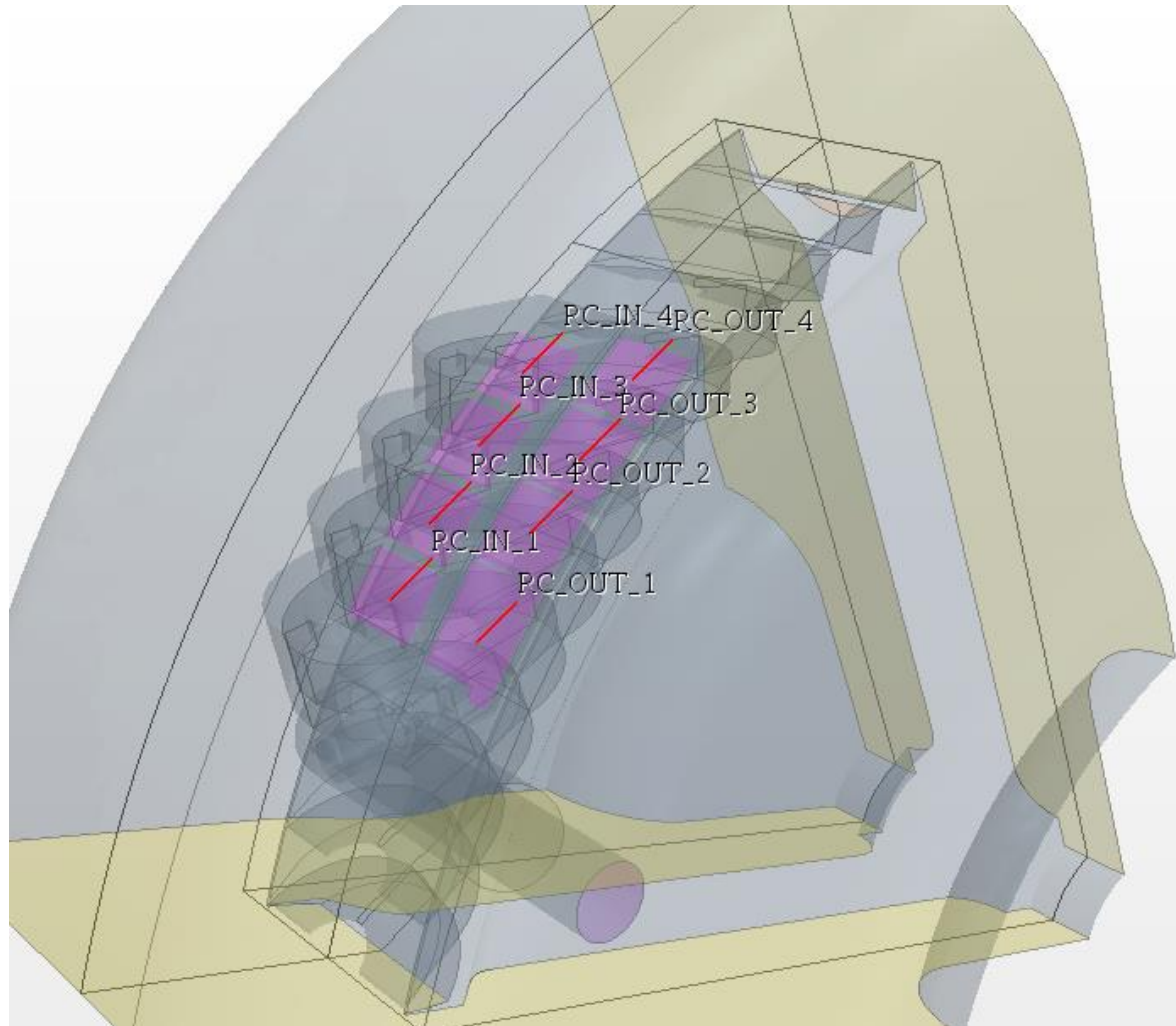


Figure 7.19 Constrained planes to compute reversing chamber loss coefficients

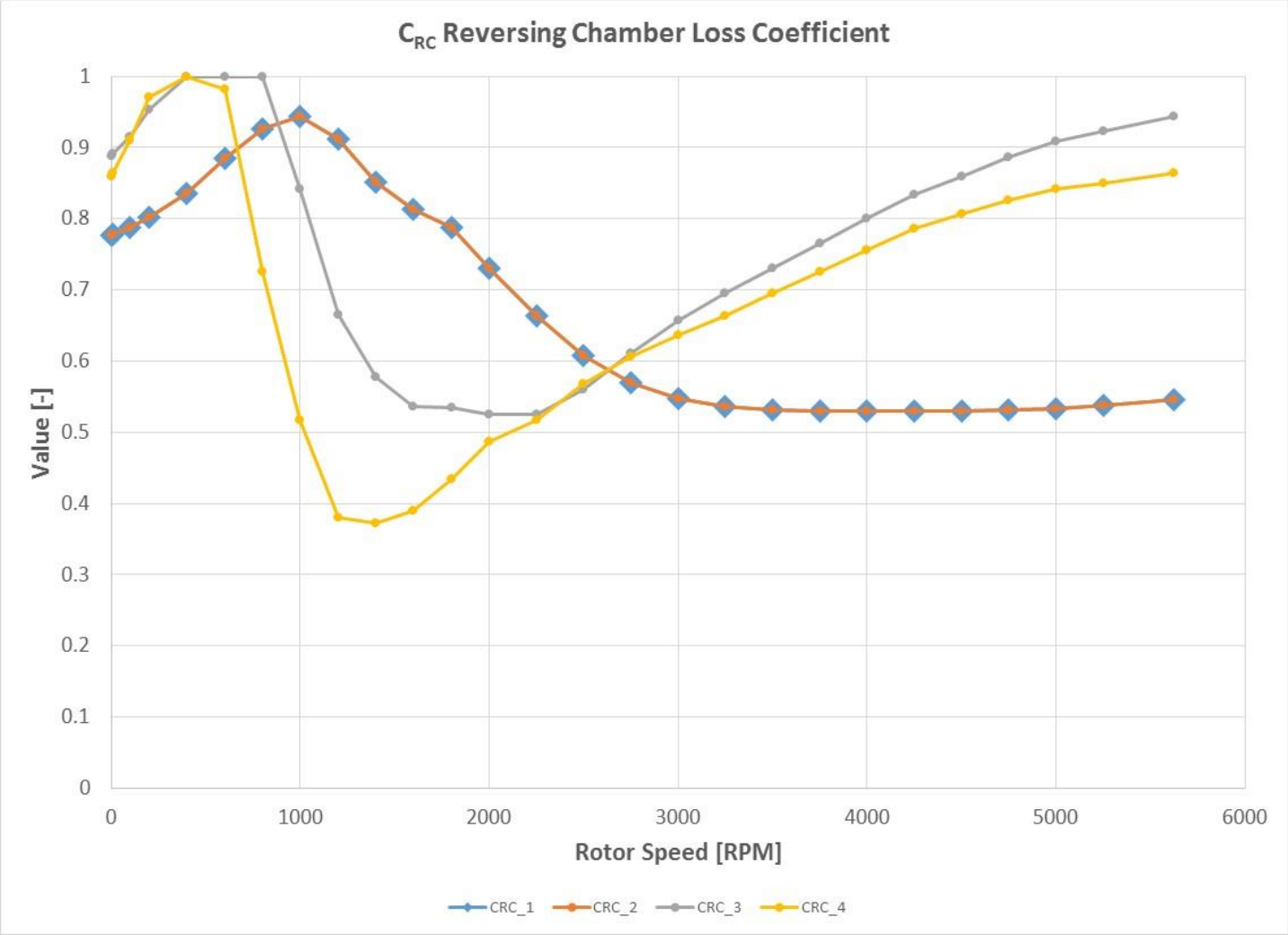


Figure 7.20 Reversing chamber loss coefficient as a function of rotational speed

Table 7.8 Reversing chamber loss coefficient data

RPM	CRC1 & CRC2	CRC3	CRC4
0	0.776	0.888	0.859
10	0.777	0.891	0.864
100	0.787	0.916	0.910
200	0.801	0.953	0.971
400	0.836	1.000	1.000
600	0.885	1.000	0.982
800	0.926	1.000	0.725
1000	0.943	0.842	0.516
1200	0.913	0.665	0.380
1400	0.851	0.577	0.372
1600	0.812	0.536	0.389
1800	0.787	0.534	0.434
2000	0.731	0.525	0.487
2250	0.664	0.525	0.516
2500	0.608	0.560	0.568
2750	0.570	0.611	0.607
3000	0.547	0.657	0.636
3250	0.536	0.696	0.664
3500	0.531	0.731	0.695
3750	0.530	0.765	0.725
4000	0.530	0.800	0.756
4250	0.530	0.834	0.786
4500	0.530	0.860	0.806
4750	0.531	0.887	0.826
5000	0.533	0.909	0.842
5250	0.538	0.923	0.850
5625	0.546	0.944	0.864

7.1.3.5 Reversing Chamber Leakage Coefficient

The reversing chamber leakage coefficient, denoted γ_{RC} in the systems-level velocity stage model, is computed for each reversing chamber using surface-averaged mass flow rates. The surfaces in question for this parameter are derived parts (specifically, constrained planes) that constitute reversing chamber crescent holes and inlets. Surface-averaged mass flow rates are calculated (via surface-average type reports) and ratios are formed between the crescent hole and the inlet. The expected fluid leakage for each reversing chamber as a function of rotor speed is thereby obtained. Figure 7.21 shows the constrained crescent hole planes while Figure 7.22 and Figure 7.23 summarize the value of this parameter as a function of rotational speed. To get the reversing chamber exit mass flow rate, the inlet mass flow rate can be multiplied by the factor γ_{RC} .

When crescent hole leakage in a reversing chamber is small, γ_{RC} is larger and vice-versa. In the earlier velocity stages, crescent hole leakage in corresponding reversing chambers is fairly constant across all rotational speeds such that at least 88% of incoming mass flow is conveyed to the other side of the chamber. In the latter velocity stages, the leakage coefficient is more variable but may be of less consequence if bucket exit angles in latter stages are such that upstream rotor buckets do not admit steam to downstream reversing chambers.

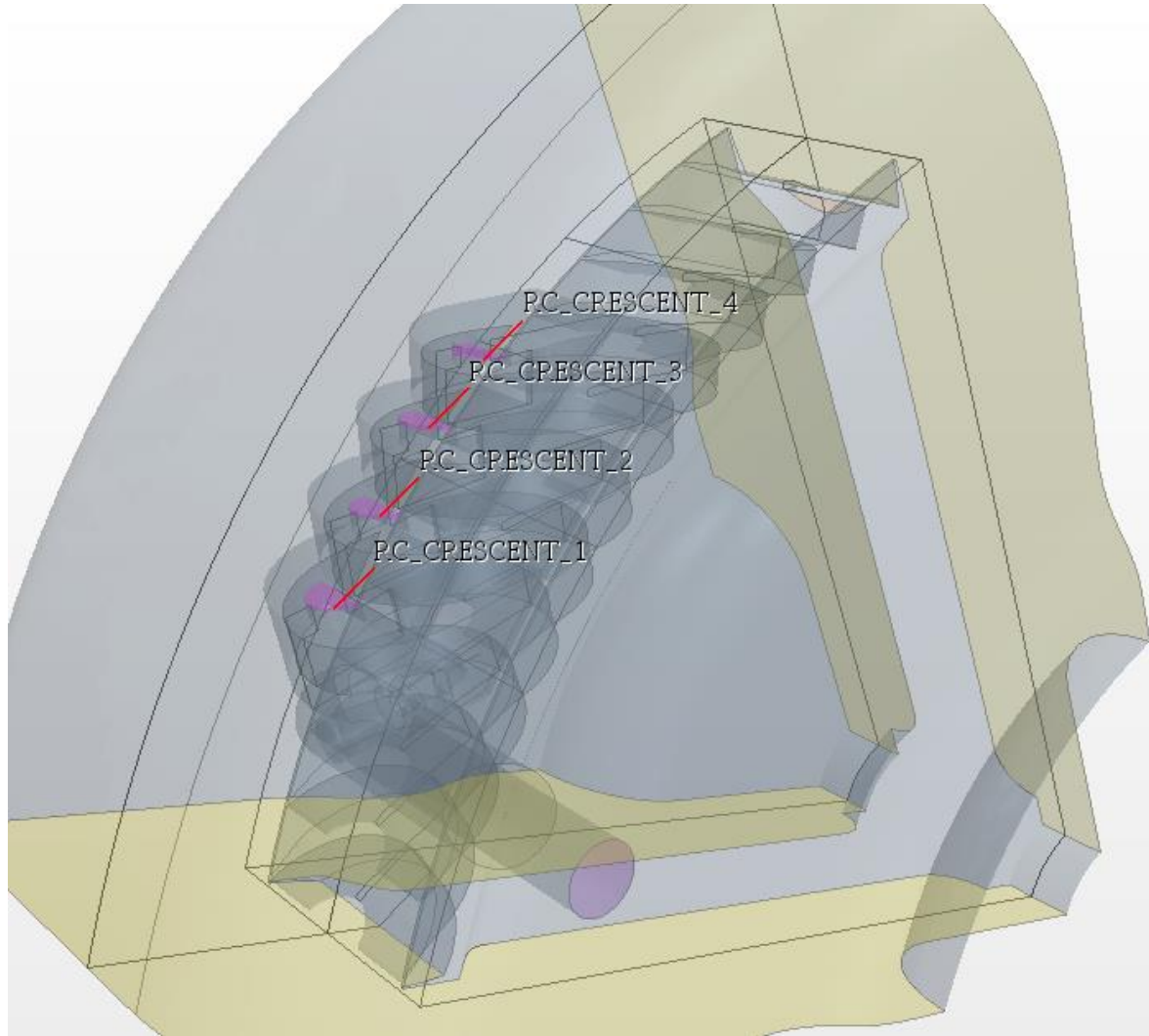


Figure 7.21 Reversing chamber crescent hole constrained planes

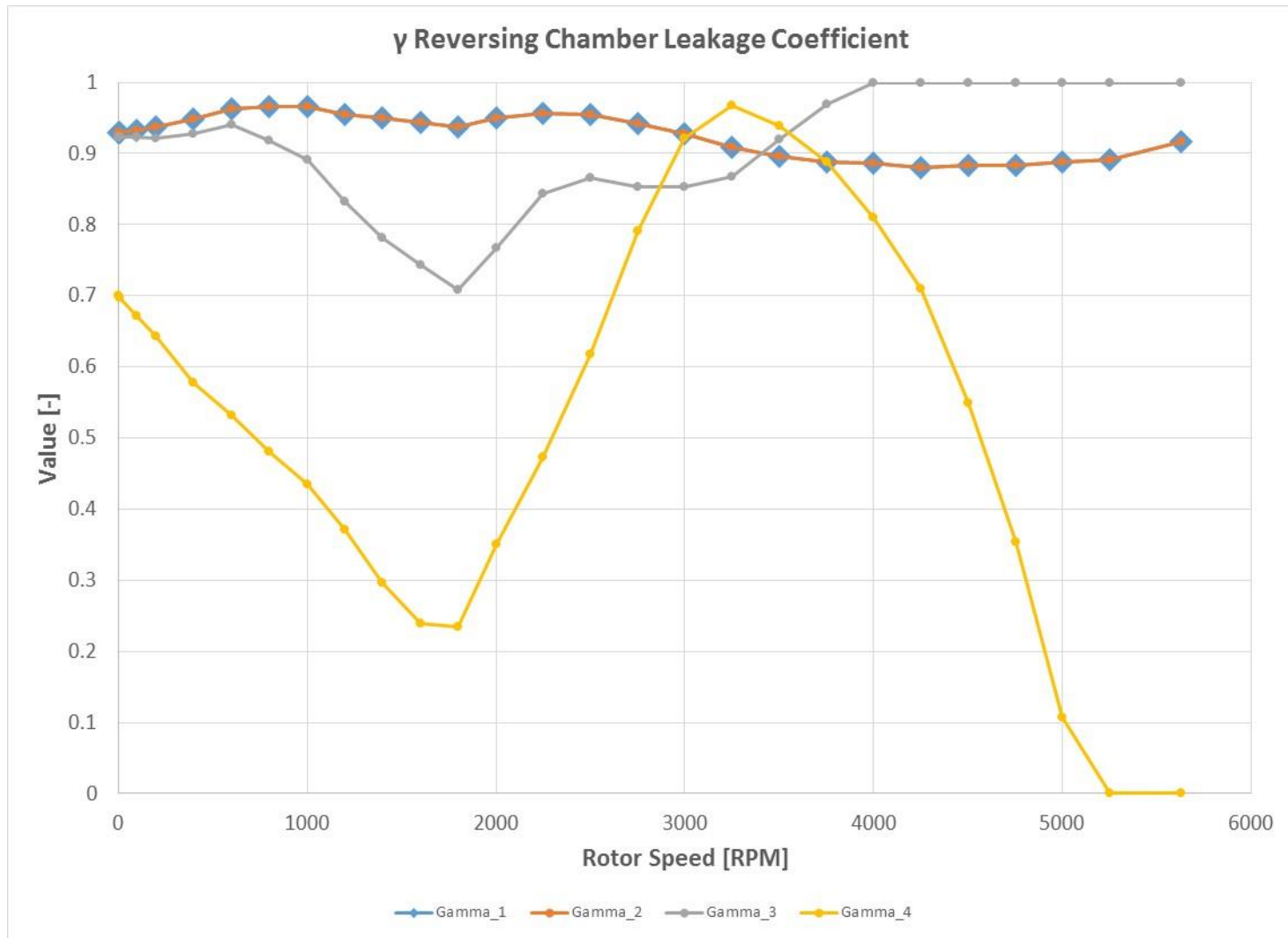


Figure 7.22 Reversing chamber leakage coefficient as a function of rotor speed

Table 7.9 Reversing chamber leakage coefficient data

RPM	GAMMA1 & GAMMA2	GAMMA3	GAMMA4
0	0.930	0.923	0.700
10	0.930	0.923	0.698
100	0.932	0.923	0.673
200	0.937	0.921	0.643
400	0.948	0.927	0.578
600	0.964	0.941	0.532
800	0.965	0.918	0.480
1000	0.966	0.892	0.435
1200	0.955	0.833	0.371
1400	0.950	0.782	0.297
1600	0.944	0.743	0.240
1800	0.937	0.708	0.234
2000	0.951	0.767	0.350
2250	0.957	0.844	0.472
2500	0.955	0.865	0.618
2750	0.942	0.852	0.791
3000	0.928	0.854	0.922
3250	0.908	0.867	0.968
3500	0.896	0.920	0.940
3750	0.889	0.968	0.887
4000	0.886	1.000	0.809
4250	0.880	1.000	0.709
4500	0.884	1.000	0.550
4750	0.884	1.000	0.353
5000	0.888	1.000	0.108
5250	0.890	1.000	0.000
5625	0.916	1.000	0.000

7.1.3.6 Carry-Over Fraction

The carry-over fraction, denoted ξ in the systems-level velocity stage model, is computed for each bucket/chamber pair using surface-averaged mass flow rates. The surfaces in question for this parameter are derived parts (specifically, constrained planes) that constitute bucket inlets and reversing chamber inlets. Since negligibly small mass flow is lost between bucket inlet and exit, the bucket inlet mass flow rate approximately equals that of its outlet. Surface-averaged mass flow rates are calculated (via surface-average type reports) and ratios are formed between bucket inlet (or outlet) and reversing chamber inlet, yielding the expected fluid loss as the gap between bucket/chamber is traversed. Figure 7.23 and Table 7.10 summarize the value of this parameter as a function of rotational speed. To get a reversing chamber inlet mass flow rate, the inlet mass flow rate of the upstream bucket can be multiplied by ξ .

For all stages – as evidenced by Figure 7.23 – the carry-over fraction is a monotonically-decreasing function of rotational speed. Thus, the latter velocity stages are efficacious in terms of secondary, tertiary, and quaternary flows only at lower rotor speed. This result is partial proof of the postulate (as made in [1]) that reversing chambers and velocity compounding do not appreciably contribute to torque at higher rotational speeds.

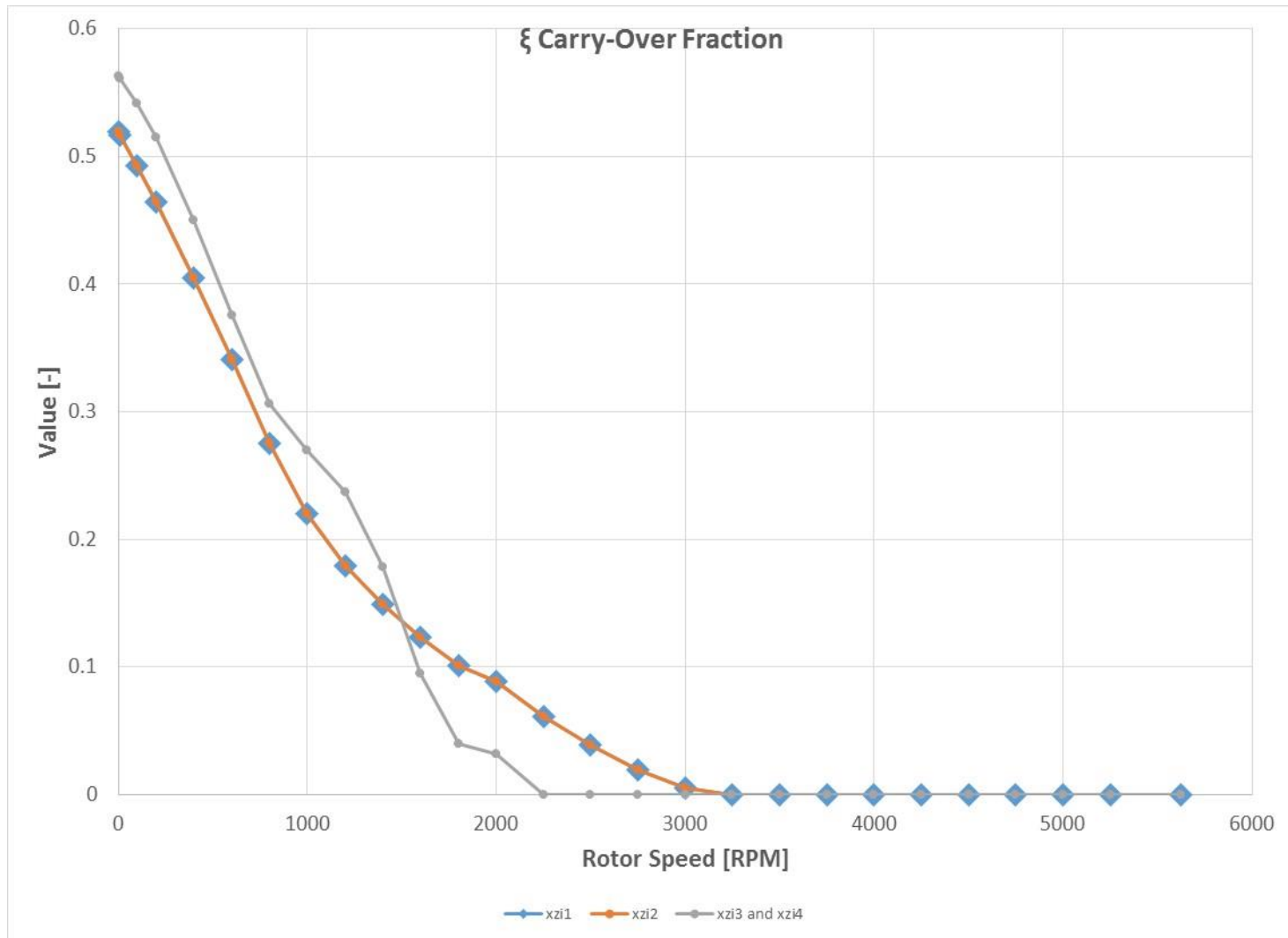


Figure 7.23 Carry-over fraction as a function of rotor speed

Table 7.10 Carry-over fraction data

RPM	XZI1 & XZI2	XZI3 & XZI4
0	0.519	0.563
10	0.517	0.561
100	0.493	0.542
200	0.465	0.515
400	0.404	0.450
600	0.340	0.375
800	0.275	0.306
1000	0.220	0.269
1200	0.180	0.237
1400	0.149	0.178
1600	0.124	0.094
1800	0.101	0.040
2000	0.089	0.032
2250	0.061	0.000
2500	0.039	0.000
2750	0.020	0.000
3000	0.005	0.000
3250	0.000	0.000
3500	0.000	0.000
3750	0.000	0.000
4000	0.000	0.000
4250	0.000	0.000
4500	0.000	0.000
4750	0.000	0.000
5000	0.000	0.000
5250	0.000	0.000
5625	0.000	0.000

7.1.3.7 Terry Turbine Steam Nozzle Expansion Rate

The steam nozzle expansion rate comes from a separate simulation. To get the best estimate of a Terry turbine nozzle expansion rate, a fully three-dimensional geometry was used with condensing steam physics models. The geometry is pictured in Figure 7.24 and Figure 7.25 below. Note that a symmetric boundary condition is employed down a vertical plane that divides the nozzle in half. This nozzle geometry is typical of a GS-1 Terry turbine but does not include the plenum upstream of the first converging section. The boundary condition types are similar to those of the two-dimensional Gyarmathy nozzle simulation (stagnation inlet, pressure outlet, no-slip walls).

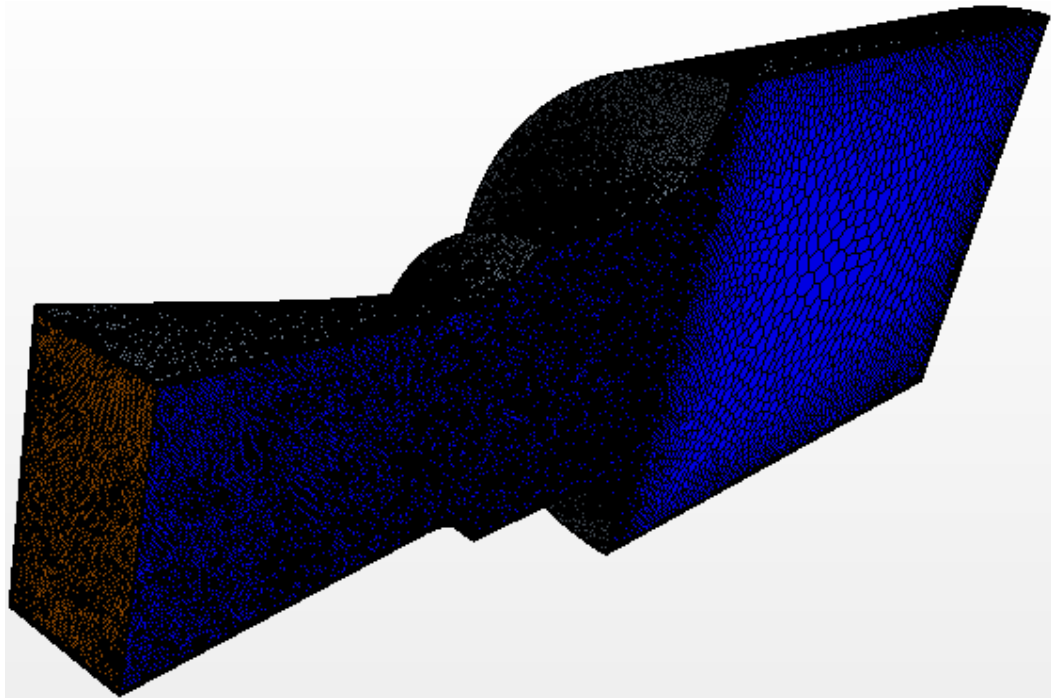


Figure 7.24 Three-dimensional Terry turbine nozzle geometry, inner side

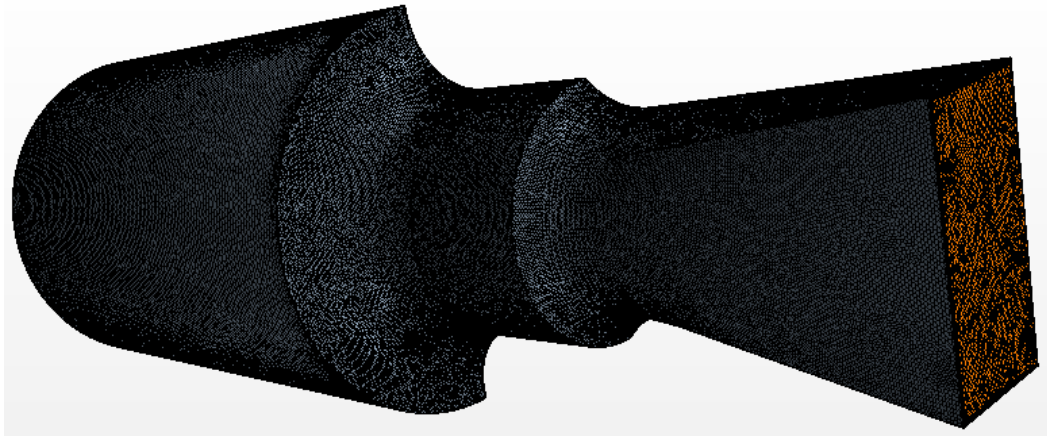


Figure 7.25 Three-dimensional Terry turbine nozzle geometry, outer side

The steam nozzle expansion rate is computed by field function according to Equation (6.113). The derivative dP/dx is approximated by a difference between the entry plane (just before the first converging section) and the nozzle exit plane. The distance between these two locations is approximately 7.24 cm and a pressure drop report can furnish the pressure decrease across the nozzle. Using the according dP/dx as a constant, a volume-average report can be applied to an expansion rate field function so as to recover a single estimate of the GS-1 Terry turbine nozzle expansion rate. The pieces to this computation are included in Table 7.11. Also, an example result (predicted nucleation rate) is included in Figure 7.26 to illustrate the performance of the steam physics models. A more complete overview of Terry turbine nozzle results is included in Appendix E. Note these results could not really be validated against any GS-1 Terry turbine experimental results as none are available.

Table 7.11 GS-1 Terry turbine expansion rate computational details

<u>Metric</u>	<u>Value</u>	<u>Units</u>
ΔP across nozzle	3.141×10^6	<i>Pa</i>
Δx across nozzle	0.0724	<i>M</i>
Vol-avg Expansion Rate	-2.259×10^3	s^{-1}

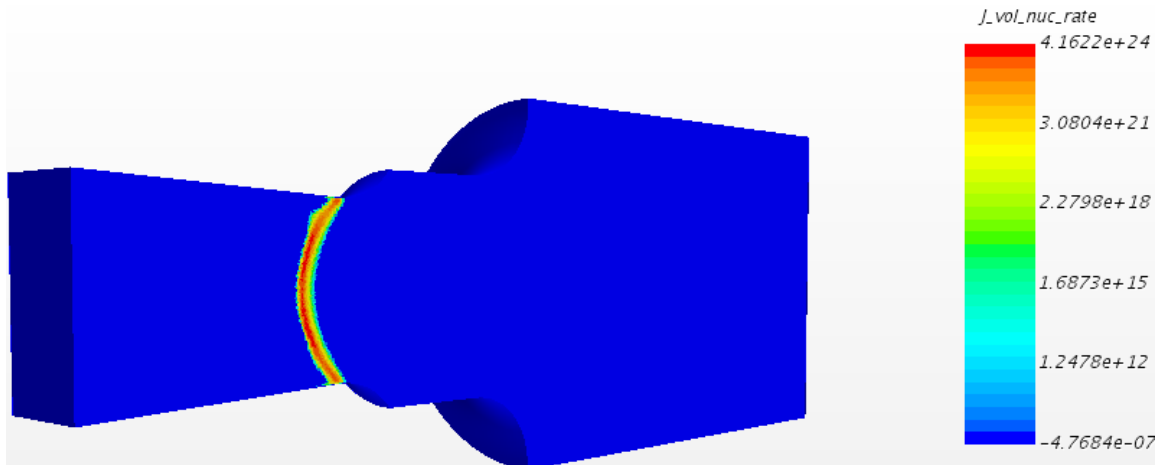


Figure 7.26 Predicted nucleation rate [drop/m³/s] for 3D Terry turbine nozzle

7.1.3.8 Discussion

To summarize some take-aways from the above results:

- From the C_B curves, there appears to be more degradation of flow velocity across rotor buckets of all velocity stages at lower rotational speeds
- From the β curves, rotor buckets seemingly convey steam flow to downstream reversing chambers only at lower rotational speeds
- From the C_{RC} curves, there appears to be more degradation of flow velocity across reversing chambers of all stages at intermediate rotational speeds
- From the γ_{RC} curves, reversing chamber leakage is roughly constant in the first two velocity stages across all rotational speeds
- From the ξ curves, flow carries over to downstream velocity stages (buckets to subsequent reversing chambers) at lower rpm
- The expansion rate should not be a strong function of boundary conditions but should rather depend on the nozzle geometry (circular-to-square transition)

All parameters characterizing the velocity stage can be specified for use in MELCOR as a function of rotational speed (either within source code as a built-in data set or as user input for a given calculation). The steam nozzle expansion rate can be specified for use in the MELCOR pressure stage (analytical Wilson point) model as a constant value. Several of the observations above underscore the notion that stage compounding is more efficacious (in terms of contributing to rotor torque) at lower rotational speeds where, presumably, it is easier for steam to “find” downstream velocity stages and to return to the rotor for further impulse exertion.

7.2 MELCOR Results

The purpose of systems-level MELCOR calculations was two-fold:

- Demonstrate the stand-alone behavior and functionality of new models in turn with simple “baby problems”, and
- Demonstrate how the new models work together in context of a pseudo-Fukushima RCIC loop model

The various test cases showcase the capabilities of new models and give examples for how a user might deploy them to predict RCIC system response.

7.2.1 *Demonstration Problems for New Models*

Typically, new MELCOR models are introduced to users with simple demonstration problems that do not include unnecessary complications. Occasionally, these baby problems represent code-to-experiment or code-to-code benchmarks. The examples outlined below are just these kinds of “baby problems”. There is a loop flow problem which demonstrates aspects of the homologous pump model and which may be compared to an example problem from RELAP5 manuals. There is also a simple benchmark calculation that compares the Terry turbine pressure stage model predictions to published results for an analytical Wilson point calculation.

7.2.1.1 *Homologous Pump Model Demonstration*

A nodalization diagram for centrifugal pump-driven loop flow problem is shown in Figure 7.27. The flow loop has two horizontal legs (volumes 1 through 4 and 10 through 14) and two vertical legs (volumes 5 through 9 and 15 through 19) with a centrifugal pump

on a flow path between volumes 19 and 1. Initially, the water-solid loop is at rest (zero velocity) and the pump is off.

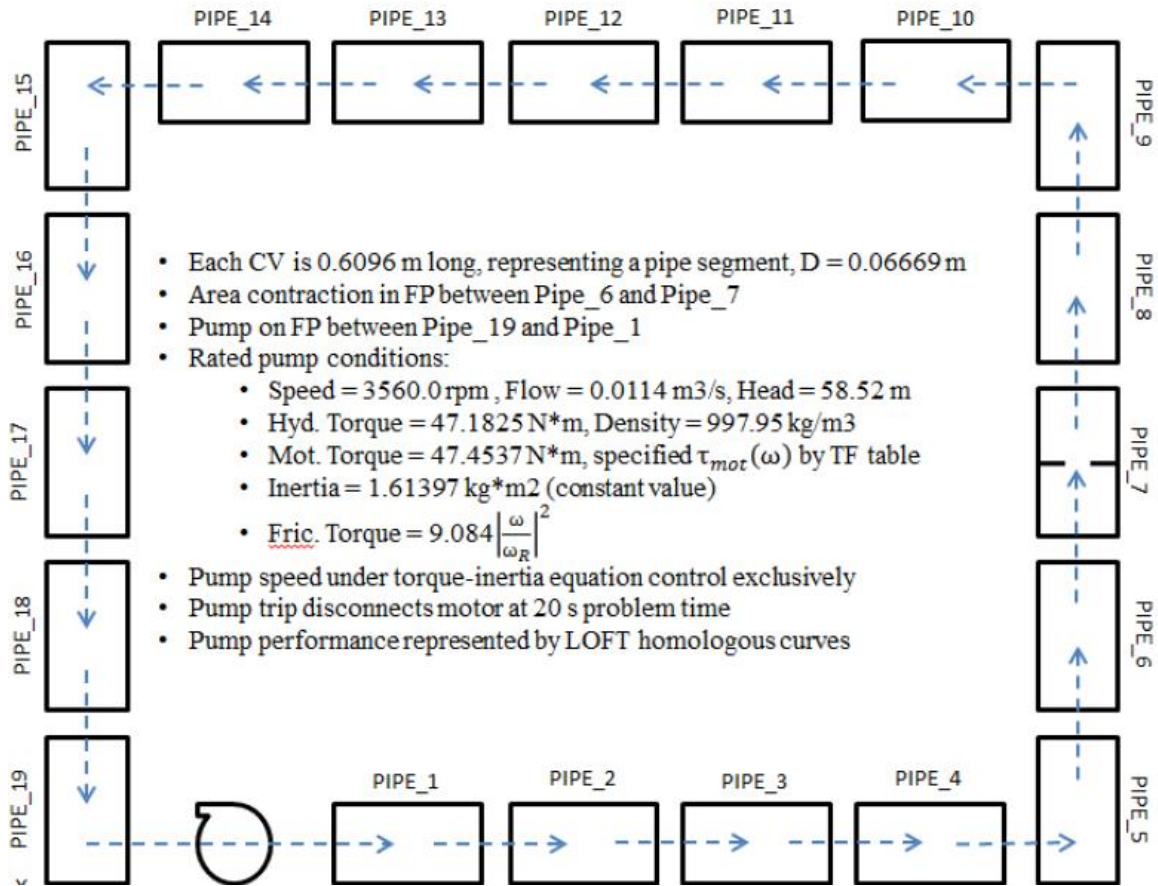


Figure 7.27 Homologous pump model demonstration problem, pump-driven flow

The parameters of interest for purposes of MELCOR-to-RELAP5 comparison are head, speed, hydraulic torque, and certain variables related to loop flow such as liquid velocities and control volume pressures. The transient progresses as:

- Action of the motor (as specified by a CF/TF control combination) causes the pump impeller speed to ramp up (motor torque outweighs friction plus hydraulic torque, driving speed higher)
- Pump speed levels off as dictated by the motor torque TF table
- At time 20 s, the pump is tripped and the driving motor is disconnected such that it provides no driving torque to the pump
- Speed coasts down as predicted by the torque-inertia equation with net negative torque on the pump
- Transient terminates at time 40 s

Comparative plots for impeller speed, pump head, and discharge water velocity are included below. The test demonstrates several features of the pump speed model:

- A speed ramp-up driven by motor torque with the ramp-up predicted by solution of the torque-inertia equation
- A leveling-off of speed as net zero torque is established due to zero net torque (consisting of friction torque, hydraulic torque, and motor torque)
- A coast-down predicted after pump trip (driving motor disconnect) causes motor torque to be zero and net torque to be negative, thus pulling down speed

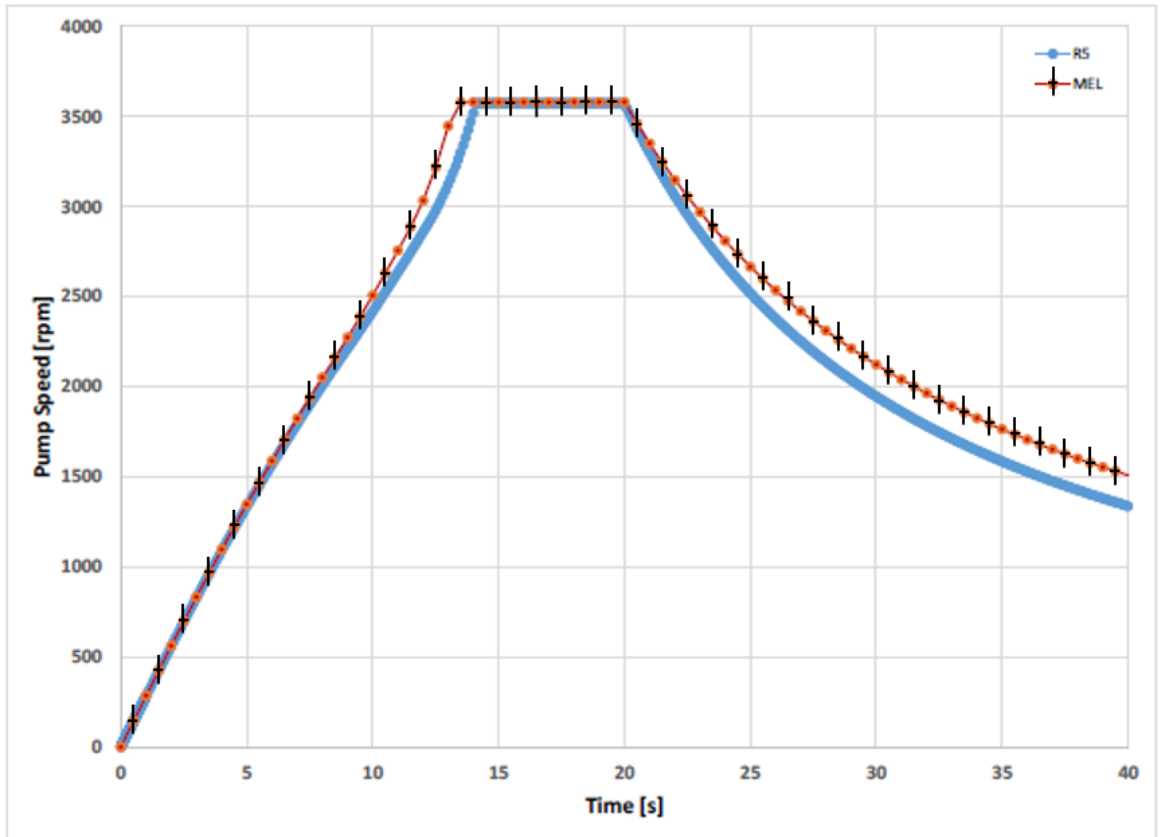


Figure 7.28 Loop flow problem, pump impeller speed

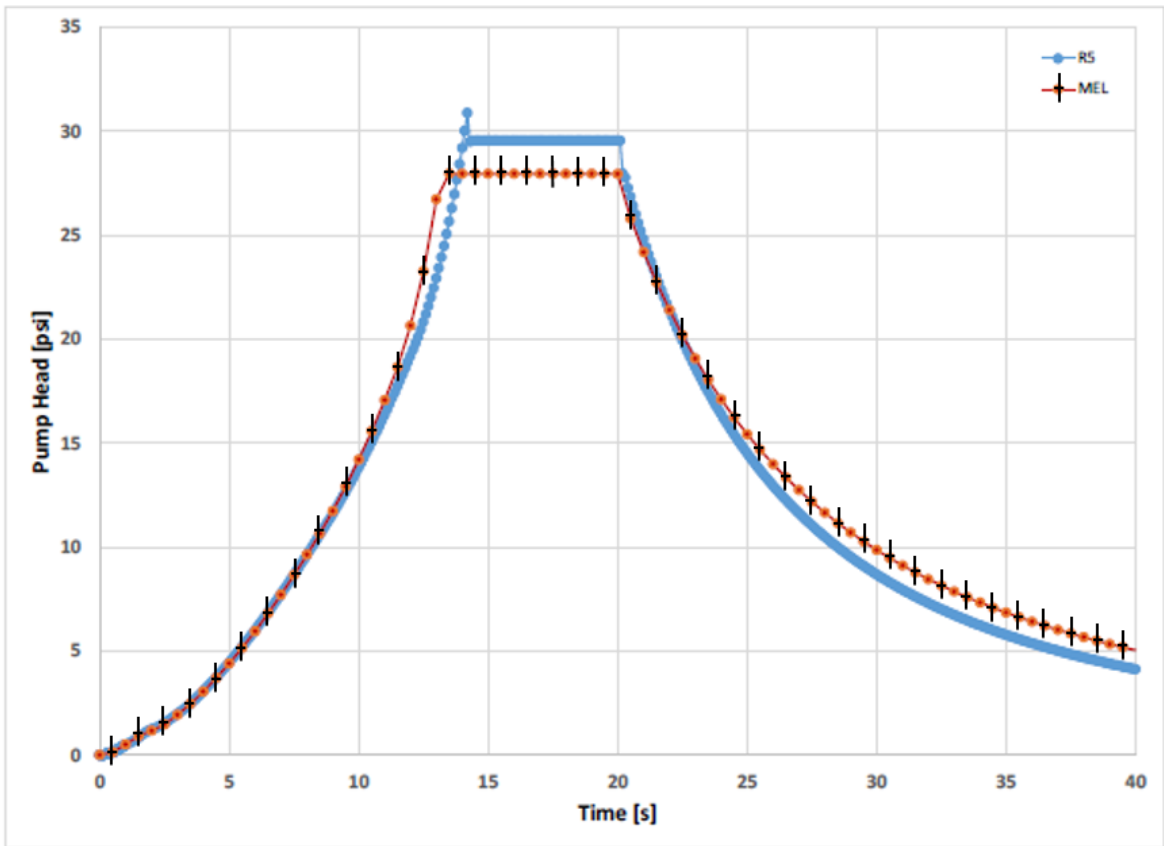


Figure 7.29 Loop flow problem, pump head

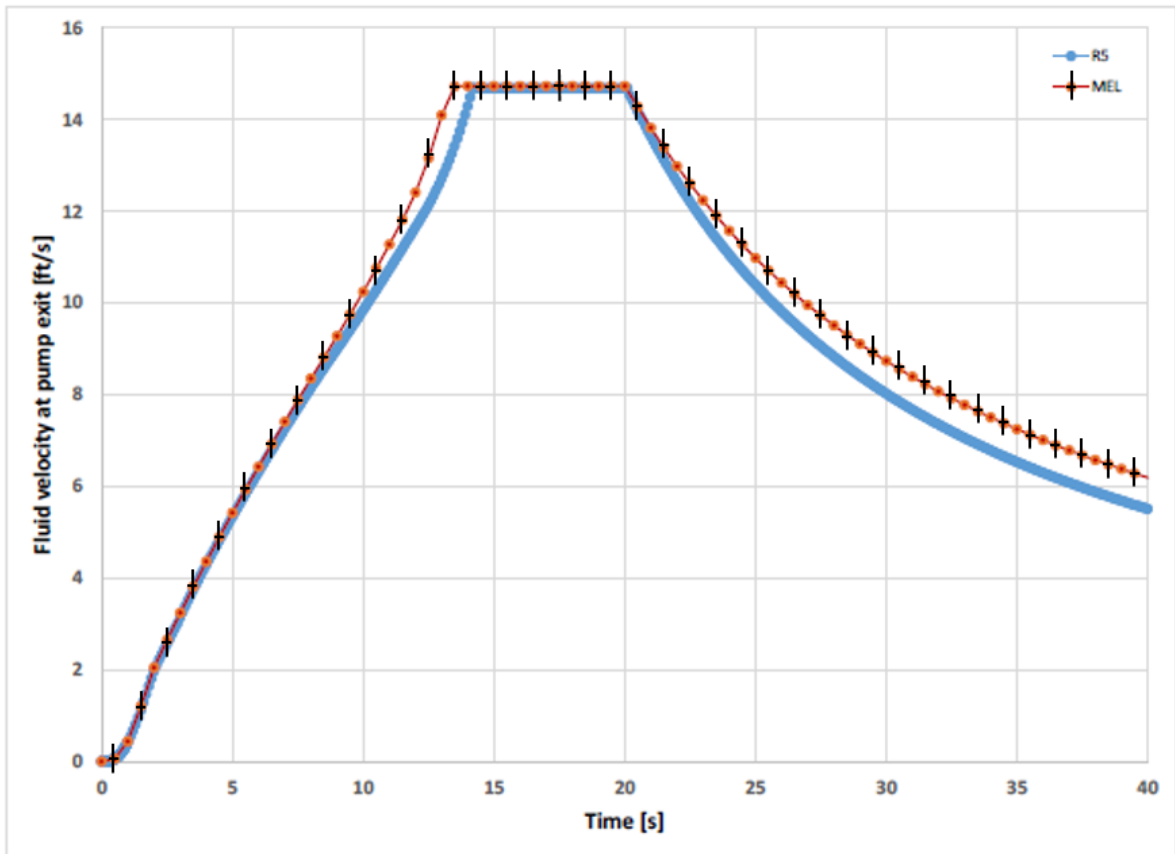


Figure 7.30 Loop flow problem, water velocity at pump discharge

The results of the loop flow test problem demonstrate that MELCOR has capabilities comparable to those of RELAP-5 in terms of centrifugal pump modeling via the homologous pump method. The results also demonstrate that the trip capability (ramp-up and coast-down), pump motor torque user specification, pump dissipation energy addition, and the torque-inertia equation solution is working properly.

7.2.1.2 Terry Turbine Pressure Stage Demonstration and Benchmark

Part of the Terry turbine pressure stage model is an analytical Wilson point solution meant to characterize any metastability associated with delayed condensation as steam rapidly expands across the nozzle. Equations are adapted from literature references on analytical Wilson point methods as previously described. The same references tabulate Wilson point computational results that are useful for comparison to MELCOR. Results are summarized in Table 7.12 below. Note the inlet boundary conditions (common to all calculations reported above) were: $P_{01} = 100.0$ kPa, $T_{01} = 413.15$ K, $\dot{P} = 3000$ 1/s.

Table 7.12 Code-to-code benchmark results, analytical Wilson point

<u>Variable</u>	<u>Units</u>	<u>Gyarmathy [55]</u>	<u>Dobbins [51]</u>	<u>MELCOR</u>
$\text{Log}_{10}(J_n)$	<i>Drop/m³/s</i>	22.2	22.01	19.554
P_n/P_{01}	-	0.28	0.281	0.26
$\Delta T_{\text{subcool}}$	<i>K</i>	37.0	36.75	36.22
U_n	<i>m/s</i>	640	644	661
T_2	<i>K</i>	-	356.65	355.0
M_a^2	-	-	2.253	2.421
T_n	<i>K</i>	-	302.77	301.28
S_n	-	-	5.455	5.423
Δh_{2n}	<i>kJ/kg</i>	-	101.3	103.2

Considering the extreme sensitivity of nucleation/growth calculations (due to their highly non-linear nature), the MELCOR results compare favorably with the two other data sets. The observable differences are likely attributable to certain features of the MELCOR solution method, e.g. Gaussian quadrature evaluation of property integrals and the use of temperature-dependent properties and/or alternative definitions of the gas constant for steam (derived from specific heat ratio instead of assumed constant). Also, the MELCOR property tables may differ somewhat from polynomial prescriptions of property temperature dependence used by Gyarmathy/Dobbins [55], [51].

7.2.2 Pseudo-Fukushima Test Variant Descriptions

A test problem similar to that of [1] was modified to use and test the new RCIC system MELCOR models. The test problem is a so-called “pseudo-Fukushima” calculation because it is a simplified 2000 MW_{th} BWR system that employs boundary conditions (wet-well pressure) taken from known Fukushima unit 2 data points. The problem models decay heat addition to an RPV, water inventory boil-off in the RPV, and RCIC system action to replenish lost coolant.

7.2.2.1 General Description and Set-Up

The original nodalization consists of an RPV and RCIC system piping on both sides of the RCIC system turbo-pump – the driving (turbine-side) loop and the pumping (pump-side) loop. The RCIC system driving loop includes:

- One CV for the RPV or “boiler”
- Two CVs for MSL piping between the boiler and the RCIC turbine
- One CV for RCIC steam line piping

- One CV for the RCIC turbine steam chest
- One CV for the RCIC turbine (i.e. inside the turbine casing)
- One CV for a relief valve sink (relief for MSL)
- Flow paths, 1 per CV pair, connections in the order as listed above

Note that there are no boundary conditions imposed on the driving loop, i.e. the code predicts the evolution of thermal-hydraulic conditions in all CVs of the driving loop. CV sizes and flow path geometry/characteristics are based on best-estimates for typical Fukushima-like BWRs with RCIC systems. Note the RPV CV contains an external source that deposits decay heat into the pool inventory. The pumping loop includes:

- Two property-specified CVs representing the wetwell and/or the CST that essentially imposing boundary conditions on the transient
- One CV for the RCIC pump inlet piping
- One CV for the RCIC pump fluid volume
- One CV for the RCIC pump outlet piping
- Flow paths connecting the pump piping CVs to the pump CV, the feedwater boundary condition CV to the pump inlet piping CV, and the pump outlet piping CV to the wetwell boundary condition CV

Figure 7.31 contains a diagram illustrating main features of the pseudo-Fukushima input. The overarching goal of the pseudo-Fukushima problem is to replicate key features of the Fukushima-II accident sequence. Ideally, MELCOR will be able to capture the feedback effect between the RPV and the RCIC system under typical SBO conditions. Table 7.13 summarizes key input values for the original pseudo-Fukushima input deck.

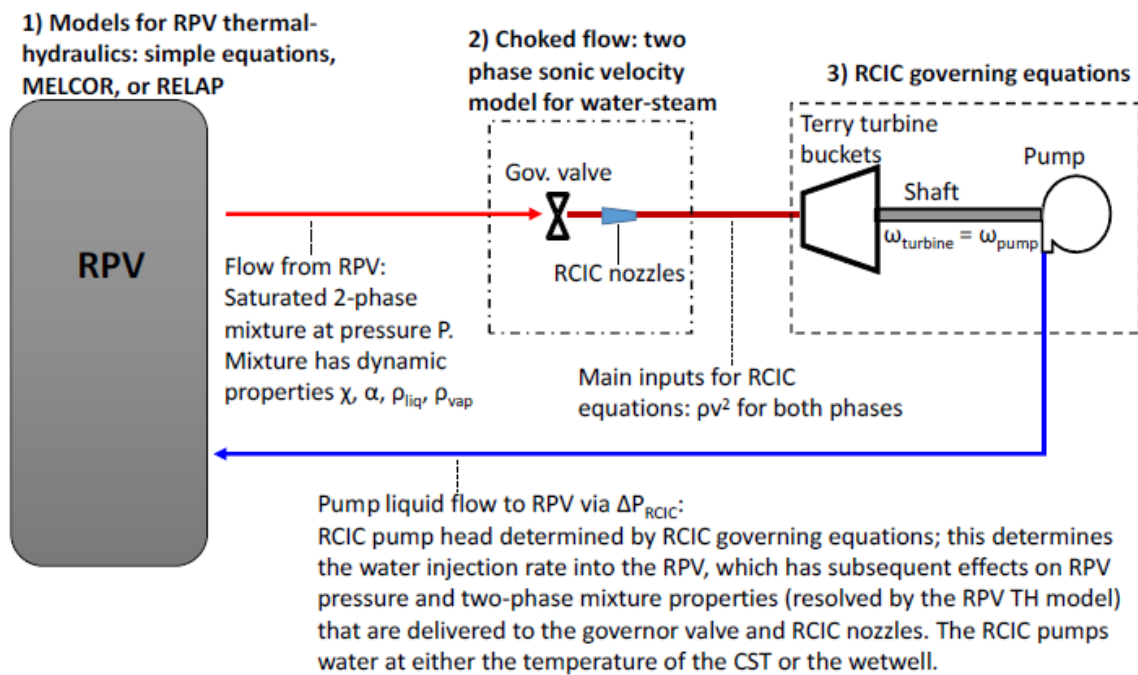


Figure 7.31 Pseudo-Fukushima RCIC system model diagram [1]

Table 7.13 Key values for original pseudo-Fukushima RCIC system input deck [1]

<u>Input Variable [units]</u>	<u>Value</u>
Turbine Rotor Radius [<i>m</i>]	0.3048
Number of Nozzles [-]	5
Turbine Moment of Inertia [<i>kg*m²</i>]	10.0
Rated RCIC Speed [<i>rpm</i>]	4300.0
Rated RCIC Pump Head [<i>Pa</i>]	$7.52 \cdot 10^6$
Rated RCIC Pump Torque [<i>N*m</i>]	449.0
Pump Injection Flow Area [<i>m²</i>]	0.0168
CST/Wetwell Pump Suction Switch [<i>hr</i>]	14
Wetwell Pool Temperature at Switch [<i>K</i>]	387.0

The problem scenario is an extended SBO with a reactor scram at time zero. The boiler is on the decay heat curve (characteristic of a general 2000 MW_{th} BWR) and receives an according thermal energy input for the duration of the transient. The only safety systems modeled are the RCIC loop and the SRV off the MSL. The RCIC system at first runs with power but eventually loses all AC and DC power. RCIC runs uncontrolled thereafter (governor valve not regulating steam admission) with the turbine governor valve full-open. Steam drives the turbine which runs the pump so as to refill the RPV. Note RCIC pump suction is initially taken from the CST boundary condition CV but later switches over to the wetwell boundary condition CV. Results from the original calculation

are documented in [1]. Note that the fully CF-specified Terry turbine model described in [1] is similar to but simpler than the velocity-stage model presented in this dissertation.

7.2.2.2 Revised Nodalization with CF Turbine Model

The original model discussed in the previous sub-section and in [1] has recently been revised in an attempt to better capture certain phenomena of interest in off-normal BWR and RCIC system operating scenarios. The input deck is largely the same with a few consequential changes:

- Altered main steam line piping dimensions
- Revised nozzle modeling, one lumped FL for “upper” nozzles, one for “lower”
- Added homologous pump model to replace quick-CF type pump
- Revised rated pump conditions and performance data based on new information
- Revised CF Terry turbine model data, informed by SNL CFD analyses

The idea behind revising the nozzle flow path modeling was to capture effects of steam line flooding, liquid water admission into the steam chest, and hence water ingestion by lower steam nozzles. The CF-specified turbine model was adjusted to account for torque from impinging water. Table 7.14 summarizes inputs for the homologous pump model.

Table 7.14 Homologous pump inputs for pseudo-Fukushima run

<u>Input Parameter</u>	<u>Value</u>	<u>Units</u>
Name, Num, Type	'RCIC_Pump' , 1 , HOM	-
Performance	USER , single-phase	-
Rated Conditions [ω , Q, H, P]	[4500, 0.026, 853, 3.43*10 ⁵]	[rpm, m ³ /s, m, W]
Inertia (App. H)	[10.0, 0.0, 0.0, 0.0, 10.0, 0.5]	-
Friction (App. H)	[1.0, 0.0, 0.0, 0.0, 1.0, 1.0, 1.0, 1.0, 0.1]	-
Misc (App. H)	TIE, SIMP, CF motor torque	-

The pseudo-Fukushima transient path is concisely summarized below and is identical for all pseudo-Fukushima calculations presented hereafter:

- Begin at “time zero” with full decay power deposition into the RPV pool as if the fission chain reaction had just been terminated by a reactor scram
- Begin the boil-down of pool inventory in the isolated RPV (there is no connection to the power-producing side of the plant)
- Assuming the RCIC turbine governor is powered and MSL relief valves are operational, steam venting from the RPV occurs as make-up coolant flows in from the CST via RCIC turbo-pump operation
- Continue until 1 hr problem time, when a loss of power (turbine control) is assumed such that the governor valve goes full-open (its default failure state)

- If the code predicts RCIC system is still operating at 14 hr problem time, model the switch-over of RCIC pump suction alignment from the CST to the Wetwell
- Terminate the transient at 66 hr problem time

7.2.2.3 Modifications to Accommodate New Models

A quick description of new input follows. Each bullet point is expounded in subsequent paragraphs. The necessary modifications include:

- Add block-CVH input for a Terry turbine object to the appropriate CV
- Revise steam nozzle flow path configurations
- Add the steam nozzle flow paths to the time-dependent tabular record if the steam expansion model will be used
- Add an FL_TSH record to associate the new rotor object with the homologous pump meant to represent
- Add whatever CFs and TFs necessary to furnish data for the velocity stages

The block CVH input for a rotor object includes identification information (rotor name, number, flow path connections) and geometry/operational characteristics (nozzle and bucket numbers, all velocity stage parameters as previously described, friction torque input, and moment-of-inertia input). For purposes of the Pseudo-Fukushima calculation, this block-CVH input consists of the information summarized by Table 7.15 below. The block-CVH input was added to the CV named 'RCIC_turbine', which represents the control volume downstream of the several nozzle flow paths which sets the turbine back-pressure and wherein the Terry turbine would reside physically reside.

Table 7.15 Block-CVH input for Terry turbine rotor object

<u>Input Parameter</u>	<u>Value</u>	<u>Units</u>
Rotor Object Name	'TERRYTURBINE'	-
Rotor Object Number	1	-
Number of Nozzles	5	-
Reversing Chambers per Nozzle	4	-
Rotor radius	0.3048	m
Rotor Inertia Inputs Order of CV_RIN, see App. H	[10.0, 0.0, 0.0, 0.0, 10.0, 0.5]	-
Rotor Friction Torque Inputs Order of CV_RFR, see App. H	[1.0, 0.0, 0.0, 0.0, 1.0, 1.0, 1.0, 0.0, 0.1]	-
Linked Nozzle Flow Paths	'Steam_nzls_Hi1' 'Steam_nzls_Hi2' 'Steam_nzls_Hi3' 'Steam_nzls_Lo1' 'Steam_nzls_Lo2'	-
Velocity Stage Parameters: Bucket Exit Angle Bucket Loss Coefficient Chamber Loss Coefficient Chamber Leakage Coefficient Carry-Over Fraction	All CF-specified	-

Experience suggested that - given the way in which the new models are presently configured - the best way to model turbine steam nozzles is with separate flow paths each assigned to represent a single nozzle. As such, the “lumped” flow paths of the modified original model were split into their constituent parts, leading to three distinct upper (or “Hi”) flow paths and two distinct lower (or “Lo”) flow paths. All five nozzles were added on the CV_NFP record (see Appendix H) so that the rotor named ‘TERRYTURBINE’ could “find” them and compute torques on the rotor due to their respective flows. All five nozzles were also specified on FL_VTM (see Appendix H) to use the new steam nozzle option. All nozzles are subject to the MELCOR flashing model (see [15], [16]) when the flow path void fraction is below 0.9 (a hard-coded value for now). Thus, two-phase choked flow can be treated when necessary. This modeling decision was made for two reasons:

- There is a rudimentary transition criterion (based on flow path void fraction) such that the steam expansion model can defer to Moody and/or Henry-Fauske two-phase critical flow models
- Water ingestion and effects of steam line flooding were deemed an important aspect of off-normal conditions that should not be neglected

The new steam nozzle flow paths were altered such that their areas and lengths were consistent with GS-1 Terry turbine nozzle dimensions. On FL_VTM (see Appendix H), all steam nozzles were given identical expansion rates (2.259×10^3 1/s) and exit-to-throat area ratios (1.644). No homologous pump model changes were made apart from linking the pump to the rotor with FL_TSH.

7.2.3 Pseudo-Fukushima Results

It is useful to present and compare certain characteristics of the system thermodynamic response for all variants of the pseudo-Fukushima test. Of particular interest are: 1) the revised original version as described above, and 2) the version(s) exercising new RCIC models. For all cases, results of interest include:

- The RPV/boiler liquid level
- The RPV/boiler pressure
- Steam nozzle characteristics (phasic mass flow, phasic velocities, etc.)
- Turbine rotor characteristics (torques)
- RCIC pump characteristics (speed, head, flow, etc.)

The RPV liquid level indicates inventory boil-off and RCIC make-up. It is the parameter that determines RCIC system actuation before total black-out conditions occur. The RPV pressure impacts SRV actuation and should respond to RCIC system intervention. The steam nozzle characteristics are especially important when all power is lost, the governor valve goes full open, and RPV over-fill leads to steam line flooding and admission of liquid water into the two lower-lying steam nozzles. The turbo-pump response during both normal and off-normal conditions is the key result for these analyses. Normal conditions exist before 1 hr problem time with the governor valve controlling steam admission and very little water, if any, passing through. Off-normal conditions develop after power is lost, the governor goes full-open, and RPV over-fill occurs. The turbine either rides out the conditions and continues to run in a sort of self-regulating mode, or trips on its mechanical over-speed set-point. Note that the conventional

assumption is mechanical over-speed shortly after loss of governor valve control. If the RCIC turbine rotor speed exceeds its trip set-point (125% of the rated speed of 4500 rpm, i.e. 5625 rpm), the RCIC system is assumed to go off-line such that it can no longer deliver make-up coolant to the RPV. Presumably the RPV pool would continue to boil off and core damage would inevitably occur (though such phenomena are not modeled in the test).

7.2.3.1 Original Version with Revisions

In this case only the first hour of the transient is considered because, using the modeling assumptions of this variant, turbine over-speed trip occurs upon loss of governor valve control. The RPV pressure holds more or less constant (subject to wiggles associated with SRV cycling) at about 8 MPa as shown in Figure 7.32. During this time, Figure 7.33 demonstrates that decay heat is boiling off the RPV liquid inventory. SRV cycling maintains the RPV pressure during steam generation. Eventually, the RPV liquid level reaches a low-low set-point (prescribed as -4.16 m in reactor coordinates) from its initial -1.9 m level. This event signals the RCIC system to start operation (at about 1500 s problem time). The turbine stop valve opens and the governor valve begins to open, ultimately to about 20% of its fully-open position (simulating governor regulation of valve open fraction). After a short period of level increase due to RCIC pump action, Figure 7.33 shows that the RPV water level turns back down beginning at around 2700 s problem time. This coincides with commencement of so-called “operator throttling” where test/recirculation lines are used to divert some make-up coolant (from RCIC) back to the suction source (i.e. the CST). This operator action is a safeguard against RPV over-fill (since the RCIC pump is typically over-sized) but does not require RCIC system

“shutdown” or closure of the turbine stop valve and/or governor valve. The RCIC pump volumetric flow does not change in response to the throttling, but the amount of inventory delivered to the RPV decreases appreciably.

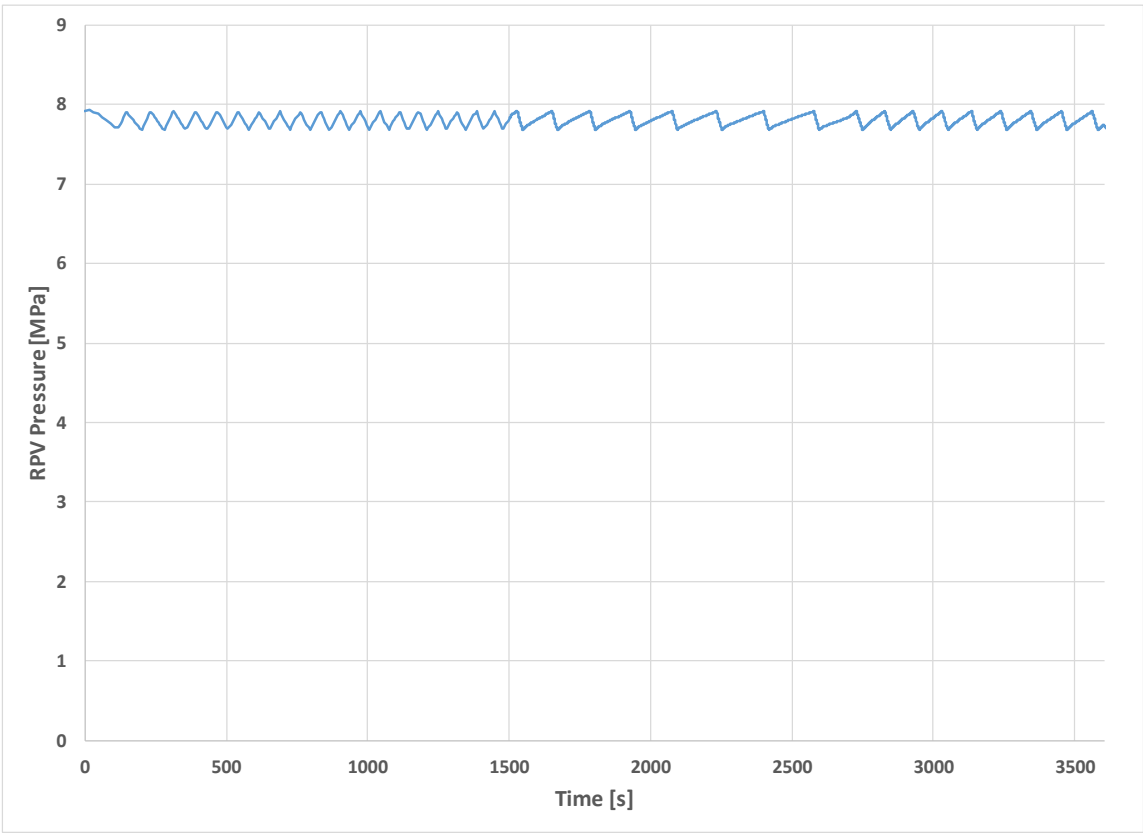


Figure 7.32 Calculated RPV pressure [Mpa]

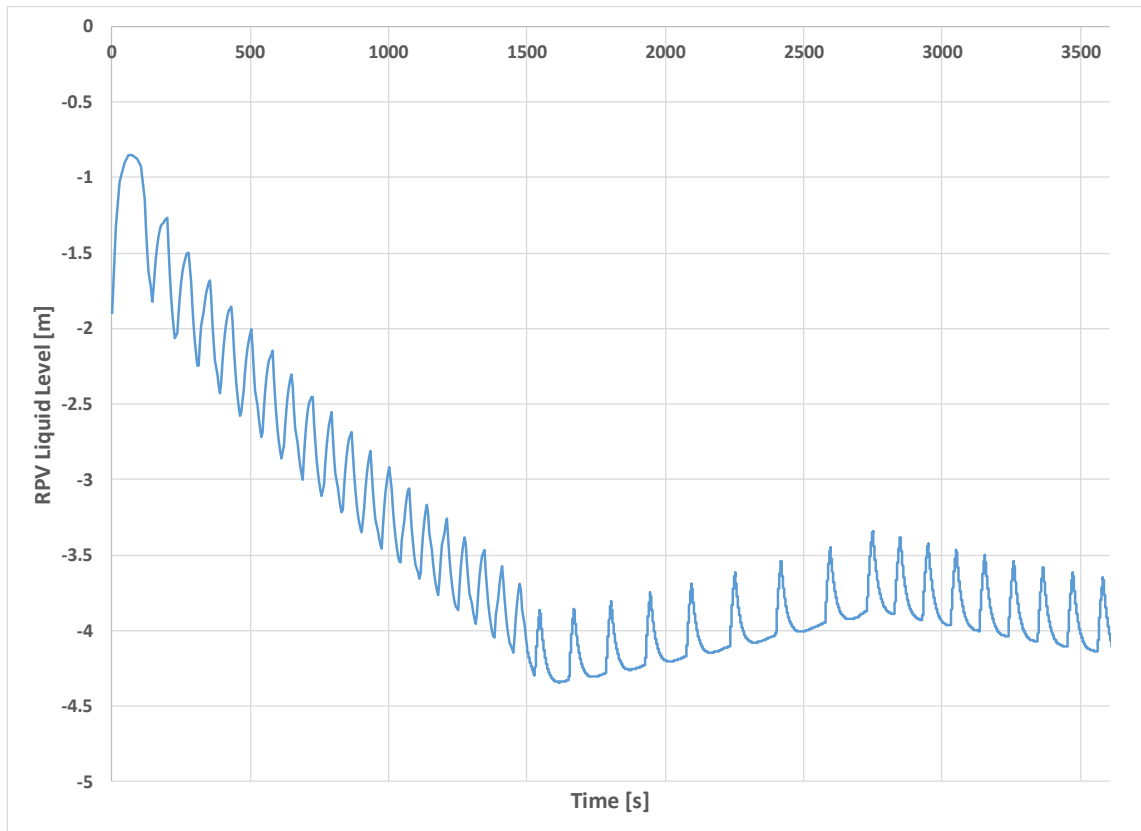


Figure 7.33 Calculated swollen RPV liquid level [m]

Turning now to the steam nozzle flow, it is first important to note that no special steam nozzle models are active here. The steam nozzle flows are treated as normal, horizontal MELCOR flow paths subject to the typical phasic velocity equation solutions and/or the choked/critical flow model. Mass flow rates and velocities are shown in Figure 7.34 to Figure 7.36 for the lumped flow paths (3 upper represented by ‘Steam_nzls_hi’, 2 lower represented by ‘Steam_nzls_lo’). The steam flow rates and velocities are very nearly identical for both of these flow paths. The lower lumped path has a slightly lower steam flow rate and velocity due to the presence of a small amount of liquid. In the first hour of

problem time, no liquid water enters the upper lumped path. As such, the lower path void fraction is very nearly one (> 0.999) and the upper path void fraction is always unity.

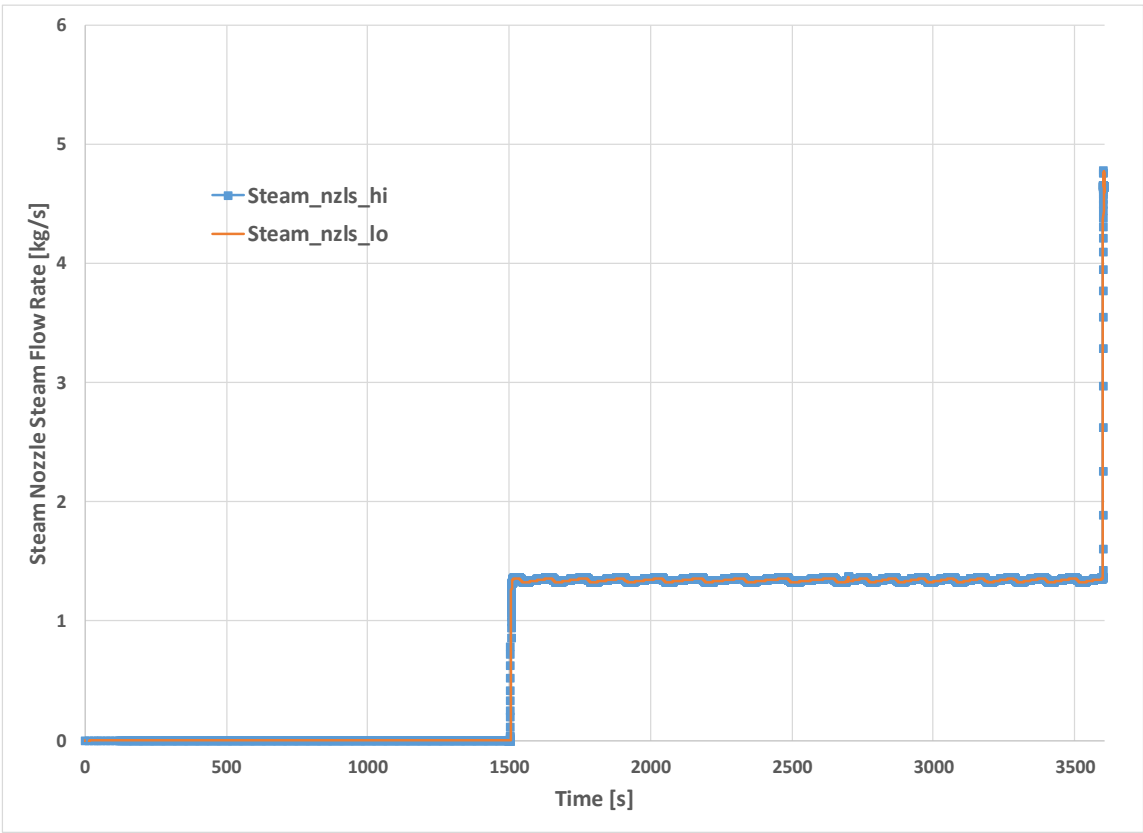


Figure 7.34 Calculated steam nozzle steam flow rates [kg/s]

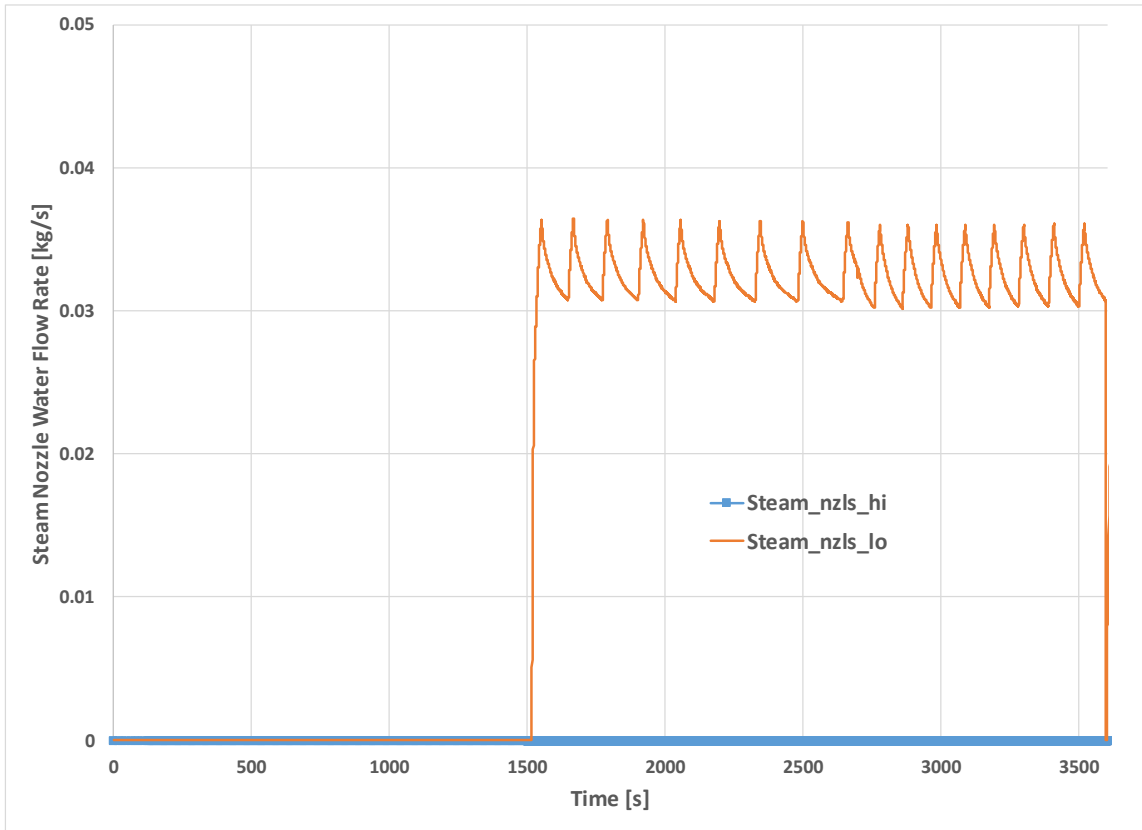


Figure 7.35 Calculated steam nozzle water flow rates [kg/s]

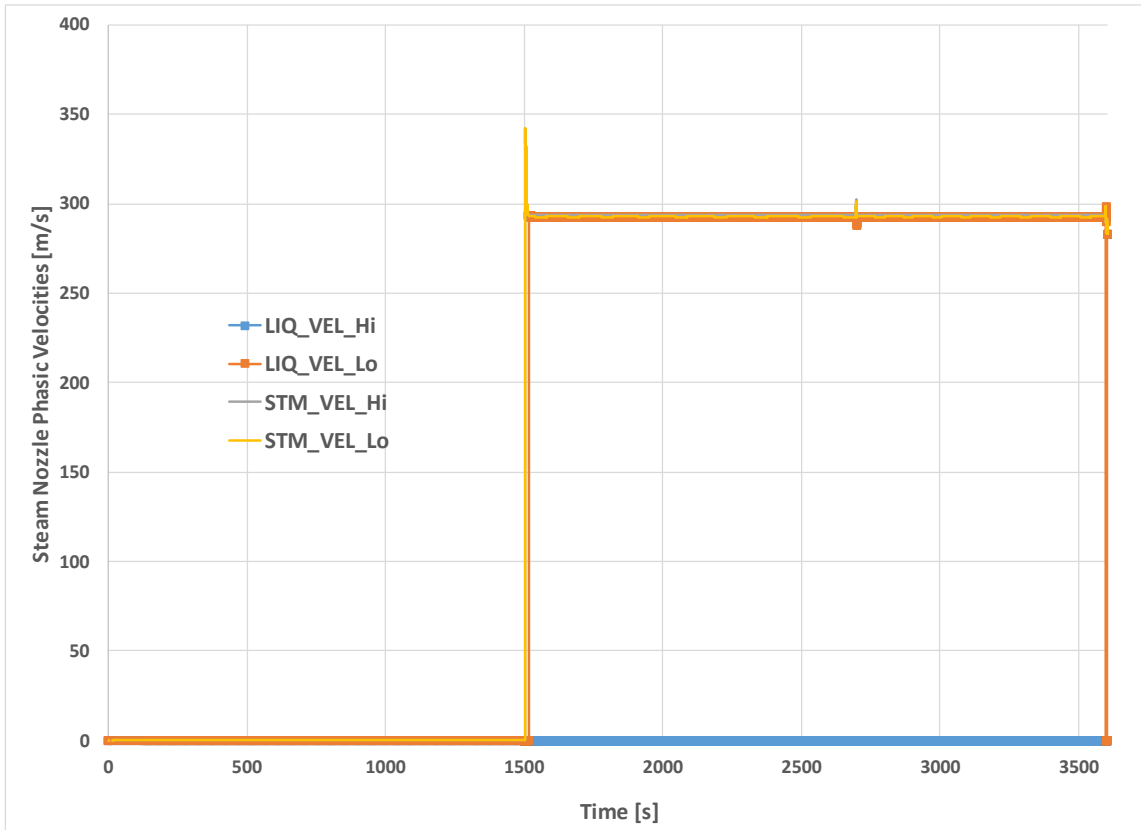


Figure 7.36 Calculated steam nozzle phasic velocities [m/s]

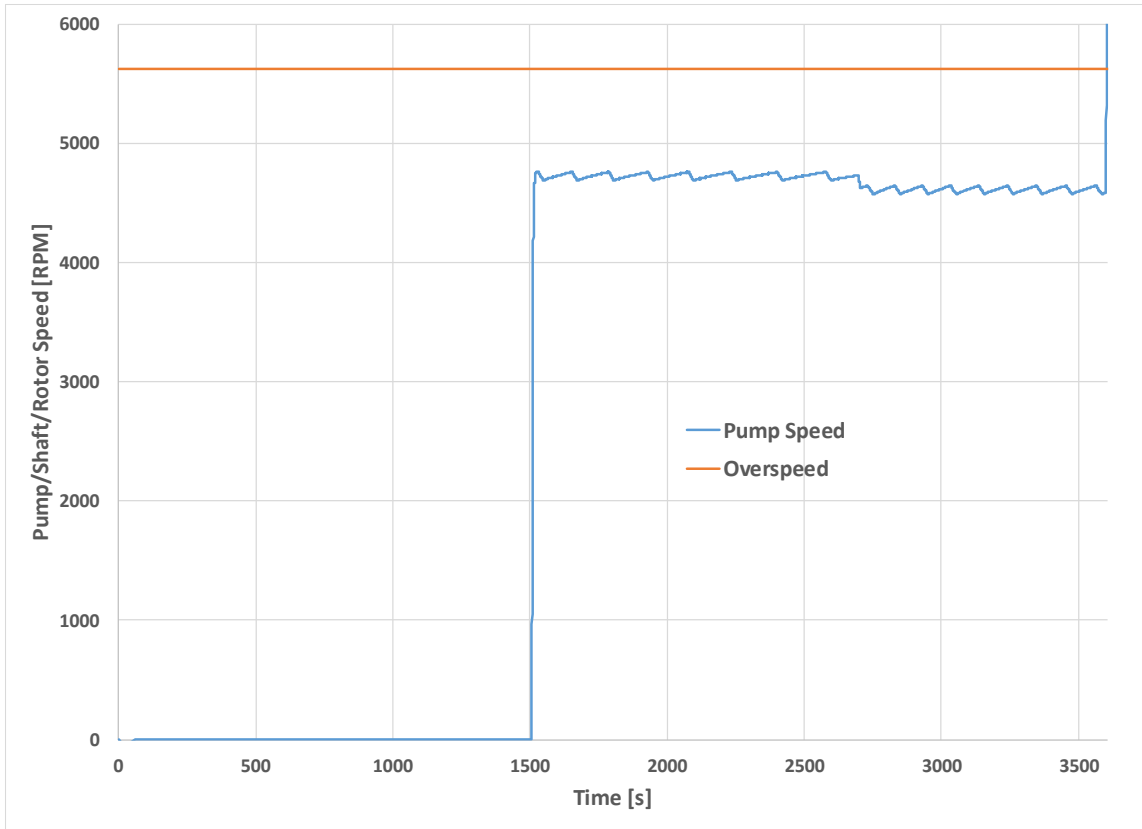


Figure 7.37 Calculated pump/shaft/rotor rotational speed [rpm]

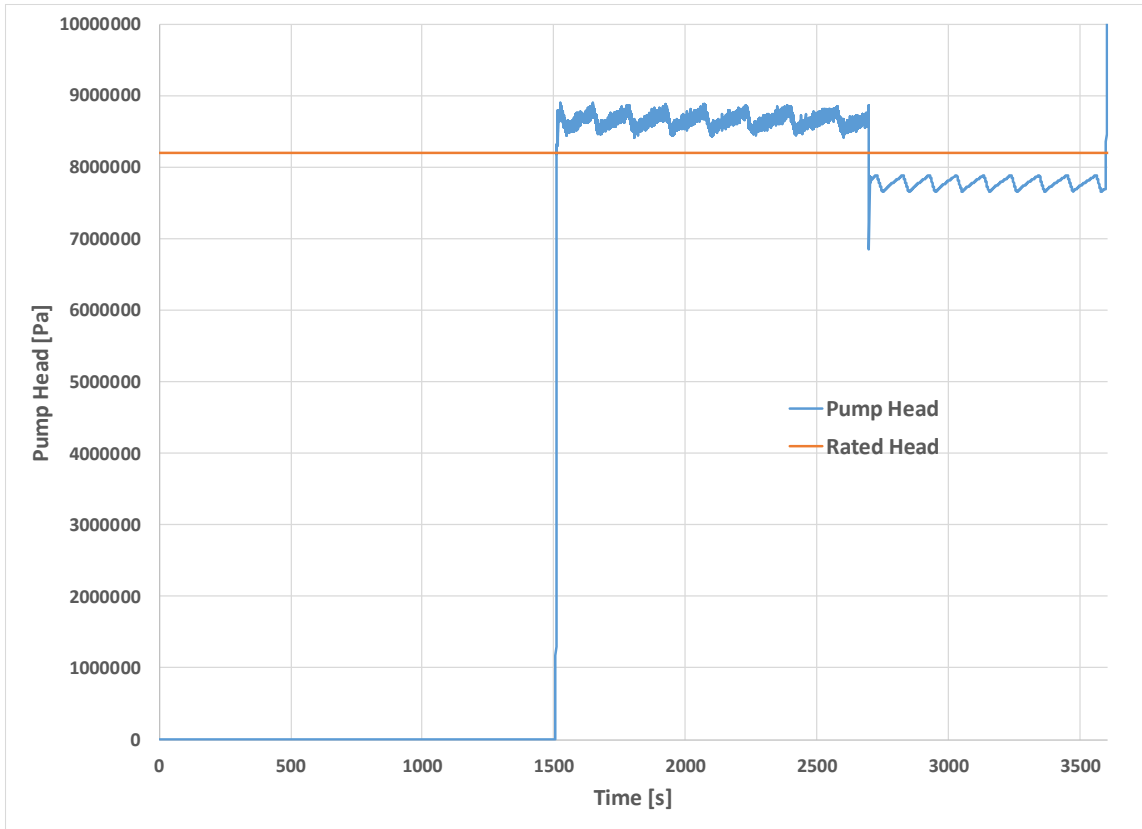


Figure 7.38 Calculated pump head [Pa]

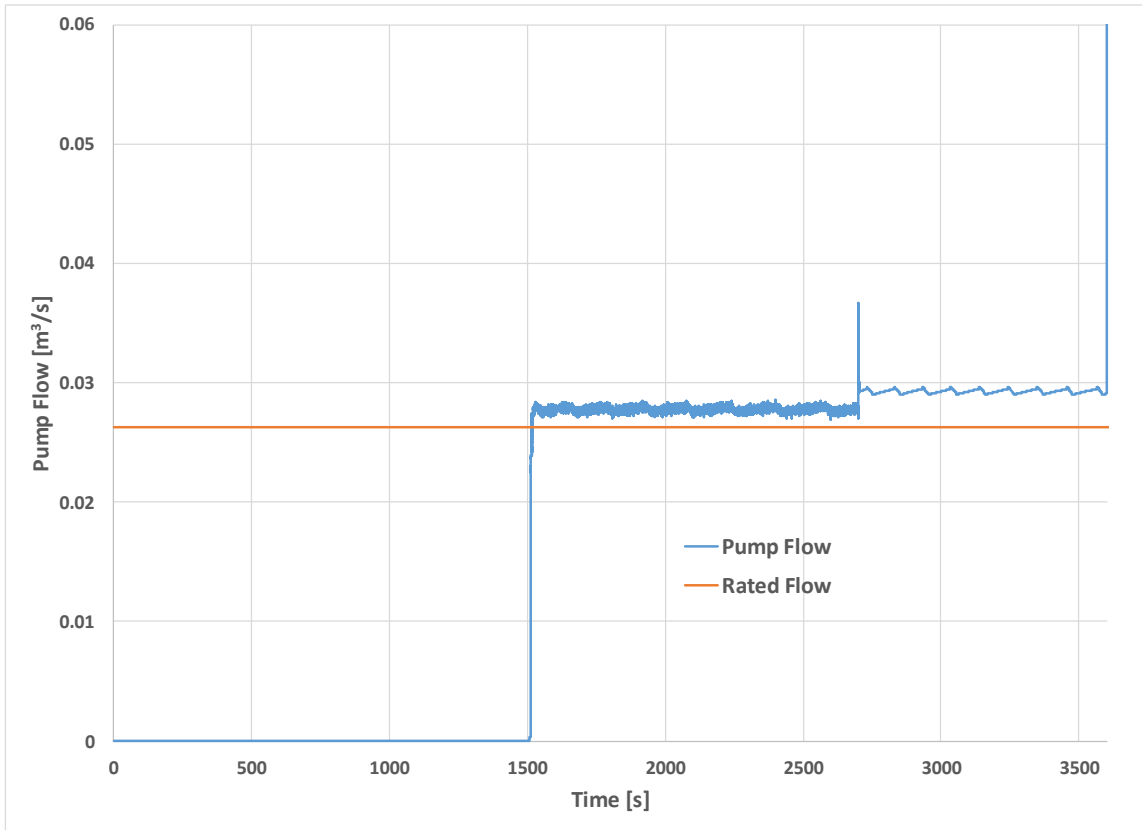


Figure 7.39 Calculated pump flow [m^3/s]

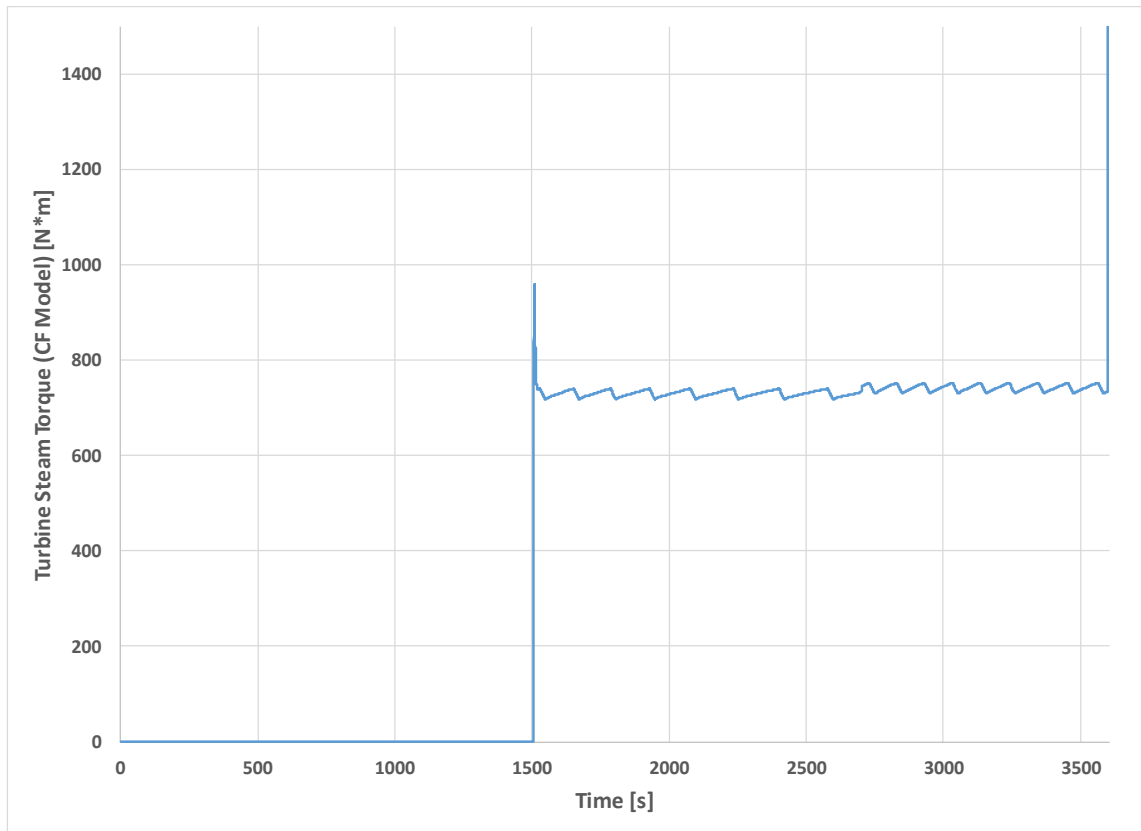


Figure 7.40 Calculated turbine torque from CF-model [N*m]

As is evident from Figure 7.37 to Figure 7.39, the start-up of CST recirculation at 2700 s problem time affects pump operation somewhat. When the turbine governor goes full-open at about 3600 s problem time, Figure 7.40 shows that the turbine torque increases drastically such that shaft speed is driven well above the mechanical over-speed trip set-point. The CF-specified model that furnishes the turbine torque involves several assumed values for constants, multipliers, etc. that may conceivably lead to an over-prediction of rotor torque. As shown in the next section, the new velocity-stage model that explicitly accounts for compounding does not predict such an over-speed. However, by estimation of this particular variant of CF turbine model, the Terry turbine cannot self-regulate upon

loss of governor valve control. Assuming no operator intervention to reset the mechanical trip and get the turbine back on-line, the RCIC system would be unable to provide coolant inventory make-up to the RPV.

7.2.3.2 *New Models, Isentropic Steam Expansion*

The same transient is run with the new velocity-stage model and with the isentropic steam expansion option active for pressure-stage modeling. For this case, all CFD-supplied systems-level velocity stage parameters are used with the exception of the bucket exit angle, which is held constant at 45°. CST recirculation (operator throttling) is deactivated for this case.

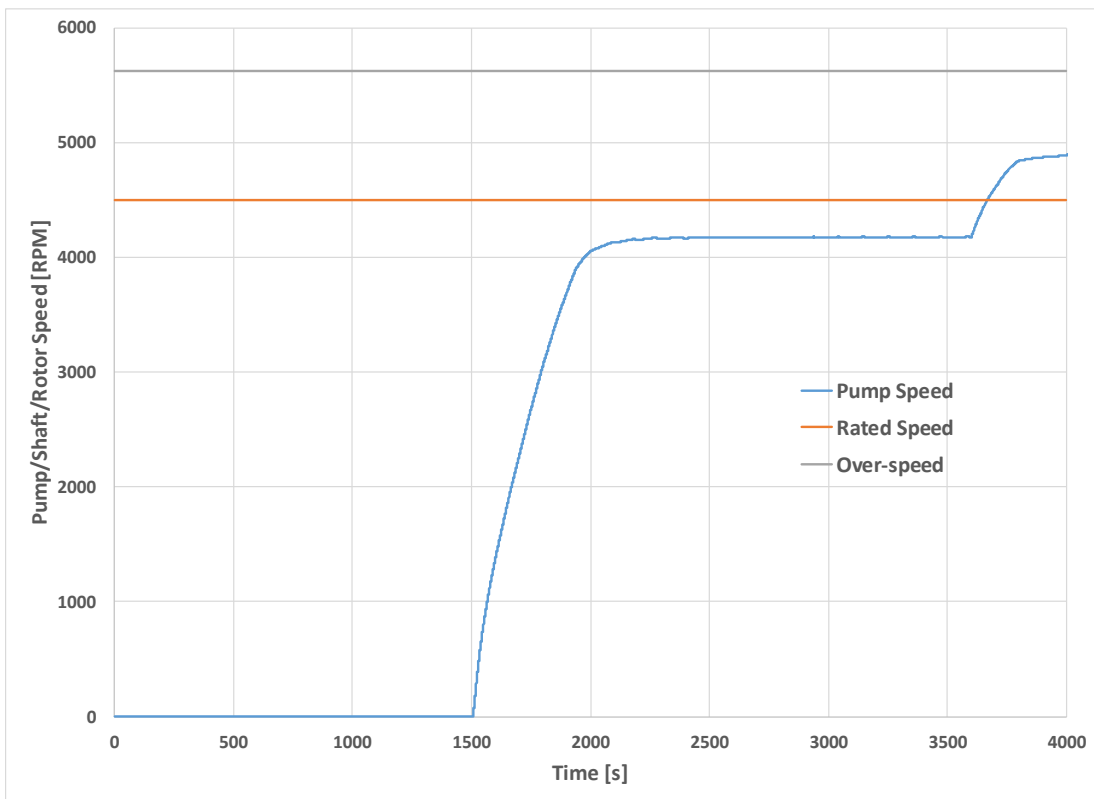


Figure 7.41 Calculated pump/shaft/rotor speed [rpm]

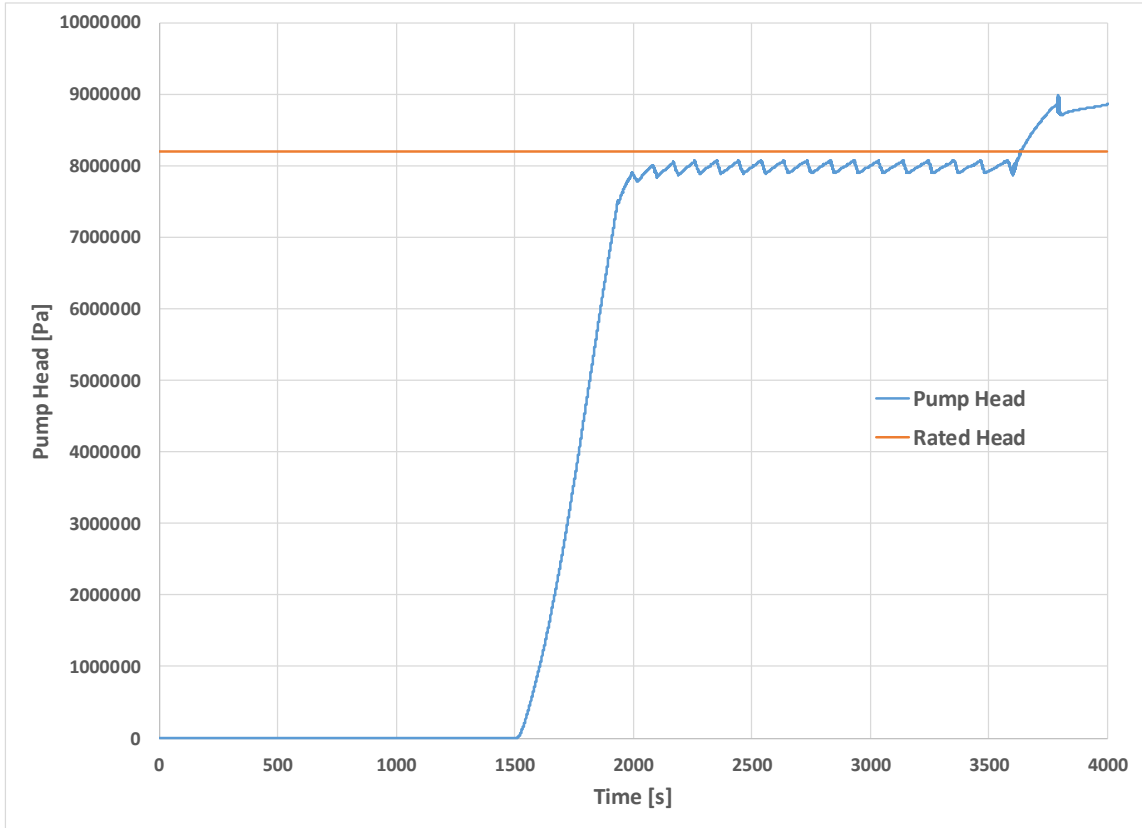


Figure 7.42 Calculated pump head [Pa]

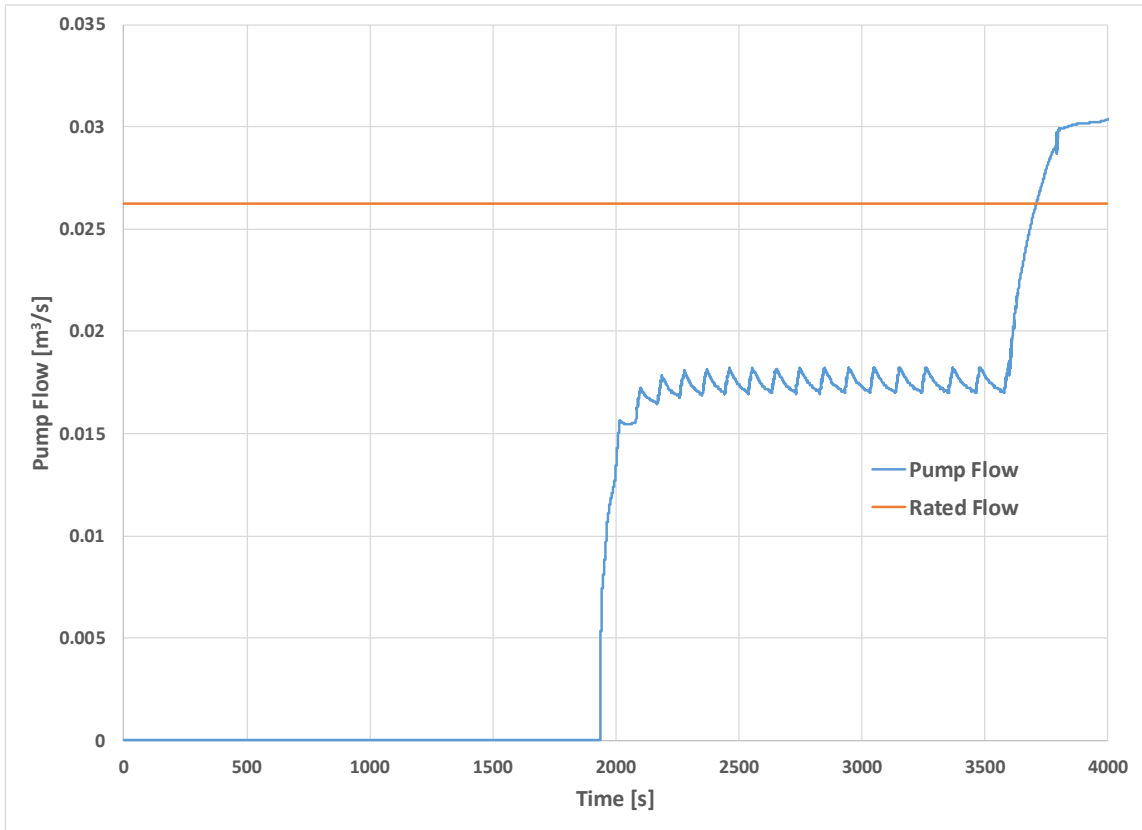


Figure 7.43 Calculated pump flow [m³/s]

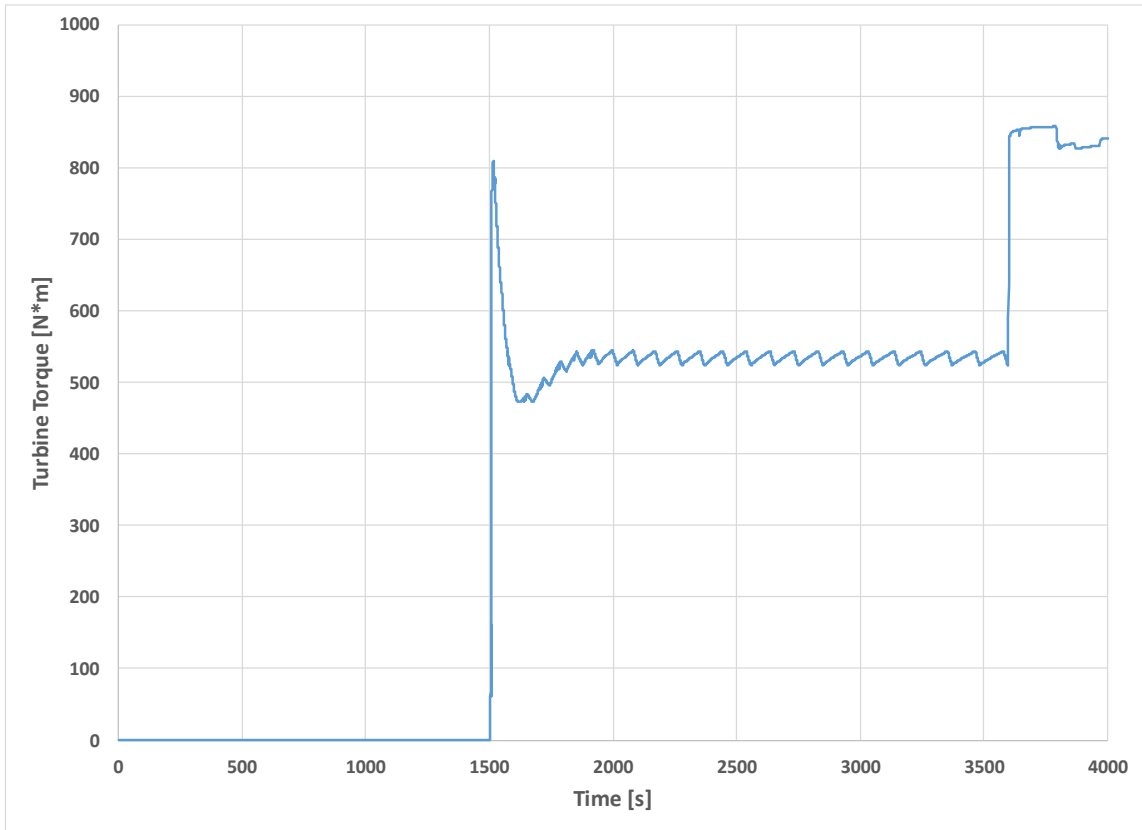


Figure 7.44 Calculated turbine torque [N*m] from compound velocity-stage model

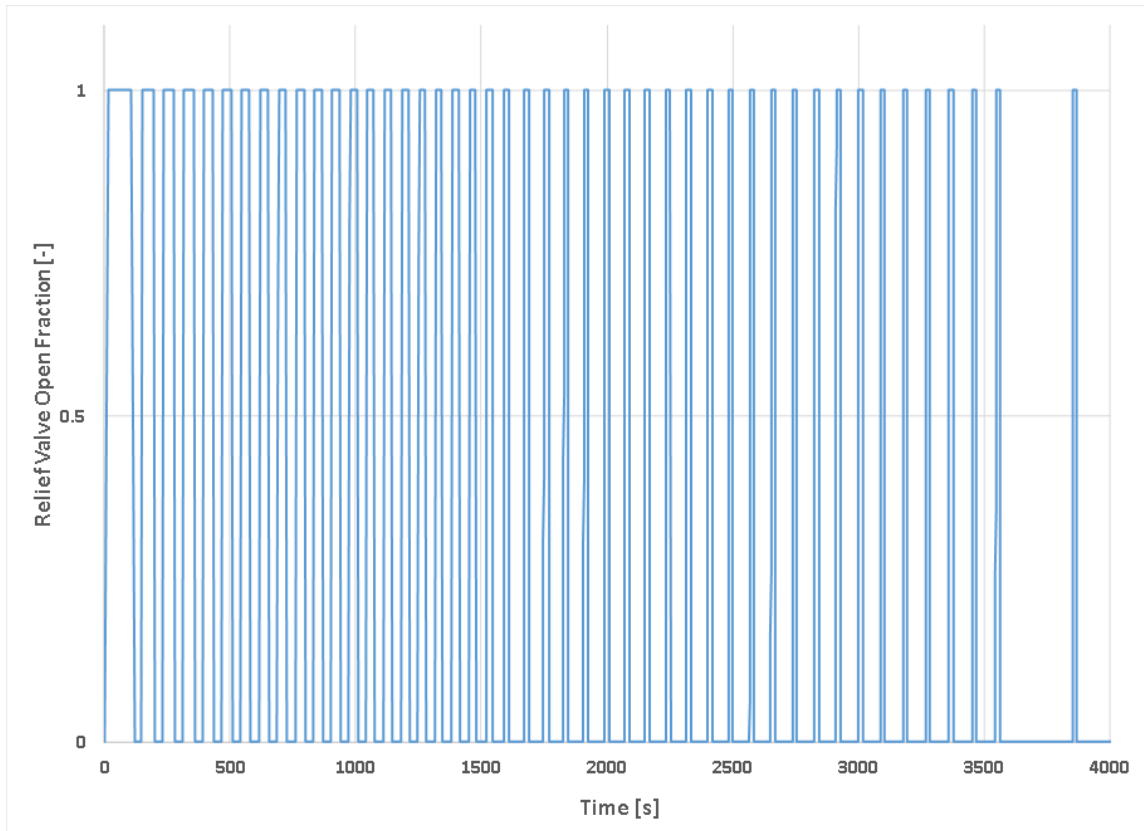


Figure 7.45 Calculated steam line relief valve open fraction

Turbine torque and RCIC pump characteristics are shown in Figure 7.41 to Figure 7.44. Relief valve cycling (via open fraction) is shown in Figure 7.45. The new RCIC system models predict that the turbo-pump can indeed survive and operate under loss-of-power conditions with a wide-open governor valve. At 3600 s problem time, the turbine torque does indeed spike, but to a more modest peak value as compared to Figure 7.40. The shaft speed, pump head, and pump flow adjust upwardly in accordance with the increased turbine steam flow. Pump speed exceeds its rated value but does not exceed its mechanical over-speed set-point. Thus, the RCIC system continues to operate and deliver make-up coolant to the RPV.

7.2.3.3 New Models, Non-Equilibrium Steam Expansion

The same transient is run with the new velocity-stage model and with the analytical Wilson point steam expansion option active for pressure-stage modeling. For this case, all CFD-supplied systems-level velocity stage parameters are used with the exception of the bucket exit angle, which is held constant at 45° as it was in the original, revised version. CST recirculation (operator throttling) is deactivated for this case. The turbine torque is somewhat different in the short-term period just after the RCIC system first actuates at about 1500 s problem time, and this is due to differences between predictions the analytical Wilson point method as opposed those of the isentropic expansion method.

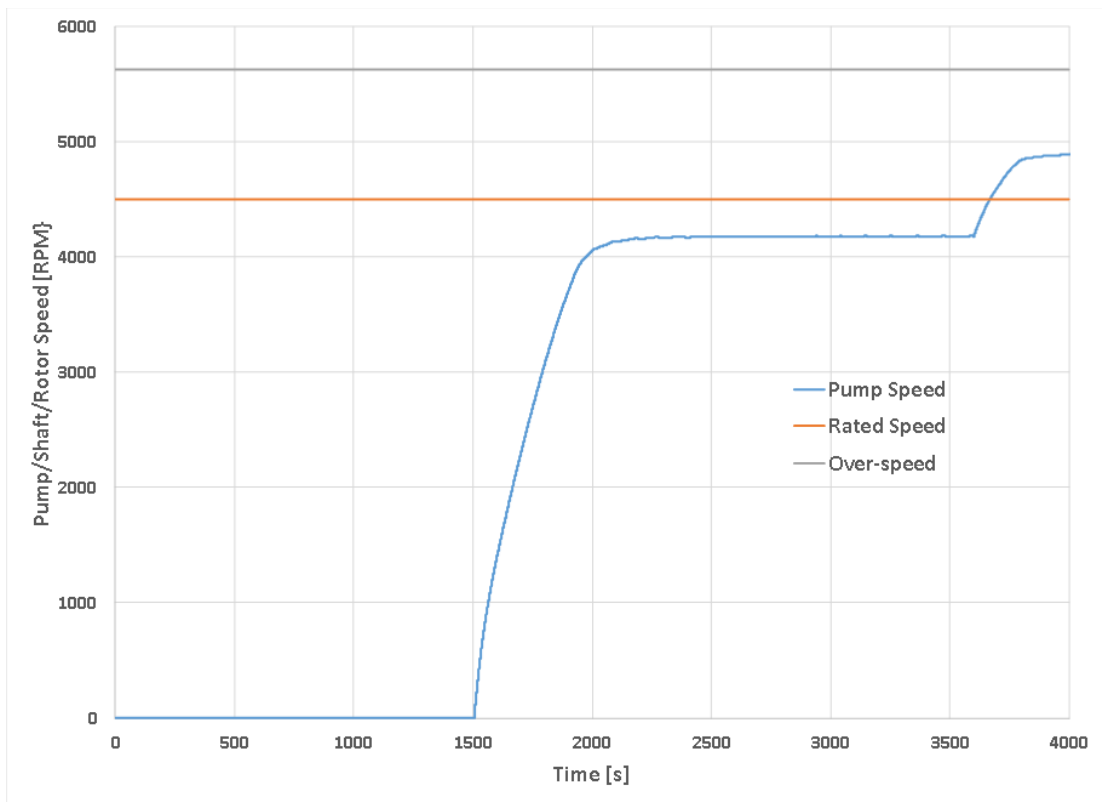


Figure 7.46 Calculated pump/shaft/rotor speed [rpm]

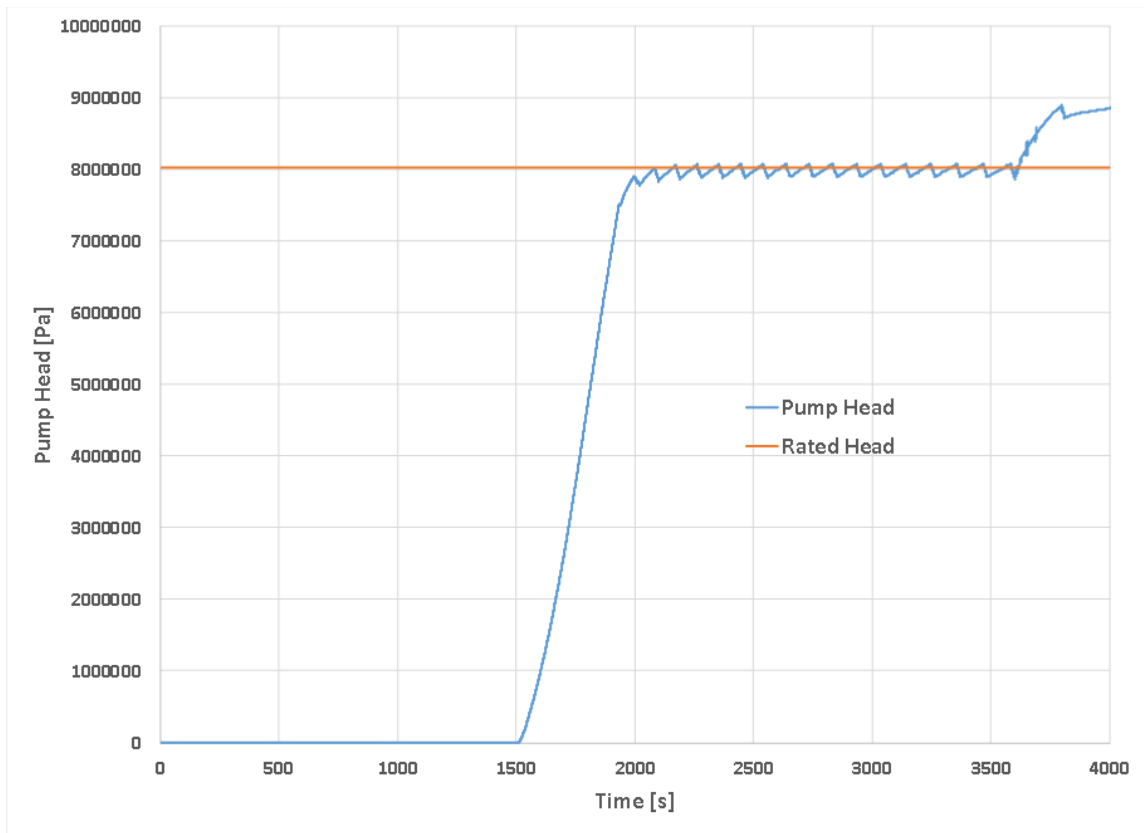


Figure 7.47 Calculated pump head [Pa]

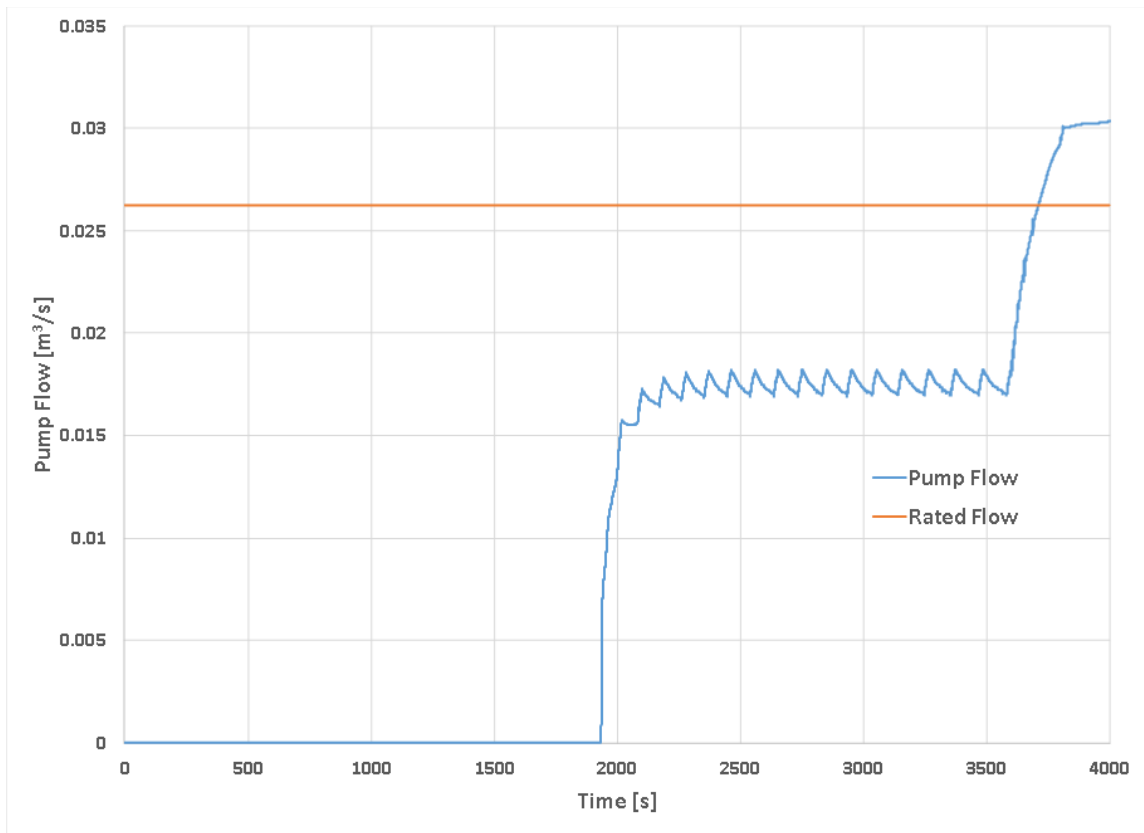


Figure 7.48 Calculated pump flow [m³/s]

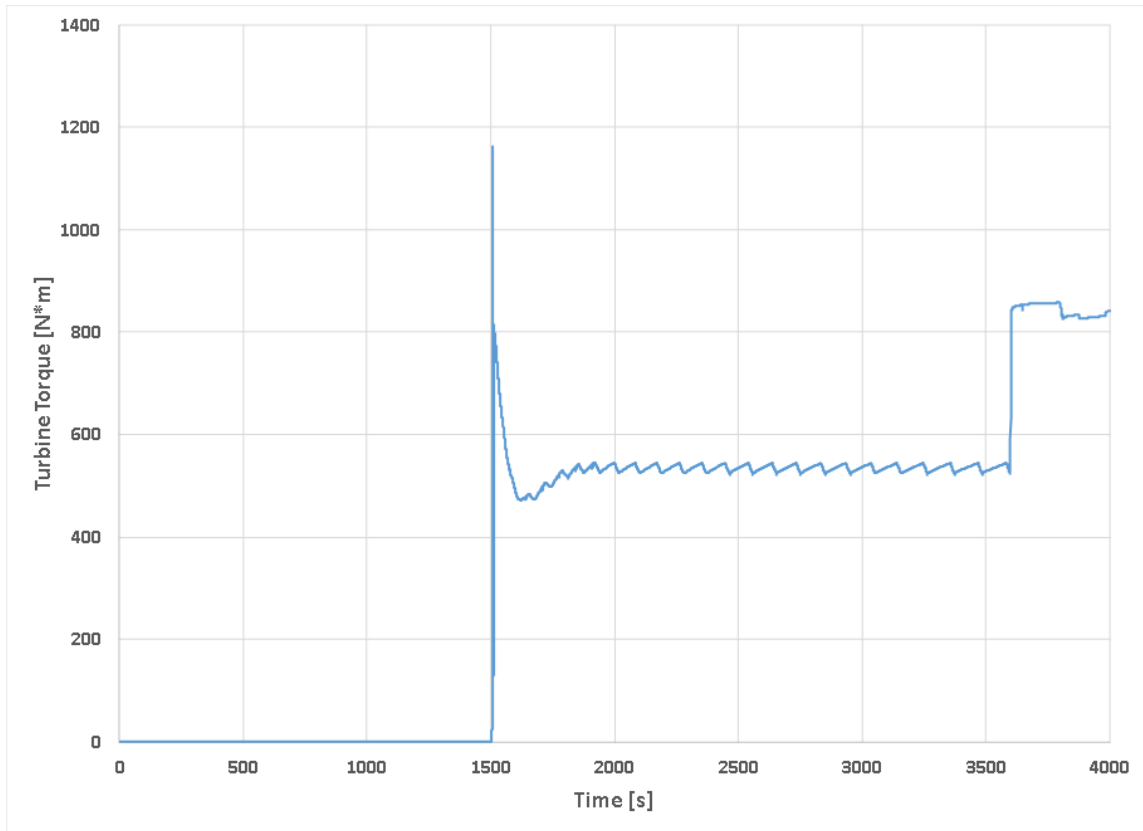


Figure 7.49 Calculated turbine torque [N*m]

Turbine torque and RCIC pump characteristics are shown in Figure 7.46 to Figure 7.49. Relief valve cycling (via open fraction) is essentially the same as depicted in Figure 7.45. The RCIC system remains capable of operating and delivering make-up coolant to the RPV with a wide-open governor, but the analytical Wilson point method predicts greater turbine torque in the short window after 1500 s problem time as the steam nozzle inlet boundary conditions adjust from superheated to saturated.

7.2.3.4 New Models, Long-Term Transient

Since the non-isentropic and isentropic pressure stage options yield identical results beyond the first hour of transient time, system response assuming isentropic expansion is presented here for the long-term (out to 66 hr problem time).

It was established in the last section that the RCIC system turbo-pump can cope with a full-open governor valve according to predictions from the new models. In the longer term as the wide-open governor admits an unregulated steam flow to the rotor, the RCIC pump flow (typically over-sized in terms of capability to re-fill the RPV) should raise the RPV liquid level (assuming no disruption of CST and/or wetwell water). In the absence of an ability to “turn off” the RCIC coolant delivery, MSL flooding could ultimately occur as the RPV over-fills. This could lead to admission of liquid water into the pressure stage of the turbine. Consequently, the turbine must deal with lower void fraction two-phase flow or with single-phase liquid flow through its nozzles. There is some concern that this could lead to over-speed, particularly just after a liquid parcel clears the rotor and higher-velocity steam is again admitted to the nozzles.

To deal with this situation in MELCOR, a capability was added whereby the steam expansion model can be bypassed in favor of the MELCOR two-phase critical flow model (Moody, Henry-Fauske curve-fitting method, see [15] and [16]). This would occur when steam nozzle flow path void fraction falls below some critical value (hard-coded at 0.9 for now, though this could easily be made into a user input value). Note that - according to the current velocity stage model – neither steam nor water can exert a torque on the rotor if the fluid velocity is less than the local rotor bucket velocity (equal to the rotor radius

[m] times rotational speed [1/s]). If the fluid velocity is less than the local bucket velocity, the relative velocity between stream and bucket is such that the stream cannot “catch up” to the bucket and therefore cannot push the bucket to go faster or to maintain speed. Note also that no modeling provisions exist for retarding effects of such a slower-moving fluid stream. If either steam or water (or both) from nozzles moves at a velocity lower than that of the rotor buckets, torque goes to zero and the rotor should slow down as it has no impulse to maintain or increase its speed. These dynamics are indeed observed below.

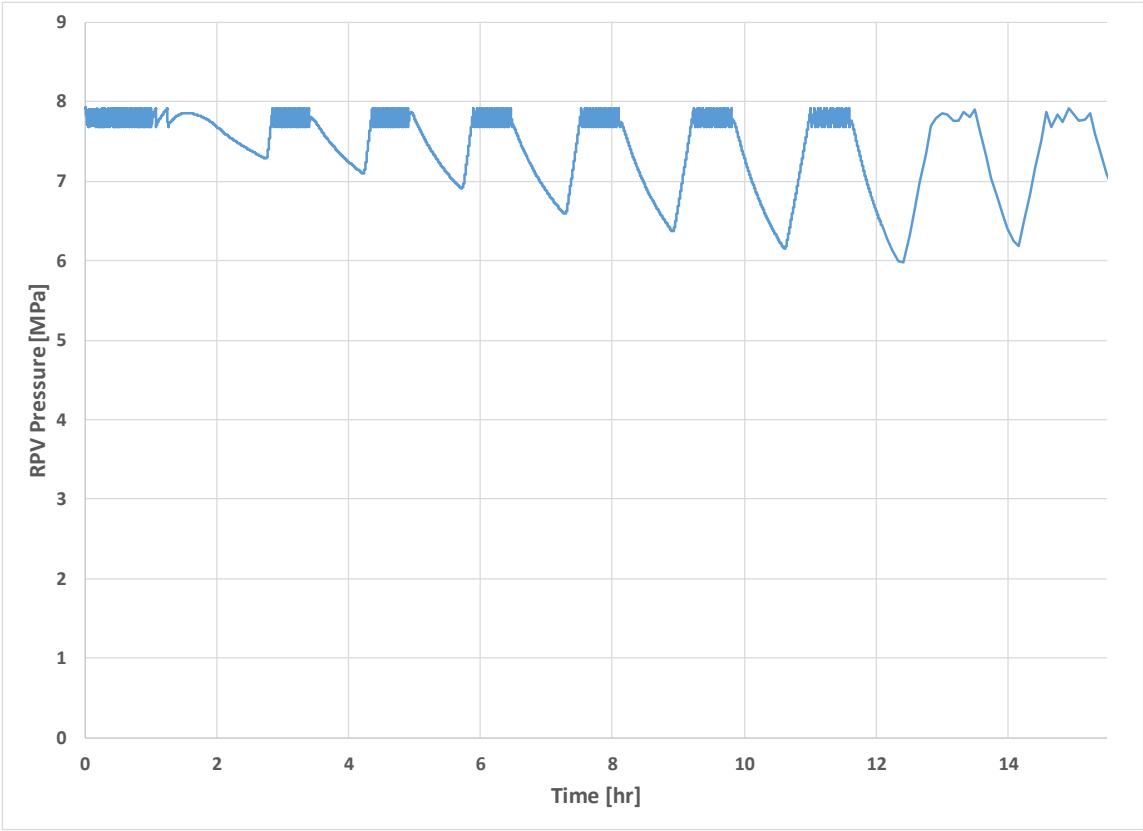


Figure 7.50 Calculated RPV pressure [MPa]

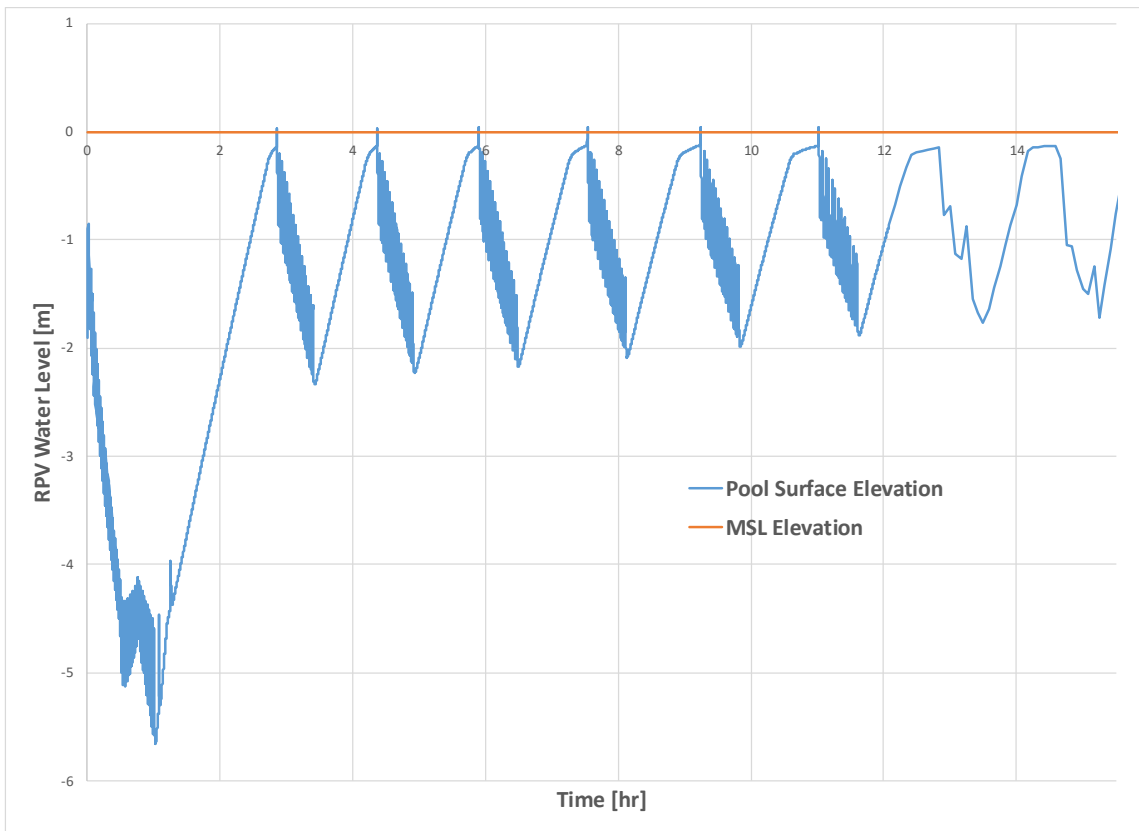


Figure 7.51 Calculated RPV liquid level [m]

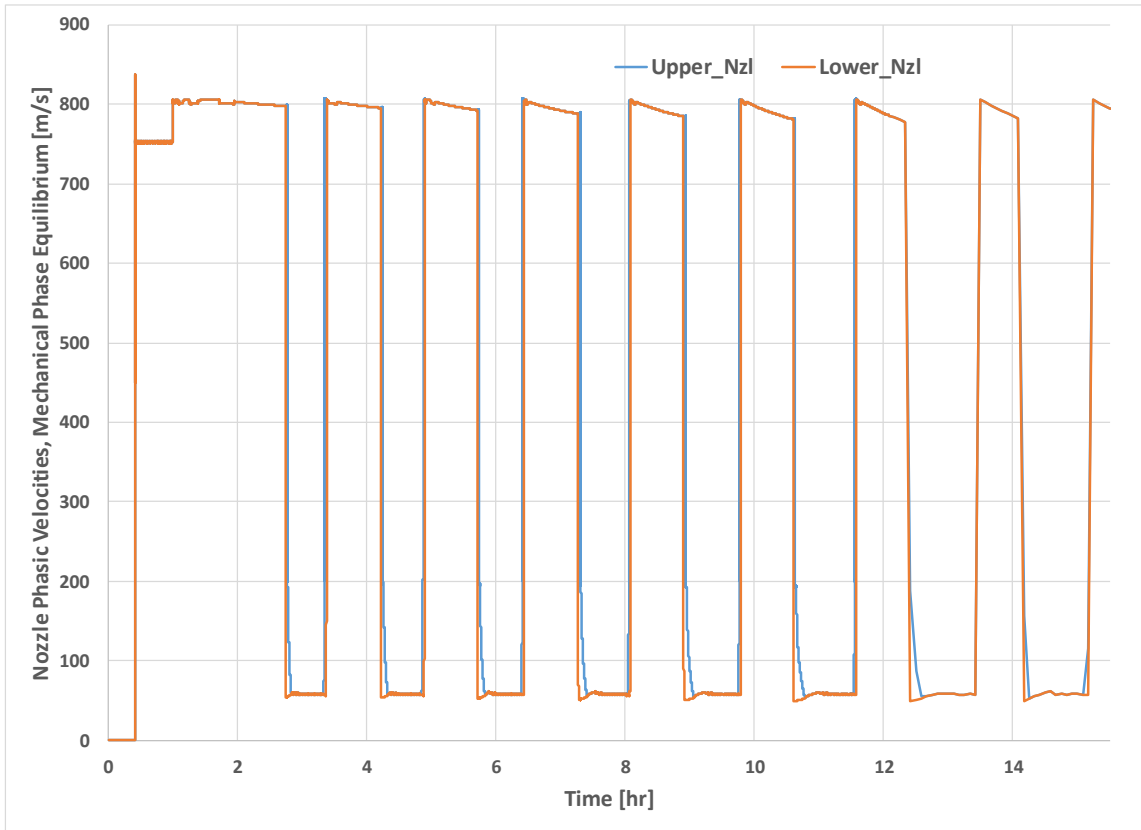


Figure 7.52 Calculated steam nozzle phasic velocities [m/s]

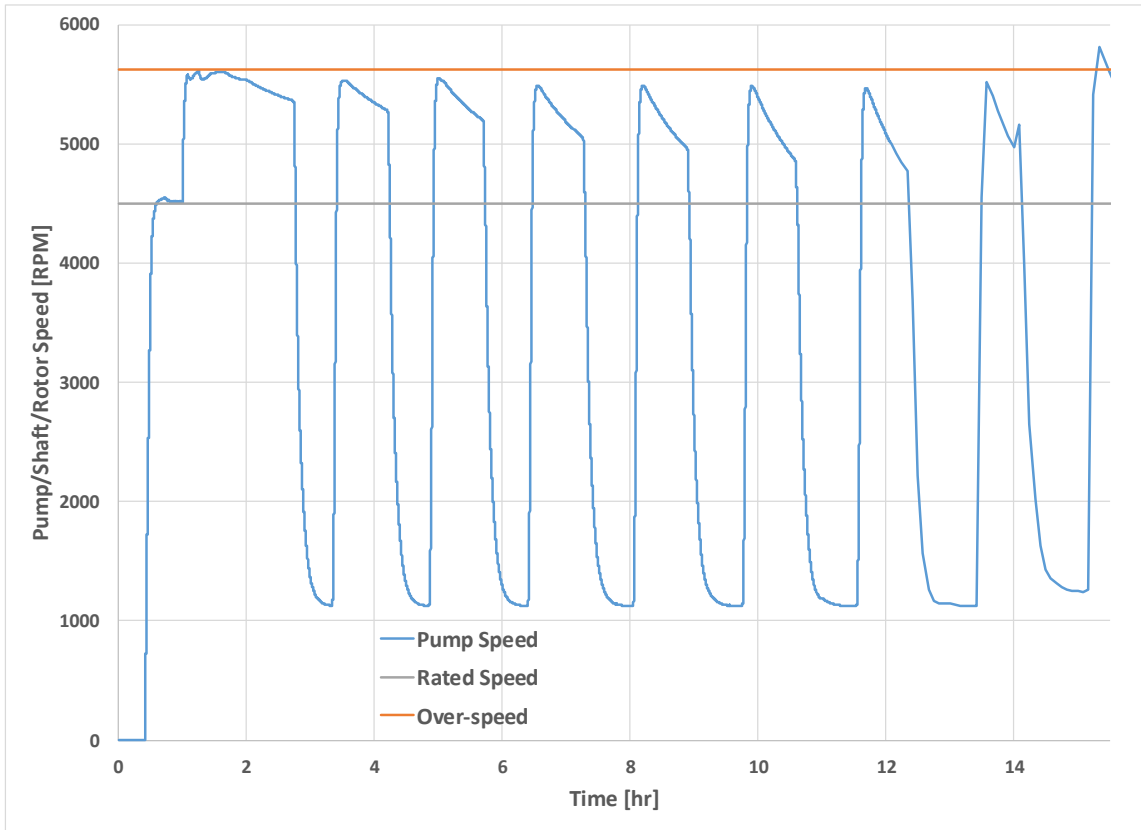


Figure 7.53 Calculated pump/shaft/rotor speed [rpm]

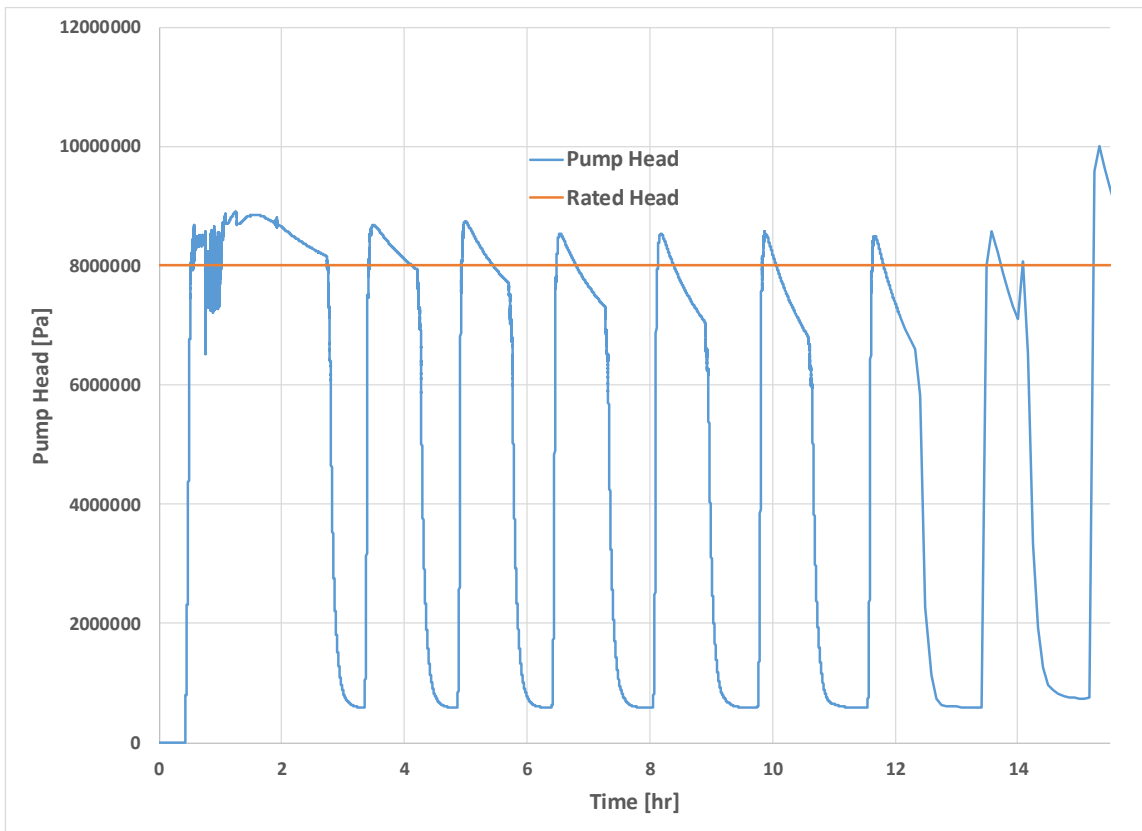


Figure 7.54 Calculated pump head [Pa]

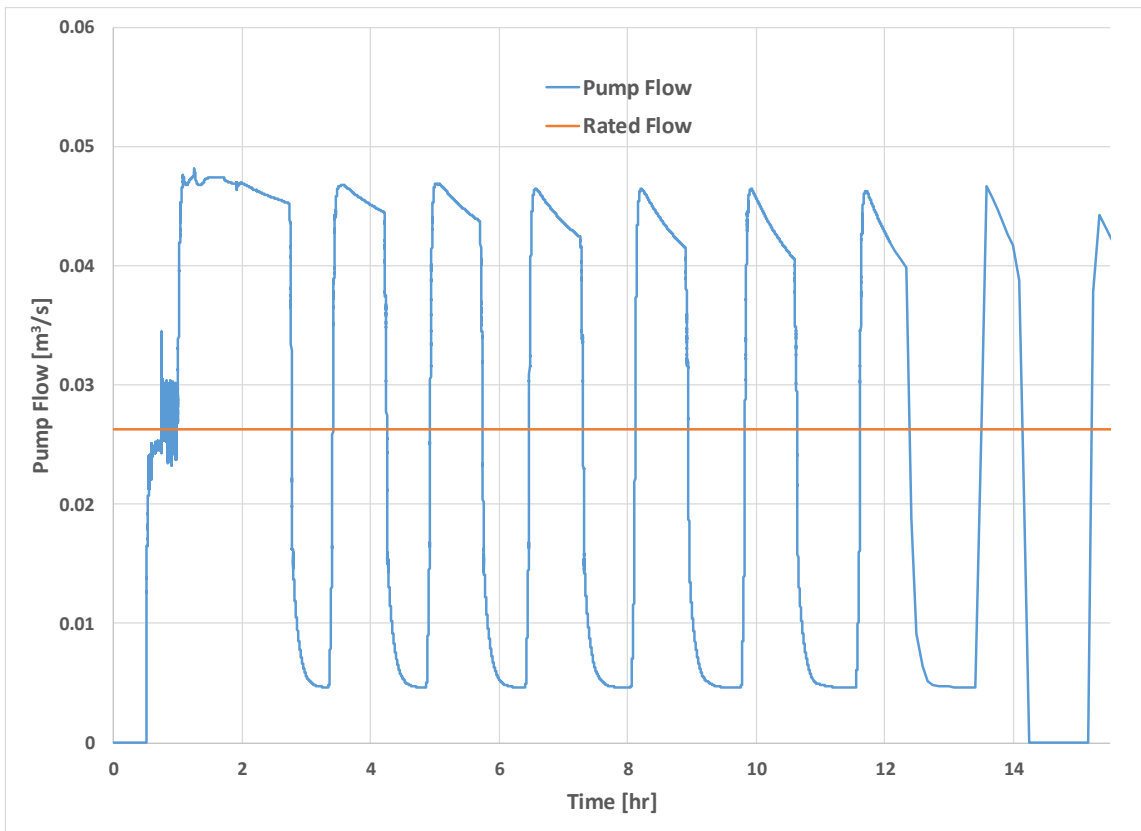


Figure 7.55 Calculated pump flow [m³/s]

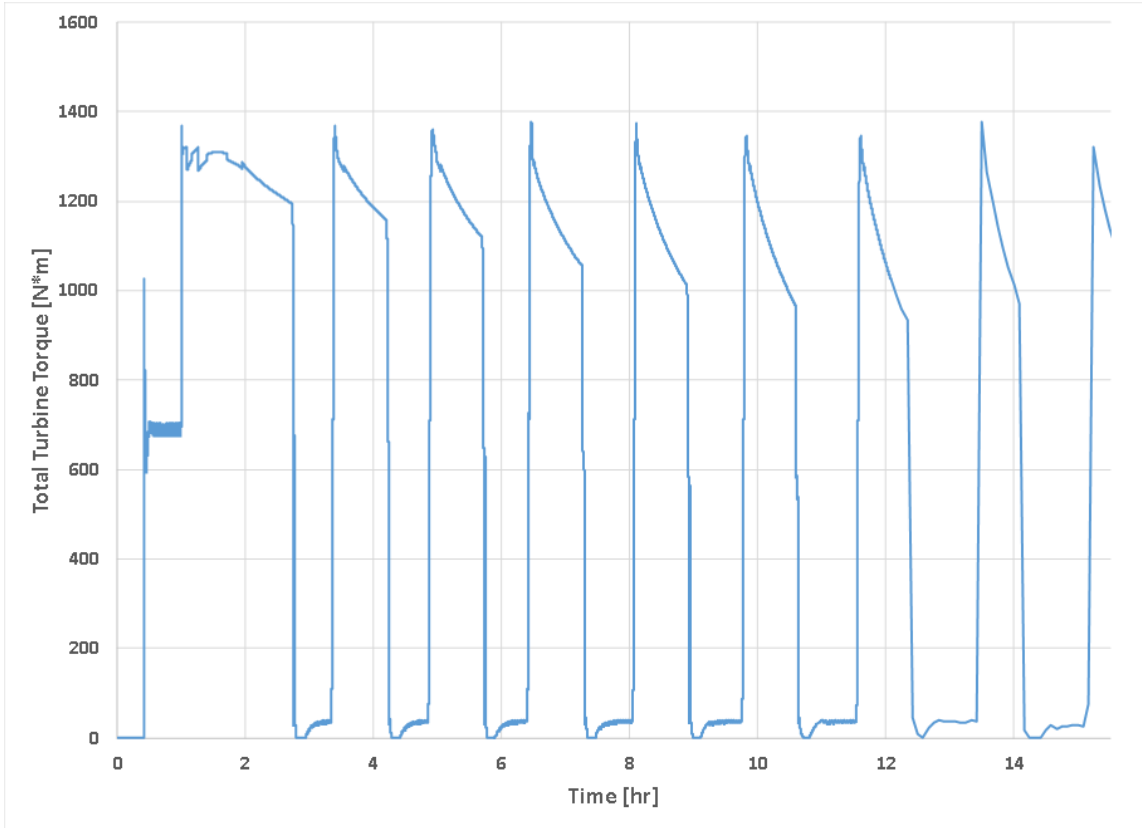


Figure 7.56 Calculated total turbine torque (both phases) [N*m]

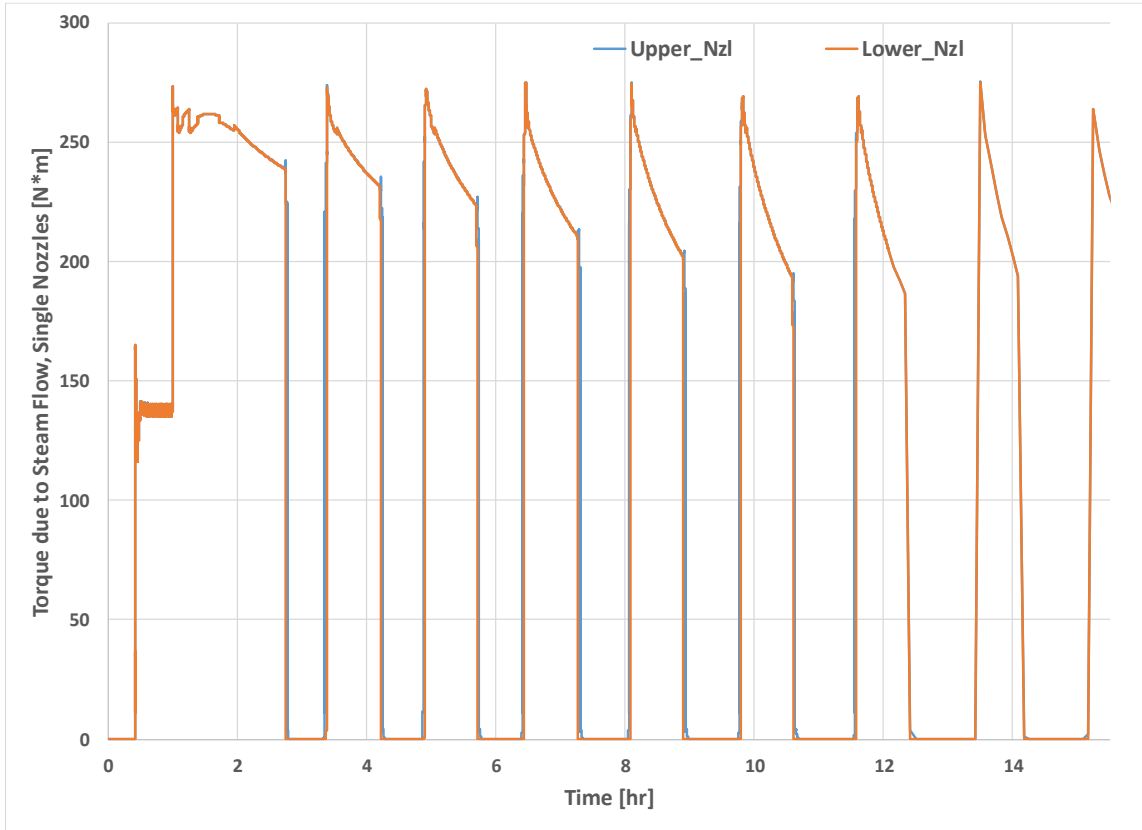


Figure 7.57 Calculated turbine torque due to steam flow [N*m]

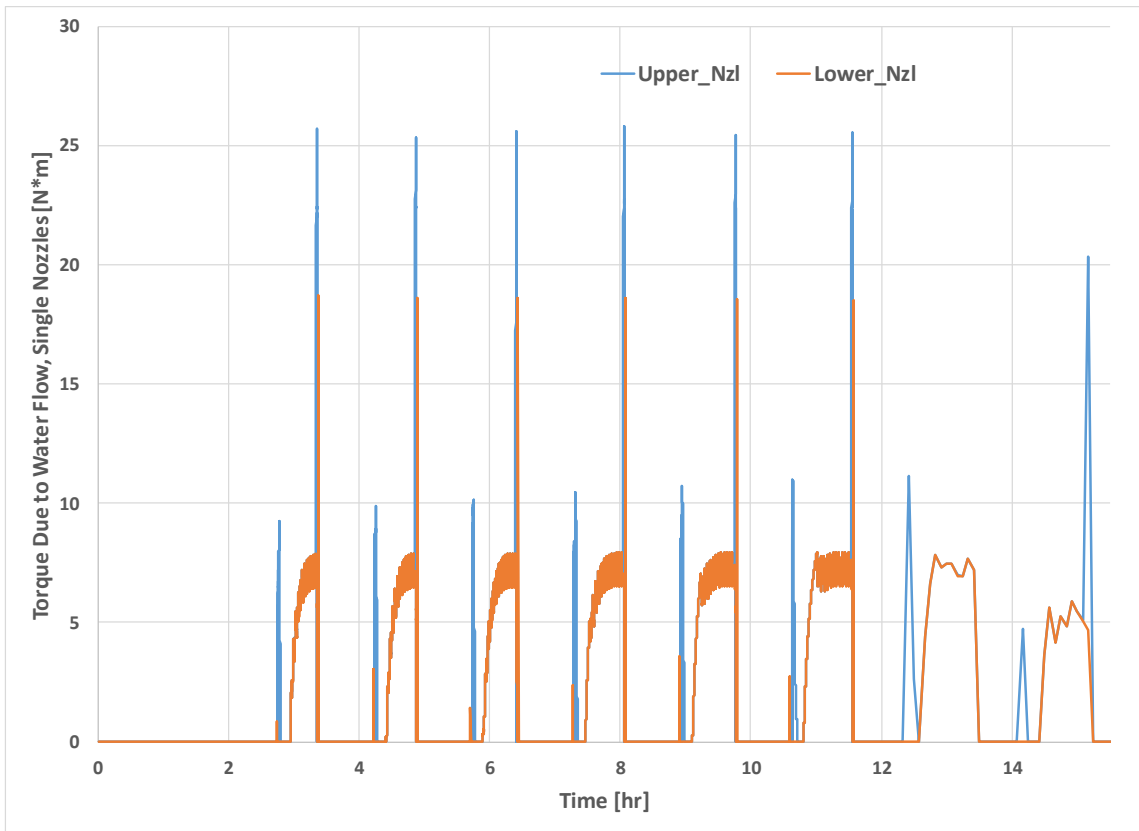


Figure 7.58 Calculated turbine torque due to water flow [N*m]

The first hour plays out as described in previous sections and the turbine does not over-speed upon loss of governor valve control. The RPV water level is at its lowest elevation at approximately 1 hr of problem time and the wide-open governor admits such a high steam flow rate to the turbine so as to drive the pump flow well above its rated value (see Figure 7.55). This quickly fills the RPV back up and by about 3 hr problem time, water enters the MSL and passes all the way through to the turbine rotor. The phasic velocity plot (Figure 7.52) shows that transitioning from the steam expansion model to the two-phase critical flow model (for void fractions below 0.9) drastically drops steam/water velocity. Note that the atmosphere phase velocity (in the absence of pool) is typical of

experimentally-observed, supersonic steam flow through converging-diverging nozzles where speeds between above Mach 1 and approaching Mach 2 are not unusual. Figure 7.56 through Figure 7.58 show the consequences for rotor torque (in total and by phase). When water displaces steam, rotor torque is smaller and is only nonzero when the water phase velocity (according to the two-phase critical flow model) exceeds the local rotor bucket velocity. This explains why the rotor slows down so much while water is flowing through nozzles. The rotor must slow down so that the comparatively lower-velocity water jets can “catch up” to the rotor that was previously driven by higher-velocity steam jets.

Apparently, the rotor speed recovery ramp-ups (when water clears and steam returns to the nozzles) do not lead to turbine over-speed until after CST-to-wetwell RCIC pump suction switch-over occurs at/after 14 hr problem time. This is partially due to the change in RCIC pump suction CV water conditions (lower density, higher temperature nearly approaching saturation). Temperature effects are shown in Figure 7.59 and clearly indicate that the CST-to-wetwell switch-over brings in water at essentially saturated conditions. Accordingly, the water entering the RCIC pump decreases in density by about 50 kg/m^3 . Recalling the definition of pump hydraulic torque (which characterizes the force exerted by pumped fluid on the impeller and “felt” as resistance by the rotor), it generally decreases when the ratio of actual-to-rated water density decreases. Lower hydraulic torque directly leads to higher turbine speed when all other variables are constant. Other effects related to the pump performance model are likely in play as well.

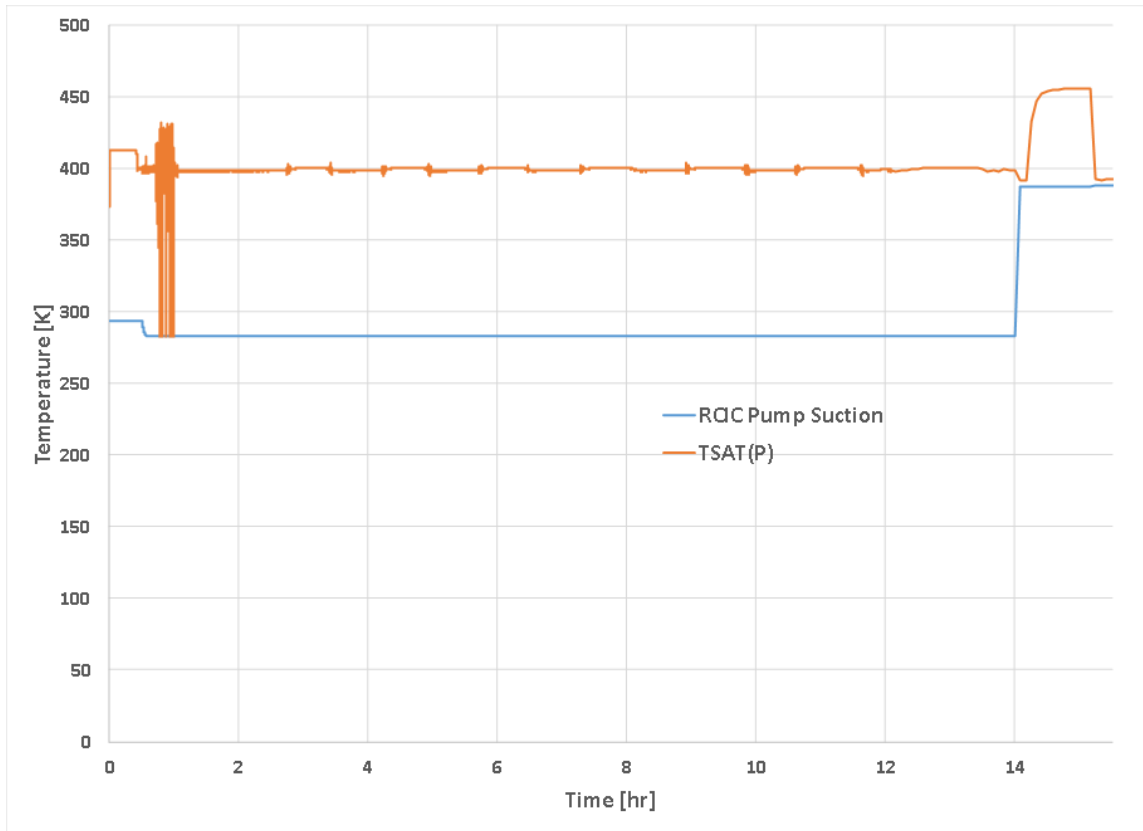


Figure 7.59 Calculated RCIC pump suction water temperature [K]

7.2.3.5 Discussion

New models predict the RCIC turbo-pump is capable of self-regulation under station blackout conditions. This stands in contrast to the results generated with the most recent CF-turbine pseudo-Fukushima test case variant. New turbo-pump models predict that the increased steam load through the wide-open governor does not drive the rotor to mechanical over-speed in the short term. Periodic patterns of rotor coast-down and ramp-up due to intermittent MSL flooding likewise do not lead to over-speed in the short term. In the intermediate term, more specifically at about 14 hr problem time, RCIC pump suction source switch-over occurs (from the CST to the wetwell), and the new models

predict turbine over-speed. The peak rotor speed is only slightly in excess of the mechanical over-speed set-point (5848 rpm relative to 5625 rpm, or about a 4% excess), so the MELCOR prediction of rotor over-speed upon CST-to-wetwell switchover is a close call that could conceivably change in light of input parameter values, dependencies, uncertainties, etc.

There are several modeling decisions and input parameters that can drastically impact the turbo-pump response. Velocity-stage parameters aside, one example that comes to mind in light of the above results involves turbine and pump friction torque polynomial prescriptions. It stands to reason that total friction torque would increase as the pump impeller and/or the rotor spin faster. If reasonable estimates of torque increase could be made, such data could be applied and an investigation of any retarding effects on shaft speed ramp-up could be conducted. Since the turbine just barely over-speeds under assumption of a speed-independent friction torque of 2.0 N*m (1.0 N*m for the turbine and 1.0 N*m for the pump), even a modest increase in total friction torque may be sufficient to pull shaft speed back below the mechanical over-speed set-point. The new models expand the toolbox for MELCOR users that they may explore the RCIC system response in greater depth and attempt to answer such questions.

8 CONCLUSIONS AND RECOMMENDATIONS

A condensing steam flow physics model was developed and successfully applied on a typical GS-1 Terry turbine pressure stage (steam nozzle) geometry with STAR-CCM+, a commercial computational fluid dynamics code. The physics model was at least indirectly and partially validated by a benchmark to available steam nozzle experimental data. Simpler ideal gas air simulations were used on a symmetric wedge of the full three-dimensional GS-1 Terry turbine (pressure and velocity stage) to ascertain certain performance characteristics (primarily pertaining to the velocity stage). These parameters were useful to the systems-level models developed for RCIC system analysis in MELCOR.

A homologous pump model, a Terry turbine rotor (compound velocity stage) model, a steam nozzle expansion (pressure stage) model, and a turbo-shaft model were conceptually developed, coded, and integrated into an up-to-date version of MELCOR. This includes all the requisite source code for mathematical models, user input acquisition, and post-processing. The new models were demonstrated with simple test problems typically used for purposes of introducing code features to the user community. Additionally, a pseudo-Fukushima RCIC system test problem was run. The results were compared to those most recently generated with a simpler CF-specified turbine model. The most important outcomes observed from that comparison were that, with new models, MELCOR:

- predicts that the RCIC system turbo-pump can survive loss of governor control and can continue to deliver make-up coolant inventory to the RPV

- predicts that the RCIC turbo-pump can ride out the periodic flow patterns associated with RPV re-fill and over-fill without over-speed upon resumption of steam flow
- predicts the possibility of over-speed when the governor is full-open (high steam load on the rotor) and the pumped fluid is close to saturation

The new models represent an expanded set of capabilities for MELCOR with which users may analyze the dynamics of RCIC system operation in normal and off-normal conditions. Even in the few preliminary calculations expounded in this dissertation, some evidence was found of RCIC system capability beyond what is typically credited and what is typically factored into plant operating procedures and/or severe accident management guidelines. In the near future, coding efforts could focus on one or all of several issues (listed below in no particular order of importance):

1. improving the robustness of the steam expansion model when the analytical Wilson point method is active, and
2. adding a capability to evolve “fog” across a steam nozzle flow path, and
3. accounting for effects of water pooling inside the turbine casing (presumably increasing the torque required to maintain shaft speed)
4. accounting for cavitation effects on the pump side
5. expanding/generalizing the turbine side of the model so as to extend it to other classes of turbomachine (e.g. reaction-type turbines)
6. Adding miscellaneous user-requested capabilities

As to the first point, the existing analytical Wilson point solution methodology is in line with that proposed by the literature [51]. While the methods were shown to work for a simple two-CV proof-of-concept problem, they may not be the best option for use in MELCOR because boundary conditions on the nozzle can rapidly change, leading to certain difficulties in resolving Wilson point conditions. The second point could have implications for aerosol and radioactivity transport within nuclear systems, particularly BWRs for which the primary and secondary loops are not separated. The third point is presently a pressing question that can hopefully be answered with forthcoming full-scale or smaller-scale experiments. If – under off-normal conditions - water tends to pool up in the casing so as to drag down the turbine rotor, the impact on net shaft torque could make the difference between over-speed (loss of the RCIC system) and continued operation. For the fourth point, cavitation effects on pump hydraulic torque could influence turbo-pump performance, particularly after RCIC pump suction switch-over from the CST. As to the fifth point, the modeling framework established by these new models could be generalized to accommodate phenomenological, mechanistic models for other types of turbines (e.g. typical reaction-type machines used on the power-production side of nuclear systems). Moving forward, modeling efforts should focus on applying the new models in increasingly more complicated, true-to-life simulations of nuclear systems be they BWRs or PWRs. Code bugs can be addressed as necessary and improvements can be made subject to user feedback. Additionally, an in-depth exploration of uncertainty and sensitivity (primarily for the CMFD results but also for MELCOR) could be a worth-while undertaking.

REFERENCES

- [1] K. Ross, J. Cardoni, C. Wilson, C. Morrow, D. Osborn and R. Gauntt, "Modeling of the Reactor Core Isolation Cooling Response to Beyond Design Basis Operations," Sandia National Laboratories, Albuquerque, 2015.
- [2] ANS Special Committee on Fukushima, Fukushima Daiichi: ANS Committee Report, La Grange Park: American Nuclear Society, 2012.
- [3] R. Gauntt, D. Kalinich, J. Cardoni, J. Phillips, A. Goldmann, S. Pickering, M. Francis, K. Robb, L. Ott, D. Wang, C. Smith, S. St. Germain, D. Schweider and C. Phelan, "Fukushima Daiichi Accident Study (Status as of April 2012)," Sandia National Laboratories, Albuquerque, 2012.
- [4] General Electric, "General Electric Systems Technology Manual, Chapter 2.7, Reactor Core Isolation Cooling System." 2012.
- [5] General Electric, "General Electric Systems Technology Manual, Chapter 6, BWR Differences" 2017.
- [6] J. A. Moyer, "Steam Turbines: A Practical and Theoretical Treatise for Engineers and Students," John Wiley & Sons, New York, 1917.
- [7] W. Leland, "Steam Turbines," American School of Correspondence, Chicago, 1910.
- [8] W. Goudie, "Steam Turbines: A Textbook for Engineering Students," Longmans, Green, and Co, London, 1917.

- [9] R. Gauntt, "RCIC Operation in Fukushima Accidents as Modeled by MELCOR and Proposed Testing," BWR Owners' Group Meeting, Key West, 2014.
- [10] S. Mizokami, "The Accident Analysis for Unit 2 at Fukushima Daiichi Nuclear Power Station," NUTHOS 9, Kaohsiung, Taiwan, 2013.
- [11] CD ADAPCO, "STAR-CCM+ User Guide," 2016.
- [12] CD ADAPCO, "STAR-CCM+ Theory Guide," CD ADAPCO, 2016.
- [13] "Revised Release on the IAPWS Industrial Formulation 1997 for the Thermodynamic Properties of Water and Steam," International Association for the Properties of Water and Steam, 2007.
- [14] MELCOR Workshop Presentation, "In Proceedings From the MELCOR Workshop," U.S. Nuclear Regulatory Commission, Bethesda, 2009.
- [15] "MELCOR Computer Code Manuals Vol 1: Primer and Users' Guide, Version 2.1. NUREG/CR-6119," Sandia National Laboratories. 2016.
- [16] "MELCOR Computer Code Manuals, Vol 2: Reference Manual, Version 2.1, NUREG/CR-6119," Sandia National Laboratories. 2016.
- [17] R. Mohsin, Z. Abdul Majid, Z. Yacob and S. Ashraf, "Water Condensation in Low Pressure Steam Turbine: A Nucleation Theory - Part I," *Journal of Chemical and Natural Resources Engineering*, vol. 2, no. 5, pp. 40-49, 2008.
- [18] J. McDonald, "Homogeneous Nucleation of Vapor Condensation I: Therodynamic Aspects," Institute of Atmospheric Physics, University of Arizona, Tucson, 1962.

- [19] J. McDonald, "Homogeneous Nucleation of Vapor Condensation II: Kinetic Aspects," Institute of Atmospheric Physics, University of Arizona, Tucson, 1962.
- [20] F. Bakhtar, J. B. Young, A. J. White and D. A. Simpson, "Classical Nucleation Theory and its Application to Condensing Steam Flow Calculations," *Proceedings of the Institution of Mechanical Engineers, Part C: Journal of Mechanical Engineering Science*, vol. 219, pp. 1315-1333, 2005.
- [21] W. G. Courtney, "Remarks on Homogeneous Nucleation," *J Chem Phys*, vol. 35, pp. 2249-2250, 1961.
- [22] A. Kantrowitz, "Nucleation in Very Rapid Vapor Expansion," *J Chem Phys*, vol. 19, pp. 1097-1100, 1951.
- [23] M. J. Moore and C. H. Sieverding, *Two-Phase Steam Flow in Turbines and Separators*, Washington: Hemisphere Publishing Company, 1976.
- [24] P. G. Hill, "Condensation of Water Vapor During Supersonic Expansion in Nozzles," *J Fluid Mech*, vol. 25, no. 3, pp. 593-620, 1966.
- [25] J. B. Young, "The Spontaneous Condensation of Steam in Supersonic Nozzles," *PhysicoChem Hydrodyn*, vol. 3, pp. 57-82, 1982.
- [26] L. Zori and F. Keleczy, "Wet Steam Flow Modeling in a General CFD Flow Solver," in *35th AIAA Fluid Dynamics Conference and Exhibit*, Toronto, 2005.
- [27] M. Giordano and P. Cinnella, "Numerical Method for Wet Steam Flows with Polydispersed Droplet Spectra," American Institute of Aeronautics and Astronautics, Lecce, Italy, 2008.

- [28] Y. Cengel and M. Boles, *Thermodynamics: An Engineering Approach*, 6th edition, New York: McGraw-Hill, 2008.
- [29] M. Z. Y. Hasril Hasini and A. M. Norhazwani, "Numerical Modeling of Wet Steam Flow in Steam Turbine Channel," Centre for Advanced Computational Engineering, Malaysia, 2012.
- [30] A. J. White and J. B. Young, "Time-Marching Method for the Prediction of Two-Dimensional, Unsteady Flows of Condensing Steam," *Journal of Propulsion and Power*, vol. 9, no. 4, pp. 579-587, 1993.
- [31] F. Bakhtar and M. Piran, "Thermodynamic Properties of Supercooled Steam," *Int J Heat & Fluid Flow*, vol. 1, no. 2, pp. 53-62, 1979.
- [32] "Release on the IAPWS Formulation 2011 for the Thermal Conductivity of Ordinary Water Substance," International Association for the Properties of Water and Steam, Plzen, Czech Republic, 2011.
- [33] "Release on the IAPWS Formulation 2008 for the Viscosity of Ordinary Water Substance," International Association for the Properties of Water and Steam, Berlin, Germany, 2008.
- [34] "Revised Release on Surface Tension of Ordinary Water Substance," International Association for the Properties of Water and Steam, 2014.
- [35] M. Mikofski, "MathWorks," 18 March 2012. [Online]. Available: <https://www.mathworks.com/matlabcentral/fileexchange/35710-iapws-if97->

- functional-form-with-no-slip?requestedDomain=www.mathworks.com. [Accessed 10 January 2017].
- [36] A. R. Avetissian, G. A. Philippov and L. I. Zaichik, "Effects of Turbulence and Inlet Moisture on Two-Phase Spontaneously Condensing Flows in Transonic Nozzles," *International Journal of Heat and Mass Transfer*, vol. 51, pp. 4195-4203, 2008.
- [37] Q.-F. Ma, D.-P. Hu, J.-Z. Jiang and Z.-H. Qiu, "A Turbulent Eulerian Multi-Fluid Model for Homogeneous Nucleation of Water Vapour in Transonic Flow," *International Journal of Computational Fluid Dynamics*, vol. 23, no. 3, pp. 221-231, 2009.
- [38] H. Tennekes and J. L. Lumley, *A First Course in Turbulence*, Cambridge: MIT Press, 1972.
- [39] D. Wilcox, *Turbulence Modeling for CFD*, La Canada: DCW Industries, Inc, 1994.
- [40] P. Bradshaw, *An Introduction to Turbulence and Its Measurement*, New York: Pergamon Press, 1971.
- [41] C. Crowe, J. Schwarzkopf, M. Sommerfeld and Y. Tsuji, *Multiphase Flows with Droplets and Particles*, 2nd Edition, Boca Raton: CRC Press, 2012.
- [42] B. L. Sawford, "Reynolds Number Effects in Lagrangian Stochastic Models of Turbulent Dispersion," *Phys Fluids*, vol. 3, no. 6, pp. 1577-1586, 1991.
- [43] Idaho National Laboratories, "RELAP5-3D Code Manual Volume II: User's Guide and Input Requirements," INEEL-EXT-98-00834 rev 2.4 p 2-44 - 2-57, 2005.

- [44] Olson, "Single and Two-Phase Performance Characteristics of the Mod-1 Semiscale Pump Under Steady State and Transient Fluid Conditions," ANCR-1165, 1974.
- [45] Reeder, "Loft System and Test Description," NUREG/CR-0247, 1978.
- [46] Lahssuny and Jedral, "Universal Correlations for Predicting Complete Pump Performance Characteristics," 2004.
- [47] Narabayashi, "Centrifugal Pump Behavior in Steady and Transient Two-Phase Flow," *Journal of Nuclear Science and Technology*, vol. 23, no. 2, pp. 136-150, 1986.
- [48] M. Kazimi and N. Todreas, *Nuclear Systems II: Elements of Thermal Hydraulic Design*, Taylor and Francis, 2001.
- [49] Press, Teukolsky, Vetterling and Flannery, *Numerical Recipes in FORTRAN 77: The Art of Scientific Computing 2nd Edition*, Cambridge University Press, 1986.
- [50] I. H. Shames, *Mechanics of Fluids*, New York : McGraw Hill Inc, 1982.
- [51] R. A. Dobbins, "A Theory of the Wilson Line for Steam at Low Pressures," *Transactions of the ASME Vol 105*, pp. 414-422, December 1983.
- [52] Ding, Wang and Zhao, "An Analytical Method for Wilson Point in Nozzle Flow with Homogeneous Nucleating," *International Journal of Heat and Mass Transfer*, vol. 73, pp. 586-594, 2013.
- [53] G. Wallis, *One-Dimensional Two-Phase Flow*, New York : McGraw-Hill Inc, 1969.

- [54] Z. Z. O. Zhao, "Development and Implementation of Mechanistic Terry Turbine Models in RELAP-7 to Simulate RCIC Normal Operating Conditions," Idaho National Laboratories, Idaho Falls, 2016.
- [55] G. Gyarmathy, "Nucleation of Steam in High Pressure Nozzle Experiments," *Proc. IMechE*, vol. 219, no. A, pp. 511-521, 2005.
- [56] N. G. Luthman Jr., "Evaluation of Impulse Turbine Performance Under Wet Steam Conditions," Masters Thesis. Texas A&M University, College Station, 2017.
- [57] J. D. Hoffman, *Numerical Methods for Engineers and Scientists 2nd Edition*, New York: CRC Press, 2001.

APPENDIX A: HOMOLOGOUS PUMP MODEL CURVES AND DATA

Homologous Pump Curves and Data: Semiscale

This section contains curves and data for the Semiscale pump (built in to MELCOR). Data was extracted from reports or manuals and often required the use of plot digitizer software.

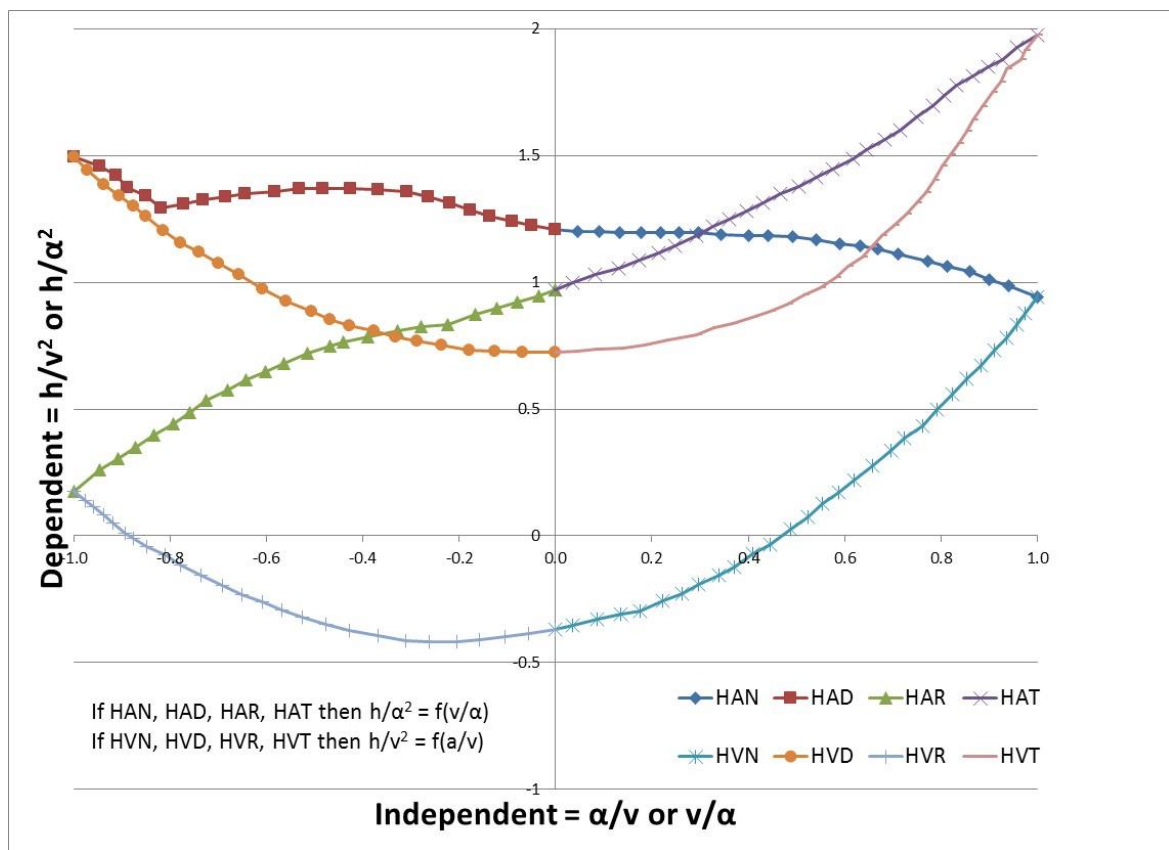


Figure A.1 Semiscale single-phase head homologous curves

Table A.1 Semiscale single-phase head homologous data (v/a octants)

HAN 1		HAD 3		HAR 7		HAT 5	
v/a	h/a ²						
0.00E+00	1.209075	0.00E+00	1.209075	0	0.969552	0	0.969552
0.045351	1.20136	-0.0496	1.22679	-0.03403	0.947262	0.036387	0.996812
0.090805	1.20114	-0.09087	1.24196	-0.07957	0.922539	0.08196	1.03152
0.13211	1.19594	-0.13626	1.26215	-0.12098	0.897794	0.131632	1.05622
0.177563	1.19571	-0.1775	1.28731	-0.16652	0.873071	0.173056	1.08595
0.218885	1.19551	-0.21873	1.31246	-0.2245	0.833439	0.21448	1.11569
0.256074	1.19532	-0.2641	1.33764	-0.27826	0.823727	0.247639	1.14546
0.297396	1.19512	-0.30949	1.35783	-0.32789	0.809004	0.29323	1.18516
0.342833	1.1899	-0.3673	1.3681	-0.38996	0.784363	0.326407	1.21992
0.400666	1.18462	-0.42515	1.36839	-0.43961	0.764651	0.359566	1.2497
0.441988	1.18441	-0.483	1.36867	-0.46859	0.749825	0.396858	1.27945
0.491556	1.17918	-0.53259	1.36892	-0.51415	0.720111	0.430035	1.31422
0.541108	1.16895	-0.58221	1.35919	-0.56387	0.680438	0.467344	1.34896
0.590643	1.15373	-0.64422	1.34952	-0.60118	0.645693	0.504636	1.37872
0.63193	1.14354	-0.68558	1.33974	-0.6426	0.615959	0.541945	1.41346
0.669086	1.13338	-0.73109	1.325	-0.67993	0.576224	0.575122	1.44823
0.710339	1.11321	-0.77246	1.31024	-0.72552	0.536531	0.61658	1.48794
0.772219	1.08296	-0.81796	1.29549	-0.75875	0.486795	0.645625	1.52273
0.813472	1.0628	-0.85087	1.34057	-0.79196	0.442049	0.682951	1.56246
0.858858	1.04261	-0.88794	1.37569	-0.83343	0.397345	0.716144	1.60222
0.900077	1.01246	-0.91258	1.42072	-0.87079	0.34763	0.749372	1.65195
0.941313	0.987306	-0.9455	1.46081	-0.90814	0.302905	0.782583	1.6967
1	0.942097	-1	1.49596	-0.94548	0.25818	0.807513	1.7365
				-1	0.176112	0.832443	1.77629
						0.865636	1.81605
						0.898813	1.85081
						0.927841	1.88061
						0.95692	1.92538
						1	1.97509

Table A.2 Semiscale single-phase head homologous data (a/v octants)

HVN 2		HVD 4		HVR 8		HVT 6	
a/v	h/v ²						
0	-0.37025	0	0.722544	0	-0.370250	0	0.722544
0.035892	-0.35552	-0.06786	0.722874	-0.05512	-0.385002	0.043729	0.727308
0.085563	-0.33081	-0.12569	0.728153	-0.10476	-0.399725	0.085085	0.737082
0.135217	-0.3111	-0.17939	0.733411	-0.15851	-0.409437	0.13882	0.741804
0.17659	-0.29634	-0.23717	0.75366	-0.204	-0.419190	0.184308	0.751557
0.22218	-0.25664	-0.28671	0.768878	-0.26185	-0.418901	0.233962	0.77127
0.263605	-0.22691	-0.33211	0.784075	-0.31142	-0.413664	0.291881	0.790941
0.296781	-0.19214	-0.37748	0.809252	-0.3692	-0.393415	0.329173	0.820696
0.338222	-0.15742	-0.427	0.829459	-0.42698	-0.373166	0.366413	0.835481
0.371399	-0.12265	-0.46823	0.854616	-0.47648	-0.347968	0.40782	0.860225
0.40876	-0.07294	-0.50532	0.884742	-0.52598	-0.322770	0.445095	0.884989
0.446086	-0.0332	-0.5589	0.924931	-0.5672	-0.292624	0.482387	0.914744
0.487612	0.026472	-0.60832	0.975079	-0.60842	-0.262477	0.515564	0.94951
0.524972	0.076187	-0.65771	1.03022	-0.64964	-0.232331	0.548724	0.979285
0.554068	0.125943	-0.69888	1.07533	-0.69084	-0.197194	0.581918	1.01904
0.587279	0.170689	-0.74005	1.12045	-0.73616	-0.157047	0.606864	1.06383
0.620507	0.220425	-0.77712	1.15557	-0.77734	-0.116920	0.635909	1.09861
0.657884	0.27513	-0.81414	1.20565	-0.81026	-0.076835	0.656706	1.13843
0.695279	0.334825	-0.85114	1.26073	-0.84733	-0.041719	0.677521	1.18324
0.724375	0.384581	-0.8758	1.30077	-0.87616	-0.011634	0.70245	1.22304
0.761735	0.434296	-0.90459	1.34084	-0.89262	0.008409	0.727397	1.26782
0.790882	0.499023	-0.93749	1.38591	-0.91727	0.048453	0.748211	1.31263
0.824144	0.558738	-0.97036	1.44097	-0.93781	0.083487	0.769009	1.35245
0.853274	0.618475	-1	1.49596	-0.95837	0.113530	0.785708	1.40226
0.882387	0.673221			-0.97481	0.138563	0.802425	1.45707
0.911517	0.732957			-1	0.176112	0.819107	1.5019
0.936481	0.782734					0.835789	1.54673
0.957312	0.832532					0.852489	1.59655
0.973995	0.87736					0.865039	1.6414
1	0.942097					0.88587	1.69119
						0.906736	1.75097
						0.923401	1.79081
						0.935969	1.84065
						0.96503	1.88042
						0.973414	1.91531
						1	1.97509

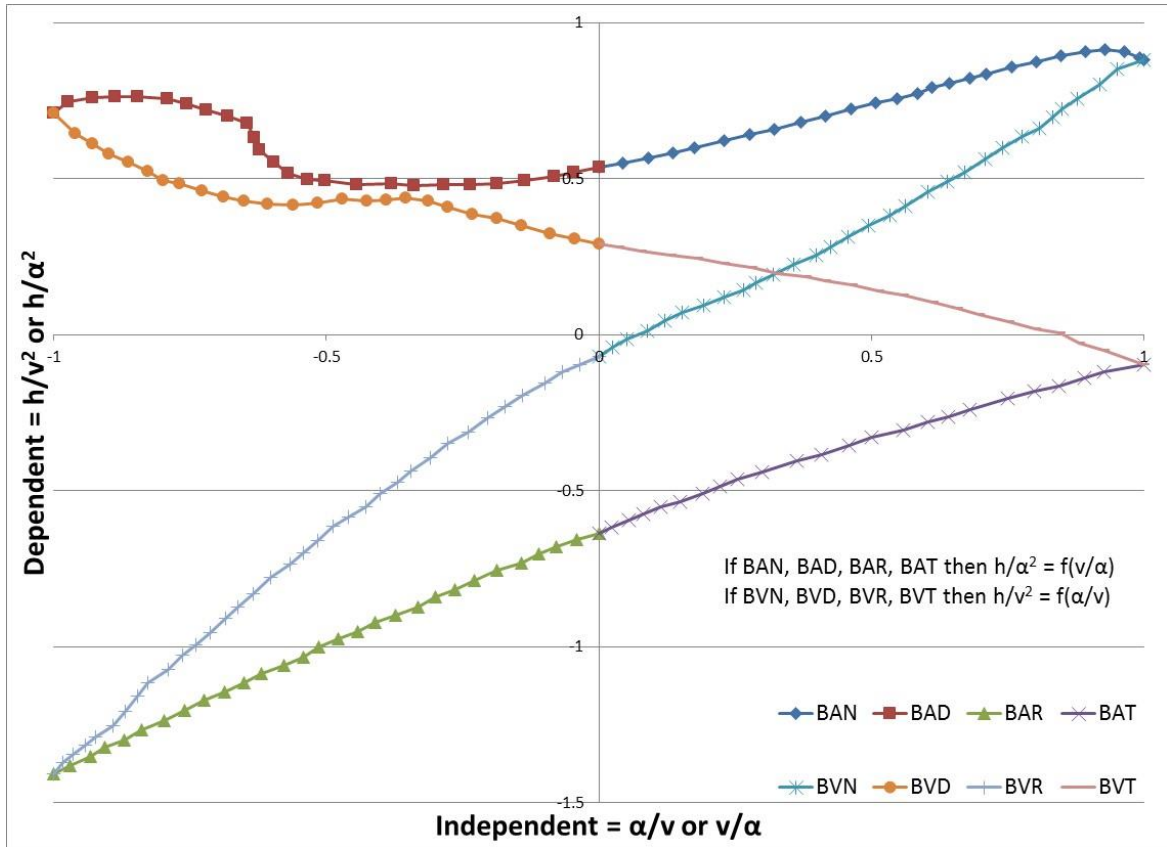


Figure A.2 Semiscale single-phase torque homologous curves

Table A.3 Semiscale single-phase torque homologous data (v/a octants)

BAN 1		BAD 3		BAR 7		BAT 5	
v/a	b/a ²						
0	0.53922	0	0.53922	0	-0.63777	0	-0.63777
0.04456	0.55239	-0.04608	0.521488	-0.04117	-0.65563	0.022489	-0.61529
0.089854	0.56556	-0.08234	0.508215	-0.07753	-0.67802	0.054342	-0.59285
0.135199	0.583292	-0.13667	0.495148	-0.10939	-0.70047	0.081631	-0.57491
0.176029	0.601075	-0.18642	0.486591	-0.14134	-0.73204	0.113484	-0.55246
0.230453	0.623266	-0.23613	0.482596	-0.18674	-0.75434	0.149801	-0.53463
0.275798	0.640998	-0.28578	0.483162	-0.22772	-0.78581	0.190733	-0.50772
0.321143	0.65873	-0.34	0.479218	-0.26419	-0.81733	0.222587	-0.48527
0.371053	0.680972	-0.38058	0.484243	-0.30056	-0.83972	0.25444	-0.46282
0.416448	0.703265	-0.44383	0.480402	-0.33252	-0.87129	0.299836	-0.44053
0.461844	0.725559	-0.50236	0.494757	-0.37345	-0.8982	0.363441	-0.40476
0.507189	0.74329	-0.53391	0.499679	-0.40982	-0.9206	0.408837	-0.38246
0.547969	0.756512	-0.56982	0.518337	-0.44177	-0.95217	0.458797	-0.35566
0.584285	0.774347	-0.59649	0.55514	-0.47814	-0.97456	0.49973	-0.32875
0.611574	0.792284	-0.62317	0.591942	-0.51456	-1.00152	0.558668	-0.30661
0.643325	0.805609	-0.63174	0.6331	-0.542	-1.03314	0.604115	-0.27976
0.679642	0.823444	-0.64477	0.678871	-0.57842	-1.0601	0.640431	-0.26192
0.711393	0.836769	-0.68063	0.702091	-0.61935	-1.08701	0.681313	-0.23958
0.756789	0.859062	-0.72105	0.720801	-0.65125	-1.11402	0.749432	-0.20386
0.802134	0.876794	-0.75696	0.73946	-0.68772	-1.14554	0.799342	-0.18162
0.847479	0.894526	-0.79287	0.758118	-0.72414	-1.1725	0.844687	-0.16388
0.892772	0.907696	-0.84699	0.763298	-0.76061	-1.20402	0.890133	-0.13703
0.928987	0.916407	-0.88762	0.763761	-0.79708	-1.23554	0.92645	-0.11919
0.964998	0.906872	-0.92829	0.759663	-0.83806	-1.267	1	-0.0948
0.991879	0.888316	-0.97359	0.746493	-0.87002	-1.29858		
1	0.881449	-1	0.710232	-0.90639	-1.32097		
				-0.93383	-1.3526		
				-0.97025	-1.37955		
				-1	-1.4065		

Table A.4 Semiscale single-phase torque homologous data (a/v octants)

BVN 2		BVD 4		BVR 8		BVT 6	
a/v	b/v ²						
0	-0.06979	0	0.290609	0	-0.06979	0	0.290609
0.024395	-0.04047	-0.04396	0.307038	-0.0349	-0.09454	0.03704	0.283303
0.051785	-0.01341	-0.0889	0.3258	-0.06675	-0.11699	0.077514	0.269155
0.088203	0.013547	-0.14281	0.349226	-0.09876	-0.15312	0.13153	0.254852
0.120159	0.045118	-0.1877	0.372549	-0.13985	-0.19372	0.181084	0.245162
0.152063	0.072128	-0.23269	0.386749	-0.17185	-0.22985	0.230586	0.230911
0.192945	0.094473	-0.27757	0.410072	-0.20386	-0.26598	0.280088	0.21666
0.229363	0.121431	-0.31348	0.428731	-0.24048	-0.31119	0.329539	0.197847
0.265731	0.143827	-0.35401	0.438318	-0.277	-0.34727	0.379092	0.188157
0.288556	0.166378	-0.39017	0.434168	-0.30911	-0.39252	0.415052	0.17406
0.32046	0.193388	-0.42633	0.430018	-0.34573	-0.43773	0.464555	0.159809
0.35693	0.224908	-0.47142	0.435095	-0.36871	-0.47397	0.514006	0.140996
0.397913	0.256376	-0.51672	0.421924	-0.40072	-0.5101	0.558994	0.126796
0.425303	0.283437	-0.56191	0.417878	-0.42826	-0.55084	0.612908	0.10337
0.457259	0.315008	-0.60705	0.418392	-0.46021	-0.58242	0.657846	0.084608
0.493779	0.35109	-0.65209	0.428031	-0.48766	-0.61404	0.698269	0.065898
0.534763	0.382558	-0.68805	0.442128	-0.51525	-0.65935	0.752183	0.042472
0.562204	0.414181	-0.72847	0.460838	-0.54279	-0.70009	0.801584	0.019097
0.60334	0.459334	-0.76884	0.484109	-0.56577	-0.73633	0.846572	0.004897
0.63981	0.490854	-0.80034	0.493593	-0.60234	-0.77697	0.882328	-0.02745
0.671765	0.522425	-0.82707	0.525834	-0.63455	-0.83135	0.927214	-0.05077
0.708336	0.563068	-0.86288	0.553616	-0.6621	-0.8721	1	-0.0948
0.740343	0.599201	-0.89868	0.581397	-0.68507	-0.90833		
0.776863	0.635283	-0.92992	0.61369	-0.71267	-0.95364		
0.808767	0.662292	-0.96117	0.645982	-0.74021	-0.99439		
0.831745	0.698528	-1	0.710232	-0.76314	-1.02606		
0.850107	0.725692			-0.79073	-1.07137		
0.877549	0.757315			-0.82735	-1.11657		
0.918685	0.802468			-0.84587	-1.15742		
0.950844	0.852286			-0.869	-1.20734		
1	0.881449			-0.89208	-1.2527		
				-0.92409	-1.28883		
				-0.94245	-1.316		
				-0.96532	-1.34311		
				-0.98369	-1.37028		
				-1	-1.4065		

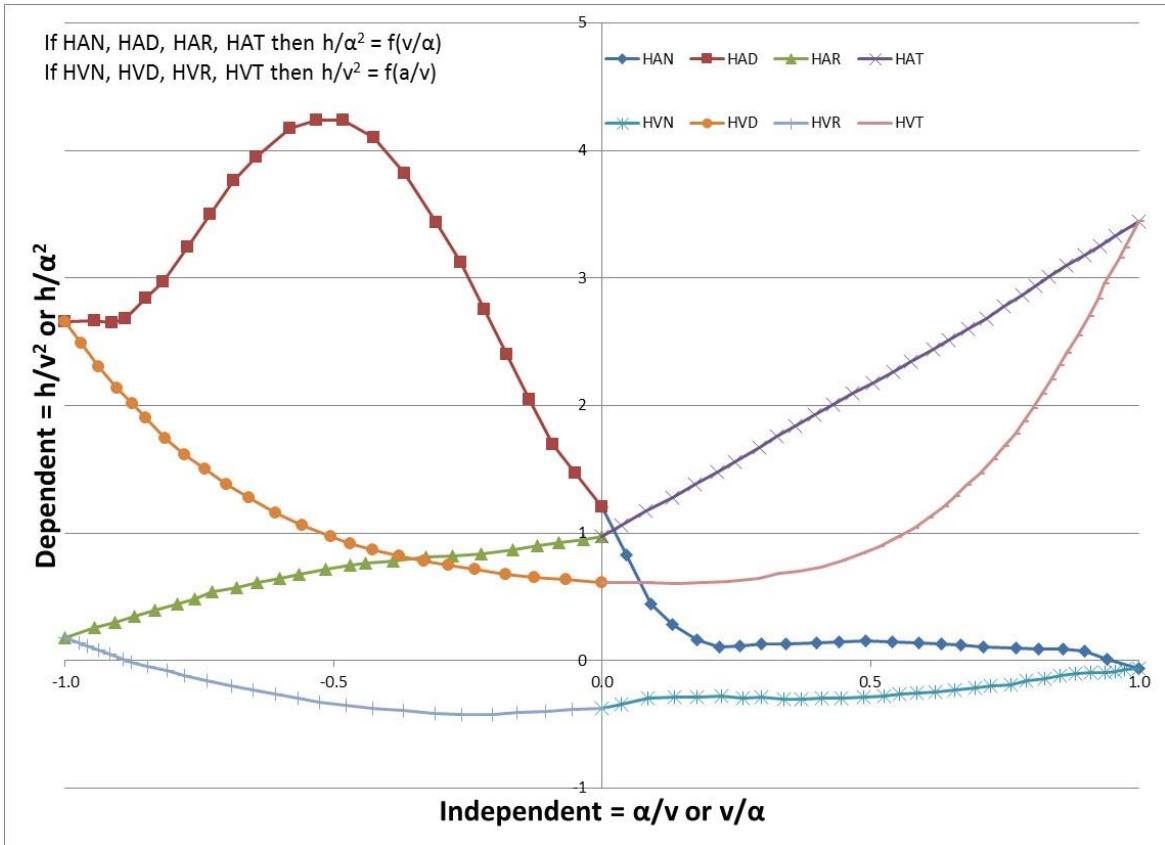


Figure A.3 Semiscale two-phase head homologous curves

Table A.5 Semiscale two-phase (fully-degraded) head homologous data (v/a octants)

HAN 1			HAD 3			HAR 7			HAT 5		
v/a	interp diff	h/a ²									
0.00E+00	0	1.209075	0.00E+00	0	1.209075	0	0	0.969552	0	0	0.969552
0.045351	0.376413	0.824947	-0.0496	-0.243	1.46979	-0.03403	0	0.947262	0.036387	-0.061858	1.05867
0.090805	0.753682	0.447458	-0.09087	-0.45435	1.69631	-0.07957	0	0.922539	0.08196	-0.139332	1.170852
0.13211	0.913486	0.282454	-0.13626	-0.787663	2.049813	-0.12098	0	0.897794	0.131632	-0.223774	1.279994
0.177563	1.03166	0.16405	-0.1775	-1.11483	2.40214	-0.16652	0	0.873071	0.173056	-0.294195	1.380145
0.218885	1.08559	0.10992	-0.21873	-1.44192	2.75438	-0.2245	0	0.833439	0.21448	-0.362444	1.478134
0.256074	1.07692	0.1184	-0.2641	-1.78212	3.11976	-0.27826	0	0.823727	0.247639	-0.41384	1.5593
0.297396	1.06727	0.12785	-0.30949	-2.07867	3.4365	-0.32789	0	0.809004	0.29323	-0.484507	1.669667
0.342833	1.05667	0.13323	-0.3673	-2.45636	3.82446	-0.38996	0	0.784363	0.326407	-0.535931	1.755851
0.400666	1.04318	0.14144	-0.42515	-2.73036	4.09875	-0.43961	0	0.764651	0.359566	-0.587327	1.837027
0.441988	1.03354	0.15087	-0.483	-2.8692	4.23787	-0.46859	0	0.749825	0.396858	-0.64513	1.92458
0.491556	1.02197	0.15721	-0.53259	-2.87089	4.23981	-0.51415	0	0.720111	0.430035	-0.692049	2.006269
0.541108	1.01794	0.15101	-0.58221	-2.81135	4.17054	-0.56387	0	0.680438	0.467344	-0.744282	2.093242
0.590643	1.01547	0.13826	-0.64422	-2.59985	3.94937	-0.60118	0	0.645693	0.504636	-0.79649	2.17521
0.63193	1.0134	0.13014	-0.68558	-2.42201	3.76175	-0.6426	0	0.615959	0.541945	-0.848723	2.262183
0.669086	1.01155	0.12183	-0.73109	-2.17657	3.50157	-0.67993	0	0.576224	0.575122	-0.895171	2.343401
0.710339	1.00638	0.10683	-0.77246	-1.93249	3.24273	-0.72552	0	0.536531	0.61658	-0.951554	2.439494
0.772219	0.984723	0.098237	-0.81796	-1.67481	2.9703	-0.75875	0	0.486795	0.645625	-0.989313	2.512043
0.813472	0.970285	0.092515	-0.85087	-1.50039	2.84096	-0.79196	0	0.442049	0.682951	-1.03784	2.6003
0.858858	0.9544	0.08821	-0.88794	-1.30392	2.67961	-0.83343	0	0.397345	0.716144	-1.08099	2.68321
0.900077	0.94	0.07246	-0.91258	-1.22994	2.65066	-0.87079	0	0.34763	0.749372	-1.12418	2.77613
0.941313	0.98	0.007306	-0.9455	-1.2036	2.66441	-0.90814	0	0.302905	0.782583	-1.16736	2.86406
1	1	-0.0579	-1	-1.16	2.65596	-0.94548	0	0.25818	0.807513	-1.20052	2.93702
						-1	0	0.176112	0.832443	-1.23542	3.01171
									0.865636	-1.28189	3.09794
									0.898813	-1.32834	3.17915
									0.927841	-1.36898	3.24959
									0.95692	-1.40969	3.33507
									1	-1.47	3.44509

Table A.5 Semiscale two-phase (fully-degraded) head homologous data (v/a octants)

HVN 2			HVD 4			HVR 8			HVT 6		
a/v	interp diff	h/v ²									
0	0	-0.37025	0	0.11	0.612544	0	0	-0.37025	0	0.11	0.612544
0.035892	-0.014357	-0.34116	-0.06786	0.089642	0.633232	-0.05512	0	-0.385	0.043729	0.118746	0.608562
0.085563	-0.034225	-0.29659	-0.12569	0.072293	0.65586	-0.10476	0	-0.39973	0.085085	0.127017	0.610065
0.135217	-0.025913	-0.28519	-0.17939	0.056183	0.677228	-0.15851	0	-0.40944	0.13882	0.135176	0.606628
0.17659	-0.009364	-0.28697	-0.23717	0.03761	0.71605	-0.204	0	-0.41919	0.184308	0.141241	0.610316
0.22218	0.02218	-0.27882	-0.28671	0.021097	0.747781	-0.26185	0	-0.4189	0.233962	0.147862	0.623408
0.263605	0.063605	-0.29051	-0.33211	0.005963	0.778112	-0.31142	0	-0.41366	0.291881	0.144416	0.646525
0.296781	0.096781	-0.28892	-0.37748	-0.014656	0.823908	-0.3692	0	-0.39342	0.329173	0.139444	0.681252
0.338222	0.142044	-0.29946	-0.427	-0.041067	0.870526	-0.42698	0	-0.37317	0.366413	0.134478	0.701003
0.371399	0.178539	-0.30119	-0.46823	-0.063056	0.917672	-0.47648	0	-0.34797	0.40782	0.125308	0.734917
0.40876	0.220074	-0.29301	-0.50532	-0.084788	0.96953	-0.52598	0	-0.32277	0.445095	0.102943	0.782046
0.446086	0.262999	-0.2962	-0.5589	-0.13301	1.057941	-0.5672	0	-0.29262	0.482387	0.080568	0.834176
0.487612	0.310754	-0.28428	-0.60832	-0.181648	1.156727	-0.60842	0	-0.26248	0.515564	0.05288	0.89663
0.524972	0.353718	-0.27753	-0.65771	-0.250794	1.281014	-0.64964	0	-0.23233	0.548724	0.016404	0.962881
0.554068	0.387178	-0.26124	-0.69888	-0.308432	1.383762	-0.69084	0	-0.19719	0.581918	-0.02011	1.03915
0.587279	0.425371	-0.25468	-0.74005	-0.386095	1.506545	-0.73616	0	-0.15705	0.606864	-0.053042	1.116872
0.620507	0.463583	-0.24316	-0.77712	-0.456528	1.612098	-0.77734	0	-0.11692	0.635909	-0.108227	1.206837
0.657884	0.506567	-0.23144	-0.81414	-0.539592	1.745242	-0.81026	0	-0.07683	0.656706	-0.147741	1.286171
0.695279	0.549571	-0.21475	-0.85114	-0.643192	1.903922	-0.84733	0	-0.04172	0.677521	-0.18729	1.37053
0.724375	0.583031	-0.19845	-0.8758	-0.71224	2.01301	-0.87616	0	-0.01163	0.70245	-0.23686	1.4599
0.761735	0.625995	-0.1917	-0.90459	-0.797442	2.138282	-0.89262	0	0.008409	0.727397	-0.306712	1.574532
0.790882	0.659514	-0.16049	-0.93749	-0.922462	2.308372	-0.91727	0	0.048453	0.748211	-0.364991	1.677621
0.824144	0.701387	-0.14265	-0.97036	-1.04737	2.48834	-0.93781	0	0.083487	0.769009	-0.423225	1.775675
0.853274	0.739256	-0.12078	-1	-1.16	2.65596	-0.95837	0	0.11353	0.785708	-0.469982	1.872242
0.882387	0.777103	-0.10388				-0.97481	0	0.138563	0.802425	-0.5197	1.97677
0.911517	0.823034	-0.09008				-1	0	0.176112	0.819107	-0.586428	2.088328
0.936481	0.872962	-0.09023							0.835789	-0.653156	2.199886
0.957312	0.914624	-0.08209							0.852489	-0.719956	2.316506
0.973995	0.94799	-0.07063							0.865039	-0.770156	2.411556
1	1	-0.0579							0.88587	-0.85348	2.54467
									0.906736	-0.947722	2.698692
									0.923401	-1.04105	2.83186
									0.935969	-1.11143	2.95208
									0.96503	-1.27417	3.15459
									0.973414	-1.32112	3.23643
									1	-1.47	3.44509

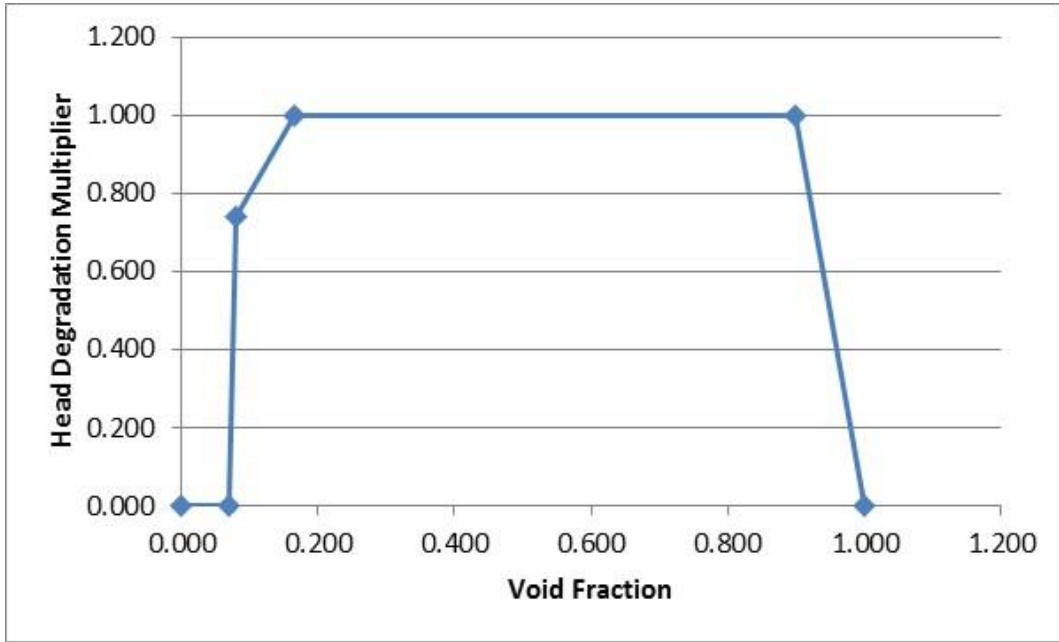


Figure A.4 Semiscale head degradation multiplier

Table A.6 Semiscale head degradation multiplier data

void	M_H
0.000	0.000
0.070	0.000
0.080	0.740
0.165	1.000
0.900	1.000
1.000	0.000

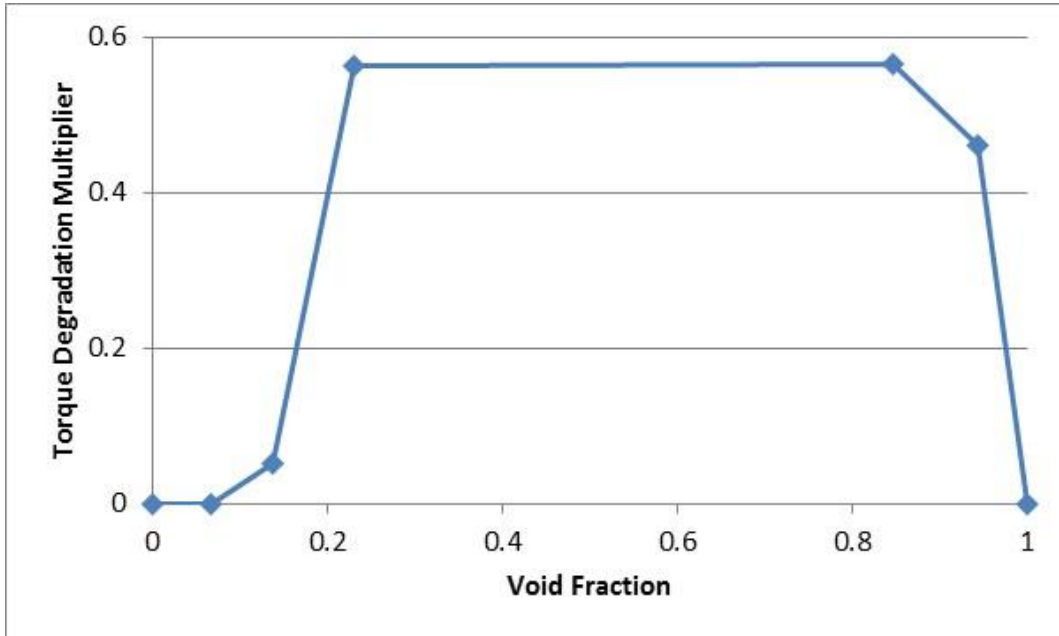


Figure A.5 Semiscale torque degradation multiplier

Table A.7 Semiscale head degradation multiplier data

void	M_T
0	0
0.067232	0
0.136755	0.052665
0.229824	0.563503
0.846779	0.563825
0.944549	0.460877
1	0.00E+00

Homologous Pump Curves and Data: Loft

This section contains curves and data for the Semiscale pump (built in to MELCOR). Data was extracted from reports or manuals and often required the use of plot digitizer software.

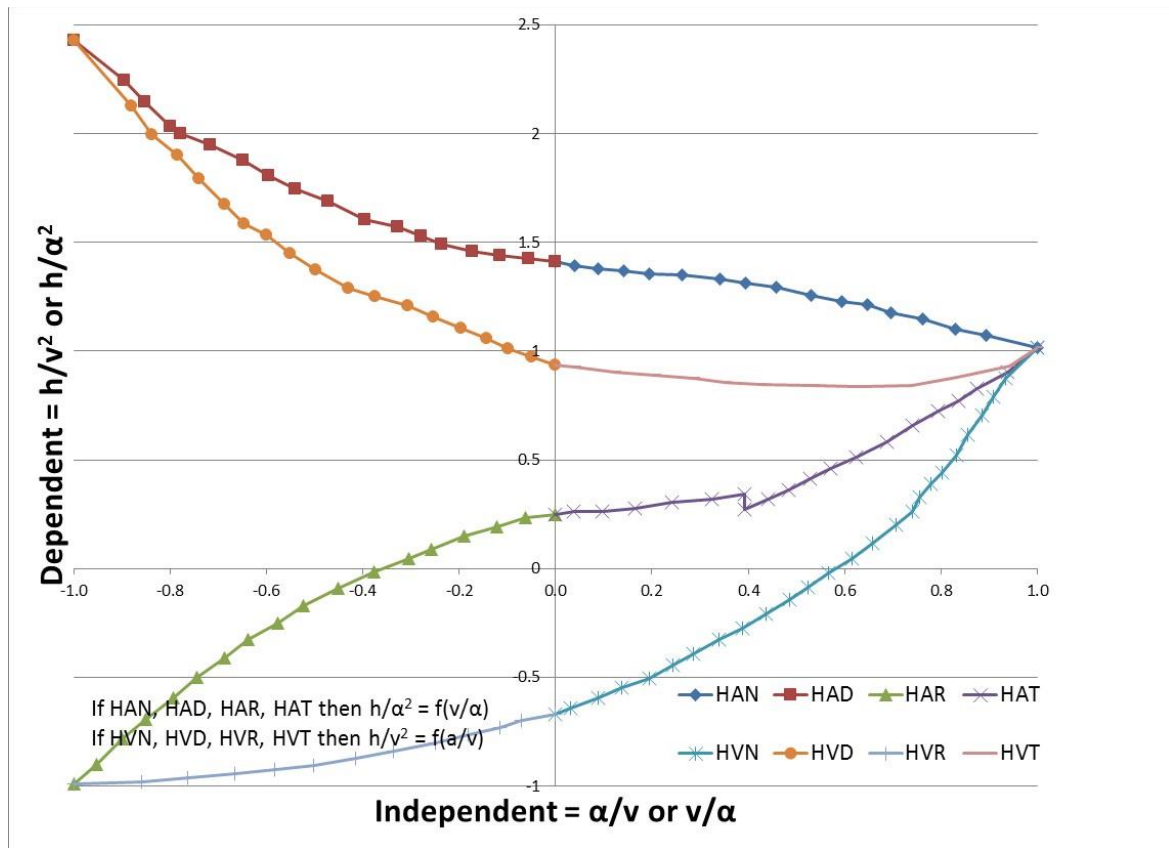


Figure A.6 Loft single-phase head homologous curves

Table A.8 Loft single-phase head homologous data (v/a octants)

HAN 1		HAD 3		HAR 7		HAT 5	
v/a	h/a ²						
0	1.4112	0	1.4112	0	0.250711	0	0.250711
0.040722	1.39274	-0.0562	1.42435	-0.06326	0.234656	0.038377	0.261481
0.089183	1.37694	-0.11435	1.44013	-0.12128	0.192013	0.096488	0.261635
0.142464	1.37177	-0.1725	1.46122	-0.18898	0.149345	0.164249	0.277748
0.195767	1.35598	-0.23553	1.49292	-0.25665	0.090743	0.241672	0.304509
0.263575	1.35085	-0.27919	1.52998	-0.30498	0.048126	0.323961	0.320661
0.341103	1.32981	-0.32771	1.57234	-0.37748	-0.0158	0.39171	0.342085
0.394407	1.31402	-0.39558	1.60403	-0.44995	-0.09035	0.391863	0.273042
0.457408	1.29294	-0.47325	1.6888	-0.52241	-0.17021	0.440183	0.32097
0.530128	1.25596	-0.54117	1.74704	-0.57551	-0.25001	0.483672	0.363574
0.593141	1.22957	-0.59457	1.80532	-0.6383	-0.32453	0.52715	0.411489
0.646444	1.21378	-0.648	1.87953	-0.68653	-0.40964	0.570628	0.459404
0.694952	1.17673	-0.71595	1.9484	-0.74445	-0.50008	0.623779	0.512656
0.762807	1.15035	-0.77902	2.00134	-0.79266	-0.59581	0.68658	0.581866
0.830709	1.10273	-0.79846	2.03316	-0.85056	-0.69156	0.739685	0.656362
0.893733	1.07103	-0.85198	2.14455	-0.89879	-0.78198	0.792801	0.725547
1	1.01552	-0.89579	2.24534	-0.9518	-0.89896	0.836278	0.773462
		-1	2.42834	-1	-0.99201	0.874902	0.826676
						0.937691	0.901197
						1	1.01816

Table A.9 Loft single-phase head homologous data (a/v octants)

HVN 2		HVD 4		HVR 8		HVT 6	
a/v	h/v ²						
0	-0.66811	0	0.935854	0	-0.66811	0	0.935854
0.030685	-0.64142	-0.05036	0.972929	-0.07088	-0.70011	0.041754	0.925374
0.088691	-0.59347	-0.09887	1.00998	-0.11439	-0.7321	0.124125	0.904348
0.137011	-0.54554	-0.14256	1.05766	-0.18212	-0.76414	0.206484	0.888634
0.195028	-0.5029	-0.19593	1.10532	-0.24983	-0.8015	0.288843	0.872919
0.243325	-0.44435	-0.25416	1.15827	-0.33692	-0.83891	0.351832	0.857153
0.286791	-0.39112	-0.30755	1.21124	-0.41433	-0.87098	0.429337	0.846737
0.339919	-0.32725	-0.37544	1.25355	-0.50143	-0.90308	0.535886	0.841709
0.388228	-0.27401	-0.42879	1.29059	-0.5837	-0.92454	0.627906	0.836642
0.436513	-0.21015	-0.49677	1.37538	-0.66599	-0.94069	0.739274	0.842249
0.484786	-0.14098	-0.5502	1.4496	-0.7628	-0.96219	0.831201	0.87967
0.52341	-0.08776	-0.59882	1.53445	-0.85961	-0.97838	0.942464	0.933077
0.566841	-0.0186	-0.64736	1.58743	-1	-0.99201	1	1.01816
0.615126	0.045259	-0.6863	1.67761				
0.658557	0.114418	-0.73983	1.79431				
0.706795	0.199523	-0.78364	1.90042				
0.740552	0.263346	-0.83712	1.99588				
0.754939	0.327117	-0.881	2.12854				
0.779012	0.390913	-1	2.42834				
0.803107	0.444088						
0.831987	0.523831						
0.856	0.614183						
0.884857	0.704548						
0.908882	0.789588						
0.932907	0.874629						
1	1.01552						

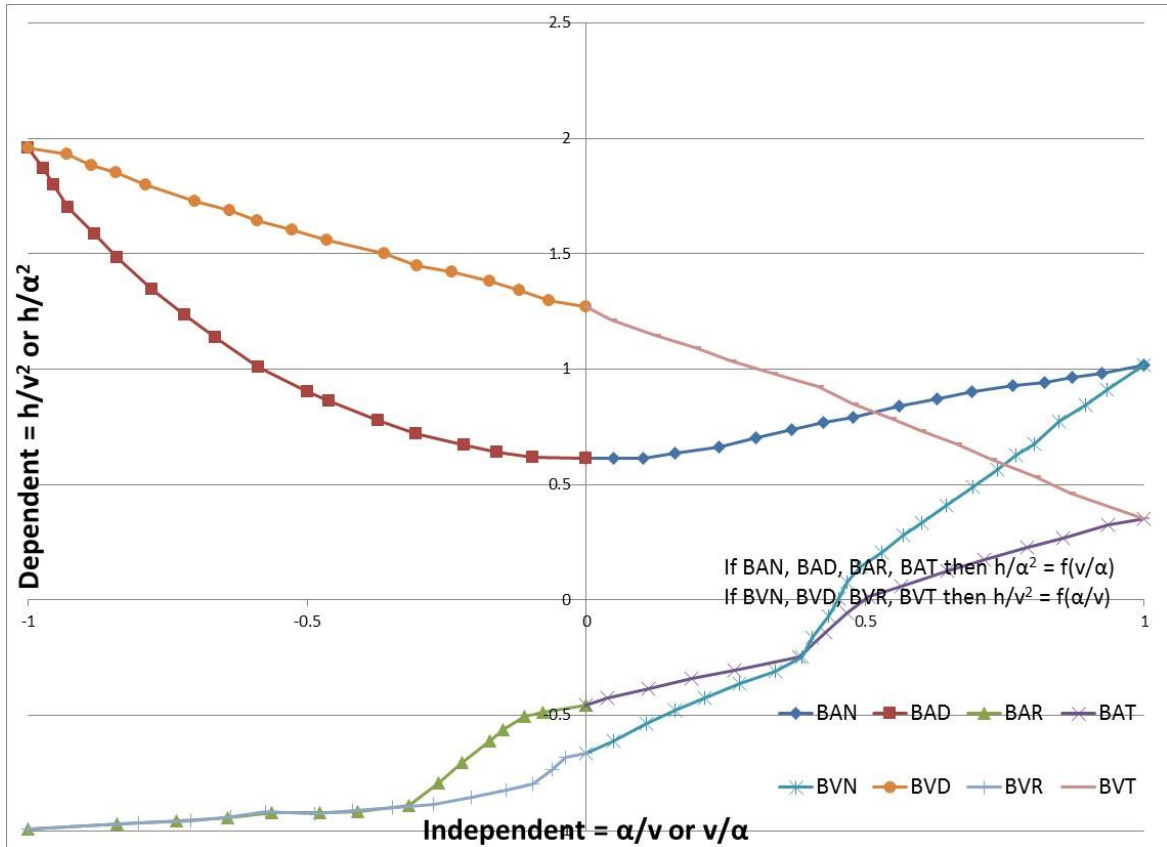


Figure A.7 Loft single-phase torque homologous curves

Table A.10 Loft single-phase torque homologous data (v/a octants)

BAN 1		BAD 3		BAR 7		BAT 5	
v/a	b/a ²						
0	0.61405	0	0.61405	0	-0.45672	0	-0.45672
0.04863	0.614428	-0.09667	0.618981	-0.07726	-0.48899	0.038676	-0.42445
0.101898	0.614712	-0.15972	0.639955	-0.11109	-0.50515	0.111149	-0.38677
0.159914	0.63633	-0.21797	0.671608	-0.14957	-0.56396	0.188418	-0.33841
0.237277	0.663379	-0.30534	0.719088	-0.17357	-0.61203	0.265757	-0.30604
0.304908	0.70103	-0.37339	0.777326	-0.2216	-0.70285	0.381719	-0.24682
0.367696	0.738656	-0.46094	0.862096	-0.26478	-0.79365	0.429675	-0.14002
0.425665	0.770928	-0.49986	0.904507	-0.31763	-0.88982	0.46804	-0.05458
0.478839	0.792521	-0.5875	1.01059	-0.40952	-0.91695	0.506475	0.014883
0.56095	0.840904	-0.66554	1.13803	-0.47729	-0.92263	0.564398	0.05781
0.628605	0.873228	-0.71923	1.23363	-0.56446	-0.9231	0.646415	0.127502
0.69144	0.900199	-0.77783	1.34519	-0.64184	-0.94482	0.713999	0.175808
0.76396	0.927222	-0.84139	1.48336	-0.7338	-0.95596	0.791245	0.229492
0.822	0.943513	-0.88058	1.58437	-0.84027	-0.97251	0.854033	0.267118
0.870331	0.965079	-0.92952	1.70131	-1	-0.992	0.936098	0.326155
0.923528	0.981345	-0.95416	1.79707			1	0.353036
1	1.01894	-0.97385	1.87155				
		-1	1.95937				

Table A.11 Loft single-phase torque homologous data (a/v octants)

BVN 2		BVD 4		BVR 8		BVT 6	
a/v	b/v ²						
0	-0.66447	0	1.26933	0	-0.66447	0	1.26933
0.049181	-0.61085	-0.06575	1.29571	-0.03768	-0.68056	0.046004	1.21107
0.106963	-0.53596	-0.11923	1.34337	-0.06166	-0.73396	0.123765	1.14756
0.159973	-0.47707	-0.17266	1.38038	-0.09527	-0.79807	0.196637	1.09467
0.213006	-0.42352	-0.24064	1.42264	-0.14358	-0.82497	0.259848	1.03641
0.2757	-0.36458	-0.30371	1.44894	-0.20639	-0.85726	0.33272	0.983525
0.338418	-0.31098	-0.36206	1.5019	-0.27407	-0.88426	0.4153	0.925364
0.386562	-0.24679	-0.46401	1.55996	-0.34664	-0.90063	0.478581	0.851119
0.405557	-0.16146	-0.52715	1.60224	-0.41923	-0.91167	0.546657	0.787555
0.434213	-0.07074	-0.59029	1.64452	-0.48695	-0.92801	0.600159	0.734567
0.453255	0.003945	-0.6389	1.68688	-0.57417	-0.91782	0.66337	0.676303
0.467454	0.078603	-0.70204	1.72916	-0.63702	-0.93947	0.726627	0.607385
0.491385	0.142658	-0.78951	1.79795	-0.70959	-0.95584	0.804436	0.533218
0.529844	0.20679	-0.84301	1.85094	-0.80155	-0.96698	0.867693	0.4643
0.568255	0.281577	-0.88674	1.88267	-1	-0.992	1	0.353036
0.601918	0.335029	-0.93053	1.93038				
0.645172	0.409842	-1	1.95937				
0.693246	0.490007						
0.7365	0.56482						
0.770116	0.628926						
0.803802	0.677051						
0.846963	0.773173						
0.895083	0.842684						
0.933518	0.912143						
1	1.01894						

Polar Homologous Pump Curves and Data: Semiscale

This section contains curves and data for the Semiscale pump (built in to MELCOR). Polar homologous data was obtained by conversion from homologous data.

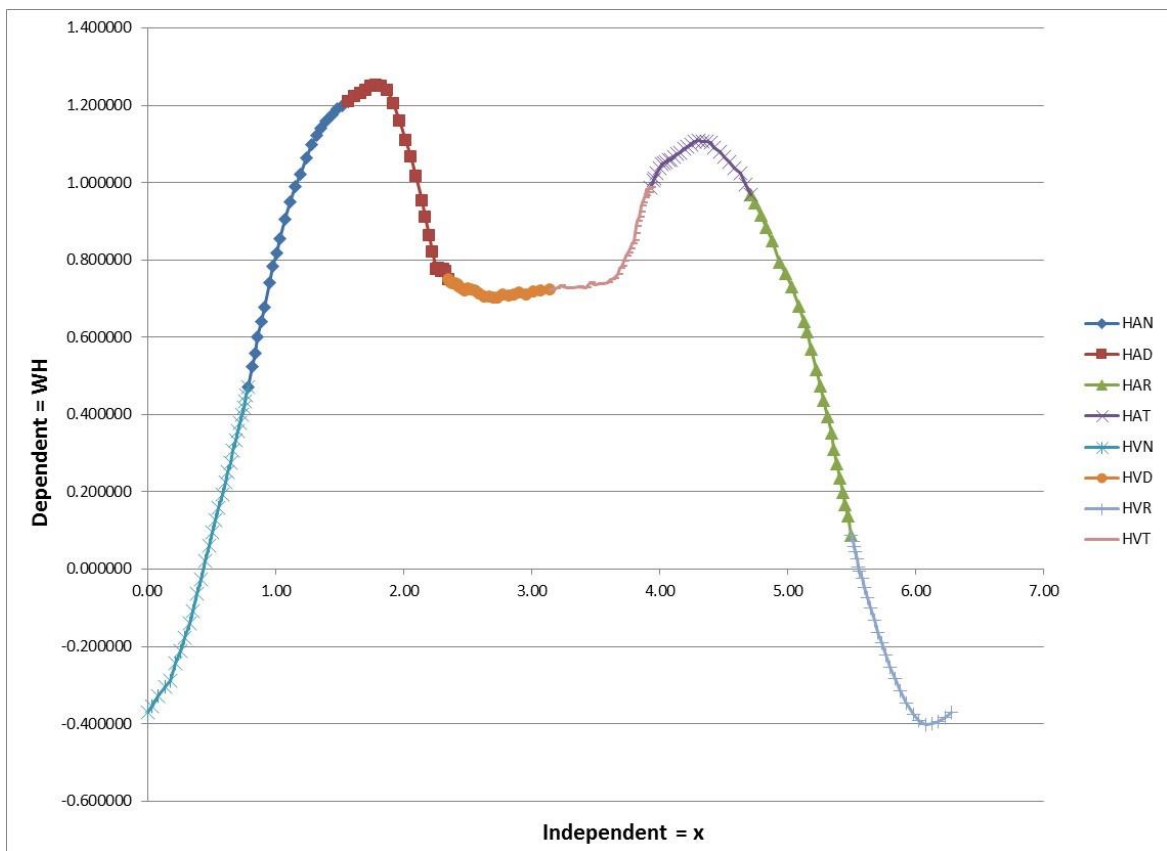


Figure A.8 Semiscale head data, polar homologous form

Table A.12 Semiscale single-phase head data, polar homologous form

x	WH	x	WH	x	WH	x	WH	x	WH	x	WH
0.000000	-0.370250	1.113927	0.949705	2.480960	0.720469	3.817811	0.886357	4.746406	0.946166	5.929512	-0.346223
0.035876	-0.355058	1.154625	0.990845	2.504490	0.723957	3.827876	0.898837	4.791791	0.916735	5.981289	-0.377094
0.085355	-0.328408	1.189716	1.020755	2.531617	0.722456	3.837778	0.910621	4.832781	0.884844	6.027089	-0.392023
0.134402	-0.305513	1.240521	1.064755	2.559814	0.719132	3.847530	0.924605	4.877391	0.849516	6.081950	-0.402443
0.174788	-0.287374	1.281730	1.098007	2.595081	0.711711	3.854753	0.938859	4.933230	0.793448	6.125985	-0.399402
0.218629	-0.244569	1.320109	1.121762	2.631942	0.704780	3.866546	0.947570	4.983779	0.764532	6.178811	-0.395386
0.257742	-0.212165	1.355310	1.140851	2.673699	0.704779	3.878117	0.960926	5.029234	0.730469	6.228123	-0.383836
0.288501	-0.176588	1.395065	1.159163	2.703681	0.700941	3.887187	0.966611	5.084210	0.680830	6.283185	-0.370250
0.326144	-0.141259	1.439447	1.175425	2.738033	0.701549	3.893928	0.981137	5.126572	0.640808		
0.355610	-0.107785	1.480240	1.191317	2.780651	0.708323	3.909197	0.973664	5.150594	0.614824		
0.388035	-0.062495	1.525476	1.198894	2.820944	0.706185	3.913520	0.983454	5.187290	0.569552		
0.419594	-0.027692	1.570793	1.209075	2.862375	0.710476	3.926991	0.987545	5.225818	0.516286		
0.453688	0.021387	1.620359	1.223779	2.908723	0.713524	3.949001	1.005055	5.253674	0.474281		
0.483425	0.059727	1.661421	1.231788	2.964091	0.710545	3.964403	1.010598	5.283546	0.435942		
0.505961	0.096361	1.706221	1.239143	3.016559	0.716829	3.980230	1.023755	5.309516	0.394053		
0.531013	0.126916	1.746462	1.247993	3.073840	0.719561	3.998887	1.038143	5.340037	0.351506		
0.555362	0.159148	1.786136	1.252535	3.141593	0.722544	4.018176	1.049221	5.361465	0.308939		
0.581898	0.192021	1.829001	1.250424	3.185294	0.725920	4.033084	1.051101	5.382207	0.271663		
0.607550	0.225713	1.870932	1.239144	3.226473	0.731784	4.048359	1.052259	5.407186	0.234476		
0.626898	0.252231	1.922800	1.205470	3.279531	0.727779	4.069290	1.057886	5.428831	0.197710		
0.650969	0.274829	1.972796	1.158912	3.323855	0.726866	4.090910	1.059065	5.449681	0.166002		
0.669156	0.306998	2.020753	1.109771	3.371421	0.731243	4.113197	1.065491	5.469770	0.136320		
0.689290	0.332738	2.060173	1.066428	3.425584	0.728847	4.139095	1.074743	5.497787	0.088056		
0.706392	0.357898	2.098031	1.015104	3.459594	0.740463	4.159867	1.078084	5.510540	0.071048		
0.722999	0.378510	2.143100	0.953708	3.492814	0.736588	4.190463	1.088269	5.519041	0.059177		
0.739142	0.400334	2.171779	0.911375	3.528822	0.737557	4.215751	1.092568	5.529867	0.044420		
0.752609	0.417014	2.202082	0.863482	3.560360	0.738654	4.245039	1.098882	5.540910	0.026313		
0.763592	0.434414	2.228516	0.820597	3.591051	0.742067	4.275206	1.107147	5.554465	0.004680		
0.772225	0.450236	2.256395	0.776178	3.617614	0.750123	4.306261	1.109112	5.563702	-0.006582		
0.785398	0.471048	2.275794	0.777604	3.643456	0.752660	4.334594	1.105360	5.580242	-0.024284		
0.815620	0.523473	2.296906	0.769216	3.668610	0.761257	4.367218	1.106627	5.602218	-0.046383		
0.837939	0.559327	2.310516	0.775166	3.687044	0.777492	4.396885	1.102462	5.622414	-0.072881		
0.861182	0.600016	2.328186	0.771298	3.707998	0.782274	4.427155	1.091324	5.648603	-0.101851		
0.887895	0.639572	2.356194	0.747980	3.722668	0.795403	4.469634	1.079273	5.678634	-0.133486		
0.913226	0.678409	2.371237	0.742158	3.737072	0.810975	4.501110	1.066624	5.707065	-0.163380		
0.953165	0.739880	2.388448	0.737624	3.753961	0.818944	4.541030	1.054373	5.736599	-0.191565		
0.981121	0.782896	2.406250	0.737425	3.770470	0.829125	4.581509	1.038231	5.767233	-0.221397		
1.007229	0.817202	2.422312	0.736138	3.783948	0.841527	4.630612	1.024637	5.798970	-0.252825		
1.037285	0.855338	2.436437	0.731096	3.797149	0.849863	4.676018	0.995494	5.838531	-0.283585		
1.074806	0.904202	2.458290	0.725063	3.807558	0.867018	4.712393	0.969552	5.879640	-0.315624		

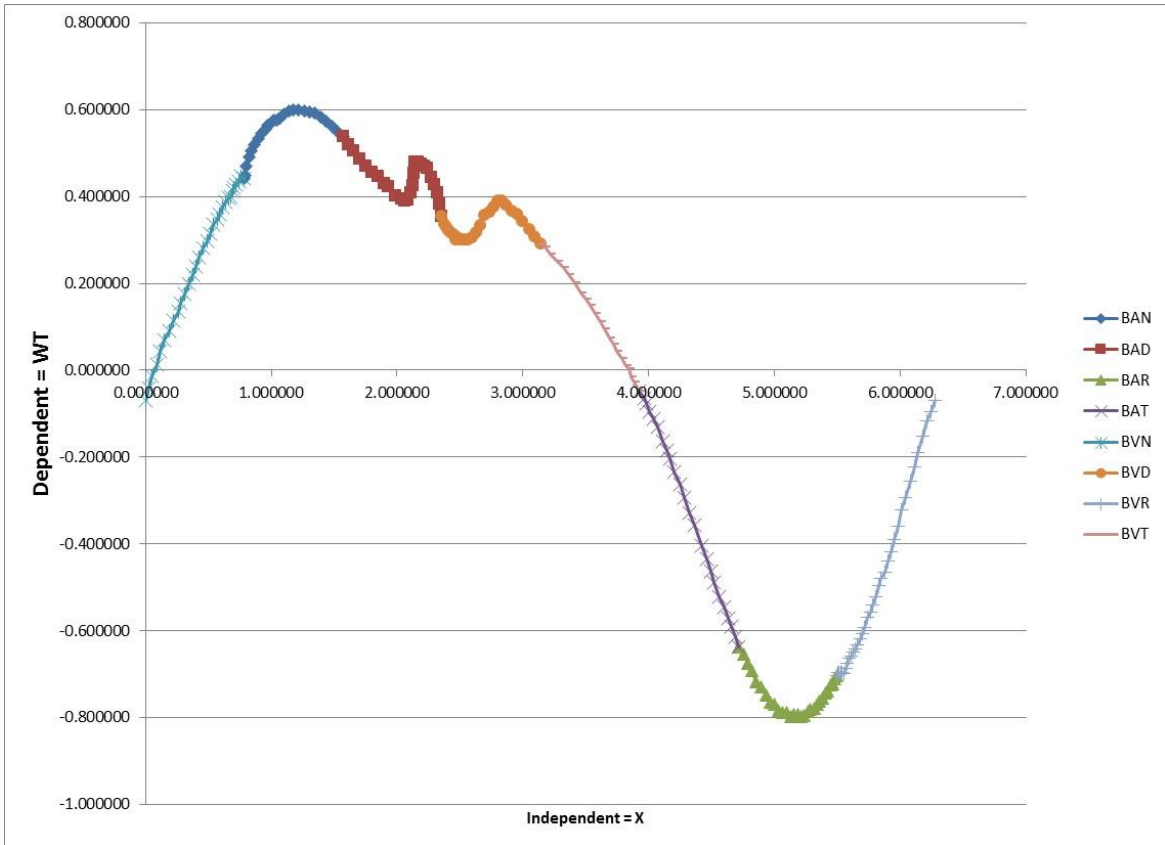


Figure A.9 Semiscale torque data, polar homologous form

Table A.13 Semiscale single-phase torque data, polar homologous form

x	WT												
0	-0.06979	0.789475	0.44778	1.84916	0.44668	2.596006	0.305728	3.786489	0.027125	4.753533	-0.65452	5.527407	-0.69696
0.02439	-0.04045	0.803209	0.469585	1.898538	0.42956	2.629653	0.317599	3.817299	0.011627	4.789769	-0.67397	5.537221	-0.69519
0.051739	-0.01338	0.822195	0.491894	1.93445	0.422978	2.664662	0.333011	3.844093	0.002853	4.821344	-0.69219	5.554764	-0.69757
0.087976	0.013442	0.841989	0.505106	1.988507	0.401344	2.701067	0.355982	3.864558	-0.01543	4.852802	-0.71771	5.567764	-0.68788
0.119586	0.044476	0.867768	0.520612	2.036329	0.395058	2.738593	0.363879	3.889241	-0.0273	4.897002	-0.72892	5.581094	-0.67469
0.150907	0.070498	0.894756	0.533518	2.0612	0.388838	2.76959	0.376806	3.926991	-0.0474	4.936293	-0.74706	5.591986	-0.66284
0.190603	0.091082	0.922964	0.546224	2.088726	0.391289	2.801354	0.389505	3.926991	-0.0474	4.97068	-0.764	5.614122	-0.6592
0.225463	0.115362	0.952465	0.555594	2.108633	0.409454	2.837815	0.39037	3.965151	-0.06414	5.004359	-0.77015	5.631329	-0.64843
0.259729	0.134341	0.973865	0.563265	2.128079	0.426366	2.870838	0.380738	3.985052	-0.07645	5.033403	-0.78455	5.645979	-0.64241
0.280925	0.153589	0.999128	0.569791	2.134227	0.452507	2.912976	0.366885	4.010987	-0.09564	5.069797	-0.78827	5.664008	-0.63243
0.31012	0.175378	1.02191	0.576616	2.143488	0.47952	2.956054	0.359871	4.038049	-0.11081	5.101328	-0.78822	5.682548	-0.6182
0.342835	0.199493	1.042012	0.577273	2.168404	0.479814	2.999741	0.342246	4.069251	-0.13054	5.128378	-0.79669	5.698354	-0.60631
0.378706	0.221332	1.069514	0.581811	2.195513	0.474237	3.05293	0.323246	4.114315	-0.16363	5.158395	-0.79322	5.717747	-0.5927
0.402127	0.240021	1.101414	0.591207	2.218738	0.470098	3.097662	0.306446	4.14277	-0.18574	5.187613	-0.79186	5.741046	-0.57012
0.428874	0.260534	1.138137	0.598005	2.241175	0.46549	3.141593	0.290609	4.168949	-0.20496	5.209067	-0.79856	5.768315	-0.55778
0.458658	0.282268	1.176192	0.599325	2.27354	0.444452	3.141593	0.290609	4.202915	-0.23368	5.236787	-0.79434	5.785893	-0.54077
0.49107	0.297486	1.215491	0.598562	2.296727	0.427192	3.178616	0.282915	4.248957	-0.26306	5.266914	-0.78564	5.807413	-0.52102
0.512165	0.31471	1.260057	0.597145	2.319025	0.408042	3.218952	0.267547	4.282244	-0.29381	5.289645	-0.78225	5.829462	-0.49607
0.542872	0.33675	1.301688	0.595687	2.342813	0.383235	3.272372	0.250518	4.324288	-0.32769	5.314827	-0.77771	5.85187	-0.48062
0.569178	0.348282	1.344298	0.591835	2.356194	0.355116	3.320735	0.237378	4.363791	-0.35753	5.339134	-0.76917	5.878558	-0.46547
0.591524	0.359978	1.396552	0.58301	2.356194	0.355116	3.368218	0.219253	4.421083	-0.40419	5.362646	-0.76275	5.902063	-0.43952
0.616299	0.374944	1.436412	0.572822	2.375993	0.335777	3.414683	0.2009	4.463236	-0.43468	5.385347	-0.75553	5.929941	-0.41724
0.637292	0.387054	1.481183	0.56103	2.392489	0.329099	3.459924	0.178466	4.493372	-0.46236	5.409912	-0.74427	5.950319	-0.39099
0.660473	0.396181	1.526266	0.551295	2.409506	0.321635	3.503946	0.164514	4.52392	-0.4899	5.42839	-0.73912	5.983393	-0.35829
0.680064	0.400393	1.570796	0.53922	2.429671	0.31734	3.535007	0.148481	4.563694	-0.52289	5.448721	-0.7252	6.01296	-0.32252
0.6938	0.41289	1.570796	0.53922	2.450563	0.312245	3.576484	0.131442	4.599388	-0.54544	5.463582	-0.72253	6.047187	-0.29417
0.704556	0.421257	1.616842	0.520383	2.466644	0.300872	3.616382	0.11153	4.630939	-0.5711	5.482687	-0.7106	6.082083	-0.25537
0.720272	0.427839	1.652955	0.504792	2.48614	0.304257	3.651315	0.096608	4.6581	-0.5911	5.497787	-0.70325	6.112996	-0.22325
0.743043	0.435182	1.706621	0.486069	2.512013	0.301069	3.691449	0.075142	4.689904	-0.61498	5.497787	-0.70325	6.144241	-0.19
0.760206	0.447605	1.755104	0.470248	2.538933	0.300071	3.723464	0.059052	4.712389	-0.63777	5.506011	-0.69641	6.184745	-0.15164
0.785398	0.440724	1.802678	0.457109	2.563751	0.300327	3.751156	0.044299	4.712389	-0.63777	5.515429	-0.69525	6.216531	-0.11647
												6.248299	-0.09443
												6.283185	-0.06979

Polar Homologous Pump Curves and Data: Loft

This section contains curves and data for the Loft pump (built in to MELCOR). Polar homologous data was obtained by conversion from homologous data.

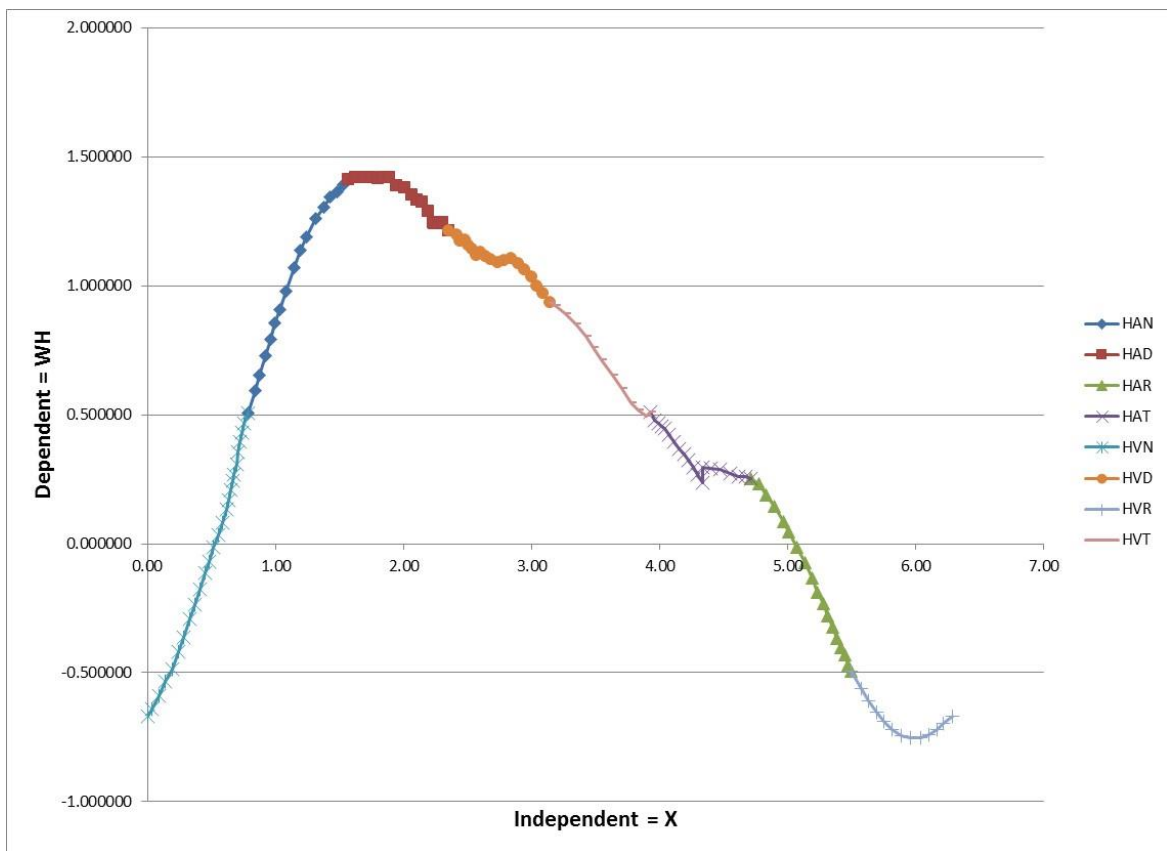


Figure A.10 Loft head data, polar homologous form

Table A.14 Semiscale single-phase head data, polar homologous form

x	WH	x	WH	x	WH	x	WH
0.000000	-0.668105	1.242069	1.191211	2.782441	1.098688	4.475264	0.287705
0.030676	-0.640818	1.313083	1.263100	2.843228	1.106576	4.549594	0.270452
0.088459	-0.588836	1.377474	1.305931	2.892703	1.087989	4.616199	0.259222
0.136163	-0.535488	1.429285	1.344482	2.948113	1.064457	4.674031	0.261096
0.192610	-0.484470	1.481848	1.366075	2.999990	1.036594	4.712385	0.250711
0.238687	-0.419509	1.530097	1.390434	3.043044	1.000203	4.712393	0.250711
0.279295	-0.361396	1.570793	1.411200	3.091275	0.970468	4.775563	0.233721
0.327666	-0.293352	1.570800	1.411200	3.141593	0.935854	4.833076	0.189230
0.370317	-0.238119	1.626937	1.419865	3.141593	0.935854	4.899164	0.144195
0.411582	-0.176513	1.684648	1.421543	3.183323	0.923764	4.963612	0.085136
0.451402	-0.114148	1.741619	1.418994	3.265086	0.890626	5.008406	0.044031
0.482200	-0.068889	1.802109	1.414455	3.345215	0.852296	5.073329	-0.013829
0.515681	-0.014079	1.843057	1.419344	3.422783	0.805699	5.135201	-0.075135
0.551467	0.032835	1.887480	1.419854	3.479899	0.762737	5.193806	-0.133713
0.582367	0.079806	1.947487	1.386989	3.547131	0.714950	5.234603	-0.187808
0.615272	0.133054	2.012815	1.379778	3.633535	0.653920	5.280492	-0.230588
0.637427	0.170074	2.066838	1.351289	3.702279	0.600059	5.314019	-0.278415
0.646655	0.208364	2.107214	1.333802	3.778194	0.544607	5.352325	-0.321761
0.661812	0.243278	2.145767	1.323697	3.835071	0.520239	5.382638	-0.365906
0.676633	0.269965	2.192148	1.288124	3.897379	0.494152	5.417208	-0.401265
0.693943	0.309556	2.232615	1.245484	3.926991	0.509080	5.444533	-0.432553
0.707967	0.354458	2.244600	1.241590	3.926991	0.509080	5.473095	-0.471669
0.724386	0.395154	2.276438	1.242592	3.959136	0.479548	5.497787	-0.496003
0.737701	0.432398	2.301278	1.245729	3.993614	0.468251	5.497787	-0.496003
0.750701	0.467637	2.356194	1.214170	4.015915	0.455149	5.573137	-0.562634
0.785398	0.507760	2.356194	1.214170	4.042053	0.445522	5.631546	-0.608268
0.785398	0.507760	2.419375	1.198395	4.075522	0.424244	5.695651	-0.651654
0.841454	0.595427	2.444622	1.173512	4.110727	0.395453	5.754836	-0.689591
0.877609	0.652473	2.476905	1.177389	4.154668	0.369056	5.818398	-0.721638
0.919149	0.727207	2.504635	1.159609	4.193847	0.346559	5.890389	-0.743367
0.963466	0.793502	2.540121	1.140451	4.227258	0.322007	5.958213	-0.753388
0.996925	0.856047	2.567076	1.118638	4.261889	0.294645	6.038364	-0.754410
1.035435	0.909569	2.602044	1.129451	4.297729	0.268873	6.103041	-0.739610
1.083338	0.980425	2.638594	1.112747	4.338917	0.236696	6.169287	-0.722639
1.141799	1.069233	2.680532	1.103145	4.339050	0.296579	6.212424	-0.696613
1.195121	1.137131	2.736520	1.090157	4.399097	0.290204	6.283185	-0.668105

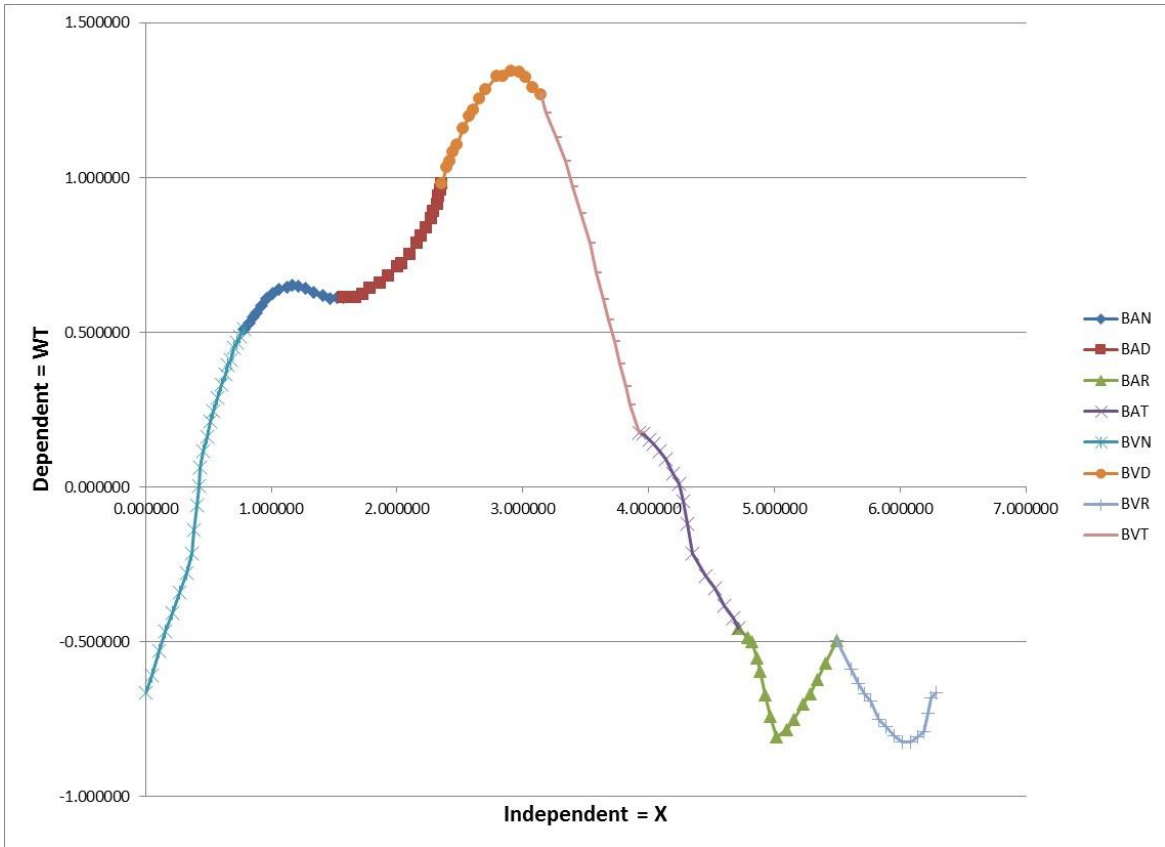


Figure A.11 Loft torque data, polar homologous form

Table A.15 Loft single-phase torque data, polar homologous form

x	WT	x	WT	x	WT	x	WT	x	WT
0.000000	-0.664470	1.059585	0.639634	2.473281	1.107573	4.092329	0.116445	5.830030	-0.750137
0.049142	-0.609372	1.124220	0.644700	2.529499	1.158287	4.138538	0.089926	5.886214	-0.775393
0.106558	-0.529893	1.168363	0.652670	2.573061	1.197905	4.198559	0.043844	5.949509	-0.804019
0.158629	-0.465169	1.218444	0.650683	2.608346	1.219573	4.243575	0.011845	6.015684	-0.822480
0.209869	-0.405136	1.274843	0.641400	2.656464	1.253823	4.274635	-0.044769	6.079650	-0.822237
0.269017	-0.338829	1.337828	0.628021	2.707152	1.283598	4.306565	-0.118196	6.140579	-0.808301
0.326320	-0.279022	1.412225	0.620463	2.794218	1.327841	4.347741	-0.215429	6.188199	-0.790892
0.368868	-0.214709	1.469249	0.608395	2.846734	1.326575	4.452636	-0.285848	6.221606	-0.731184
0.385288	-0.138650	1.522204	0.612978	2.905441	1.344766	4.526154	-0.326810	6.245524	-0.679599
0.409648	-0.059517	1.570796	0.614050	2.970619	1.340421	4.601694	-0.382050	6.283185	-0.664470
0.425557	0.003273	1.570796	0.614050	3.022925	1.324541	4.673733	-0.423813		
0.437273	0.064507	1.667165	0.613250	3.075938	1.290133	4.712389	-0.456719		
0.456732	0.114912	1.729174	0.624037	3.141593	1.269330	4.712389	-0.456719		
0.487237	0.161462	1.785405	0.641148	3.141593	1.269330	4.789499	-0.486090		
0.516750	0.212846	1.867146	0.657763	3.187564	1.208512	4.823025	-0.498996		
0.541829	0.245928	1.928158	0.682210	3.264731	1.130247	4.860860	-0.551618		
0.572974	0.289386	2.002707	0.711030	3.335752	1.053919	4.884251	-0.594133		
0.606179	0.330954	2.034334	0.723685	3.395818	0.970857	4.930465	-0.669953		
0.634805	0.366188	2.101971	0.751283	3.462791	0.885498	4.971233	-0.741649		
0.656252	0.394787	2.158018	0.788687	3.535219	0.789240	5.019940	-0.808274		
0.677055	0.411307	2.194311	0.813048	3.587959	0.692507	5.101075	-0.785253		
0.702728	0.450214	2.231873	0.838114	3.641866	0.606355	5.157705	-0.751449		
0.730092	0.467853	2.270272	0.868507	3.682129	0.540047	5.226263	-0.700054		
0.751028	0.487398	2.292777	0.892392	3.727309	0.469635	5.283008	-0.669154		
0.785398	0.509470	2.319684	0.912716	3.769966	0.397507	5.345443	-0.621374		
0.785398	0.509470	2.332739	0.940672	3.819033	0.323728	5.411206	-0.570038		
0.825133	0.529625	2.342949	0.960562	3.856269	0.264877	5.497787	-0.496000		
0.854617	0.549128	2.356194	0.979685	3.926991	0.176518	5.497787	-0.496000		
0.882784	0.563061	2.356194	0.979685	3.926991	0.176518	5.607499	-0.588730		
0.918421	0.585502	2.392165	1.034567	3.959984	0.173831	5.666051	-0.635732		
0.965838	0.609029	2.416155	1.053950	4.005558	0.154460	5.715987	-0.668279		
1.009609	0.625905	2.441170	1.081999	4.043009	0.141133	5.761979	-0.690265		

Universal Correlation Curves and Data

Table A.16 Data corresponding to Figure 6.3

Data From Paper $WH(nq) = A(nq^0) + B(nq^1) + C(nq^2) + D(nq^3)$							
x	A	B	C	D	v/a	a/v	x_polar
3.141593	1.094580	0.008814	-9.56000E-06	0.00000E+00	0.000000		0.000000
3.212992	1.085510	0.007712	-8.24430E-06	0.00000E+00	0.071521		0.071400
3.284392	1.081270	0.006259	-5.38570E-06	0.00000E+00	0.143778		0.142800
3.355792	1.048570	0.004888	-2.65355E-06	0.00000E+00	0.217537		0.214199
3.427192	0.994794	0.003750	-1.00626E-06	0.00000E+00	0.293626		0.285599
3.498592	0.950790	0.002139	2.79052E-06	0.00000E+00	0.372981		0.356999
3.569992	0.904765	0.001132	4.18123E-06	0.00000E+00	0.456685		0.428399
3.641391	0.850766	0.000716	3.43250E-06	0.00000E+00	0.546041		0.499799
3.712791	0.745394	0.001201	7.62472E-07	0.00000E+00	0.642661		0.571199
3.784191	0.624030	0.001707	-2.19598E-06	0.00000E+00	0.748591		0.642598
3.855591	0.549354	0.001157	-1.99221E-06	0.00000E+00	0.866505		0.713998
3.926991	0.500000	0.000000	0.00000E+00	0.00000E+00	1.000000		0.785398
3.998391	0.451514	-0.006158	0.00000E+00	0.00000E+00		0.866505	0.856798
4.069790	0.363014	-0.001000	0.00000E+00	0.00000E+00		0.748591	0.928198
4.141190	0.259533	-0.002105	7.11626E-06	-1.74007E-08		0.642661	0.999598
4.212590	0.213805	-0.002544	-5.87277E-07	1.04944E-08		0.546041	1.070997
4.283990	0.137520	-0.003782	2.60360E-06	9.21642E-09		0.456685	1.142397
4.355390	0.121829	-0.006303	1.23903E-05	0.00000E+00		0.372981	1.213797
4.426790	0.020028	-0.006467	-2.84207E-07	4.99101E-08		0.293626	1.285197
4.498189	-0.197520	0.002157	-1.75575E-04	1.16209E-06		0.217537	1.356597
4.569589	0.013000	-0.014295	3.81799E-05	1.09954E-08		0.143778	1.427997
4.640989	0.054105	-0.018352	5.78271E-05	-8.71503E-09		0.071521	1.499396
4.712389	0.270364	-0.034571	2.00409E-04	-3.29514E-07		0.000000	1.570796

Table A.17 Data corresponding to Figure 6.4

WT(nq) = A(nq ⁰) + B(nq ¹) + C(nq ²) + D(nq ³)					
x	A	B	C	D	x_polar
3.141593	0.301400	0.006800	-1.000E-06	0.000E+00	0.000000
3.212992	0.338500	0.006500	-3.000E-06	0.000E+00	0.071400
3.284392	0.390900	0.005600	-2.000E-06	0.000E+00	0.142800
3.355792	0.437000	0.004100	2.000E-07	0.000E+00	0.214199
3.427192	0.453200	0.004400	-1.000E-05	3.000E-08	0.285599
3.498592	0.457700	0.004400	-2.000E-05	5.000E-08	0.356999
3.569992	0.499200	0.002100	-1.000E-06	0.000E+00	0.428399
3.641391	0.523500	0.001600	-1.000E-06	0.000E+00	0.499799
3.712791	0.457300	0.001800	-3.000E-06	0.000E+00	0.571199
3.784191	0.438200	0.001600	-3.000E-06	0.000E+00	0.642598
3.855591	0.475000	0.000700	-1.000E-06	0.000E+00	0.713998
3.926991	0.429400	0.000800	-2.000E-06	0.000E+00	0.785398
3.998391	0.408900	0.000200	-6.000E-07	0.000E+00	0.856798
4.069790	0.354000	0.000010	-2.000E-06	0.000E+00	0.928198
4.141190	0.337100	-0.001200	-3.000E-07	0.000E+00	0.999598
4.212590	0.352200	-0.004800	3.000E-05	-6.000E-08	1.070997
4.283990	0.270400	-0.003900	6.000E-06	0.000E+00	1.142397
4.355390	0.354700	-0.010800	6.000E-05	-1.000E-07	1.213797
4.426790	0.361400	-0.015300	8.000E-05	-1.000E-07	1.285197
4.498189	0.381400	-0.019000	1.000E-04	-1.000E-07	1.356597
4.569589	0.412300	-0.022700	1.000E-04	-1.000E-07	1.427997
4.640989	0.313400	-0.021000	7.000E-05	0.000E+00	1.499396
4.712389	0.375600	-0.025700	8.000E-05	0.000E+00	1.570796

APPENDIX B: TERRY TURBINE VELOCITY STAGE MODEL DERIVATIONS

Angular Momentum Equation Term Derivations:

The angular momentum equation for a Terry turbine control volume is:

$$\mathbf{B.1} \quad \underbrace{\oint \mathbf{r} T_{\theta} dA}_{(1)} + \underbrace{\iiint \mathbf{r} \mathbf{B}_{\theta} dV}_{(2)} = \underbrace{\oint \mathbf{r} u_{\theta} (\rho \bar{\mathbf{u}} * d\bar{\mathbf{A}})}_{(3)} + \underbrace{\frac{\partial}{\partial t} \iiint \rho \mathbf{r} u_{\theta} dV}_{(4)}$$

Term 1:

$$\mathbf{B.2} \quad \oint \mathbf{r} T_{\theta} dA = -T_{pump} = -T_{shaft} \quad (\text{shaft torque crosses CV boundary})$$

Term 2:

$$\mathbf{B.3} \quad \iiint \mathbf{r} \mathbf{B}_{\theta} dV = \mathbf{0} \quad (\text{neglect body forces})$$

Term 3:

$$\mathbf{B.4} \quad \oint \mathbf{r} u_{\theta} (\rho \bar{\mathbf{u}} * d\bar{\mathbf{A}}) = \sum_{OUT} \left[|\bar{\mathbf{R}} \times \bar{\mathbf{u}}|_{out} \dot{m}_{out} \right] - \sum_{IN} \left[|\bar{\mathbf{R}} \times \bar{\mathbf{u}}|_{in} \dot{m}_{in} \right]$$

= Net moment-of-momentum flux across CV boundaries (control surface)
multiplied by in/out surface areas

Term 4:

$$\mathbf{B.5} \quad \frac{\partial}{\partial t} \iiint \rho \mathbf{r} u_{\theta} dV = \text{Time rate of change of angular momentum,}$$

Terms 3 and 4 may be further developed from velocity triangles analysis and mathematical manipulations, respectively.

Moment-of-Momentum Flux Term Development:

Figures D.1 through D.3 contain illustrations that help interpret the net moment-of-momentum flux term from the CV angular momentum conservation equation. This term accounts for all fluid streams entering/exiting the Terry turbine CV. The IN summation term counts a jet from the nozzle and ‘n’ jets entering rotor buckets. The OUT summation term counts ‘n’ jets exiting rotor buckets. Note ‘n’ is the number of reversing chambers paired to a given steam nozzle. A velocity triangles analysis as in Figure D.3 on helps resolve the two terms of the net moment-of-momentum flux term.

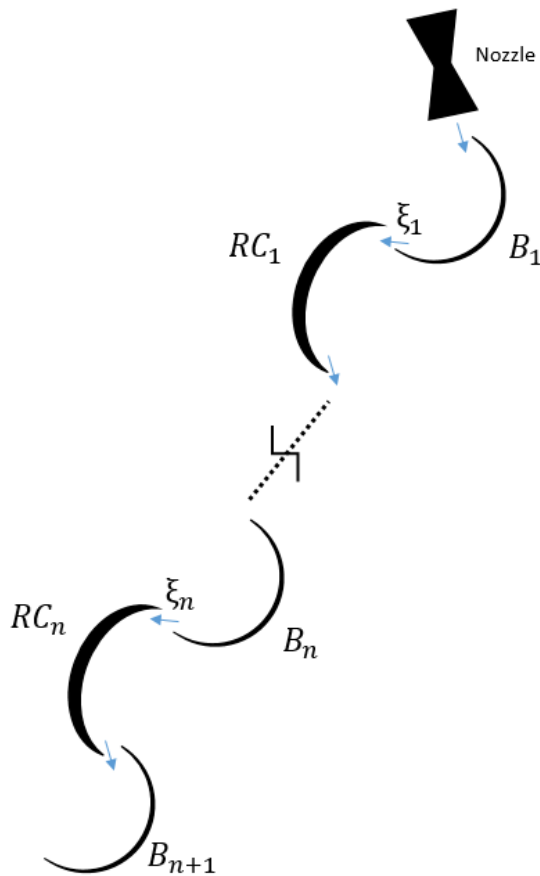


Figure B.1 Compound velocity stage for a nozzle associated with n reversing chambers

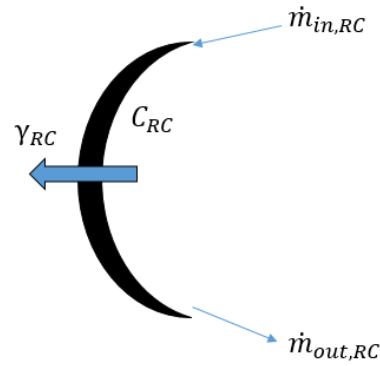


Figure B.2 A single reversing chamber showing leakage and loss coefficients

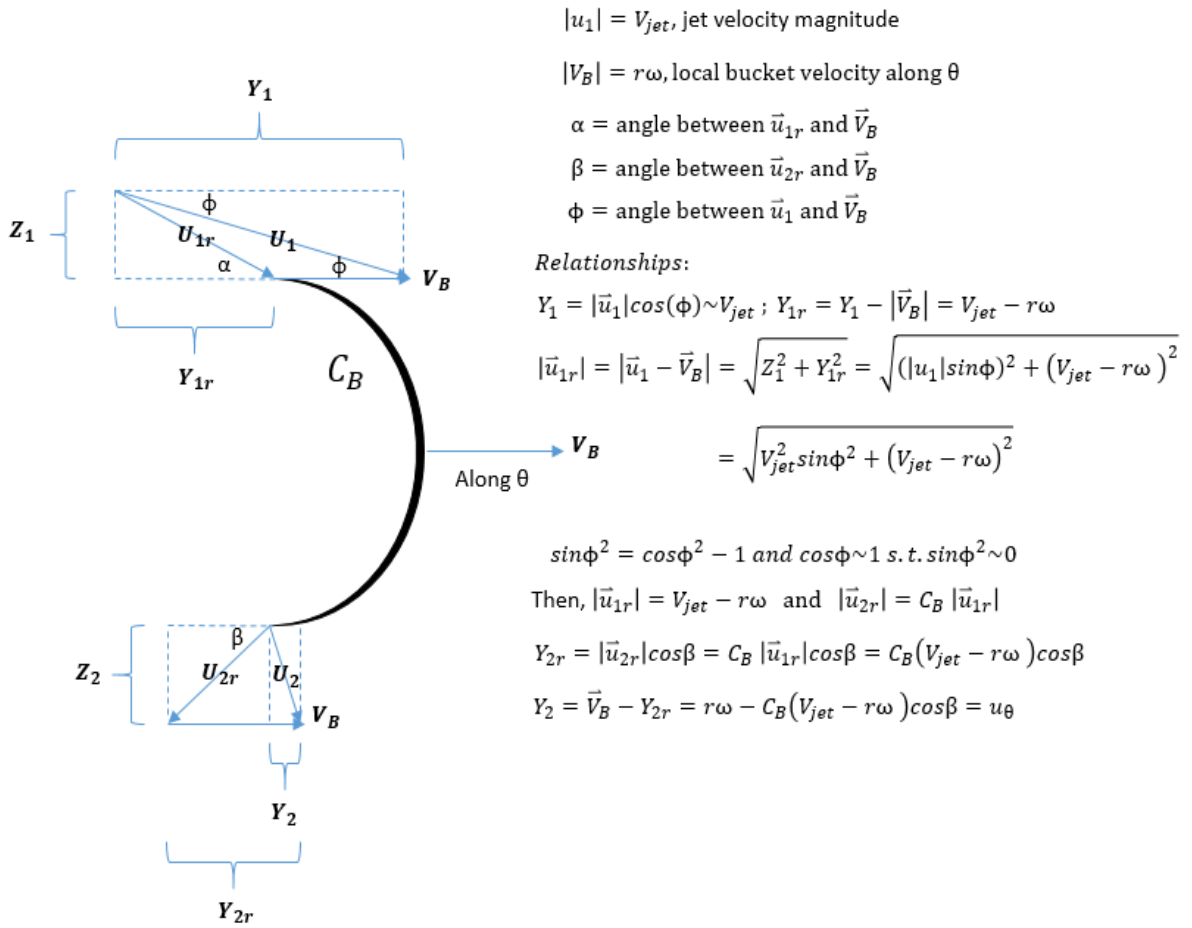


Figure B.3 A single rotor bucket showing velocity triangles, loss coefficient, exit angle

The OUT sum of the net moment-of-momentum flux term looks like (Equation (6.34):

$$\mathbf{B.6} \quad \sum_{OUT} \left[\left[\bar{\mathbf{R}} \times \bar{\mathbf{u}} \right]_{out} \dot{m}_{out} \right] = \sum_{i=1}^{n+1} r u_{\theta,i} \dot{m}_{out,i} = \sum_{i=1}^{n+1} r u_{\theta,i} \dot{m}_{in,i}$$

The IN sum of the net moment-of-momentum flux term looks like (Equation (6.35):

$$\mathbf{B.7} \quad \sum_{IN} \left[\left[\bar{\mathbf{R}} \times \bar{\mathbf{u}} \right]_{in} \dot{m}_{in} \right] = \sum_{i=1}^{n+1} r \left(V_{j,i} \cos(\beta_i) \right) \dot{m}_{in,i}$$

To recover Equation (6.36), one simply substitutes the definition of u_{θ} into D.6 and does some algebraic re-arranging. Putting the moment-of-momentum flux term back together with the other terms of the turbine torque-inertia equation, one obtains an algebraic expression (Equation 6.30) consisting of a summation over all velocity stages. In light of Equation 6.31 and 6.32, the individual terms in the compound velocity summation of Equation 6.30 are apparently coupled. The steam velocity and steam mass flow rate entering a rotor bucket (at each given stage) depends on the characteristics of the upstream reversing chamber, bucket, and steam flow. The first stage obviously depends on nozzle flow only. Equations 6.31 and 6.32 express the stage-to-stage coupling of the 2nd through last velocity stages.

Equation 6.31 says that the i^{th} stage incoming mass flow rate is either equal to the nozzle jet mass flow rate ($i=1$) or equal to the previous stage incoming mass flow rate augmented by two separate loss coefficients:

- γ for leakage across the reversing chamber upstream from the bucket in question
- ξ for loss as steam crosses gap between upstream bucket and reversing chamber

The leakage factor γ is shown in Figure D.2. The loss factor ξ is shown in Figure D.1 between bucket and reversing chamber pairs.

Equation 6.32 says that the i^{th} stage steam velocity is either equal to the nozzle jet velocity ($i=1$) or equal to a value related to:

- Previous stage incoming steam velocity
- Bucket and reversing chamber loss coefficients
- Steam exit angle from the upstream bucket

The loss coefficients are written such that they simply capture the multiplicative factor by which the velocity magnitude decreases across a reversing chamber or a bucket. The velocity triangle relationships (Figure D.3) relate bucket entrance velocities across stages by considering exit angle and relative velocity effects (due to bucket motion)

Transient Term Simplification:

$$\begin{aligned}
 \text{B.8} \quad \frac{\partial}{\partial t} \iiint \rho r u_{\theta} dV &= \sum_{i=1}^{n+1} \left[\frac{\partial}{\partial t} \iiint_{CV} r u_{\theta,i} \rho dV \right], \text{ using expression for } u_{\theta}: \\
 &= \sum_{i=1}^{n+1} \left[\frac{\partial}{\partial t} \iiint_{CV} \rho r \left(r\omega - C_{B,i} (V_{j,i} - r\omega) \cos(\beta_i) \right) dV \right], \text{ expanding:} \\
 &= \sum_{i=1}^{n+1} \left[\frac{\partial}{\partial t} \iiint_{CV} [\rho r^2 \omega - \rho r C_{B,i} V_{j,i} \cos(\beta_i) + \rho r^2 \omega C_{B,i} \cos(\beta_i)] dV \right]
 \end{aligned}$$

Separating terms yields:

B.9

$$\begin{aligned}
 \sum_{i=1}^{n+1} \left[\frac{\partial}{\partial t} \iiint_{CV} [\rho r^2 \omega (1 + \cos(\beta_i))] dV \right] & \quad (1) \\
 - \sum_{i=1}^{n+1} \left[\frac{\partial}{\partial t} \iiint_{CV} [\rho r C_{B,i} V_{j,i} \cos(\beta_i)] dV \right] & \quad (2)
 \end{aligned}$$

Term (2) goes to zero as in [1] and term (1) can be expanded further:

$$\begin{aligned}
 \text{B.10} \quad \sum_{i=1}^{n+1} (1 + \cos(\beta_i)) \left[\frac{\partial}{\partial t} \iiint_{CV} [\rho r^2 \omega] dV \right] \\
 = \sum_{i=1}^{n+1} \left[\left(1 + C_{B,i} \cos(\beta_i) \right) \right] \frac{\partial \omega}{\partial t} I_T
 \end{aligned}$$

Finally, Equation 6.29 can be recovered:

$$\frac{\partial}{\partial t} \iiint \rho r u_{\theta} dV = I_T \frac{\partial \omega}{\partial t} \sum_{i=1}^{n+1} \left(1 + C_{B,i} \cos(\beta_i) \right)$$

APPENDIX C: TERRY TURBINE PRESSURE STAGE MODEL DERIVATIONS

Gaussian Quadrature Numerical Integration

Gaussian quadrature is a numerical integration procedure that can evaluate, for example, temperature-dependent specific heat integrals. Consider the definite integral:

$$C.1 \quad \int_a^b f(x) dx = \sum_{i=1}^n C_i f(x_i)$$

x_i are locations at which the integrand - function $f(x)$ - is known and C_i are weighting factors. The locations x_i and the factors C_i can be chosen such that the integral of a polynomial of degree $2n-1$ is exact. Omitting a more lengthy derivation [53]:

$$C.2 \quad \int_a^b f(x) dx = \int_{-1}^1 F(t) (m dt) = \\ \left(\frac{b-a}{2}\right) \int_{-1}^1 F(t) dt = \left(\frac{b-a}{2}\right) \sum_{i=1}^n C_i F(t_i)$$

Where:

$$x = mt + c$$

$$m = \frac{b-a}{2}$$

$$c = \frac{b+a}{2}$$

$$F(t) = f(mt + c)$$

For a 7th order (n=4, four point formula) Gaussian quadrature approximation:

Table C.1 Gaussian quadrature t and C values

t _i	C _i
-0.8611363116	0.3478548451
-0.3399810436	0.6521451549
+0.3399810436	0.6521451549
+0.8611363116	0.3478548451

So, if evaluating an isobaric specific heat integral between two temperature values:

$$C.3 \quad \int_{T_2}^{T_1} c_p(T) dT = \left(\frac{T_1-T_2}{2}\right) \sum_{i=1}^4 C_i * c_p\left(\left(\frac{T_1-T_2}{2}\right) t_i + \frac{T_1+T_2}{2}\right)$$

On the right-hand side, the specific heat is obtained from some assumed functional dependence, a table look-up, etc.

LaPlace's Method

Laplace's method can be used to approximate integrals of exponential functions as integrals of Gaussian functions under certain assumptions that hold for the so-called "nucleation pulse" over which nucleation-growth integrals are evaluated. For a definite integral of an exponential function:

$$\text{C.4} \quad \int_a^b e^{Mf(x)} dx$$

Assume:

- $f(x)$ a twice differentiable function, M some large number
- a, b could be $-\infty, +\infty$
- $f(x)$ has a local maximum at x_0 such that $f(x_0) > f(x \neq x_0)$
- With $Mf(x)$, ratio $Mf(x_0) / Mf(x)$ remains the same, but $e^{Mf(x)}$ increases

As the constant M increases, the exponential function more closely approximates a Gaussian function and significant contributions come from the vicinity of x_0 . Expanding the function $f(x)$ in a Taylor series about the point x_0 :

$$\text{C.5} \quad f(x) = f(x_0) + f'(x_0)(x - x_0) + \frac{f''(x_0)}{2}(x - x_0)^2 + \mathbf{O(3)}$$

If a local maximum exists at x_0 , then $f'(x_0)$ is zero and $f''(x_0)$ is negative, hence:

$$\text{C.6} \quad f(x) \approx f(x_0) - \frac{|f''(x_0)|}{2} (x - x_0)^2$$

Plugging into the exponential integral and evaluating:

$$\text{C.7} \quad \int_a^b e^{Mf(x)} dx \approx e^{Mf(x_0)} \int_a^b e^{-M \frac{|f''(x_0)|}{2} (x-x_0)^2} dx$$

The integral on the right-hand side is a Gaussian integral if a and b are $-/\pm \infty$ and indeed if other assumptions above hold, this is a good approximation because the exponential decays away very quickly for x away from x_0 . Employing the known result of integrating a Gaussian function:

$$\text{C.8} \quad \int_a^b e^{Mf(x)} dx \approx e^{Mf(x_0)} \left(\frac{2\pi}{M|f''(x_0)|} \right)^{1/2}$$

This is a better and better approximation as M grows larger. This result can be applied to nucleation-growth integral evaluation.

Nucleation-Growth Equations and Closures for Steam Wetness

The complete set of nucleation-growth relationships (at the Wilson point \mathbf{n}) are written below. Note the wetness and wetness derivative equations (Y_n, Y'_n) are derived from application of Laplace' method to evaluate nucleation-growth integrals [51]

$$\text{C.9} \quad Y_n = \frac{2\pi}{3} \rho_l I_n \alpha^4 c_{gn}^3 (1 + g_1(\zeta))$$

$$\text{C.10} \quad g_1(\zeta) = \frac{3\sqrt{\pi}}{2} \zeta + 3\zeta^2 + \sqrt{\pi} \zeta^3$$

$$\text{C.11} \quad Y'_n = \pi^{3/2} \rho_l I_n \alpha^3 c_{gn}^3 (1 + g_2(\zeta))$$

$$\text{C.12} \quad g_2(\zeta) = \frac{4}{\sqrt{\pi}} \zeta + 2\zeta^2 + \frac{4}{3\sqrt{\pi}} \zeta^3$$

$$\text{C.13} \quad \zeta = \frac{r_n^*}{c_{gn} \alpha}$$

$$\text{C.14} \quad \alpha = \left(\frac{2}{B_n \eta_n'} \right)^{1/2}$$

$$\text{C.15} \quad I_n = A_n e^{-B_n \eta_n}$$

$$\text{C.16} \quad \eta_n = \frac{1}{T_n^3 (\ln(S_n))^2}$$

$$\text{C.17} \quad A_n = \frac{\rho_g}{\rho_l} \left(\frac{2\sigma(T_n)}{\pi m_v^3} \right)^{1/2}$$

$$\text{C.18} \quad B_n = \frac{16\pi\sigma(T_n)^3}{K(\rho_l R)^2}$$

$$\text{C.19} \quad r_n^* = \frac{2\sigma(T_n)}{\rho_l R T_n \ln(S_n)}$$

$$\text{C.20} \quad c_{gn} = \frac{\rho_g c_p(T_n) \Delta T_n}{2.4 \rho_l (h_{fg} Pr_g)_n} \sqrt{RT_n}$$

Auxiliary expressions for $\eta'_n, T'_n, \eta''_n, T''_n$:

$$\text{C.21} \quad T'_n = -\frac{2T_n}{\omega \ln(S_n)} f_p \dot{P}$$

$$\text{C.22} \quad f_p \dot{P} = \left(-\frac{1}{P} \frac{dP}{dt} \right)_{t_n}$$

$$\text{C.23} \quad \omega = \frac{2A_1}{T_n \ln(S_n)} + \frac{4A_2}{T_n^2 \ln(S_n)} - 3$$

$$\text{C.24} \quad \eta''_n = \frac{\eta_n}{T_n} \omega T''_n - \frac{2\eta_n}{\ln(S_n)^2} (1 - \xi) (f_p \dot{P})^2$$

$$\text{C.25} \quad \xi = \frac{1}{\omega^2} \left((\omega - 3)^2 + \frac{4A_1}{T_n \ln(S_n)} - 12 \right)$$

$$\text{C.26} \quad f_p = \frac{M_a^2 - 1}{(\gamma - \kappa) M_a^2 - 1}$$

$$\text{C.27} \quad \kappa = \frac{2\gamma}{\omega \ln(S_n)}$$

$$\text{C.28} \quad T''_n = \frac{(M_a^2 - 1) (\dot{P} R (T_a T_n)^{1/2} (1 - \phi))^2}{(c_p h_{fg})_n Y_n (\gamma M_a^2 - 1)}$$

$$\text{C.29} \quad \phi = \left(\frac{\kappa}{\gamma - 1} \right) f_p$$

$$\text{C.30} \quad Y'_n = \frac{RT_a \dot{P} (M_a^2 - 1) (1 - \phi)}{h_{fg} (\gamma M_a^2 - 1)}$$

Wetness Iteration

An iterative approach to solving for a self-consistent set of conditions at the isentropic reference state \mathbf{a} and the Wilson point \mathbf{n} is employed along with “wetness iteration” within step three of the Terry turbine expansion stage pressure model. The method is based on solving two disparate nucleation pulse half-width (α) expressions in such a way as to iteratively converge on a nucleation characteristics and Wilson point temperature and wetness. Note that, as explained in [51], certain assumptions related to mathematical modeling of the nucleation process leads to the set of equations C.9 to C.30. This long list of equations dictates nucleation/condensation (evolved wetness) under those assumptions and for some given set of conditions.

As explained in [51], the full complement of closures (C.9 to C.30 above) can be used to derive two nucleation pulse half-width expressions which can then be employed in an iterative approach to ultimately resolve \mathbf{a} and \mathbf{n} . The expressions used for the iterative method in MELCOR resemble those of Appendix C in [51]. The mathematical approach taken to ultimately converge on wetness is likely different from [51]. The equations for α yield an α_A and an α_B that ought to agree when \mathbf{a} and \mathbf{n} conditions are consistent. The relative agreement can be gauged by taking the logarithm (base 10) of each quantity and subtracting one from the other. Then, using Wilson point temperature as the variable x for the nonlinear equation $f(x) = \log(\alpha_A) - \log(\alpha_B)$, a Regula-Falsi approach can be used to settle on the Wilson point temperature that enables $\alpha_A \sim \alpha_B$. The first expression for nucleation pulse half-width α_A is a 3rd order polynomial that comes from combining C.11 and C.30 so as to eliminate Y'_n :

$$\text{C.31 } \alpha_A^3 + Y_A \alpha_A^2 + Y_B \alpha_A + Y_C + Y_D = 0$$

Where:

$$Y_A = \left(\frac{4}{\sqrt{\pi}} \right) \left(\frac{r_n^*}{c_{gn}} \right)$$

$$Y_B = 2 \left(\frac{r_n^*}{c_{gn}} \right)^2$$

$$Y_C = \left(\frac{4}{3\sqrt{\pi}} \right) \left(\frac{r_n^*}{c_{gn}} \right)^3$$

$$Y_D = - \left(\frac{RT_a \dot{P} (1 - \phi)}{I_n c_{gn}^3 \rho_l h_{fg} \pi^{2/3}} \right) \left(\frac{\gamma M a^2 - 1}{M a^2 - 1} \right)$$

The second expression for nucleation pulse half-width α_B is a 2nd order polynomial that comes from combining C.9, C.11, C.14, C.24, C.28, and C.30.

$$\text{C.32 } \alpha_B^2 + Y_E \alpha_B + Y_F = 0$$

Where:

$$Y_E = \left(\frac{3}{4\pi^{1/3}} \right) \left(\frac{\gamma - 1}{\gamma} \right) \left(\frac{\omega(1 - \phi)}{(1 - \zeta) \left(1 + g_1(\zeta) / 1 + g_2(\zeta) \right)} \right) \left(\frac{(\ln(S_n))^2}{f_p^2 \dot{P}} \right)$$

$$Y_F = \frac{-(\ln(S_n))^2}{2B_n \eta_n (1 - \xi) f_p^2 \dot{P}^2}$$

Equation C.32 is obtained by a series of steps:

- Substitute C.24 into C.14 and rearrange to recover:

$$\text{C.33} \quad \alpha_B^2 \left[\left(\frac{\eta_n}{T_n} \right) \omega T_n'' + \left(\frac{2\eta_n}{(\ln(S_n))^2} \right) (1 - \xi) f_p^2 \dot{P}^2 \right] - \frac{2}{B_n} = 0$$

- Substitute C.28 into C.33 and expand to recover:

$$\text{C.34} \quad \alpha_B^2 \left(\frac{\eta_n}{T_n} \right) \omega \left(\frac{\left(\frac{\dot{P} R (T_a T_n)^{\frac{1}{2}} (1 - \phi)}{(c_p h_{fg})_n} \right)^2}{\left(\frac{M_a^2 - 1}{\gamma M_a^2 - 1} \right) \left(\frac{1}{Y_n} \right)} \right) +$$

$$\alpha_B^2 \left(\frac{2\eta_n}{(\ln(S_n))^2} \right) (1 - \xi) f_p^2 \dot{P}^2 - \frac{2}{B_n} = 0$$

- Pull out factor of α_B^2 , divide through by $\left(\frac{2\eta_n}{(\ln(S_n))^2} \right) (1 - \xi) f_p^2 \dot{P}^2$ and use the C.9 relationship as a substitute for $\frac{1}{Y_n}$ along with C.30 for Y'_n to recover:

$$\text{C.35} \quad \alpha_B^2 + \alpha_B \left(\frac{3}{4\sqrt[3]{\pi}} \right) \left(\frac{\gamma - 1}{\gamma} \right) \left(\frac{\omega(1 - \phi)}{(1 - \xi) \left(\frac{1 + g_1(\zeta)}{1 + g_2(\zeta)} \right)} \right) \left(\frac{(\ln(S_n))^2}{f_p^2 \dot{P}} \right)$$

$$- \frac{(\ln(S_n))^2}{2B_n \eta_n (1 - \xi) f_p^2 \dot{P}^2} = 0$$

Equation C.31 can be solved by a combination of bisection and the quadratic formula (to get all three roots), whereas equation C.32 can be solved with the quadratic formula. Equations C.31 and C.32 can be solved for any guess or latest-iterate T_n and for known conditions at expansion states **01** and **2**. Within the context of a regula-falsi approach and a searching algorithm, the value of T_n which leads to self-consistent Wilson point and isentropic reference conditions can be found.

Newton Iteration

Newton's method (or the Newton-Rhapson method) is a popular, straight-forward way of solving non-linear equations or systems thereof. The following descriptions are from [53].

Single Equation F(x):

A function $f(x)$ – usually nonlinear – is solved iteratively for x via repetitive application (to convergence) of:

$$C.37 \quad x_{i+1} = x_i - \frac{f(x_i)}{f'(x_i)}$$

Note that $f(x)=0$ and a derivative function $f'(x)$ must exist and must be calculated. Eventually, the iteration-to-iteration values of x stop changing appreciably and/or the function value $f(x)$ converges to a value sufficiently close to zero.

System of Equations:

A system of two or more equations can be solved by a similar application of Newton's method. A system (two equations here for illustrative purposes) is written as:

$$C.38 \quad \begin{cases} f(x, y) = 0 \\ g(x, y) = 0 \end{cases}$$

Following a Taylor series expansion of each function, a new system can be constructed:

$$\text{C.39} \quad \begin{cases} f'_x \Delta x_i + f'_y \Delta y_i = -f_i \\ g'_x \Delta x_i + g'_y \Delta y_i = -g_i \end{cases} \text{ and } \begin{cases} x_{i+1} = x_i + \Delta x_i \\ y_{i+1} = y_i + \Delta y_i \end{cases}$$

Thus, the derivative functions f'_x , f'_y , g'_x , and g'_y must be computed and the system in C.39 is solved (by whatever linear algebra method) for the incremental quantities Δx and Δy such that next-iterate x and y are derived from last-iterate values and the deltas.

Lagrange Polynomials

For any general set of $n+1$ data points $([a, f(a)], [b, f(b)], \dots, [k, f(k)])$ an n^{th} degree polynomial $P_n(x)$ passing through all $n+1$ points is [53]:

$$\begin{aligned} \text{C.40 } P_n(x) = & \frac{(x-b)(x-c)\dots(x-k)}{(a-b)(a-c)\dots(a-k)} f(a) + \frac{(x-a)(x-c)\dots(x-k)}{(b-a)(b-c)\dots(b-k)} f(b) \dots + \\ & \dots \frac{(x-a)(x-b)\dots(x-j)}{(k-a)(k-b)\dots(k-j)} f(k) \end{aligned}$$

For $n=3$, a three-point (quadratic) Lagrange polynomial for $([a, f(a)], [b, f(b)], [c, f(c)])$ is:

$$\text{C.41 } P_3(x) = \frac{(x-b)(x-c)}{(a-b)(a-c)} f(a) + \frac{(x-a)(x-c)}{(b-a)(b-c)} f(b) + \frac{(x-a)(x-b)}{(c-a)(c-b)} f(c)$$

A derivative formula is straightforward to compute if need be. The polynomial can be used in the context of a Newton iteration solution or can be interpolated for function values at some $x \neq (a, b, c)$. There is no requirement that (a, b, c) are equally or unequally spaced.

Bisection (Interval Halving)

For some non-linear equation $f(x)=0$, it is sometimes necessary to find one or more roots (or zeros) on a prescribed, closed domain $[a,b]$. Regula-Falsi and bisection are two different approaches to finding such a root.

Bisection takes the closed domain limits a and b as an interval and halves it to get a value c . function evaluations $f(a)$, $f(b)$, and $f(c)$ are made and interval limits are revised according to the interval half (a,c) or (c,b) within which the root is decidedly located. As the process is repeated, the interval narrows and eventually converges to the root by virtue of a small $f(c)$ value or a sufficiently narrow interval width $[a,b]$. From [54] :

$$\text{C.42 } c = (a + b)/2$$

$$\begin{cases} \text{if } f(a)f(c) < 0: \text{ keep } a = a \text{ and move } b = c \\ \text{if } f(a) * f(c) > 0; \text{ move } a = c \text{ and keep } b = b \end{cases}$$

Regula-Falsi (False Position)

Regula-Falsi – relative to bisection – is similar in theory, but simply changes the assumption about the value c . The nonlinear function $f(x)=0$ is approximated as a linear function $g(x)$ on $[a,b]$ and c is calculated as the x value where $g(x)=0$. The derivative of $g(x)$ is used in ascertaining c [54]:

$$\text{C.43 } g'(x) = \frac{f(b)-f(a)}{b-a} \text{ so that if } f(c) = 0: c = b - \frac{f(b)}{g'(x)}$$
$$\begin{cases} \text{if } f(a)f(c) < 0: \text{ keep } a = a \text{ and move } b = c \\ \text{if } f(a) * f(c) > 0; \text{ move } a = c \text{ and keep } b = b \end{cases}$$

APPENDIX D: MELCOR USER INPUT FOR NEW MODELS

This appendix summarizes new and modified input records to facilitate the homologous pump model and the new RCIC Terry turbine models. New input records that did not previously exist have their respective record names highlighted in green, for instance:

FL_RPD – Rated Pump Data

Note that none of the body of the description for new input records is highlighted with color since the green heading implies the entire record is new to MELCOR. Modified input records have their respective record names highlighted in yellow as:

FL_PMP – Pump Input Data

Additionally, the modified fields on modified records are highlighted in yellow and some input structures of such records are omitted if they have not changed due to new models (these omissions are denoted by *bold, red, italic text*). The format of presentation in this appendix follows that of the MELCOR User Guide [15]

Homologous Pump Model Input Records

FL_PMP – Pump Input Data

Optional

Only one pump may be input for a given flow path

(1) NPUMP

Number of pumps

(type = integer, default = none, units = none)

The following data are input as a table with length NPUMP

(1) NP

Table row index

(type = integer, default = none, units = none)

(2) PNAME

Name of the pump

(type = character*16, default = none, units = dimensionless)

(3) FLNAME

Name of the flow path connected to this pump

(type = character*16, default = none, units = dimensionless)

(4) PTYPE

Pump type

(a) FANA

...No changes to current UG

(b) QUICK-CF

... No changes to current UG

(c) HOM

The HOM pump type allows access to a centrifugal pump performance model that uses input or built-in homologous pump data to predict pump head and torque. Single and two phase performance can be modeled, and the trip capability is preserved. A torque-inertia equation to predict pump speed is also available with this type. Coupling to the momentum equation is either explicit or semi-implicit in time depending upon input for FL_PNT as described subsequently.

(d) UNIV

The UNIV pump type allows access to a centrifugal pump performance model that requires only pump specific speed in order to predict pump head and torque (in the normal mode of operation only and for single-phase only). The trip capability is preserved and the torque-inertia equation is also available for use with this type. Coupling to the momentum equation is either explicit or semi-implicit in time depending upon input for FL_PNT as described subsequently.

(type = character, default = none, units = dimensionless)

The additional data required to define a pump depend on the pump type. These data are interpreted according to the pump type flag.

If PTYPE = FANA

... No changes to current UG

If PTYPE = QUICK-CF

... No changes to current UG

If PTYPE = HOM

(5) PHSOPT

Pump performance modeling phase option

(a) ONE

Only single-phase performance is modeled

(b) TWO

Two-phase performance is modeled. Note if two-phase modeling is selected but only single-phase conditions are present, there is no difficulty in the solution method

(type = character*3, default = TWO, units = dimensionless)

(6) DATOPT

Pump performance modeling data source

(a) USER

A full complement of homologous pump data will be input by the user in accordance with the selected PHSOPT

(b) SEMI

The built-in data corresponding to the Semiscale experiments will be used, compatible with either choice of PHSOPT

(c) LOFT

The built-in data corresponding to the LOFT experiments will be used. Note LOFT data only covers single-phase operation so Semiscale two-phase data will be used as well.

(type = character*4, default = SEMI, units = dimensionless)

(7) ITRIP ... *same as entry for trip on FANA type pump*

(8) CFNAME/TFNAME...*same as entry for trip on FANA type pump*

If PTYPE = UNIV

(5) PHSOPT

Pump performance modeling phase option

(a) ONE

Only single-phase performance is modeled. Note the universal correlation only covers the normal mode of pump operation. Thus, if the pump conditions should depart from the normal mode, Semiscale or LOFT data will be used depending upon DATOPT.

(b) TWO

Two-phase performance is modeled. Note the universal correlation does not cover two-phase conditions. Thus, if two-phase conditions exist, the two-phase component of head and torque calculations are performed with Semiscale data.

(type = character*3, default = TWO, units = dimensionless)

(6) DATOPT

Pump performance modeling data source for purposes of single-phase, outside normal mode of pump operation. Note if two-phase conditions occur, Semiscale data is used for the two-phase component of head and torque computations.

(a) SEMI

The built-in data corresponding to the Semiscale experiments will be used.

(b) LOFT

The built-in data corresponding to the LOFT experiments will be used.

(type = character*4, default = SEMI, units = dimensionless)

(7) ITRIP ... *same as entry for trip on FANA type pump*

(8) CFNAME/TFNAME...*same as entry for trip on FANA type pump*

Examples:

```
FL_PMP 9 ! NP PNAME FLNAME PTYPE ...
  1 'Pump1' FL280 QUICK-CF 'CF266'
  2 'Pump2' FANA 5.0 2.0
  3 'Pump3' FANA 5.0 2.0 5.0 ON
  4 'Pump4' FANA 5.0 2.0 5.0 CF 'CF101'
  5 'Pump5' FANA 5.0 2.0 5.0 TF 'TF282'
  6 'Pump6' HOM ONE USER ON
  7 'Pump7' HOM TWO USER CF 'CF101'
  8 'Pump8' HOM TWO SEMI TF 'TF282'
  9 'Pump9' UNIV ONE LOFT ON
```

FL_RPD – Rated Pump Data

Required if PTYPE = HOM or PTYPE = UNIV for any pump defined on FL_PMP. One set of rated conditions is required per each HOM/UNIV type pump on FL_PMP. Note that to determine rated motor torque, the shaft power at rated conditions and the rated speed are used. To determine the rated hydraulic torque and hence the brake power at rated conditions, the friction torque (evaluated at rated conditions) is subtracted from the rated motor torque. The tacit assumption here is steady-state (net zero torque) operation at rated conditions.

(1) NPHUP

Number of HOM and UNIV type pumps

(type = integer, default = none, units = dimensionless)

The following data are input as a table with length NPHUP

(1) NP

Table row index

(type = integer, default = none, units = none)

(2) PNAME

Name of the pump

(type = character*16, default = none, units = dimensionless)

(3) OMEGAR

Rated impeller speed (i.e. pump speed), factors into the rated brake power

(type = real, default = none, units = rpm)

(4) SPDRAT

Ratio of initial impeller speed to rated impeller speed

(type = real, default = none, units = dimensionless)

(5) QR

Pump rated volumetric flow rate, factors into the rated hydraulic power

(type = real, default = none, units = m³/s)

(6) HR

Pump rated head, factors into the rated hydraulic power

(type = real, default = none, units = m)

(7) PSHR

Shaft power at rated conditions (equals rated motor torque times rated speed)

(type = real, default = none, units = W)

(8) RHOR

Rated density of pumped fluid

(type = real, default = none, units = kg/m³)

Example:

FL_RPD 1

1 'Pump1' 3560.0 0.0 0.0114 58.52 1.769E+4 997.95

FL_SPH – Single-phase head performance data

Required if PTYPE = HOM and DATOPT = USER for any pump defined on FL_PMP (regardless of PHSOPT). HAN and HVN (normal mode octants) are required, remaining six octants are optional.

(1) NPHUP

Number of HOM and UNIV type pumps

(type = integer, default = none, units = dimensionless)

The following data are input as a table with length NPHUP

(1) PNAME

Name of the pump

(type = character*16, default = none, units = dimensionless)

(2) HAN

TF name for data of normal pump operating mode, range A

(type = character*16, default = none, units = dimensionless)

(3) HVN

TF name for data of normal pump operating mode, range V

(type = character*16, default = none, units = dimensionless)

(4) HAD or placeholder ‘-‘

TF name for data of dissipation pump operating mode, range A (or ‘-‘)

(type = character*16, default = none, units = dimensionless)

(5) HVD or placeholder ‘-‘

TF name for data of dissipation pump operating mode, range V (or ‘-‘)

(type = character*16, default = none, units = dimensionless)

(6) HAT or placeholder ‘-‘

TF name for data of turbine pump operating mode, range A (or ‘-‘)

(type = character*16, default = none, units = dimensionless)

(7) HVT or placeholder ‘-‘

TF name for data of turbine pump operating mode, range V (or ‘-‘)

(type = character*16, default = none, units = dimensionless)

(8) HAR or placeholder ‘-‘

TF name for data of reversal pump operating mode, range A (or ‘-‘)

(type = character*16, default = none, units = dimensionless)

(9) HVR or placeholder ‘-‘

TF name for data of reversal pump operating mode, range V (or ‘-‘)

(type = character*16, default = none, units = dimensionless)

Example:

FL_SPH 2

1 ‘Pump1’ ‘HANTF’ ‘HVNTF’ ‘HADTF’ ‘HVDTF’ ‘HATTF’ ‘HVTTF’ ‘HARTF’ ‘HVRTF’

2 ‘Pump2’ ‘HANTF2’ ‘HVNTF2’ ‘HADTF2’ ‘HVDTF2’ ‘-‘ ‘-‘ ‘-‘ ‘-‘

FL_TPH – Two-phase head performance data

Required if PTYPE = HOM and DATOPT = USER and PHSOPT = TWO for any pump defined on FL_PMP. HAN2 and HVN2 (normal mode octants) are required, the remaining six octants are optional. If any two-phase data is entered, the head multiplier TF is required.

(1) NPHUP

Number of HOM and UNIV type pumps

(type = integer, default = none, units = dimensionless)

The following data are input as a table with length NPHUP

(1) PNAME

Name of the pump

(type = character*16, default = none, units = dimensionless)

(2) HAN2

TF name for data of normal pump operating mode, range A

(type = character*16, default = none, units = dimensionless)

(3) HVN2

TF name for data of normal pump operating mode, range V

(type = character*16, default = none, units = dimensionless)

(4) HAD2 or placeholder ‘-‘

TF name for data of dissipation pump operating mode, range A (or ‘-‘)

(type = character*16, default = none, units = dimensionless)

(5) HVD2 or placeholder ‘-‘

TF name for data of dissipation pump operating mode, range V (or ‘-‘)

(type = character*16, default = none, units = dimensionless)

(6) HAT2 or placeholder ‘-‘

TF name for data of turbine pump operating mode, range A (or ‘-‘)

(type = character*16, default = none, units = dimensionless)

(7) HVT2 or placeholder ‘-‘

TF name for data of turbine pump operating mode, range V (or ‘-‘)

(type = character*16, default = none, units = dimensionless)

(8) HAR2 or placeholder ‘-‘

TF name for data of reversal pump operating mode, range A (or ‘-‘)

(type = character*16, default = none, units = dimensionless)

(9) HVR2 or placeholder ‘-‘

TF name for data of reversal pump operating mode, range V (or ‘-‘)

(type = character*16, default = none, units = dimensionless)

(10) HMULT or placeholder ‘-‘

TF name for data of head multiplier (or ‘-‘)

(type = character*16, default = none, units = dimensionless)

Example:

FL_TPH 2

```
1 'Pump1' 'HAN2TF' 'HVN2TF' 'HAD2TF' 'HVD2TF' 'HAT2TF' 'HVT2TF' 'HAR2TF' 'HVR2TF' 'HMULT'  
2 'Pump2' 'HAN2TF2' 'HVN2TF2' '- ' '- ' '- ' '- ' '- ' '- ' 'HMULT2'
```

FL_TPT – Two-phase torque performance data

Required if PTYPE = HOM and DATOPT = USER and PHSOPT = TWO for any pump defined on FL_PMP. BAN2 and BVN2 (normal mode octants) are required, the remaining six octants are optional. If any two-phase data is entered, the torque multiplier TF is required.

(1) NPHUP

Number of HOM and UNIV type pumps

(type = integer, default = none, units = dimensionless)

The following data are input as a table with length NPHUP

(1) PNAME

Name of the pump

(type = character*16, default = none, units = dimensionless)

(2) BAN2

TF name for data of normal pump operating mode, range A

(type = character*16, default = none, units = dimensionless)

(3) BVN2

TF name for data of normal pump operating mode, range V

(type = character*16, default = none, units = dimensionless)

(4) BAD2 or placeholder ‘-‘

TF name for data of dissipation pump operating mode, range A (or ‘-‘)

(type = character*16, default = none, units = dimensionless)

(5) BVD2 or placeholder ‘-‘

TF name for data of dissipation pump operating mode, range V (or ‘-‘)

(type = character*16, default = none, units = dimensionless)

(6) BAT2 or placeholder ‘-‘

TF name for data of turbine pump operating mode, range A (or ‘-‘)

(type = character*16, default = none, units = dimensionless)

(7) BVT2 or placeholder ‘-‘

TF name for data of turbine pump operating mode, range V (or ‘-‘)

(type = character*16, default = none, units = dimensionless)

(8) BAR2 or placeholder ‘-‘

TF name for data of reversal pump operating mode, range A (or ‘-‘)

(type = character*16, default = none, units = dimensionless)

(9) BVR2 or placeholder ‘-‘

TF name for data of reversal pump operating mode, range V (or ‘-‘)

(type = character*16, default = none, units = dimensionless)

(10) TMULT

TF name for data of torque multiplier (or ‘-‘)

(type = character*16, default = none, units = dimensionless)

Example:

FL_TPT 2

```
1 'Pump1' 'BAN2TF' 'BVN2TF' 'BAD2TF' 'BVD2TF' 'BAT2TF' 'BVT2TF' 'BAR2TF' 'BVR2TF' 'TMULT'  
2 'Pump2' 'BAN2TF2' 'BVN2TF2' 'BAD2TF2' 'BVD2TF2' '- ' '- ' '- ' '- ' 'TMULT2'
```

FL_PFR – Pump friction torque data

Required if PTYPE = HOM or PTYPE = UNIV for any pump defined on FL_PMP. The pump friction torque is described in terms of pump speed via input of coefficients and exponents.

(1) NPHUP

Number of HOM and UNIV type pumps

(type = integer, default = none, units = dimensionless)

The following data are input as a table with length NPHUP

(1) PNAME

Name of the pump

(type = character*16, default = none, units = dimensionless)

(2) TCOEFFC

Constant (zeroth) friction torque coefficient

(type = real, default = none, units = N*m)

(3) TCOEFF1

First friction torque coefficient

(type = real, default = none, units = N*m)

(4) TCOEFF2

Second friction torque coefficient

(type = real, default = none, units = N*m)

(5) TCOEFF3

Third friction torque coefficient

(type = real, default = none, units = N*m)

(6) TEXP1

First friction torque exponent, greater than, less than, but not equal to zero

(type = real, default = none, units = dimensionless)

(7) TEXP2

Second friction torque exponent, greater than, less than, but not equal to zero

(type = real, default = none, units = dimensionless)

(8) TEXP3

Third friction torque exponent, greater than, less than, but not equal to zero

(type = real, default = none, units = dimensionless)

(9) TFRC

Friction torque used below pump friction critical speed ratio

(type = real, default = none, units = N*m)

(10) TSPCRT

Pump friction torque critical speed ratio

(type = real, default = none, units = dimensionless)

Example:

FL_PFR 1

1 'PUMP1' 451.0 100.0 50.0 25.0 1.1 2.2 3.3 451.0 0.25

FL_PIN – Pump moment of inertia data

Required if PTYPE = HOM or PTYPE = UNIV for any pump defined on FL_PMP, The pump moment of inertia is given in terms of pump speed and user-supplied polynomial coefficients. Note this is a positive, non-zero quantity and such constraints are enforced by MELGEN and MELCOR.

(1) NPHUP

Number of HOM and UNIV type pumps

(type = integer, default = none, units = dimensionless)

The following data are input as a table with length NPHUP

(1) PNAME

Name of the pump

(type = character*16, default = none, units = dimensionless)

(2) ICOEFFC

Constant inertia coefficient

(type = real, default = none, units = kg*m2)

(3) ICOEFF1

First (linear) inertia coefficient

(type = real, default = none, units = kg*m2)

(4) ICOEFF2

Second (quadratic) inertia coefficient

(type = real, default = none, units = kg*m2)

(5) ICOEFF3

Third (cubic) inertia coefficient

(type = real, default = none, units = kg*m2)

(6) INRC

Moment of inertia below critical speed ratio, exceeds zero unless ISPCRT = 0

(type = real, default = none, units = kg*m2)

(7) ISPCRT

Pump inertia critical speed ratio

(type = real, default = none, units = dimensionless)

Example:

FL_PIN 1

1 'PUMP1' 1.43 1.0 0.5 0.25 1.43 0.25

FL_SMT – Pump speed and motor torque data

Required if PTYPE = HOM or PTYPE = UNIV for any pump defined on FL_PMP. The pump speed and motor torque options must be specified. Note the motor torque CF or TF should return dimensional motor torque (units of N*m). Also note that the user-implied value of rated motor torque (following from PSHR on FL_RPD) is not applied to the motor torque CF or TF, thus the user should ensure that rated motor torque is consistent with CF or TF values.

(1) NPHUP

Number of HOM and UNIV type pumps

(type = integer, default = none, units = dimensionless)

The following data are input as a table with length NPHUP

(1) PNAME

Name of the pump

(type = character*16, default = none, units = dimensionless)

(2) SMTopt

Option governing the pump speed computation,

(a) CFTF-ONLY

Choose this option if the pump speed is under CF or TF control (or equals the constant rated speed) for the entirety of the calculation. The torque-inertia equation will never be used to compute pump speed.

(b) CFTF-TIE

The pump speed is under CF or TF control (or equals the constant rates speed) until the trip (specified on FL_PMP) indicates switchover to torque-inertia equation solutions.

(c) TIE

The pump speed is initialized according to SPDRAT on FL_RPD and is governed by the torque-inertia equation for the entirety of the calculation.

(type = character, default = none, units = kg*m²)

(3) SFLAG

Flag indicating pump speed CF, TF, or constant value

(a) NO

The pump speed, for SMTopt = CFTF-ONLY or CFTF-TIE (before trip), equals the constant, rated value specified as OMEGAR on FL_RPD

(b) CF

The pump speed, for SMTopt = CFTF-ONLY or CFTF-TIE (before trip), is CF-specified

(c) TF

The pump speed, for SMTopt = CFTF-ONLY or CFTF-TIE (before trip), is TF-specified

(type = character*2, default = none, units = dimensionless)

If SFLAG = NO then

(4) ‘-‘

Use ‘-‘ as a placeholder

If SFLAG = CF then

(5) CFNAME

Name of the control function used for pump speed

(type = character*16, default = none, units = dimensionless)

If SFLAG = TF then

(5) TFNAME

Name of the tabular function used for pump speed

(type = character*16, default = none, units = dimensionless)

(6) MTFLAG

Flag indicating motor torque CF, TF, or constant value

(a) NO

The motor torque equals the constant, rated value specified as MOTTR on FL_RPD

(b) CF

The motor torque, for SMTopt = CFTF-ONLY or CFTF-TIE (before trip), is CF-specified

(c) TF

The motor torque, for SMTopt = CFTF-ONLY or CFTF-TIE (before trip), is TF-specified

(type = character*2, default = none, units = dimensionless)

If MTFLAG = NO then

(7) '-'

Use '-' as a placeholder

If MTFLAG = CF then

(7) CFNAME

Name of the control function used for pump speed

(type = character*16, default = none, units = dimensionless)

If MTFLAG = TF then

(7) TFNAME

Name of the tabular function used for pump speed

(type = character*16, default = none, units = dimensionless)

Example:

FL_SMT 3

1 'PUMP1' CFTF-ONLY CF 'OmegaCF' CF 'TauMotCF'

2 'PUMP2' CFTF-TIE TF 'OmegaTF' NO '-'

3 'PUMP3' TIE NO '-' TF 'TauMotTF'

FL_PNT – Pump numerical treatment

Required if PTYPE = HOM or PTYPE = UNIV for any pump defined on FL_PMP
The pump numerical option must be specified.

(1) NPHUP

Number of HOM and UNIV type pumps

(type = integer, default = none, units = dimensionless)

The following data are input as a table with length NPHUP

(1) PNAME

Name of the pump

(type = character*16, default = none, units = dimensionless)

(2) PNTopt

Option governing the pump numerical treatment,

(a) SIMP

Choose this option for a semi-implicit pump numerical treatment. Pump head figures into the flow path velocity solutions in a semi-implicit manner with this choice.

(b) EXP

Choose this option for a totally explicit pump numerical treatment similar to that applied to FANA and QUICK-CF type pumps.

(type = character, default = none, units = dimensionless)

(3) DISopt

Option governing pump dissipation energy treatment

(a) YES

Split the calculated dissipation energy across pool and atmosphere (according to the prescription outlined in the reference manual) and add to the discharge (“to”) control volume with respect to the flow path containing the pump. This amounts to adding a type AE and a type PE external source (RATE interpretation) to the discharge volume.

(b) NO

Calculate the overall dissipation energy (available as a CF argument and plot variable) but do not add any energy to the contents of the discharge control volume.

Example:

FL_PNT 1

1 ‘PUMP1’ SIMP YES

Block CVH Input Records for Terry Turbine Velocity Stage Model

CV_ROT – Terry turbine rotor object definition

Required if a Terry turbine rotor object is desired in a given control volume.

Defines the name, sequencing number, and some characteristics of a rotor object.

(1) ROTNAM

Object name of Terry turbine rotor

(type = character, default = none, units = dimensionless)

(2) ROTNUM

Object number of Terry turbine rotor

(type = integer, default = none, units = dimensionless)

(3) NUMNZL

Number of defined steam nozzle flow paths associated with this rotor object.

Note this does not factor in any steam nozzle multiplicity, rather it counts only defined flow paths with block FL input.

(type = integer, default = none, units = dimensionless)

(4) NUMRC

Number of reversing chambers coupled to a single steam nozzle for this rotor.

This defines the number of velocity stages for the turbine. Every nozzle associated with the rotor must have the same number of coupled reversing chambers.

(type = integer, default = none, units = dimensionless)

(5) ROTRAD (optional)

Radius of Terry turbine rotor, factors into rotor torque computation as the moment arm at which the impinging steam force acts on the rotor.

(type = real, default = 0.3048, units = m)

Example:

CV_ROT 'TerryTurbine' 1 2 4 ! note no 5th field, so default ROTRAD = 0.3048

CV_ROT 'TerryTurbine' 1 2 4 0.1524

CV_RIN – Terry turbine moment of inertia data

Required if a Terry turbine rotor is defined on CV_ROT.

The rotor moment of inertia is given in terms of turbo-shaft speed and user-supplied polynomial coefficients. Note this is a positive, non-zero quantity and such constraints are enforced by MELGEN and MELCOR.

(1) ICOEFFC

Constant inertia coefficient

(type = real, default = none, units = kg*m2)

(2) ICOEFF1

First (linear) inertia coefficient

(type = real, default = none, units = kg*m2)

(3) ICOEFF2

Second (quadratic) inertia coefficient

(type = real, default = none, units = kg*m2)

(4) ICOEFF3

Third (cubic) inertia coefficient

(type = real, default = none, units = kg*m2)

(5) INRC

Moment of inertia below critical speed ratio, exceeds zero unless ISPCRT = 0

(type = real, default = none, units = kg*m2)

(6) ISPCRT

Rotor inertia critical speed ratio

(type = real, default = none, units = dimensionless)

Example:

FL_RIN 1.43 1.0 0.5 0.25 1.43 0.25

CV_RFR – Terry turbine friction torque data

Required if a Terry turbine rotor is defined on CV_ROT.

The rotor friction torque is described in terms of turbo-shaft speed via input of coefficients and exponents.

- (1) TCOEFFC
Constant (zeroth) friction torque coefficient
(type = real, default = none, units = N*m)
- (2) TCOEFF1
First friction torque coefficient
(type = real, default = none, units = N*m)
- (3) TCOEFF2
Second friction torque coefficient
(type = real, default = none, units = N*m)
- (4) TCOEFF3
Third friction torque coefficient
(type = real, default = none, units = N*m)
- (5) TEXP1
First friction torque exponent, greater than, less than, but not equal to zero
(type = real, default = none, units = dimensionless)
- (6) TEXP2
Second friction torque exponent, greater than, less than, but not equal to zero
(type = real, default = none, units = dimensionless)
- (7) TEXP3
Third friction torque exponent, greater than, less than, but not equal to zero
(type = real, default = none, units = dimensionless)
- (8) TFRC
Friction torque used below critical speed ratio
(type = real, default = none, units = N*m)
- (9) TSPCRT
Rotor friction torque critical speed ratio
(type = real, default = none, units = dimensionless)

Example:

FL_RFR 451.0 100.0 50.0 25.0 1.1 2.2 3.3 451.0 0.25

CV_RBE – Terry turbine rotor bucket exit angle data

Required if a Terry turbine rotor is defined on CV_ROT.

The rotor bucket exit angles factor into the computation of rotor torque contributions of each velocity stage. Constants or control functions may define these angles. The table length must equal the number of nozzles (NUMNZZL on CV_ROT) and the number of entries on each tabular record must equal the number of reversing chambers (NUMRC on CV_ROT) plus one to account for the bucket downstream of the last reversing chamber.

(1) NTAB

Number of tabular rows in CV_RBE table, must equal NUMNZZL on CV_ROT

(type = integer, default = none, units = dimensionless)

The following data are input as a table with length NTAB

(1) NROW

Tabular row identifier

(type = integer, default = none, units = dimensionless)

(2) BETA_BK_1

Bucket exit angle for first bucket associated with steam nozzle described by current tabular record

(a) CONSTVALU

A constant value of bucket exit angle for current bucket of current nozzle

(type = real, default = none, units = radians)

(b) CFNAME

An object name signifying the control function that specifies bucket exit angle for current bucket of current nozzle

(type = character, default = none, units = dimensionless)

... entries for bucket 2 to bucket NUMRC+1

Example:

CV_RBE 2 ! 2 defined steam nozzle flow paths, assume 4 rev cham per nzl

1 0.5236 0.5236 0.5236 0.5236 0.5236 ! constant value 45 degrees for all

2 'BETA_1' 'BETA_2' 'BETA_3' 'BETA_4' 'BETA_5'

CV_RCB – Terry turbine rotor bucket loss coefficient data

Required if a Terry turbine rotor is defined on CV_ROT.

The rotor bucket loss coefficients factor into the computation of rotor torque contributions of each velocity stage. They characterize the velocity decrease across a bucket. Constants or control functions may define these coefficients. The table length must equal the number of nozzles (NUMNZZ on CV_ROT) and the number of entries on each tabular record must equal the number of reversing chambers (NUMRC on CV_ROT) plus one to account for the bucket downstream of the last reversing chamber.

(1) NTAB

Number of tabular rows in CV_RCB table, must equal NUMNZZ on CV_ROT

(type = integer, default = none, units = dimensionless)

The following data are input as a table with length NTAB

(1) NROW

Tabular row identifier

(type = integer, default = none, units = dimensionless)

(2) CB_BK_1

Bucket loss coefficient for first bucket associated with steam nozzle described by current tabular record

(a) CONSTVALU

A constant value of loss coefficient for current bucket of current nozzle

(type = real, default = none, units = radians)

(b) CFNAME

An object name signifying the control function that specifies loss coefficient for current bucket of current nozzle

(type = character, default = none, units = dimensionless)

... entries for bucket 2 to bucket NUMRC+1

Example:

CV_RCB 2 ! 2 defined steam nozzle flow paths, assume 4 rev cham per nzl

1 0.95 0.95 0.95 0.95 0.95 ! 5% loss of velocity across all buckets

2 'CB_1' 'CB_2' 'CB_3' 'CB_4' 'CB_5'

CV_RGR – Terry turbine reversing chamber leakage coefficient data

Required if a Terry turbine rotor is defined on CV_ROT.

The reversing chamber leakage coefficients factor into the computation of rotor torque contributions of each velocity stage. They characterize the mass decrease across a reversing chamber due to out-flow through crescent holes in chambers. Constants or control functions may define these coefficients. The table length must equal the number of nozzles (NUMNZL on CV_ROT) and the number of entries on each tabular record must equal the number of reversing chambers (NUMRC on CV_ROT).

(1) NTAB

Number of tabular rows in CV_RGR table, must equal NUMNZL on CV_ROT

(type = integer, default = none, units = dimensionless)

The following data are input as a table with length NTAB

(1) NROW

Tabular row identifier

(type = integer, default = none, units = dimensionless)

(2) GR_RC_1

Leakage coefficient for first chamber associated with steam nozzle described by current tabular record

(a) CONSTVALU

A constant value of leakage coefficient for current chamber of current nozzle

(type = real, default = none, units = radians)

(b) CFNAME

An object name signifying the control function that specifies leakage coefficient for current chamber of current nozzle

(type = character, default = none, units = dimensionless)

... entries for chamber 2 to chamber NUMRC

Example:

CV_RGR 2 ! 2 defined steam nozzle flow paths, assume 4 rev cham per nzl

1 0.95 0.95 0.95 0.95 ! 5% loss of mass across all chambers

2 'CB_1' 'CB_2' 'CB_3' 'CB_4'

CV_RCR – Terry turbine reversing chamber loss coefficient data

Required if a Terry turbine rotor is defined on CV_ROT.

The reversing chamber loss coefficients factor into the computation of rotor torque contributions of each velocity stage. They characterize the velocity decrease across a reversing chamber. Constants or control functions may define these coefficients. The table length must equal the number of nozzles (NUMNZL on CV_ROT) and the number of entries on each tabular record must equal the number of reversing chambers (NUMRC on CV_ROT).

(1) NTAB

Number of tabular rows in CV_RCR table, must equal NUMNZL on CV_ROT

(type = integer, default = none, units = dimensionless)

The following data are input as a table with length NTAB

(1) NROW

Tabular row identifier

(type = integer, default = none, units = dimensionless)

(2) CR_RC_1

Chamber loss coefficient for first bucket associated with steam nozzle described by current tabular record

(a) CONSTVALU

A constant value of loss coefficient for current chamber of current nozzle

(type = real, default = none, units = radians)

(b) CFNAME

An object name signifying the control function that specifies loss coefficient for current chamber of current nozzle

(type = character, default = none, units = dimensionless)

... entries for chamber 2 to chamber NUMRC

Example:

CV_RCR 2 ! 2 defined steam nozzle flow paths, assume 4 rev cham per nzl

1 0.95 0.95 0.95 0.95 ! 5% loss of velocity across all chambers

2 'CR_1' 'CR_2' 'CR_3' 'CR_4'

CV_RXZI – Terry turbine carryover fraction data

Required if a Terry turbine rotor is defined on CV_ROT.

The carryover fractions factor into the computation of rotor torque contributions of each velocity stage. They characterize the loss of mass as steam traverses the gap between a rotor bucket and its downstream reversing chamber. Constants or control functions may define these coefficients. The table length must equal the number of nozzles (NUMNZL on CV_ROT) and the number of entries on each tabular record must equal the number of reversing chambers (NUMRC on CV_ROT).

(1) NTAB

Number of tabular rows in CV_RXZI table, must equal NUMNZL on CV_ROT

(type = integer, default = none, units = dimensionless)

The following data are input as a table with length NTAB

(1) NROW

Tabular row identifier

(type = integer, default = none, units = dimensionless)

(2) XZI_RC_1

Carryover fraction for first bucket/chamber pair associated with steam nozzle described by current tabular record

(a) CONSTVALU

A constant value of carryover fraction for current bucket/chamber pair

(type = real, default = none, units = radians)

(b) CFNAME

An object name signifying the control function that specifies carryover fraction for current bucket/chamber pair

(type = character, default = none, units = dimensionless)

... entries for chamber 2 to chamber NUMRC

Example:

CV_RXZI 2 ! 2 defined steam nozzle flow paths, assume 4 rev cham per nzl

1 0.95 0.95 0.95 0.95 ! 5% loss of mass flow across all bucket/chamber gaps

2 'XZI_1' 'XZI_2' 'XZI_3' 'XZI_4'

CV_NFP – Terry turbine rotor associated steam nozzle flow paths

Required if a Terry turbine rotor is defined on CV_ROT.

This record connects defined steam nozzle flow paths (with FL_ID records and block FL input) to a rotor object. It also allows specification of a steam nozzle “multiplicity” such that the effects of a given steam nozzle flow path on turbine torque can be multiplied.

(1) NTAB

Number of tabular rows in CV_NFP table, must equal NUMNZN on CV_ROT

(type = integer, default = none, units = dimensionless)

The following data are input as a table with length NTAB

(1) NROW

Tabular row identifier

(type = integer, default = none, units = dimensionless)

(2) FPNAME

Object name of a flow path meant to represent a steam nozzle. Note the flow path does not necessarily have to be listed on FL_VTM as a steam nozzle type flow path.

(3) MULT

Multiplicity of flow path FPNAME. The torque contribution of steam/water through FPNAME will be multiplied by MULT and factored into the overall rotor torque calculation without the need to define a new flow path. Note multiplicity is not accounted for in NUMNZN on CV_ROT.

Example:

CV_NFP 2

1 ‘Stm_Nzl_Hi’ 3 ! one FP in FL input, but 3 identical FP’s seen by rotor

2 ‘Stm_Nzl_Lo’ 2 ! one FP in FL input, but 2 identical FP’s seen by rotor

FL Input Records for Terry Turbine Pressure Stage Model

FL_VTM – Time-Dependent Flow Path

The velocity through the flow path may be defined using tabular or control functions. The pool and atmosphere velocities are identical. Only one time dependent flow path dataset may be entered for a flow path.

(1) NVOFT

Number of time-dependent flow paths

(type = integer, default = none, units = dimensionless)

The following data are input as a table with length NVOFT

(1) NFLT

Table row index

(type = integer, default = none, units = none)

(2) FLNAME

Name of flow path that will be time dependent

(type = character, default = none, units = dimensionless)

(3) NTFLAG

Time dependent flow path type flag

(a) 1 or TF

Use tabular function name NFUN to define velocity versus time

(b) -1 or CF

Use control function name NFUN to define velocity versus time

(c) 2 or STMNZL

Use steam expansion model to compute atmosphere velocity

(type = integer|character, default = none, units = dimensionless)

If NTFLAG = 1|TF or if NTFLAG = -1|CF

(4) NFUN

Tabular or control function name to define the velocity versus time. The interpretation is dependent on the value of NTFLAG

(type = character, default = none, units = dimensionless)

If NTFLAG = 2|STMNZL

(4) PDOT

Steam nozzle expansion rate for use in analytical Wilson point calculation

(type = real, default = 2259.0, units = 1/s)

(5) Ae2At

Steam nozzle area ratio, exit-to-throat

(type = real, default = 1.644, units = dimensionless)

(6) ISENTEXP

Expansion calculation option

(a) 0

Use analytical Wilson point method, don't force purely isentropic expansion

(b) 1

Force purely isentropic expansion, discounting any metastability in expansion

(type = integer, default = 0, units = dimensionless)

Example

FL_VTM 3

- 1 FlowPath190 TF TF19
- 2 FlowPath700 CF CF700
- 3 'Stm_Nzl_Hi' 2 2.259e+3 1.644 1

FL_TSH – Turboshaft object association

Required for a Terry turbine rotor defined on CV_ROT to be linked to a homologous pump defined on FL_PMP.

A turboshaft linking two defined code objects (a rotor object and a pump object) is implicitly defined here by specifying the object names of the rotor and pump.

(1) NTAB

Number of tabular rows in FL_TSH table

(type = integer, default = none, units = dimensionless)

The following data are input as a table with length NTAB

(1) NROW

Tabular row identifier

(type = integer, default = none, units = dimensionless)

(2) ROTNAM

Object name of a Terry turbine rotor defined on CV_ROT of some control volume meant to represent a steam nozzle. Note the flow path does not necessarily have to be listed on FL_VTM as a steam nozzle type flow path.

(3) PNAME

Multiplicity of flow path FPNAME. The torque contribution of steam/water through FPNAME will be multiplied by MULT and factored into the overall rotor torque calculation without the need to define a new flow path. Note multiplicity is not accounted for in NUMNZZL on CV_ROT.

Example:

CV_NFP 2

- 1 'Stm_Nzl_Hi' 3 ! one FP in FL input, but 3 identical FP's seen by rotor
- 2 'Stm_Nzl_Lo' 2 ! one FP in FL input, but 2 identical FP's seen by rotor

APPENDIX E: 3D NOZZLE SIMULATION DETAILS AND RESULTS

Mesh, Geometry, and Boundary Conditions

The nozzle region of the full 3D Terry turbine model was extracted and meshed as shown in Figure E.1 below for purposes of a pure pressure stage simulation. Because no particular experimental benchmark exists for the simulation, boundary conditions similar to those of the 2D Gyarmathy nozzle simulation were imposed.

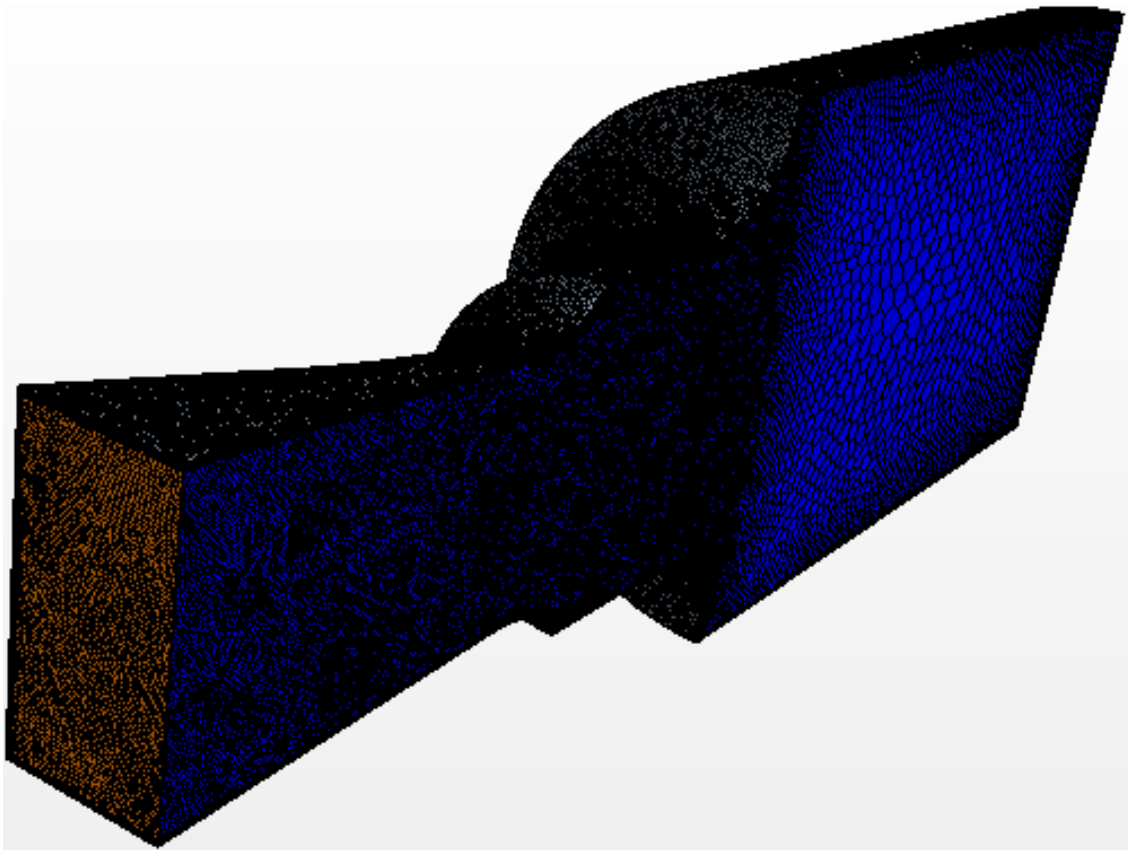


Figure E.1 Computational mesh for 3D Terry turbine nozzle CMFD simulation

Solution Profiles

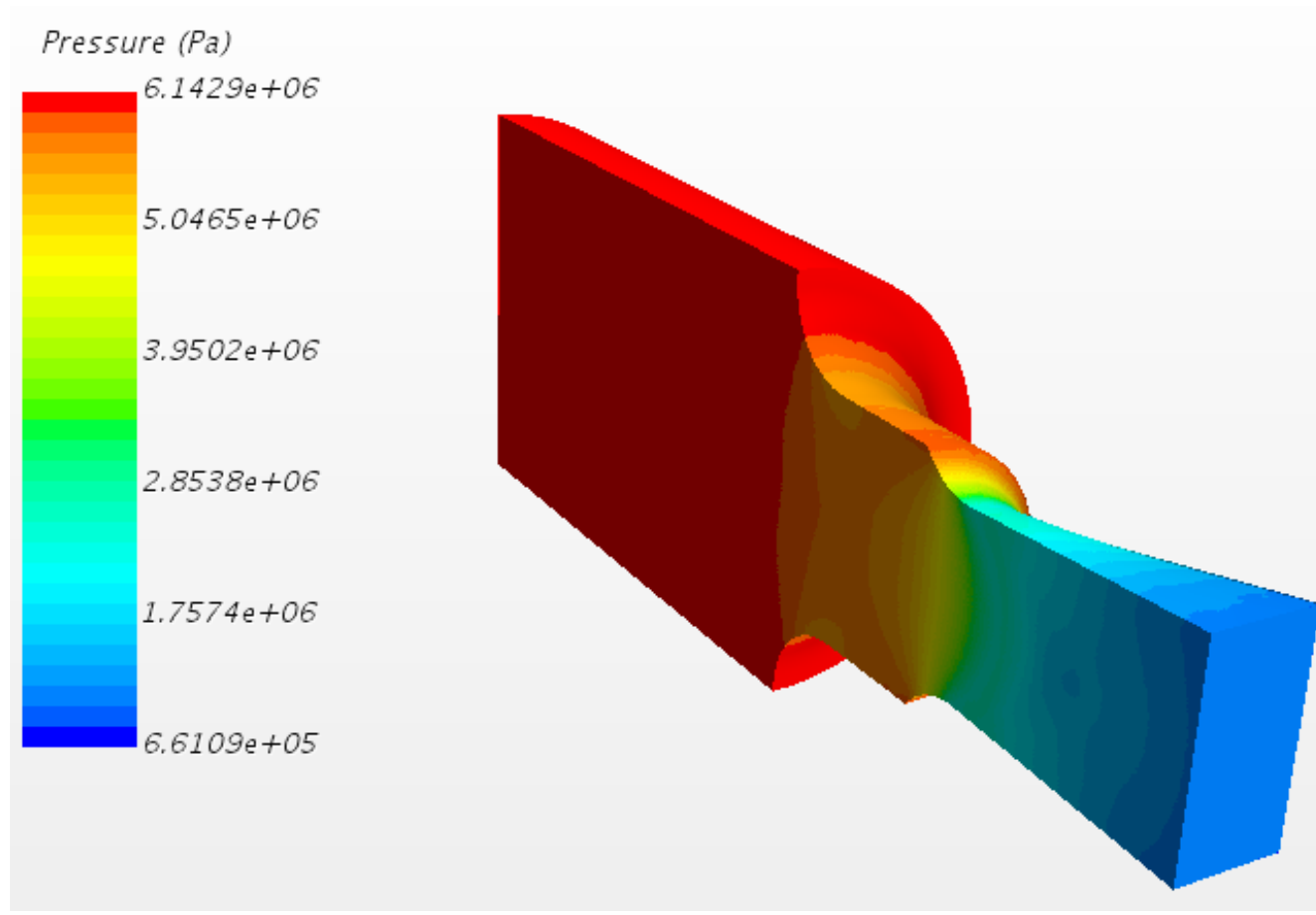


Figure E.2 Pressure distribution for 3D Terry turbine nozzle simulation

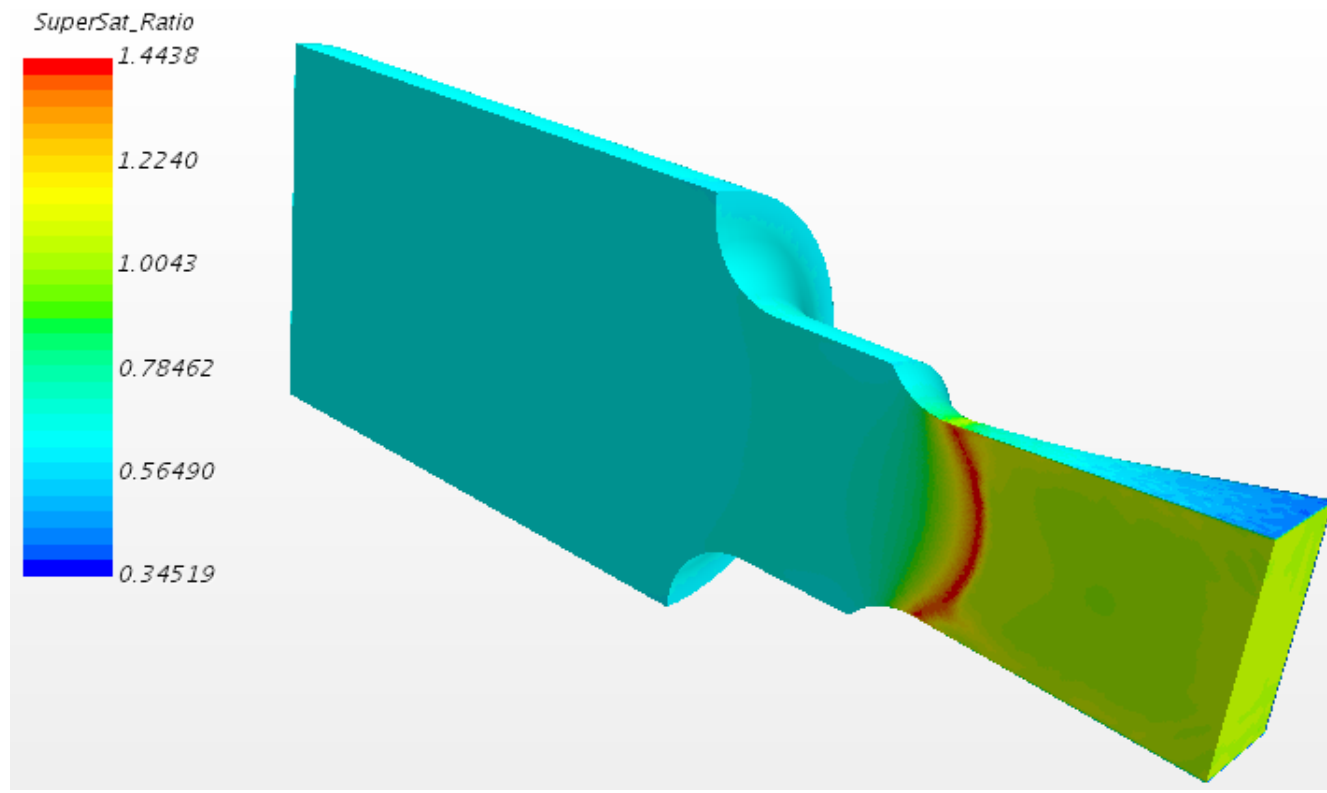


Figure E.3 Super-saturation ratio for 3D Terry turbine nozzle simulation

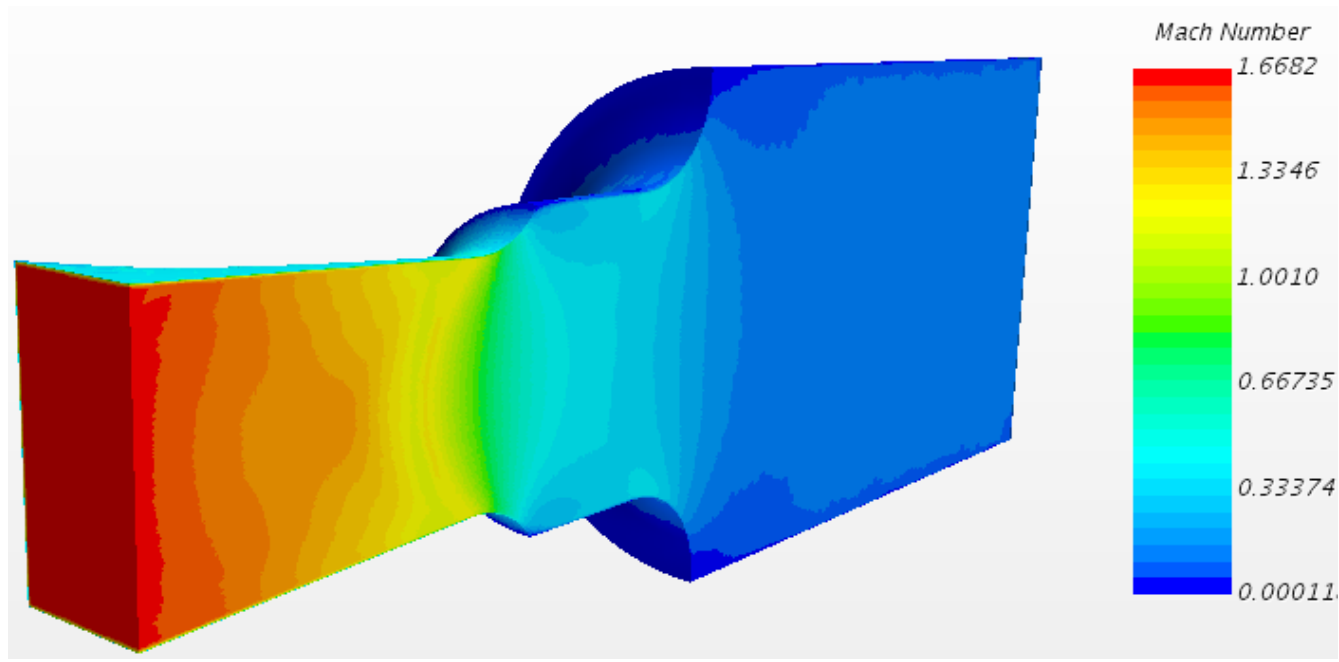


Figure E.4 Mach number for 3D Terry turbine nozzle simulation

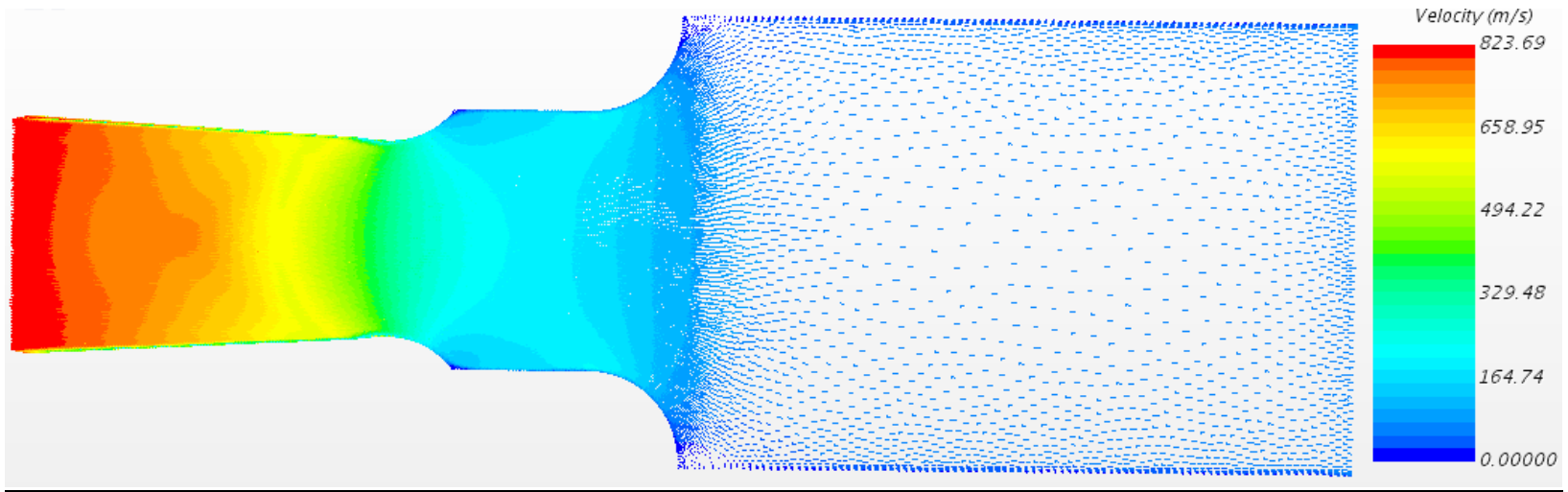


Figure E.5 Velocity vectors for 3D Terry turbine nozzle simulation

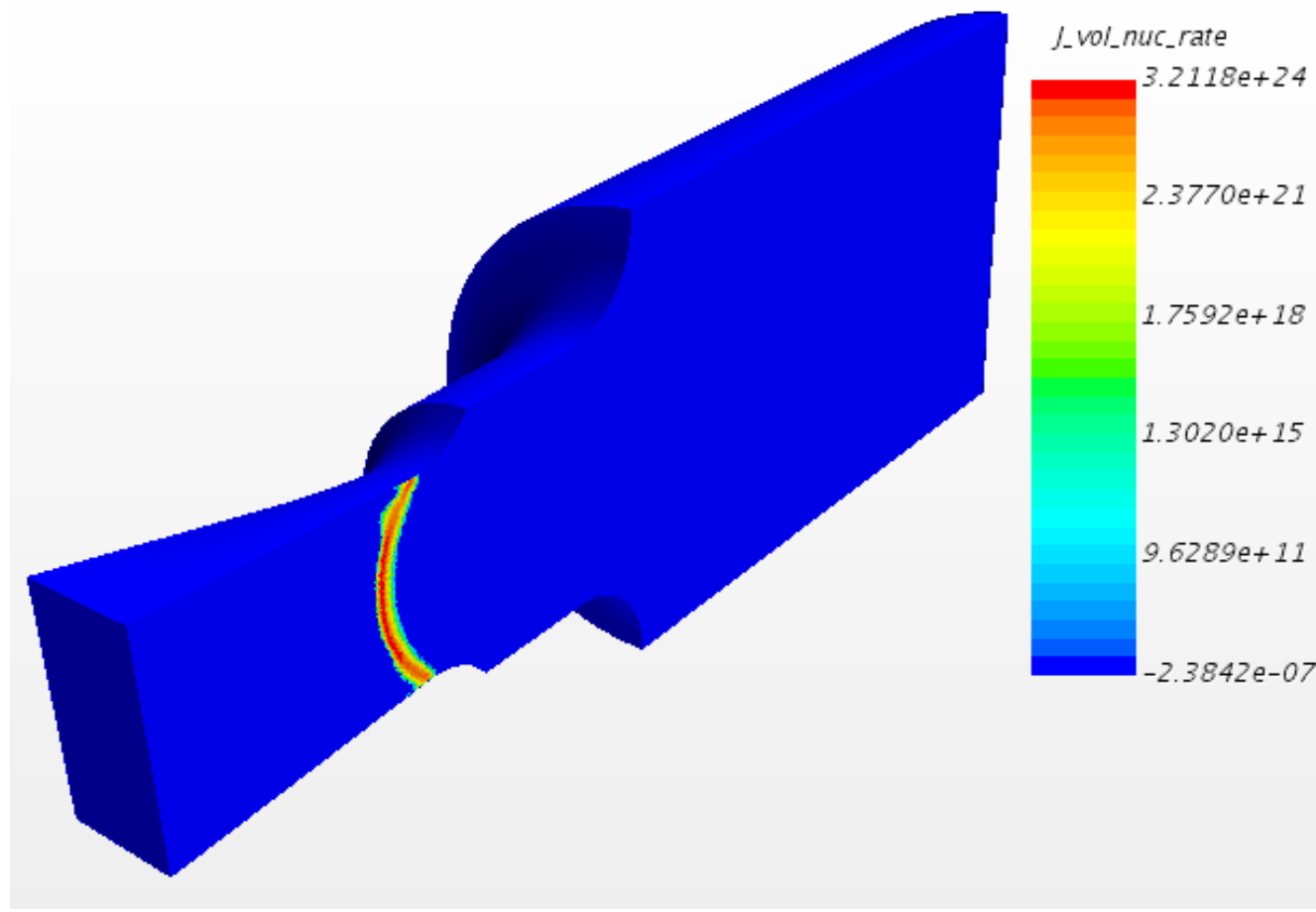


Figure E.6 Nucleation rate for 3D Terry turbine nozzle simulation

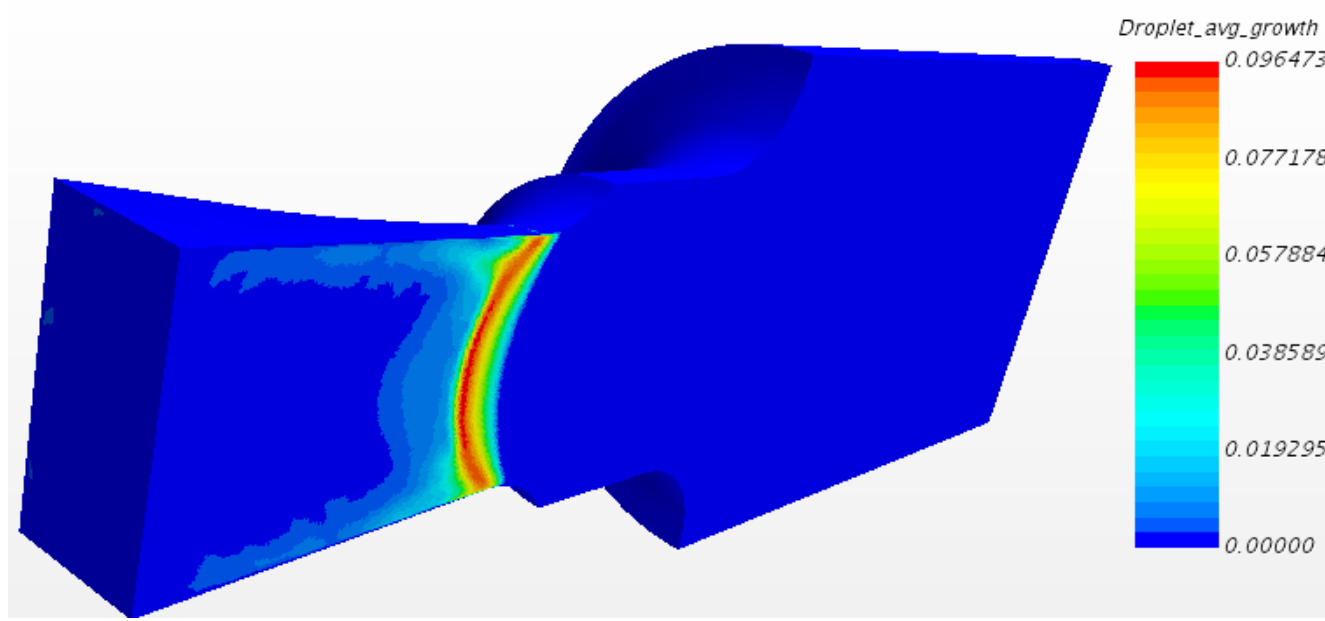


Figure E.7 Condensation rate for 3D Terry turbine nozzle simulation

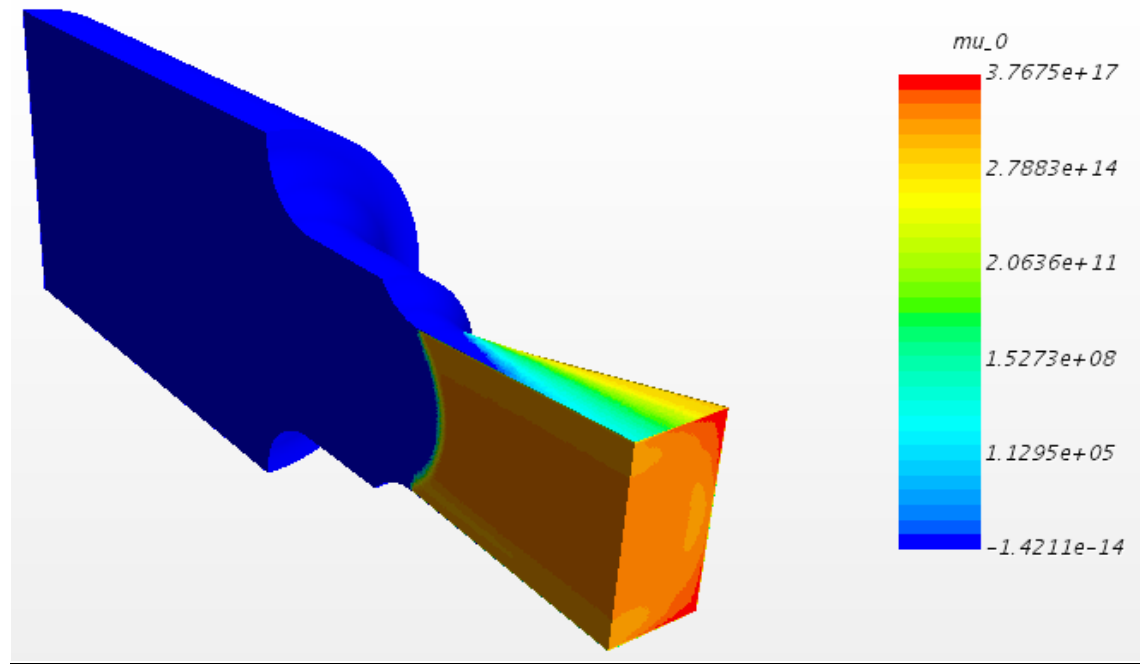


Figure E.8 First drop size distribution moment [drop/kg] for 3D Terry turbine nozzle simulation

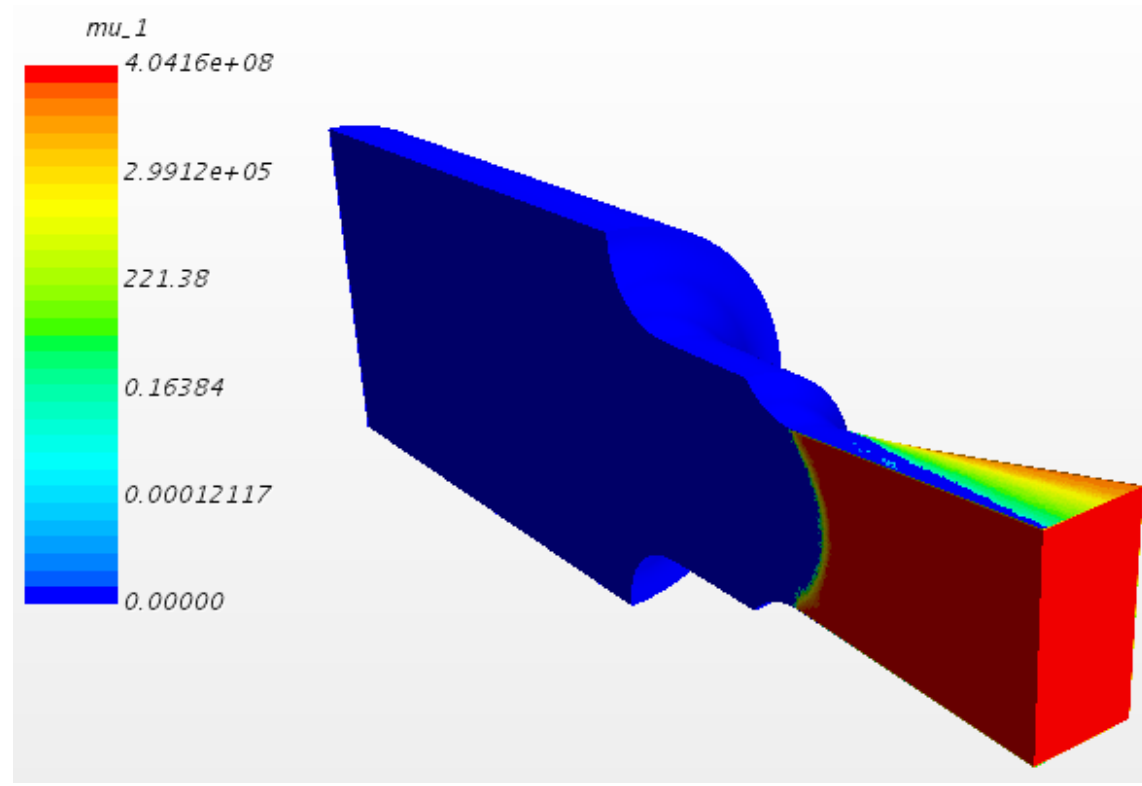


Figure E.9 Second drop size distribution moment [drop*m/kg] for 3D Terry turbine nozzle simulation

APPENDIX F: MODIFIED HEM FOR DISPERSED TWO-PHASE FLOW

Assuming one-dimensional, steady, homogeneous-equilibrium (thermal, mechanical equilibrium) flow in a duct, the following conservation equations apply [53]:

Continuity:

$$\mathbf{F.1} \quad \dot{m} = \mathbf{const} = \rho_{mix}VA$$

Momentum (neglecting gravity):

$$\mathbf{F.2} \quad \dot{m} \frac{dV}{dx} = -A \frac{dP}{dx} - P\tau_{wall}$$

Energy (neglecting wall heat transfer, work terms, and gravity):

$$\mathbf{F.3} \quad 0 = \dot{m} \frac{d}{dx} \left(h + \frac{V^2}{2} \right)$$

Where: ρ_{mix} = Mixture density [kg/m³]; V = Flow velocity [m/s]; A = Area [m²]

\dot{m} = Mass flow rate [kg/s]; P = Perimeter [m]; τ_{wall} = Shear [Pa/m²]

h = Specific enthalpy [J/kg]

The conventional one-dimensional equations of isentropic, ideal gas dynamics may be derived from F.1 through F.3 above (when paired with the Ideal gas law and Tds

relations). Consider a pseudo-gas consisting of 1) a continuous ideal gas, and 2) a dilute dispersed phase in mechanical equilibrium with and exchanging thermal energy with the gas. In this case, the pseudo-gas has a mixture density of:

$$\mathbf{F.4} \quad \rho_{mix} = \rho_{gas}(1 + Y)$$

Where: Y = Mass fraction of droplets in continuous phase [kg/kg]

Assuming heat transfer occurs such that thermal equilibrium is preserved between the two parts of the pseudo-gas, for isentropic flow the combined entropy remains constant. Thus, the entropy equation is:

$$\mathbf{F.5} \quad \frac{dT}{T} (C_{p,gas} + Y C_{p,liq}) - R \frac{dP}{P} = 0$$

Where: T = gas/drop temperature [K] ; R = steam gas constant ; P = Pressure [Pa]

$C_{p,\phi}$ = specific heat of phase ϕ [J/kg/K]

Then, the expansion law for the pseudo-gas is:

$$\mathbf{F.6} \quad P^{\gamma-1/\gamma} / T = \mathbf{const}, \quad \frac{\gamma-1}{\gamma} = \frac{R}{C_{p,gas} + Y C_{p,liq}}$$

APPENDIX G: INL VIRTUAL NOZZLE JET EXPANSION MODEL

The proposed RCIC Terry turbine pressure stage furnishes nozzle exit plane conditions including an exit plane pressure. If nozzle exit plane pressure exceeds the turbine back-pressure, further expansion of the steam jet occurs downstream of the nozzle exit plane. The attending expansion to the turbine back pressure is called a “virtual nozzle” as illustrated in Figure G.1. Assuming no mass flux through the jet boundary and using mass, momentum, and energy balance concepts plus the ideal gas law, algebraic equations for velocity, temperature, and density at the end of the virtual nozzle can be derived. These are equations (6.107, (6.108, and 6.109.

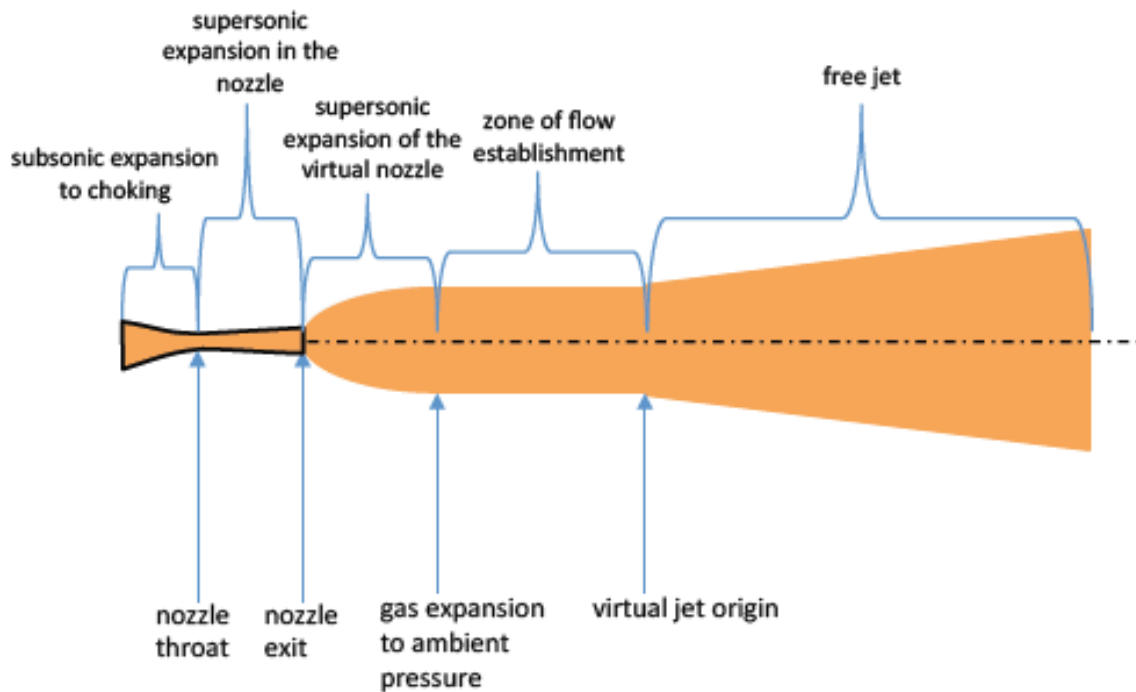


Figure G.1 Converging/Diverging nozzle expansion diagram [54]

APPENDIX H: PLOTTING AND CONTROL FUNCTIONS

This appendix summarizes new plot variables and control functions for the homologous pump model and the new RCIC Terry turbine models. The format of presentation in this appendix follows that of the MELCOR User Guide [15]

Homologous Pump Model Control Functions

FL-PMP-HEAD(NameFP)	The head (momentum source) for flow path NameFP added by a pump (PTYPE = HOM or UNIV) (Pa)
FL-PMP-THYD(NameFP)	The hydraulic torque exerted on fluid in flow path NameFP by a pump (PTYPE = HOM or UNIV) (N*m)
FL-PMP-SPD(NameFP)	The impeller speed of a pump (PTYPE = HOM or UNIV) associated with flow path NameFP (rpm)
FL-PMP-TFR(NameFP)	The friction torque of a pump (PTYPE = HOM or UNIV) associated with flow path NameFP (N*m)
FL-PMP-PIN(NameFP)	The moment of inertia of a pump (PTYPE = HOM or UNIV) associated with flow path NameFP (kg*m ²)
FL-PMP-DISS(NameFP)	The energy dissipation of a pump (PTYPE = HOM or UNIV) associated with flow path NameFP (W)
FL-PMP-EFF(NameFP)	The efficiency (based on the ratio of power used for pressure head to power delivered by impeller) of a pump (PTYPE = HOM or UNIV) associated with flow path NameFP (%)
FL-PMP-TMOT(NameFP)	The motor torque for a pump (PTYPE = HOM or UNIV) associated with flow path NameFP

	(N*m)
FL-PMP-DHDQ(NameFP)	The head derivative (as a function of flow) used during the semi-implicit solution associated with flow path NameFP (m/(m ³ /s))
FL-PMP-DELPOW(NameFP)	The power delivered by the pump impeller to the working fluid for flow path NameFP, equal to hydraulic torque times speed (W)

Homologous Pump Model Plot Variables

FL-PMP-HEAD.n	The head (momentum source) for flow path n added by a pump (PTYPE = HOM or UNIV) (Pa)
FL-PMP-THYD.n	The hydraulic torque exerted on fluid in flow path n by a pump (PTYPE = HOM or UNIV) (N*m)
FL-PMP-SPD.n	The impeller speed of a pump (PTYPE = HOM or UNIV) associated with flow path n (rpm)
FL-PMP-TFR.n	The friction torque of a pump (PTYPE = HOM or UNIV) associated with flow path n (N*m)
FL-PMP-PIN.n	The moment of inertia of a pump (PTYPE = HOM or UNIV) associated with flow path n (kg*m ²)
FL-PMP-DISS.n	The energy dissipation of a pump (PTYPE = HOM or UNIV) associated with flow path n (W)
FL-PMP-EFF.n	The efficiency (based on the ratio of power used for pressure head to power delivered by impeller) of a pump (PTYPE = HOM or UNIV) associated with flow path n (%)
FL-PMP-TMOT.n	The motor torque for a pump (PTYPE = HOM or UNIV) associated with flow path n (N*m)

FL-PMP-DHDQ.n	The head derivative (as a function of flow) used during the semi-implicit solution associated with flow path n (m/(m ³ /s))
FL-PMP-DELPOW.n	The power delivered by the pump impeller to the working fluid for flow path n, equal to hydraulic torque times speed (W)
FL-PMP-QFLO.n	The total volumetric flow rate through the pump flow path n (m ³ /s)

Terry Turbine Pressure Stage Plot Variables

FL-STMNZL-T01.n	The stagnation inlet (way-point 01) temperature for time-dependent steam nozzle type flow path n (K)
FL-STMNZL-P01.n	The stagnation inlet (way-point 01) pressure for time-dependent steam nozzle type flow path n (Pa)
FL-STMNZL-T2.n	The static temperature at expansion way-point 2 for time-dependent steam nozzle type flow path n (K)
FL-STMNZL-P2.n	The static pressure at expansion way-point 2 for time-dependent steam nozzle type flow path n (Pa)
FL-STMNZL-M2.n	The Mach number at expansion way-point 2 for time-dependent steam nozzle type flow path n (-)
FL-STMNZL-Ta.n	The static temperature at expansion way-point a for time-dependent steam nozzle type flow path n (K)
FL-STMNZL-Pa.n	The static pressure at expansion way-point a for time-dependent steam nozzle type flow path n (Pa)
FL-STMNZL-Ma.n	The Mach number at expansion way-point a for time-dependent steam nozzle type flow path n (-)

FL-STMNZL-Tn.n	The static temperature at expansion way-point n for time-dependent steam nozzle type flow path n (K)
FL-STMNZL-Pn.n	The static pressure at expansion way-point n for time-dependent steam nozzle type flow path n (Pa)
FL-STMNZL-Mn.n	The Mach number at expansion way-point n for time-dependent steam nozzle type flow path n (-)
FL-STMNZL-Yn.n	The wetness fraction at expansion way-point n for time-dependent steam nozzle type flow path n (kg _l /kg _g)
FL-STMNZL-Ypn.n	The time derivative of wetness fraction at expansion way-point n for time-dependent steam nozzle type flow path n ((kg _l /kg _g)/s)
FL-STMNZL-T3.n	The static temperature at expansion way-point 3 for time-dependent steam nozzle type flow path n (K)
FL-STMNZL-P3.n	The static pressure at expansion way-point 3 for time-dependent steam nozzle type flow path n (Pa)
FL-STMNZL-M3.n	The Mach number at expansion way-point 3 for time-dependent steam nozzle type flow path n (-)
FL-STMNZL-Y3.n	The wetness fraction at expansion way-point 3 for time-dependent steam nozzle type flow path n (kg _l /kg _g)

FL-STMNZL-X3.n	The quality at expansion way-point 3 for time-dependent steam nozzle type flow path n (-)
FL-STMNZL-T4.n	The static temperature at expansion way-point 4 for time-dependent steam nozzle type flow path n (K)
FL-STMNZL-P4.n	The static pressure at expansion way-point 4 for time-dependent steam nozzle type flow path n (Pa)
FL-STMNZL-M4.n	The Mach number at expansion way-point 4 for time-dependent steam nozzle type flow path n (-)
FL-STMNZL-Y4.n	The wetness fraction at expansion way-point 4 for time-dependent steam nozzle type flow path n (kg _l /kg _g)
FL-STMNZL-X4.n	The quality at expansion way-point 4 for time-dependent steam nozzle type flow path n (-)
FL-STMNZL-T4p.n	The static temperature at expansion way-point 4p for time-dependent steam nozzle type flow path n (K)
FL-STMNZL-P4p.n	The static pressure at expansion way-point 4p for time-dependent steam nozzle type flow path n (Pa)
FL-STMNZL-M4p.n	The Mach number at expansion way-point 4p for time-dependent steam nozzle type flow path n (-)

Terry Turbine Velocity Stage Plot Variables

CVH-TURBIN.n	The moment of inertia for Terry turbine rotor object in control volume n (kg*m ²)
CVH-TURBFR.n	The friction torque for Terry turbine rotor object in control volume n (N*m)
CVH-TURBTORQ.n	The torque exerted by fluid on Terry turbine rotor object in control volume n (N*m)
CVH-TURBDELPOW.n	The power delivered by rotor (transmitted by turboshaft) for Terry turbine rotor object in control volume n (W)
CVH-TURBSTMTORQ.k.m.n	The torque exerted by steam in velocity stage k of nozzle m in Terry turbine rotor object in control volume n (N*m)
CVH-TURBWATTORQ.m.n	The torque exerted by water in nozzle m in Terry turbine rotor object in control volume n (N*m)
CVH-TURBSTGVEL.k.m.n	The velocity of fluid in velocity stage k of nozzle m in Terry turbine rotor object in control volume n (m/s)
CVH-TURBSTGMFR.k.m.n	The mass flow rate of fluid in velocity stage k of nozzle m in Terry turbine rotor object in control volume n (kg/s)